DISSERTATION

submitted to the
Combined Faculties for the Natural Sciences and for Mathematics
of the Ruperto-Carola University of Heidelberg, Germany
for the degree of

Doctor of Natural Sciences

Put forward by

Diplom-Physiker Marc Florian Marhauser

born in Offenbach am Main, Germany

Oral examination: October 14th ,2009

Confinement in Polyakov gauge
and the
QCD phase diagram

Referees: Prof. Dr. Jan Martin Pawlowski
Prof. Dr. Jürgen Schaffner-Bielich

Quarkeinschluß in Polyakov Eichung
und das
Phasendiagramm der Quantenchromodynamik

Wir untersuchen die Quantenchromodynamik (QCD) im Rahmen der funktionalen Renormierungsgruppenmethoden (fRG). Darin beschreiben wir den Zentrumsphasenübergang von der Phase mit Quarkeinschluß in die Quark-Gluon-Plasma Phase. Wir konzentrieren uns dabei auf eine physikalische Eichung, in der der Mechanismus des Phasenübergangs deutlich wird. Wir finden gute Übereinstimmung mit Gitter-QCD Ergebnissen, sowie mit Resultaten aus funktionalen Methoden erzielt in anderen Eichungen. Der Phasenübergang ist, wie erwartet, von zweiter Ordnung und wir berechnen kritische Exponenten. Verschiedene Erweiterungen des Modells werden diskutiert.

Im Zusammenhang mit der Untersuchung des QCD Phasendiagramms, berechnen wir die Effekte die dynamische Quarks auf das Verhalten der Eichkopplung ausüben. Auch untersuchen wir wie sich diese auf den Zentrumphasenübergang auswirken, damit ermöglichen die Quarks, ein chemisches Potential zu berücksichtigen. Im weiteren stellen wir eine Verbindung zwischen dem Quarkeinschluß und chiraler Symmetrybrechung her, die für die Masse der Hadronen verantwortlich gemacht wird.

Die während der Rechnungen auftretenden Skalenabhängigkeiten der Felder werden zum Abschluß der Arbeit im Rahmen der funktionalen Renormierungsgruppenmethodik auf ein einheitliches Fundament gestellt.

Confinement in Polyakov Gauge
and the
Phasen Diagram of Quantum Chromodynamics

We investigate Quantum Chromodynamics (QCD) in the framework of the functional renormalisation group (fRG). Thereby describing the phase transition from the phase with confined quarks into the quark-gluon-plasma phase. We focus on a physical gauge in which the mechanism driving the phase transition is discernible. We find results compatible with lattice QCD data, as well as with functional methods applied in different gauges. The phase transition is of the expected order and we computed critical exponents. Extensions of the model are discussed.

When investigating the QCD phase diagram, we compute the effects of dynamical quarks at finite density on the running of the gauge coupling. Additionally, we calculate how these affect the deconfinement phase transition, also, dynamical quarks allow for the inclusion of a finite chemical potential. Concluding the investigation of the phase diagram, we establish a relation between confinement and chiral symmetry breaking, which is tied to the dynamical generation of hadron masses.

In the investigations, we often encounter scale dependent fields. We will investigate a footing on which these can be dealt with in a uniform way.

Contents

1 The QCD phase diagram

"Je größer die Schwierigkeiten, desto größer der Sieg"
Marcus Tulius Cicero

It is widely believed that Quantum Chromodynamics (QCD) is the correct quantum field theory of strong interactions at energy scales accessible in experiments today. In the high energy limit QCD can be successfully treated perturbatively, in an expansion in powers of the coupling constant. The validity of this expansion is a consequence of asymptotic freedom, the notion that at asymptotically short distances the coupling strength vanishes. The discovery of this property has been awarded with the Nobel prize [1, 2] and was one keystone to establish QCD as the theory of strong interactions consistent with experiments.

The perturbative treatment fails in the low and intermediate energy regime, where phenomena like chiral symmetry breaking (χSB) or confinement, i.e. the permanent enclosure of all coloured degrees of freedom inside colour neutral objects (hadrons) occur. Due to the non-Abelian nature of the gauge symmetry of QCD, it describes not only interactions between quarks and gluons, but also among the gluons themselves. It is expected that this self-interaction generates confinement.

Confinement leads to the challenging situation that the theoretical formulation of QCD is surprisingly straightforward, while the connection to observables is not. It is therefore not only essential to understand the underlying QCD phenomena, but also to compute hadronic observables from the fundamental theory.

χSB manifests itself in the bound state spectrum, with hadrons having masses of the order of 1 GeV, quite independently of the current quark masses. Again the situation arises, that while the underlying theory is well know, getting predictions proves to be very difficult.

As both phenomena, χSB and confinement, root in the theory, it is highly desirable to have an understanding of their interplay and occurrence. There are indications, that both phenomena are closely related and in the context of the phase diagram share a common phase boundary. Yet, there is no rigourous prove of the latter, which is an active area of research.

Related to the understanding of QCD phenomena like confinement or chiral symmetry breaking is knowledge about the QCD phase diagram. A version of the QCD phase diagram, as it is conjectured nowadays, is displayed in Fig. 1.1. Shortly after establishing QCD as the theory of strong interactions, it has already been argued, that hadrons, which consist out of quarks and gluons should dissociate at high enough temperatures or densities [3, 4]. This area of research has recently attracted a lot of attention, since much progress has been made from the experimental as well as from the theoretical side.

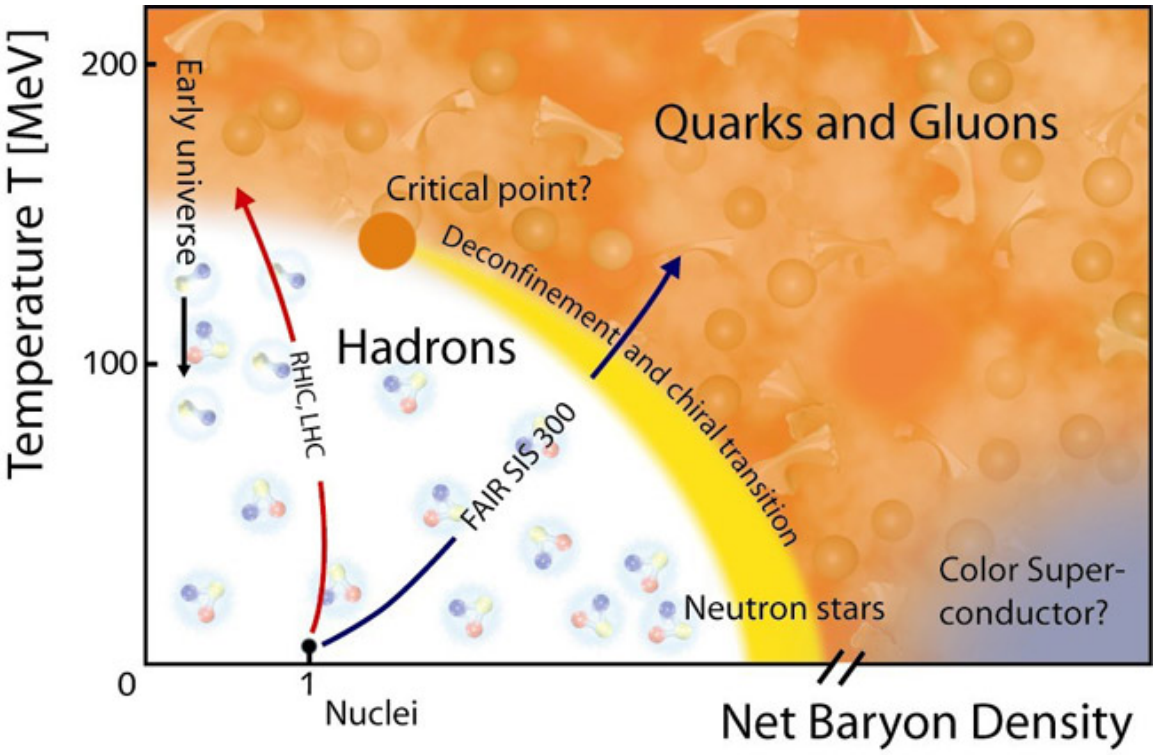

Figure 1.1: Sketch of the QCD phase diagram [5].

Moreover, it is also relevant for cosmology, as e.g. the early universe underwent the confinement and chiral phase transition from the Quark-Gluon-Plasma phase into the hadronic phase, some few microseconds after the Big Bang. Another important thermodynamic property, the equation of state has implications for the formation of compact stars. For neutron stars as indicated in Fig. 1.1, the region of very low temperatures and intermediate densities is relevant. Their properties are also dependent on the location and type of the chiral phase transition. In supernovae explosions, a region that extends up to 50 MeV in the temperature direction is relevant, as is the influence of the chiral phase transition.

The phases of QCD, of course, depend on many thermodynamical parameters and each combination covers different aspects of the underlying physics. We want to focus on the phase diagram arising for different temperatures and baryon densities, which are ultimately related to the chemical potential.

Indicated are the phases of the Quark-Gluon-Plasma in the high temperature regime, the hadron gas in the low temperature, low density regime and the domain of colocolourr superconductivity in the low temperature, high density regime. This sketch also shows where future experiments will work.

Theoretically easily accessible are the domains of high temperature or density, where perturbation theory is applicable. In order to get a full insight into the phase diagram,

methods going beyond perturbation theory have to be applied.

Various non-perturbative approaches have been put forward, which allowed for much insight in the nature of the strong interactions and the phase diagram. These approaches comprise models mimicking QCD interactions, lattice gauge theory and functional methods. They all have advantages and shortcomings, therefore, a combined approach, bundling the strengths of these methods seems promising to resolve the phase structure of the QCD phase diagrams.

More precisely, QCD model theories allow for an easy computation of QCD processes and have therefore been used extensively to investigate the structure of the QCD phase diagram. An often used model is the Nambu-Jona-Lasinio (NJL) model, which is very useful to study χSB and colour superconductivity, see e.g. [6]. In parts of this work, we will also use a model derived from the NJL model.

If we stick to the temperature axis and neglect high densities, lattice QCD simulations are possible and we can study thermodynamic properties and the chiral and deconfinement phase transition [7]. Lattice QCD is the conventional method for *ab-initio* calculations. The theory is formulated on a discrete and finite volume of space-time and the path-integral, which then has a statistical interpretation, is performed numerically, see e.g. [8]. Due to the notorious sign problem there is currently no reliable simulation available that covers the parts of the phase diagram with non-vanishing density.

Functional methods, like Dyson-Schwinger equations or the functional renormalisation group (fRG) do not suffer from this limitation. Moreover, the physical mechanisms, that are at work become apparent. Due to the nature of functional methods, there is no measure of the quality of the calculation, as in perturbation theory. Therefore, it is necessary to have a good physical insight into the problem and, whenever possible, to compare the result with limiting cases, that can be calculated with an exact method. Functional methods and lattice QCD should be viewed as complementary approaches, where the one approach has difficulties, the other usually does well. By combining the two approaches, lattice QCD and functional methods, it is possible to overcome the individual weaknesses and gain much insight into the physical problem at hand. We use the lattice to measure the quality of our results.

Recently, there have been attempts to map out the phase diagram, using lattice, as well as functional methods. On the lattice imaginary chemical potential techniques, circumventing the sign problem have been used, as well as Taylor expansions [9–17]. With this techniques, it was possible, to extract the curvature of the chiral phase boundary. Albeit within continuum approaches real chemical potential is not an issue, it is a huge effort to compute the full phase diagram. Therefore, in [18] the curvature of the phase boundary has been determined using an expansion of the observables in terms of the chemical potential. The question whether the phase boundary of the confined and the chirally symmetric phase coincide has not been answered conclusively. The general expectation is that they coincide, but recently it has also been conjectured that there might be a new, so-called quarkyonic phase which is still confining by chirally symmetric [19]. A good theoretical description of the phase transitions is therefore indispensable for a better understanding of the experimental data [20, 21].

In this work we aim at a first principle description of QCD using functional renormalisation group (fRG) techniques, working in different gauges, Polyakov and Landau gauge. By the use of different gauges, we can check the gauge invariance of the results. Polyakov gauge [22] is a physical gauge in the sense that we can relate the gauge fields directly to observables, like the confinement order parameter, which we want to compute in different settings. Landau gauge is technically easy accessible, due to a non-renormalisation theorem analytically tractable in the low momentum regime. Therefore, there exist many results with high accuracy, the agreement amongst these results is remarkable. Non-perturbative methods being indispensable in the investigation of the QCD phase diagram come in various fashions other than the fRG, that we choose as a tool to investigate the non-pertubative physics. It has the advantage of having a simple one-loop structure, there is no need for a regularisation and we can systematically check and extend our truncations. It has been applied successfully in high-energy physics, as well as in condensed matter physics or the physics of ultracold atoms. Furthermore, the RG in general is a powerful tool to study physics, which has also been used for proves of renormalisability.

This work is organised in the following form:

In chapter 2 we will provide the basics of QCD and functional methods. The relevant quantities and concepts are introduced, while some of the derivations are deferred to later chapters.

In chapter 3 we propose a new scheme to compute the deconfinement phase transition within functional methods. We discuss the truncation and methods to solve the resulting equations. Results are presented and compared to existing computations. The scheme is at the current stage limited to the case of vanishing density.

Having discussed the deconfinement phase transition, we turn towards the full QCD phase diagram in chapter 4, where we employ various approaches towards the full theory. We first discuss the chiral phase transition and its implications for the phase diagram, when we incorporate non-perturbative gluon dynamics. Thereafter, we compute the effects dynamical quarks have on the deconfinement phase transition, that we described in chapter 3. Finally, we explore the relation between χSB and confinement.

Throughout the work, we encounter many situations, in which an apt parameterisation of the degrees of freedom is crucial to get physically correct results. In chapter 5 we want to elaborate on getting the right parameterisation in situations, where the degrees of freedom change when going from one physical regime to the other.

We conclude this work in chapter 6 with a summary of the results and possible further investigations.

Part of this work has already been published, the results of Sec. 3.1 were published in ref. [23]. A very condensed form of Sec. 4.4 has been published in [24].

2 Introduction

"Omne initium difficile est"

2.1 QCD basics

Quantum Chromodynamics, the quantum field theory of strong interactions, is a non-Abelian gauge theory. Therefore, we start with defining the field contents of the theory and a discussion of its symmetries.

Field contents

The quark fields are spin-1/2 fermions transforming in the fundamental representation of the gauge group $SU(N_c)$, N_c being the number of colours. In this work we will focus on $N_c \in \{2, 3\}$, where the case of two colours serves as a model theory to set up and asses our fRG approach. Note also that 2-colour QCD on the lattice does not face the sign problem and is therefore an ideal benchmarking environment for a discussion of finite chemical potential in functional methods. We will see that the insight gained in 2-colour QCD will have significant implications for the physical theory.

Quarks come in different flavours, the number of which is N_f. The quark fields therefore form N_f fundamental representations of $SU(N_c)$ on a Cartesian product of Dirac spinors. Flavour is an extension of the concept of isospin, where the latter was invented to explain the mass degeneracy of the proton and the neutron.

The kinetic term of a fermion field, obeying renormalisibility, locality, gauge symmetry and Poincaré invariance, is given by

$$\bar{\psi}\left(-i\not{D} + m + i\mu\gamma^0\right)\psi \tag{2.1}$$

where we introduced the mass matrix m, containing the current quark masses of the quark fields. We used the standard notation $\bar{\psi} = \psi^\dagger\gamma^0$, introduced the quark chemical potential μ and the covariant derivative

$$D_\mu = \partial_\mu + igA_\mu \ . \tag{2.2}$$

We used the standard abbreviation $\not{D} = \gamma_\mu D_\mu$ with antihermitian γ-matrices, defined in appendix A.1.

A_μ are the gluon fields taking values in the Lie algebra of $SU(N_c)$ and are therefore locally parametrised by $A_\mu = A_\mu^a T^a$, with the T^a being the generators of $SU(N_c)$. Their properties are detailed in appendix A.1.

The gluon fields A^a_μ are non-Abelian gauge fields, transforming according to the adjoint representation of the gauge group $SU(N_c)$. The corresponding field strength tensor and the covariant derivative in the adjoint representation are given by

$$F^a_{\mu\nu} = \partial_\mu A^a_\nu - \partial_\nu A^a_\mu - g f^{abc} A^b_\mu A^c_\nu \,, \tag{2.3}$$

$$D^{ab}_\mu = \partial_\mu \delta^{ab} + g f^{abc} A^c_\mu. \tag{2.4}$$

Here g is the (unrenormalised) coupling constant of the theory and f^{abc} are the structure constants of the gauge group $SU(N_c)$.

Gauge invariance is an important concept in modern quantum field theory. It is one of the building blocks of the standard model of particle physics. Additionally the dynamical breaking of gauge symmetry is a beautiful concept to explain the emergence of superconductivity [25]. Under local gauge transformations fermion fields transform as

$$\psi \to U\psi = \exp(-i\alpha^a(x)T^a)\psi, \tag{2.5}$$

with $\alpha^a(x)$ being arbitrary fields, which will of course be identified with the gauge fields. In order for the kinetic term to be invariant under gauge transformations, the covariant derivative has to transform as

$$D_\mu \to U D_\mu U^{-1}. \tag{2.6}$$

This can easily be achieved by requiring a certain transformation property of the gauge field, this is

$$A_\mu \to U A_\mu U^{-1} - (\partial_\mu U) U^{-1}. \tag{2.7}$$

In continuum studies of QCD we have to ensure the gauge invariance of physical objects. This is a challenge that we will come back to. In any case, we have collected all the ingredients to formulate the theory.

Generating functional and gauge fixing

Investigating equilibrium thermodynamics goes along with working in Euclidean space-time. The generating functional governing the dynamics of the quantum field theory of quarks and gluons is given by

$$\begin{aligned} Z[J,\eta,\bar\eta] = e^{W[J,\eta,\bar\eta]} &= \int \mathcal{D}[A\bar\psi\psi] \exp\left\{ -S[A,\psi,\bar\psi] + \int d^4x \left(A^a_\mu J^a_\mu + \bar\eta\psi + \bar\psi\eta \right) \right\} \\ \text{with} \quad S[A,\psi,\bar\psi] &= \int d^4x \, \mathcal{L}_{\mathrm{QCD}} = \int d^4x \left(\bar\psi \left(-i\not{D} + m + \mu\gamma^0 \right) \psi + \frac{1}{4} F^a_{\mu\nu} F^a_{\mu\nu} \right). \end{aligned} \tag{2.8}$$

$\bar\eta$ and η are Grassmann valued sources for the quark fields ψ and $\bar\psi$ and J^a_μ is the source for the gauge field A^a_μ. We elaborate on the role of the generating functional later on.

This generating functional is manifestly gauge invariant, i.e. unchanged under the transformations in eq. (2.5) and eq. (2.7). In the limit of vanishing quark masses it is also invariant under chiral symmetry, which we will discuss later. We tacitly assume

the path integral to be meaningful, at least after a proper renormalisation has been performed.

The path-integral definition of the generating functional is at the current stage not complete since we integrate over physically equivalent gauge field configurations due to gauge invariance. These configurations are said to lie in the same gauge orbit, meaning that they can be connected simply by a gauge transformation. A gauge orbit is defined by

$$[A^U] = \left\{ (UAU^\dagger + UdU^\dagger) : U \in SU(N_c) \right\}. \tag{2.9}$$

Integrating over each gauge orbit, we get an infinite constant - the volume of the gauge group. We have to single out gauge orbits and restrict the path-integral to an integration solely over one configuration of each orbit. The volume of the gauge group can be absorbed in the normalisation.

Gauge invariance also hinders the definition of a (perturbative) gauge field propagator. This is a consequence of the zero eigenmodes that reside in the quadratic part of the gauge field Lagrangian, which therefore cannot be inverted. The troublesome modes are the modes that are gauge equivalent to $A^a_\mu = 0$.

There are various ways to circumvent the problem. In this work we will resort to the Faddeev-Popov procedure. The underlying idea is to separate the integration over the gauge fields in an integration over different gauge orbits and an integration along those orbits.

On the level of the path-integral this is achieved by inserting the identity

$$1 = \int \mathcal{D}\alpha \; \delta\left[G(A^\alpha)\right] \mathrm{Det}\left[\frac{\delta G(A^\alpha)}{\delta \alpha}\right] \tag{2.10}$$

into the partition function, where $\mathrm{Det}[\delta G(A^\alpha)/\delta\alpha]$ is called *Faddeev-Popov determinant* and $G(A^\alpha)$ is a function that encodes the gauge fixing condition. A^α is the gauge field A, transformed through a finite gauge transformation:

$$(A^\alpha)^a_\mu t^a = e^{-i\alpha^a t^a}\left[A^b_\mu t^b + \frac{i}{g}\partial_\mu\right] e^{i\alpha^c t^c}. \tag{2.11}$$

Usually one writes the determinant as an integral over anticommuting scalar fields, called Faddeev-Popov ghosts, c and $\bar{c}$, and the gauge fixing term with the δ-distribution as a Gaussian integral. Therefore, gauge fixing amounts to adding a ghost and a gauge-fixing term to the Lagrangian. For covariant gauges these terms are:

$$\int d^4x \left(\frac{(\partial_\mu A^a_\mu)^2}{2\xi} - i\bar{c}(-\partial_\mu D^{ab}_\mu)c \right), \tag{2.12}$$

where we introduced the gauge fixing parameter ξ. Landau gauge corresponds to $\xi = 0$, note that strictly speaking this is only defined of taking the limit $\xi \to 0$. Feynman gauge can be achieved by setting $\xi = 1$.

For the calculations in Polyakov gauge, we want to pursue another path and leave the gauge fixing, as it stands. In Polyakov gauge, one can explicitly show that in a

static approximation the longitudinal gauge degrees of freedom and the Faddeev-Popov determinant cancel. We explain our choice of gauge and its effect further when we discuss the confinement-deconfinement phase transition.

The Faddeev-Popov procedure comes with its own problems, the most severe of which is the Gribov problem [26]. It has been conjectured, that this is one of the reasons for the discrepancy in the results for the infrared (IR) behaviour of the propagators in Landau gauge between gauge fixed lattice QCD and functional methods.

On the lattice there is no need to fix a gauge, because one does not work with the gauge fields themselves, but rather with the elements of the gauge group. In Polyakov gauge, we also do not face the problem of Gribov copies and hence mention only the existence of the Gribov problem.

The Lagrangian (2.8) is defined in terms of bare quantities, in order to get physically meaningful result these have to be renormalised, to compensate for loop effects. The correspondence between the bare Lagrangian (2.8) and its renormalised version including counterterms is given by the following rescaling transformations

$$A^a_\mu \rightarrow \sqrt{Z_3} A^a_\mu, \qquad \bar{c}^a c^b \rightarrow \tilde{Z}_3 \bar{c}^a c^b, \qquad \bar{\Psi}\Psi \rightarrow Z_2 \bar{\Psi}\Psi, \tag{2.13}$$

$$g \rightarrow Z_g g, \qquad \alpha \rightarrow Z_\alpha \alpha, \qquad \lambda \rightarrow Z_\lambda \lambda, \tag{2.14}$$

where six independent renormalisation constants $Z_3, \tilde{Z}_3, Z_2, Z_g, Z_\alpha$ and Z_λ have been introduced.

Finite temperature QCD

As we are interested in the QCD phase diagram, we have to treat QCD in a thermodynamical context. This is naturally formulated in imaginary time, i.e. Euclidean space, which is why we formulated the generating functional eq. (2.8) in Euclidean space right from the start, for reviews see e.g. [27, 28].

In order to obtain equilibrium observables at finite temperature T we use the Matsubara or imaginary time formalism. This amounts to a compactification of time and entails a genuine Euclidean formulation. Explicit Lorentz symmetry is lost and we have to keep track of dependencies perpendicular and parallel to the heat bath. The action is unchanged except for the x_0 integration:

$$\int d^4x \, \mathcal{L}_{\mathrm{QCD}} \rightarrow \int_0^\beta d\tau \int d^3x \, \mathcal{L}_{\mathrm{QCD}} =: \int_T d^4x \, \mathcal{L}_{\mathrm{QCD}}, \tag{2.15}$$

where $\beta = 1/T$. For vanishing temperature, the integral naturally reduces to the four dimensional integral over uncompactified four-dimensional space-time. According to the Kubo-Martin-Schwinger relation, gluons and ghosts obey periodic boundary conditions, while quarks obey anti-periodic boundary conditions. This is reflected in the Matsubara frequencies.

The Matsubara sum is a direct consequence of finite temperature. Working in Fourier space, all quantities now depend on the three-momenta $\vec{p}$ and the Matsubara frequencies

ω_n individually. The Matsubara frequencies are

$$\omega_n = \begin{cases} 2n\pi T & \text{bosons,} \\ (2n+1)\pi T & \text{fermions.} \end{cases} \tag{2.16}$$

2.2 Symmetries

Symmetries are always a fortunate circumstance in field theory as symmetries simplify the analysis and quite often allow for obtaining exact or semi-exact results. The richer the symmetry, the stronger the results obtained. Sometimes symmetries even determine the full solution of the theory, c.f. the exact solution of $\mathcal{N} = 2$ supersymmetric Yang-Mills theory by Seiberg and Witten [29]. Certainly, in QCD symmetries do not allow for a solution solely based on them, however, useful insight can be gained and will play an important role in our analysis.

QCD exhibits many symmetries in nature most of these are broken in the ground state of the theory, but can be restored under extreme conditions. In our investigations of the phase diagram we will encounter phase transitions, where on one side of the phase boundary, a particular symmetry is broken, whereas on the other side it is restored. We will discuss the order parameter related to the symmetries in the next section.

Chiral Symmetry

Chiral symmetry is related to the quark fields and the spectrum of the Dirac operator. For the discussion of the symmetries in the quark sector we can neglect the chemical potential that we introduced earlier, as the chemical potential term in the Lagrangian is chirally symmetric. The quark sector of the QCD Lagrangian eq. (2.8) is then

$$\mathcal{L}_{\mathcal{M}} = \bar{\psi}\left(-i\not{D} + m\right)\psi \,, \tag{2.17}$$

where m is a diagonal matrix containing the masses of six different flavours of quarks, generated in the electroweak sector of the standard model, see e.g. [30]. In the *chiral limit*, i.e. $m = 0$ the Lagrangian is invariant under global vector and axial-vector $SU(N_f)$ transformations.

$$SU(N_f)_V: \quad \psi \to \exp(i\Theta_V^a T^a)\psi \quad \text{and} \quad SU(N_f)_A: \quad \psi \to \exp(i\gamma_5\Theta_V^a T^a)\psi, \tag{2.18}$$

where T^a are the generators of $SU(N_f)$. The vector transformation is still a symmetry if all flavours have degenerate masses. In physical QCD, chiral symmetry is a useful concept for the two-flavour (up/down) case, as the current quark masses are very small. Particularly at finite temperature, where the Matsubara mass in the Quark-Gluon-Plasma phase is generically higher than these masses.

The observation that there are nearly degenerate $SU(N_f)$ multiplets in the hadron spectrum reflects that $SU(N_f)_V$ is also an approximate symmetry of the QCD vacuum. If the axial symmetry was also a symmetry of the vacuum, every hadron would possess

a "chiral partner" having opposite parity. As these states are not observed, we conclude that chiral symmetry is spontaneously broken in the QCD vacuum. An observable, which is not invariant under $SU(N_f)_A$ is the quark condensate $\langle\bar{\psi}\psi\rangle$, often called chiral condensate. A non-vanishing chiral condensate is an indication for chiral symmetry breaking.

Chiral symmetry also plays an important role in our understanding of the low masses of the pions in nature. This can be understood quite naturally by identifying the pions as the Goldstone bosons of the broken chiral symmetry. The smallness of their mass can be understood in terms of the small current quark masses of up- and down-quarks. In the three flavour case the corresponding Goldstone bosons are in the pseudoscalar meson octet. They all obey several low-energy theorems, providing a basis for chiral perturbation theory χPT, for reviews see e.g. [31–34]). χPT is an expansion in quark masses and momenta. It is a effective theory of the low-energy regime of QCD, where the coupling strength α_s of QCD is large. In this regime, the reformulation of the generating functional of QCD in terms of pion degrees of freedom permits to set up a well-defined perturbative expansion scheme. An ordinary perturbative expansion in the coupling strength would be ill-defined.

In the chiral limit the quark fields can be separated into left- and right-handed Weyl-spinors

$$\psi_R = \frac{1+\gamma_5}{2}\psi\,, \qquad \psi_L = \frac{1-\gamma_5}{2}\psi. \tag{2.19}$$

The Noether currents corresponding to chiral symmetry are

$$\begin{aligned} j_\mu &= \bar{\psi}\gamma_\mu\psi\,, && (2.20)\\ j^5_\mu &= \bar{\psi}\gamma_\mu\gamma_5\psi\,, && (2.21)\\ j^a_\mu &= \bar{\psi}\gamma_\mu T^a\psi\,, && (2.22)\\ j^{5,a}_\mu &= \bar{\psi}\gamma_\mu\gamma_5 T^a\psi\,, && (2.23) \end{aligned}$$

where $T^a = \frac{\lambda^a}{2}$ denote the generators of SU(3) flavour transformations given by the Gell-Mann matrices λ^a. On the classical level, these currents are conserved. However, due to quantum corrections, the axial current, eq. (2.21) is no longer conserved.

In the presence of a non-vanishing mass matrix m and including the effects of the axial anomaly we find the divergences of these currents to be

$$\begin{aligned} \partial_\mu j_\mu &= 0\,, && (2.24)\\ \partial_\mu j^5_\mu &= 2i\bar{\psi}m\gamma_5\psi - \frac{g^2}{16\pi^2}\epsilon^{\mu\nu\sigma\rho}F^a_{\mu\nu}F^a_{\sigma\rho}\,, && (2.25)\\ \partial_\mu j^a_\mu &= \bar{\psi}\,[T^a, m]\,\psi\,, && (2.26)\\ \partial_\mu j^{5,a}_\mu &= \bar{\psi}\,\{T^a, m\}\,\psi\,. && (2.27) \end{aligned}$$

Thus only one current, eq. (2.24), is conserved and it describes baryon number conservation in strong interaction processes. The vector current, eq. (2.26), is conserved in the case of identical quark masses and thus describes the approximate flavour symmetry in the light quark sector of QCD.

The axial vector current, eq. (2.27), is not conserved if we have a non-vanishing quark mass matrix in the Lagrangian of QCD. This is called *explicit chiral symmetry breaking*. Since the current quark masses of the up and down quark are very small, we still expect approximately degenerate parity partners of the lowest lying hadron spectra, if the current masses were the only reason for broken chiral symmetry. However, such parity partners are not observed in nature. Therefore, we must assume that there is another source for chiral symmetry breaking. This notion is met by the phenomenon of *dynamical chiral symmetry breaking*.

Within lattice simulations it is difficult to implement chiral symmetry However, there is work going on in lattice gauge theory investigation the chiral phase transition.

Center Symmetry and the Deconfinement Phase Transition

Next we discuss one symmetry of the gauge sector which has an intimate relation to confinement, *center symmetry*. Center symmetry is a symmetry of the gauge field action $\int d^4x F_{\mu\nu}F_{\mu\nu}$. In Yang-Mills theory (YM) it is an exact symmetry. $SU(N_c)$ YM is obtained from eq. (2.8) in the limit $m \to \infty$, which is the opposite of the chiral limit. Center symmetry reflects the fact, that after gauge fixing we still have a residual symmetry of the gauge fields, that is we can transform the fields with a center element of the gauge group $SU(N_c)$, this center is Z_{N_c}. It can be shown that broken center symmetry signals confinement, whereas the center symmetric phase of YM is deconfined.

In the presence of dynamical quarks center symmetry is explicitely broken. However, the order parameter related to center symmetry can still be used to infer information on the confinement phase transition. We expect a smooth crossover from the low temperature into the high temperature phase.

Order Parameter

In QCD with static quarks, this means infinitely heavy quarks, the expectation value of a static quark $\langle\psi(\vec{x})\rangle$ serves as an order parameter for confinement. It is proportional to the free energy F_q of such a state, $\langle\psi(\vec{x})\rangle \sim \exp(-\beta F_q)$, where $\beta = 1/T$ is the inverse temperature. In the confining phase the free energy of a static quark is infinite, corresponding to the fact that it is impossible to put a single quark into the theory. Hence in the confining phase at low temperature the expectation value vanishes, whereas in the deconfined phase at high temperatures it is finite.

It is heuristically easily seen, that $\langle\psi(\vec{x})\rangle$ relates to the free energy of a static quark. Let us consider a simplified example, a static *electron*. By inspecting the Dirac equation of the electron, it can be visualised, that the Polyakov loop, which we will introduce next is the creation operator of a static quark and is closely tied to the free energy. The free Dirac equation is

$$\frac{\partial\psi}{\partial\tau} = igA_0\psi \quad \Rightarrow \quad \psi(\vec{x},\tau) = \mathcal{P}\exp\left(ig\int_0^\tau d\tau'\ A_0(\vec{x},\tau')\right)\psi(\vec{x},0), \tag{2.28}$$

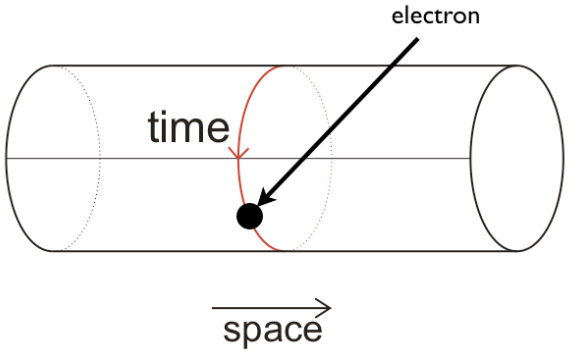

Figure 2.1: An electron winding around Euclidian time. In QCD the integration of the gauge field along this orbit constitutes the Polyakov loop.

where $\mathcal{P}$ stands for path ordering. This electron then generates a current,

$$j^{\mu}(\vec{x},\tau) = \delta^{\mu 0} \int_0^{\beta} d\tau \delta(x - x(\tau)) \tag{2.29}$$

where $x(\tau)$ denotes the worldline of the electron. The situation is depicted in Fig. 2.1. The free energy F of this electron is simply

$$\exp\left(-\beta F\right) = \langle \mathcal{P}\ e^{ig\int d^4x\ A_{\mu}(x)\ j^{\mu}(x)} \rangle = \langle \mathcal{P}\ e^{ig\int_0^{\beta}\ d\tau\ A_0(\vec{x},\tau)} \rangle. \tag{2.30}$$

Returning with our focus to QCD, the Polyakov loop variable [22] is the creation operator for a static quark,

$$L(\vec{x}) = \frac{1}{N_c} \mathrm{Tr}\, \mathcal{P}(\vec{x})\,, \tag{2.31}$$

where the trace in eq. (2.31) is done in the fundamental representation, and the Polyakov loop operator is a Wegner-Wilson loop in time direction,

$$\mathcal{P}(\vec{x}) = \mathcal{P}\ \exp\left(\mathrm{i}g \int_0^{\beta} dx_0\, A_0(x_0,\vec{x})\right)\,. \tag{2.32}$$

Here $\mathcal{P}$ stands for path ordering. We conclude with the insight gained from eq. (2.28), that $\langle \psi(\vec{x}) \rangle \simeq \langle L(\vec{x}) \rangle$. Thus the negative logarithm of the Polyakov loop expectation value relates to the free energy of a static fundamental color source. Also, $\langle L \rangle$ measures whether center symmetry is realised by the ensemble under consideration, see e.g. [35].

Therefore, we inspect the behaviour of the Polyakov loop under center transformations. More specifically we consider gauge transformations $U(x_0, x)$ with

$$U(0,\vec{x}) U^{-1}(\beta,\vec{x}) = Z, \tag{2.33}$$

where Z is a center element. In $SU(2)$ the center is Z_2, whereas in physical QCD with $SU(3)$ it is Z_3. Under such center transformations the Polyakov loop operator $\mathcal{P}(\vec{x})$ in eq. (2.32) is multiplied with a center element Z,

$$\mathcal{P}(\vec{x}) \to Z\, \mathcal{P}(\vec{x})\,, \tag{2.34}$$

and so does the Polyakov loop, $L(\vec{x}) \to Z\, L(\vec{x})$. As the expectation value of the Polyakov loop $\langle L \rangle$, is a sum over all configurations, i.e. over all center transformed configurations, the center-symmetric confining (disordered) ground state ensures $\langle L \rangle = 0$, whereas deconfinement $\langle L \rangle \neq 0$ signals the ordered phase and center-symmetry breaking,

$$\begin{aligned} T < T_c: &\qquad \langle L(\vec{x}) \rangle = 0\,, \quad F_q = \infty\,, \\ T > T_c: &\qquad \langle L(\vec{x}) \rangle \neq 0\,, \quad F_q < \infty\,. \end{aligned} \tag{2.35}$$

The expectation value of the Polyakov loop can be deduced from the equations of motion of its effective potential $V_L[\langle L \rangle]$. We shall argue that the computation of the latter greatly simplifies within an appropriate choice of gauge. Indeed, gauge fixing is nothing but the choice of a specific parameterisation of the path integral, and a conveniently chosen parameterisation can simplify the task of computing physical observables.

Note that the product of two Polyakov loops can be viewed as a closed Wegner-Wilson loop, for a pedagogical introduction see e.g. [8].

Polyakov gauge

The Polyakov loop is a complicated object which can in general not be computed analytically. However, with an appropriately chosen gauge we may simplify this computation significantly.

In the present case our choice of gauge is guided by the demand of a particularly simple representation of the Polyakov loop variable eq. (2.31). A gauge ensuring time-independent A_0 leads to both, a trivial integration in eq. (2.32) and renders the path ordering irrelevant. Having done this, one can still rotate the Polyakov loop operator $\mathcal{P}(\vec{x})$, eq. (2.32), into the Cartan subgroup.

For example in $SU(2)$, Polyakov gauge is implemented by the gauge fixing conditions

$$\partial_0 \mathrm{Tr}\, \sigma_3 A_0 = 0\,, \qquad \mathrm{Tr}\, (\sigma_1 \pm i\sigma_2) A_0 = 0\,, \tag{2.36}$$

where the σ_i are the Pauli matrices. However, the gauge fixing eq. (2.36) is not complete. It is unchanged under time-independent gauge transformations in the Cartan sub-group. These remaining gauge degrees of freedom are completely fixed by the following conditions,

$$\partial_1 \int dx_0\, \mathrm{Tr}\, \sigma_3 A_1 = 0\,, \quad \partial_2 \int dx_0 dx_1\, \mathrm{Tr}\, \sigma_3 A_2 = 0\,, \partial_3 \int dx_0 dx_1 dx_2\, \mathrm{Tr}\, \sigma_3 A_3 = 0\,. \tag{2.37}$$

The gauge fixings eq. (2.37) are integral conditions and are the weaker the more integrals are involved. Basically they eliminate the corresponding zero modes. This can be seen directly upon putting the theory into a box with periodic boundary conditions, i.e. on a four torus T^4, see e.g. [36, 37].

In Polyakov gauge, the evaluation of the Polyakov loop simplifies drastically. As A_0 is in the Cartan and independent of time, the path ordering is implemented automatically. The integration over imaginary time is trivial and for $SU(2)$ we get:

$$L(\vec{x}) = \frac{1}{2} \mathrm{Tr}\, e^{ig \int_0^\beta A_0^3(\vec{x}) \sigma^3} = \frac{1}{2} \mathrm{Tr}\, e^{i\beta g A_0^3 \sigma^3} = \cos\left(\frac{1}{2} g \beta A_0^3 \right). \tag{2.38}$$

An analogous computation can be done for any gauge group with higher rank N_c. This makes the advantages of Polyakov gauge apparent: it directly relates the zero component of the gauge field to the order parameter of confinement. As we detail below we are now able to set up simple truncation schemes based on the properties of the Polyakov loop.

Another advantageous feature of Polyakov gauge is, that we can compute the Faddeev-Popov determinant explicitely. The gauge fixing conditions eq. (2.36),eq. (2.37) lead to the following Faddeev-Popov determinant

$$\Delta_{FP}[A] = (2T)^2 \left[\prod_x \sin^2 \left(\frac{g A_0^3(\vec{x})}{2T} \right) \right] . \tag{2.39}$$

The computation of which is detailed in App. B.1. The integration over the longitudinal gauge fields precisely cancels the Faddeev-Popov determinant in the static approximation $\partial_i A_0^c = 0$, see App. B.1.

2.3 Functional Methods

Functional methods are in general methods for solving a quantum field theory that are based on functionals derived from the path integral. From these functionals, we can derive the quantum equations of motion for observables as well as important thermodynamic properties like the pressure or the free energy.

We already introduced the generating functional of QCD, as we shall see, it encodes all the physical information of the theory. In general it is impossible to solve the functional integral. We either have to apply some expansion scheme like perturbation theory, resort to a numerical simulation or work with models deduced from this functional.

We want to pursue another approach, by solving the path integral successively by integrating out momentum modes inspired by Kadanoff's block-spin transformation [38]. This idea has been extended by Wegner and Wilson to contiuum quantum field theory [39, 40].

First we will discuss the properties of the functional that the formalism is based upon, before we turn towards the flow equation with which will compute it.

Effective Action

Since symmetries are important it is highly desirable to have a formulation of the dynamics of the fields that respects these symmetries and allows to access them straightforwardly. In this work we choose the effective action as the central quantity on which we build our description. The effective action Γ governs the dynamics of the field expectation values in a quantum field theory. It has many appealing properties, which we discuss in the following. For simplicity let us consider only a real scalar field φ in d dimensions. With minor modifications the following discussion also holds for other fields like fermions or gauge fields. All n-point correlation functions are encoded in the generating functional

$Z[J]$,

$$Z[J] \equiv \mathrm{e}^{W[J]} = \int \mathcal{D}\varphi \, \mathrm{e}^{-S[\varphi]+\int J\varphi}, \tag{2.40}$$

where we abbreviated the source term $\int J\varphi = \int d^d x \, J(x)\varphi(x)$.

As long as the integration measure and the source term is invariant under the symmetries of the action, these symmetries are carried over into the generating functional. When we switch to the effective action, these symmetries are preserved.

All n-point functions are obtained by functional differentiation with respect to the source and setting the source to zero at the end of the computation

$$\langle \varphi(x_1) \dots \varphi(x_n) \rangle = \frac{1}{Z[0]} \left(\frac{\delta^n Z[J]}{\delta J(x_1) \dots \delta J(x_n)} \right)_{J=0}. \tag{2.41}$$

It is apparent, that we have a solution of the theory, if we can compute the generating functional. That is, all physical information of the theory is stored in it. The correlation functions derived from the generating functional contain also disconnected pieces of the correlations functions, which do not contribute to the S-Matrix. Therefore, we want to discuss a functional, in which the physical information is stored more efficiently.

In eq. (2.40), we introduced the generating functional of connected correlation functions $W[J] = \ln Z[J]$. In this functional, no disconnected contributions to the correlation functions are left. This functional is more suitable for computations, however, the correlation functions generated by this functional still contain contributions, that are disconnected upon cutting one internal line. We can build up all correlation functions from contributions that are not disconnected if we cut one internal line. These contributions are said to be one-particle irreducible (1PI) and the functional that generates these correlation functions is the effective action Γ. One can also define functionals that generate correlation functions that are not disconnected if we cut more than one internal line. This leads to 2PI techniques or even NPI with $N > 2$ [41].

The effective action Γ is obtained upon performing a Legendre transform of $W[J]$ w.r.t. to J

$$\Gamma[\phi] = \sup_J \left(\int J\phi - W[J] \right). \tag{2.42}$$

For any given ϕ, one $J \equiv J_{\sup} = J[\phi]$ is singled out for which $\int J\phi - W[J]$ approaches its supremum. Note that this definition of Γ automatically guarantees convexity.

We want to elucidate the meaning of the variable ϕ. Therefore, we consider the derivative of the effective action at its supremum, $J = J_{\sup}$, assuming that $\Gamma[\phi]$ is differentiable, and obtain

$$0 \stackrel{!}{=} \frac{\delta}{\delta J} \left(\int J\phi - W[J] \right) \quad \Rightarrow \quad \phi = \frac{\delta W[J]}{\delta J} = \frac{1}{Z[J]} \frac{\delta Z[J]}{\delta J} = \langle \varphi \rangle_J. \tag{2.43}$$

This implies that ϕ corresponds to the expectation value of φ in the presence of the source J. The meaning of Γ becomes clear by studying its derivative at $J = J_{\sup}$

$$\frac{\delta \Gamma[\phi]}{\delta \phi(x)} = -\int_y \frac{\delta W[J]}{\delta J(y)} \frac{\delta J(y)}{\delta \phi(x)} + \int_y \frac{\delta J(y)}{\delta \phi(x)} \phi(y) + J(x) \stackrel{(2.43)}{=} J(x). \tag{2.44}$$

This is the *quantum equation of motion* by which the effective action $\Gamma[\phi]$ governs the dynamics of the field expectation value. It includes the effects of all quantum fluctuations.

From the definition of the generating functional we can straightforwardly derive an equation for the effective action:

$$\mathrm{e}^{-\Gamma[\phi]} = \int_\Lambda \mathcal{D}\varphi \, \exp\left(-S[\phi+\varphi] + \int \frac{\delta\Gamma[\phi]}{\delta\phi}\,\varphi\right). \tag{2.45}$$

Here, we have performed a shift of the integration variable, $\varphi \to \varphi + \phi$. We observe that the effective action is determined by a nonlinear first-order functional differential equation, the structure of which is itself a result of a functional integral. An exact determination of $\Gamma[\phi]$ and thus an exact solution has so far been found only for rare, special cases.

As a first example of a functional technique, approximate solutions can be constructed from a *vertex expansion* of $\Gamma[\phi]$,

$$\Gamma[\phi] = \sum_{n=0}^{\infty} \frac{1}{n!} \int d^dx_1 \ldots d^dx_n \, \Gamma^{(n)}(x_1,\ldots,x_n)\,\phi(x_1)\ldots\phi(x_n), \tag{2.46}$$

where the expansion coefficients $\Gamma^{(n)}$ correspond to the *one-particle irreducible (1PI) proper vertices*. Inserting eq. (2.46) into eq. (2.45) and comparing the coefficients of the field monomials results in an infinite tower of coupled integro-differential equations for the coefficients $\Gamma^{(n)}$: the Dyson-Schwinger equations. This functional method of constructing approximate solutions to the theory via truncated Dyson-Schwinger equations, i.e., via a finite truncation of the series (2.46) has its own merits and advantages; their application to gauge theories is well developed, see e.g. [42, 43].

Flow equation

A versatile approach to the computation of Γ is based on RG concepts [44]. Whereas a computation via eq. (2.45) or via Dyson-Schwinger equations corresponds to integrating-out all fluctuations at once, we can implement Wilson's idea of integrating out modes momentum shell by momentum shell.

In order to compute Γ, we introduce a scale-dependent action Γ_k, called the *effective average action*, with scale parameter k. We want Γ_k to have special properties which allow for a computation of the effective action Γ. These properties are that for $k \to \Lambda$, Γ_k corresponds to the bare action we want to quantise and that the full quantum action Γ is obtained for $k \to 0$,

$$\Gamma_{k\to\Lambda} \simeq S_{\mathrm{bare}}, \quad \Gamma_{k\to 0} = \Gamma. \tag{2.47}$$

We can construct such an action from the generating functional. Therefore, we define the IR regulated functional Z_k, note that we work in momentum space, where the ideas

of Wegner and Wilson are straightforwardly implemented:

$$\begin{aligned} \mathrm{e}^{W_k[J]} &\equiv Z_k[J] := \exp\left(-\Delta S_k\left[\frac{\delta}{\delta J}\right]\right) Z[J] \\ &= \int_\Lambda \mathcal{D}\varphi\, \mathrm{e}^{-S[\varphi]-\Delta S_k[\varphi]+\int J\varphi}, \end{aligned} \tag{2.48}$$

where we introduced the regulator term

$$\Delta S_k[\varphi] = \frac{1}{2}\int \frac{d^dq}{(2\pi)^D}\,\varphi(-q)R_k(q)\varphi(q), \tag{2.49}$$

which is quadratic in φ. We can view it as a modification of the kinetic term and therefore as a modification of the propagator.

Since we want to achieve a suppression of infrared modes in the modified theory, the regulator function $R_k(q)$ should satisfy the condition

$$\lim_{q^2/k^2\to 0} R_k(q) > 0, \tag{2.50}$$

enforcing a regularisation in the infrared. For instance, if $R_k \sim k^2$ for $q^2 \ll k^2$, the regulator acts like a mass term $m^2 \sim k^2$ for the IR modes.

Furthermore, in order to implement the conditions in eq. (2.47), we demand

$$\lim_{k^2/q^2\to 0} R_k(q) = 0. \tag{2.51}$$

This implies that the regulator vanishes for $k \to 0$. Then it is not difficult to see that we automatically recover the standard generating functional as well as the full effective action in the limit $k \to 0$: $Z_{k\to 0}[J] = Z[J]$ and therefore $\Gamma_{k\to 0} = \Gamma$.

The third condition relates to the requirement that we recover the bare action in the limit $k \to \Lambda$, i.e. the theory is unchanged in the ultraviolet. The condition is

$$\lim_{k^2\to\Lambda\to\infty} R_k(q) \to \infty. \tag{2.52}$$

In this limit the functional integral is dominated by the stationary point of the action. Then it is appropriate to use the saddle-point approximation in which we approximate the effective action by the bare action, $\Gamma_{k\to\Lambda} \to S + \text{const.}$. A sketch of a typical regulator that satisfies these three requirements is shown in Fig. 2.2.

Note that in the literature the regulator is frequently written as

$$R_k(p^2) = p^2\, r(p^2/k^2), \tag{2.53}$$

with $r(y)$ being a dimensionless regulator shape function with a dimensionless momentum argument. The conditions we posed for the regulator trivially translate into those for the regulator shape function.

Imposing such a cut-off function for a study of scalar field theories is in general unproblematic. However, for gauge theories the presence of a cut-off breaks gauge symmetry.

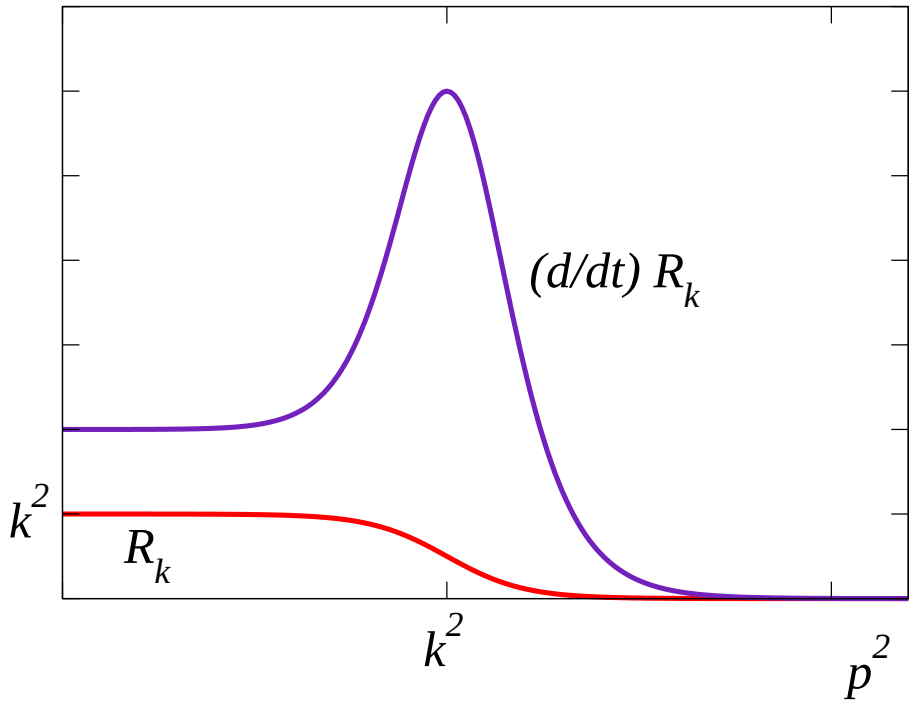

Figure 2.2: Sketch of a regulator function $R_k(p^2)$ (lower curve) and its derivative $\partial_t R_k(p^2)$ (upper curve). The regulator regularises all modes with $p^2 \lesssim k^2$ Its derivative enforces the Wilsonian idea of integrating out fluctuations within a momentum shell near $p^2 \simeq k^2$.

This is a consequence of condition (2.50), which requires the cut-off function to behave like a mass term for small momenta. Mass terms for gauge fields break gauge symmetry, it is therefore manifest that the cut-off term breaks gauge symmetry. While at first this seems to be a severe problem of the fRG, it is not an issue at all. Since in a path-integral approach, we have to fix a gauge anyway, already the the gauge-fixing breaks gauge invariance manifestly. Gauge invariance is however not lost, it is merely hidden in the formulation of the theory. Gauge symmetry is manifest in the Ward-Takahashi identities, as long as these are fulfilled, gauge invariance is not broken.

The cut-off function is therefore just another source of gauge-symmetry breaking and it modifies the Ward-Takahashi identities. In order to recover gauge invariance in the fRG setting, we now have to deal with modified Ward-Takahashi identities [45–47].

In our studies of Polyakov gauge QCD we do not face such complications, since in this gauge we can reduce the theory effectively to a scalar theory theory before introducing the cut-off. We will see this when we derive the flow for QCD. At this point let us proceed with the derivation of the flow equation.

Now that we know that the scale dependent effective action Γ_k exhibits the correct limits, let us study its behaviour in between the two limits. To that end we derive a first order differential equation which controls the scale dependence of the effective action.

We define the following abbreviations

$$t = \ln \frac{k}{\Lambda}, \qquad \partial_t = k\frac{d}{dk}. \tag{2.54}$$

Keeping the source J fixed, i.e. independent of k, the scale derivative of the scale dependent generating functional $W_k[J]$ is

$$\begin{aligned} \partial_t W_k[J] &= -\frac{1}{2}\int \mathcal{D}\varphi\, \varphi(-q)\, \partial_t R_k(q)\, \varphi(q) \mathrm{e}^{-S-\Delta S+\int J\varphi} \\ &= -\frac{1}{2}\int \frac{d^dq}{(2\pi)^d}\, \partial_t R_k(q)\, G_k(q) + \partial_t \Delta S_k[\phi]. \end{aligned} \tag{2.55}$$

In the last line, we have defined the *connected* propagator

$$G_k(p) = \left(\frac{\delta^2 W_k}{\delta J \delta J}\right)(p) = \langle\varphi(-p)\varphi(p)\rangle - \langle\varphi(-p)\rangle\langle\varphi(p)\rangle. \tag{2.56}$$

Now, we are able to define the scale dependent effective action Γ_k by a slightly modified Legendre transform, which takes care of the modifications introduced by adding the cutoff:

$$\Gamma_k[\phi] = \sup_J \left(\int J\phi - W_k[J]\right) - \Delta S_k[\phi]. \tag{2.57}$$

Since we later want to study Γ_k as a functional of a k-independent field ϕ, it is clear from eq. (2.57) that the source $J \equiv J_{\mathrm{sup}} = J[\phi]$ for which the supremum is approached is necessarily k dependent. As before, we get at $J = J_{\mathrm{sup}}$:

$$\phi(x) = \langle\varphi(x)\rangle_J = \frac{\delta W_k[J]}{\delta J(x)}. \tag{2.58}$$

The quantum equation of motion receives a regulator modification,

$$J(x) = \frac{\delta\Gamma_k[\phi]}{\delta\phi(x)} + \big(R_k\phi\big)(x). \tag{2.59}$$

In order to proceed, we have to apply a field derivative on this equation. Note that for case of fermionic Grassmann-valued fields, the field derivative should act on eq. (2.59) from the right.

The result is:

$$\frac{\delta J(x)}{\delta\phi(y)} = \frac{\delta^2\Gamma_k[\phi]}{\delta\phi(x)\delta\phi(y)} + R_k(x,y). \tag{2.60}$$

Also from eq. (2.58), we obtain

$$\frac{\delta\phi(y)}{\delta J(x')} = \frac{\delta^2 W_k[J]}{\delta J(x')\delta J(y)} \equiv G_k(y-x'). \tag{2.61}$$

We combine the two equations to get the important identity

$$\begin{aligned}\delta(x-x') &= \frac{\delta J(x)}{\delta J(x')} = \int d^d y \, \frac{\delta J(x)}{\delta \phi(y)} \frac{\delta \phi(y)}{\delta J(x')} \\ &= \int d^d y \, (\Gamma_k^{(2)}[\phi] + R_k)(x,y) G_k(y-x'),\end{aligned} \tag{2.62}$$

which can in operator notation be written in the compact form

$$\mathbb{1} = (\Gamma_k^{(2)} + R_k)\, G_k, \tag{2.63}$$

where we have introduced the short-hand notation for the field derivative acting on the scale dependent effective action

$$\Gamma_k^{(n)}[\phi] = \frac{\delta^n \Gamma_k[\phi]}{\delta\phi \dots \delta\phi}. \tag{2.64}$$

Collecting all ingredients, we can finally derive the flow equation for Γ_k for fixed ϕ and at $J = J_{\text{sup}}$ [44], recently named "Wetterich's equation":

$$\begin{aligned}\dot{\Gamma}_k[\phi] := \partial_t \Gamma_k[\phi] &= -\partial_t W_k[J]|_\phi + \int (\partial_t J)\phi - \partial_t \Delta S_k[\phi] = -\partial_t W_k[J]|_J - \partial_t \Delta S_k[\phi] \\ &\overset{(2.55)}{=} \frac{1}{2} \int \frac{d^d q}{(2\pi)^D} \, \partial_t R_k(q)\, G_k(q) \\ &\overset{(2.63)}{=} \frac{1}{2} \operatorname{Tr} \left[\partial_t R_k \left(\Gamma_k^{(2)}[\phi] + R_k \right)^{-1} \right].\end{aligned} \tag{2.65}$$

This equation is the exact evolution equation for the scale dependent effective action. Given initial conditions and a regulator function, we can, in principal, compute the flow of the scale dependent effective action. This is visualised in Fig. 2.3, where the initial conditions are fixed at the UV scale Λ by the classical action S_{cl}. Then we integrate the equation from the UV scale down to the infrared.

This flow equation is a nonlinear functional differential equation, that involves the second functional derivative of the scale dependent effective action. Despite its simple one-loop structure, it is important that the loop is not a perturbative loop, rather it contains the full propagator, thereby summing up arbitrarily high loop orders by integrating the flow equation [48].

A commonly used method to solve the flow equation eq. (2.65), is the vertex expansion technique. The strategy for studying a quantum field theory with the fRG using this technique is the following: We write down the most general Ansatz for the effective action, including all operators (n-point functions) compatible with the symmetries of the theory. From eq. (2.65) we obtain the flow of all n-point functions. Already from the structure of the flow equation we see, that the flow of an n-point function is obtained from information of higher correlation functions, i.e. $(n+1)$- and $(n+2)$-point functions. This implicates that we obtain an infinite tower of coupled flow equations, possibly carrying a complicated momentum structure.

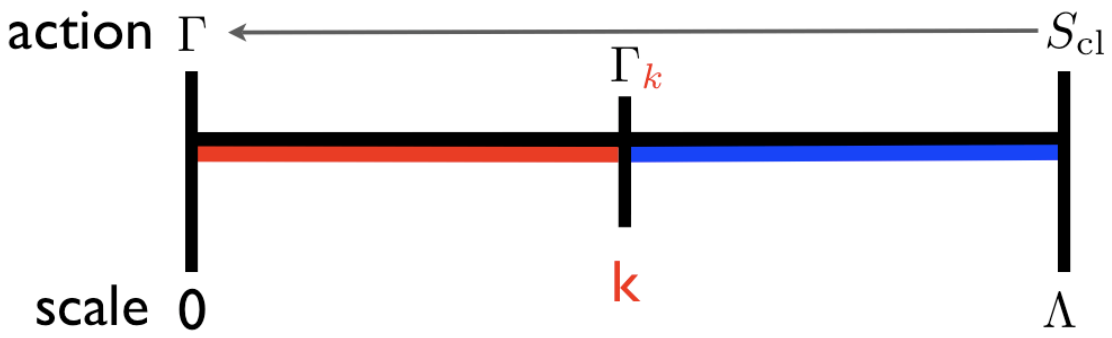

Figure 2.3: The idea of the fRG, we start with the classical action S_{cl} at a high scale Λ and evolve the action downward towards the full effective action Γ

To keep the problem manageable, we truncate the effective action by reducing the complexity of the momentum structure of n-point functions to a simple momentum dependence or even treat them as contact terms. Furthermore we choose a maximum number $N_{\max}$ of n-point functions that we want to take into account, i.e. we neglects all n-point functions with $n > N_{\max}$ right from the onset of our calculation. That is, because we cannot compute the whole tower at once and also do not aim at this in our investigations. The beauty of the approach is that we are able to see the underlying physics mechanism at work. Therefore, the ultimate goal is not to find and solve a huge system of correlation functions, but to find the subset of correlation functions that covers the essential physics at hand and study their behaviour. We will see in the course of this work that quite a simple truncation can capture the physics and leads to beautiful results.

Put another way, as it is impossible to study the flow of an effective action containing all operators which are allowed by the symmetries, we have to restrict ourselves to a subspace of operators which we expect to be relevant for the physical problem under consideration. This step is obviously the most difficult one and requires much physical insight into the problem in order to truncate towards the correct subspace of operators. Note that truncating the effective action and thereby the tower of flow equations is not an expansion in a small parameter as in perturbation theory. The tacit assumption is that the neglected operators have only a small back reaction onto the operators contained in the truncation, which has to be checked.

Once we have chosen a certain truncation scheme we need to assess how reliable the results and thereby the assumptions we made are. A clear signal that the truncation is unreliable is an unstable RG flow. The prime example here can be seen in the flow of four-fermion interactions, which shows a divergence at a finite scale $k = k_{cr}$. In this example there is a physical reason for the instability, as it indicates the onset of chiral symmetry breaking which we will see in sec. 4.1. Upon adding additional bosonic operators and shovelling parts of the flow into these, the instability vanishes and we obtain meaningful

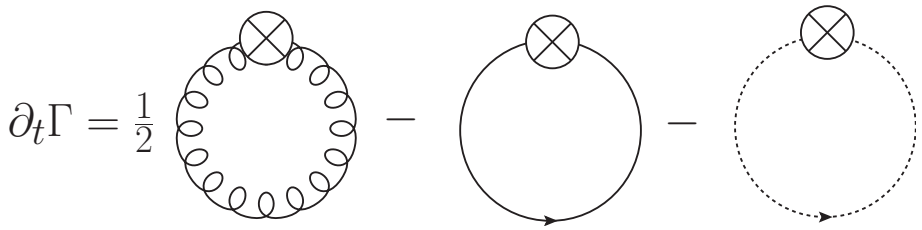

Figure 2.4: Flow equation for QCD including gluons, quarks and ghosts. Regulator insertions are represented by crossed circles. Note that the propagators in the loops are full propagators!

results [49–51].

In order to check a chosen truncation, we can extend it by adding more operators and survey whether the results obtained from the larger truncation are in agreement with the results from the smaller truncation. If the results change drastically, we have to reconsider and extend the truncation, particularly with the insight gained from extending the truncation. There is, however, no guarantee that we have included all relevant operators in our truncation, even if the results are insensitive to the added operators. This is because different physical observables might be sensitive to different sets of operators, therefore, it is important to be aware of the observables, we want to compute.

Varying the cut-off function R_k and checking if the results depend on the choice of it is another possibility to verify the reliability of the truncation. It is based on the fact that physical observables should be independent of the regularisation scheme, which is given by the cut-off function. Therefore, physical observables should not depend on the choice of R_k, if they do, this is a signal that the truncation is insufficient.

The quintessence is that an approximate solution of the flow equation can describe non-perturbative physics reliably, if we include the operators corresponding to the relevant degrees of freedom in our truncation of the effective action. Sometimes these degrees of freedom will change, making the analysis more difficult or even meaningless. It is then necessary to introduce scale-dependent fields. It is obvious that the derivation of the flow equation has to be modified. Therefore, we get a different flow equation. We will come back to this problem in chapter 5.

The derivation of the flow equation we gave extends naturally to theories with more complicated field content. For completeness, we have given the schematical picture of the flow equation for QCD in Fig. 2.4. Note the minus sign in front of the quark and ghost loop, it is a consequence of the fermionic nature of these fields.

3 QCD in Polyakov gauge

"Dum spiro spero"

In this chapter, we propose a new approach towards the confinement-deconfinement phase transition using the functional RG in Polyakov gauge. Polyakov gauge provides us with a direct access to the physical observable, the Polyakov loop, which is an order parameter for confinement. Confinement is an infrared property of QCD and therefore, it is obvious that this phase transition cannot be described in a perturbative setting. On the lattice, the Polyakov loop is an observable that is computed easily and it is well understood. In the continuum, writing down the expression for the Polyakov loop is not difficult, however, there have for a long time been no successful attempts to compute the phase transition from first principle, i.e. without imposing additional assumptions onto the theory. Recently there have been attempts to relate the Polyakov loop to the chiral condensate, giving interesting insight in the interplay between confinement and chiral symmetry breaking. We will discuss such a relation in the course of this work.

The behaviour of the Polyakov loop in the high-temperature phase was first discussed by Weiss [52], and exhibited deconfinement as expected. Some time later, attempts have been made in perturbative calculations to see confining properties. These were found with the help of additional parameters, particularly depending on the regularisation [53, 54]. In the course of these investigations it became obvious that within a perturbative approach confinement could not be described from first principle.

The fRG, being a non-perturbative method allows us to access the infrared region of the theory and is therefore a promising tool to investigate the confinement phase transition. Polyakov gauge allows direct access to the order parameter and we can employ controlled approximations of the theory in the fRG. We can relate the order parameter to the effective potential of the gluons. We shall argue, that the Polyakov loop has a massive propagator and therefore, the effective action can be kept rather simple. The physics is essentially captured by the effective potential.

First studies of the Polyakov loop using the fRG [55] in an approximation guided by this idea did not show confinement. With the insight we gain from our analysis, this is not surprising, because the confining properties of the theory were artificially removed by an inappropriate choice of boundary conditions.

Recently, the fRG was used to compute the Polyakov loop potential with the aid of propagators in Landau gauge Yang-Mills theory [56]. It was possible to compute the effective potential of the gluons from the propagators employing background field methods. In this approach confinement can be related directly to the anomalous dimension of the propagators. The condition for confinement is compatible with results for the propagators found using functional methods, as well as with propagators computed on

the lattice. Note that this approach is quite different from the one we will develop in this work, as it rests on the non-trivial momentum structure of propagators in Landau gauge.

3.1 Confinement Phase Transition in $SU(2)$

While there are two Cartan directions for $SU(3)$ there is only one Cartan direction for $SU(2)$. In general there are $N_c - 1$ Cartan directions. The number of Cartan directions defines the number of variables we use in our calculations.

In order to set up our scheme, we start with the technically less involved color gauge group $SU(2)$. This obviously simplifies things drastically, later on, we will also see, that the results from $SU(2)$ are an important input for the calculations of the confinement phase transition in $SU(3)$.

This section is organised as follows, first we set the theoretical framework that allows for the easiest access to the confinement phase transition, then we set up the flow equations. We discuss their solutions and eventually the results emerging from the flow.

3.1.1 Theoretical Setup

In order to set up our flow equations, we first show that the expectation value of the Polyakov loop $\langle L[A_0]\rangle$ and Polyakov loop of the expecatition value of the gauge field $L[\langle A_0\rangle]$ are equivalent order parameters for the deconfinement phase transition.

Reformulation of the Order Parameter

We showed, that Polyakov gauge entails a incredibly simple relation between A_0 and L,

$$L(\vec{x}) = \cos\frac{1}{2}g\beta A_0(\vec{x})\,. \tag{3.1}$$

Note that this simple relation is not valid on the level of expectation values of L and A_0, in $SU(2)$ we have $\langle L\rangle \neq \cos\frac{1}{2}g\beta\langle A_0\rangle$. However, in the present work we consider an approach that gives direct access to the effective potential $V_{\text{eff}}[\langle A_0\rangle]$ for the gauge field, as distinguished to those for the Polyakov loop, $U_{\text{eff}}[\langle L\rangle]$ [1].

Here, we argue that $L[\langle A_0\rangle]$ also serves as an order parameter: To that end we show that the order parameter $\langle L[A_0]\rangle$ is bounded from above by $L[\langle A_0\rangle]$. It follows that $L[\langle A_0\rangle]$ is non-vanishing in the center-broken phase. Furthermore we show that in the center-symmetric phase with vanishing order parameter, $\langle L[A_0]\rangle = 0$, the observable $L[\langle A_0\rangle]$ vanishes. For the sake of simplicity we restrict the explicit proof to $SU(2)$, but it straightforwardly extends to general gauge groups $SU(N_c)$. First we note that eq. (3.1) can be used for expressing the expectation value of A_0 in terms of L,

$$\frac{1}{2}g\beta\langle A_0\rangle = \langle\arccos L\rangle\,. \tag{3.2}$$

[1] A reformulation in terms of the Polyakov loop variable along the lines outlined in [41] is in progress.

We emphasise that the RHS of eq. (3.2) defines an observable as it is the expectation value of an gauge invariant object. This observable happens to agree with $\langle A_0 \rangle$ in Polyakov gauge. It follows from the Jensen inequality that the expectation value of the Polyakov loop, the order parameter for confinement, is bounded from above by $L[\langle A_0 \rangle]$, see [56]

$$L[\langle A_0 \rangle] \geq \langle L[A_0] \rangle \,. \tag{3.3}$$

for gauge fields $g\beta\langle A_0 \rangle/2 \in [0, \pi/2]$. Note that it is sufficient to consider the above interval due to periodicity and center symmetry of the potential. This means we restrict the Polyakov loop expectation value to $\langle L \rangle \geq 0$. Negative values for $\langle L \rangle$ are then obtained by center transformations, $L \to \pm L$. Eq. (3.3) is easily proven for $SU(2)$ from eq. (3.1) as $\cos(x)$ is concave for $x \in [0, \pi/2]$. Thus, for $\langle L \rangle > 0$ it necessarily follows that $g\beta\langle A_0 \rangle/2 < \pi/2$.

In turn we can show that $g\beta\langle A_0 \rangle/2 = \pi/2$, if the Polyakov loop variable $\langle L[A_0] \rangle$ vanishes. This entails that $L[\langle A_0 \rangle] = 0$. To that end we expand L about its mean value $\langle L \rangle$, that is $L = \langle L \rangle + \delta L$. Inserting this expansion into eq. (3.2) we arrive at

$$\frac{1}{2} g\beta\langle A_0 \rangle = \arccos\langle L \rangle - \frac{1}{\sqrt{1 - \langle L \rangle^2}} \langle \delta L \rangle + O\left(\langle \delta L^2 \rangle\right) \,. \tag{3.4}$$

In the center-symmetric phase we have $\langle L \rangle = 0$, c.f. eq. (2.35). Under center transformations L transforms according to (2.34), $L \to Z\,L$ with $Z = \pm 1$, and hence $\delta L \to Z\,\delta L$. It follows that $\langle \delta L^{2n+1} \rangle = Z \langle \delta L^{2n+1} \rangle = 0$, and all odd powers in eq. (3.4) vanish. The even powers vanish since the arccos function is an odd function and hence has vanishing even Taylor coefficients. Thus, in the center-symmetric phase we have

$$\frac{1}{2} g\beta\langle A_0 \rangle = \arccos\langle L \rangle = \frac{\pi}{2} \,. \tag{3.5}$$

In summary we have shown

$$\begin{aligned} T < T_c: \quad & L[\langle A_0 \rangle] = 0 \quad \Leftrightarrow \quad \tfrac{1}{2} g\beta\langle A_0(\vec{x}) \rangle = \tfrac{\pi}{2} \,, \\ T > T_c: \quad & L[\langle A_0 \rangle] \neq 0 \quad \Leftrightarrow \quad \tfrac{1}{2} g\beta\langle A_0(\vec{x}) \rangle < \tfrac{\pi}{2} \,. \end{aligned} \tag{3.6}$$

We conclude that $\langle A_0 \rangle$ in Polyakov gauge serves as an order parameter for the confinement-deconfinement (order-disorder) phase transition, as does $L[\langle A_0 \rangle]$. Thus, we only have to compute the effective potential $V_{\text{eff}}[\langle A_0 \rangle]$ in order to extract the critical temperature, and e.g. critical exponents. This potential is more easily accessed than that for the Polyakov loop. It is here were the specific gauge comes to our aid as it allows the direct physical interpretation of a component of the gauge field. This property has been already exploited in the literature, where it has been shown that $\langle A_0 \rangle$ in Polyakov gauge is sensitive to topological defects related to the confinement mechanism [36, 37, 57, 58].

Weiss Potential

We start with a discussion of the Weiss potential [52] which is an essential building block for our description of the deconfinement phase transition. The derivations done here

are also used for the derivation of the flow equations. Starting point is the standard Yang-Mills action, which simplifies upon imposing Polyakov gauge. We already showed the result for the Fadeev-Popov determinant, eq. (2.39), its derivation is deferred to App. B.1. In Polyakov gauge it cancels precisely the longitudinal components of the spatial gluon fields A_i. This can be seen upon comparing the contributions to the generating functional from the Fadeev-Popov determinant and from the longitudinal components of the gauge fields [52].

In App. B.2 we show the steps leading from the gauge fixed Yang-Mills action with longitudinal gluons already integrated out to the action that can be used to compute the effective potential of the Polyakov loop. The action is

$$S_{\text{eff}}[A] \simeq -\frac{1}{2}\beta \int d^3x\, A_0 \vec{\partial}^2 A_0 - \frac{1}{2}\int_T d^dx\, A^a_{\perp,i}\left[(D_0^2)^{ab} + \vec{\partial}^2\delta^{ab}\right] A^a_{\perp,i} + \mathcal{O}(A^3_{\perp,i}) \tag{3.7}$$

with $D_0^{ab} = \partial_0\delta^{ab} + A_0^3 g f^{a3b}$ and transversal spatial gauge fields, $\partial_i A_{\perp,i} = 0$. The notation $\int_T$ indicates the summation over Matsubara frequencies when going to momentum space, in real space this means $\int_T d^dx = \int d^3x \int_0^T dx_0$.

The generating functional of Yang-Mills theory in Polyakov gauge then reads

$$Z[J] = \int dA_0\, dA_{\perp,i}\, \exp\Big\{-S_{\text{eff}}[A] + \int d^3x\, J_0 A_0 + \int_T d^dx\, J_{\perp,i} A_{\perp,i}\Big\}. \tag{3.8}$$

In eq. (3.8) we have normalised the temporal component J_0 of the current with a factor β. The classical action S_{eff} is inherently non-local as is contains one-loop terms, the Faddeev-Popov determinant as well as the integration over the longitudinal gauge fields.

The perturbative calculation for $SU(2)$ Yang-Mills theory was done by N. Weiss. He showed that the integration and the Matsubara frequency summation can be done analytically, where he used the special features of Polyakov gauge which we just described.

The resulting potential is

$$V_W(\varphi) = -(\tilde{\varphi} - \pi)^2/(6\beta^4) + (\tilde{\varphi} - \pi)^4/(12\pi^2\beta^4)\,, \tag{3.9}$$

with the dimensionless variables $\varphi = g\beta A_0$, and $\tilde{\varphi} = \varphi \mod 2\pi$. The potential is shown in Fig. 3.1 for one period. It is obvious that it is deconfining, as the minima are located at $\langle g\beta A_0\rangle \in \{0, 2\pi n\}, n \in \mathbb{Z}$. Therefore, the Polyakov loop expectation value is zero.

Extending the calculation done by Weiss to gauge groups larger than $SU(2)$ is not difficult. The corresponding Weiss potential in four dimensions is given by

$$V_{W,SU(N)} = \beta^{-4}\frac{2}{\pi^2}\sum_{l=1}^{N_c^2-1}\sum_{n=1}^{\infty}\frac{\cos(n\nu_l)}{n^4}, \tag{3.10}$$

where the ν_l denote the eigenvalues of the hermitian color matrix $\varphi_n T^n = g\beta A_0^n T^n$. The matrices T^n are the generators of $SU(N)$. Note that in Polyakov gauge φ_n has components only in the Cartan directions.

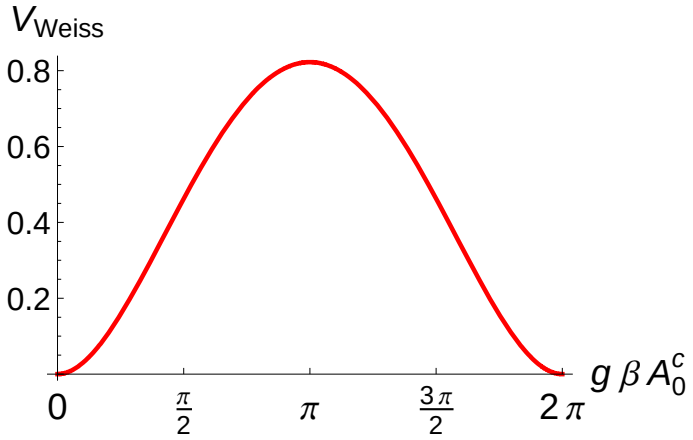

Figure 3.1: The Weiss potential for $SU(2)$

For $SU(3)$ the potential can be written as a sum of one dimensional potentials, the Weiss potentials of $SU(2)$:

$$V_{W,SU(3)}(\varphi_3, \varphi_8) = V_W(\varphi_3) + V_W(\frac{\varphi_3 + \sqrt{3}\varphi_8}{2}) + V_W(\frac{\varphi_3 - \sqrt{3}\varphi_8}{2}), \tag{3.11}$$

φ_3 and φ_8 are the Cartan directions. The resulting potential is depicted in Fig. 3.2. The periodicity in φ_3 and φ_8 direction is obvious. There are however more symmetries of

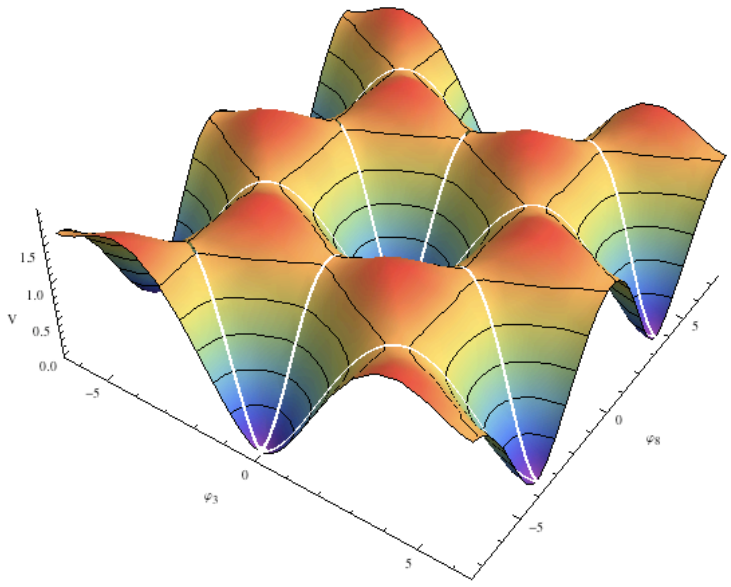

Figure 3.2: The Weiss potential for $SU(3)$. The maxima of the potential are located at combinations of field values, where the Polyakov loop vanishes.

the potential, which we will discuss in more detail when we deal with the flow of $SU(3)$. There we will also introduce the Weyl chambers, which are indicated by the white lines in the potential.

Truncation

Guided by the insight we gained from the calculation of the Weiss potential, we treat spatial and temporal gauge fields independently. We shall argue that in Polyakov gauge a rather simple approximation to the full effective action already suffices to describe the confinement-deconfinement phase transition and in particular to estimate the critical temperature.

Therefore let us analyse the expected propagation behaviour of the Polyakov loop. The expectation value $\langle L(\vec{x})\rangle$, or $L[\langle A_0\rangle]$, is used to determine the phase transition temperature T_c as well as the critical exponents. The temperature-dependence of the Polyakov loop two-point function relates to the string tension. In the confining phase, for $T < T_c$, and large separations $|\vec{x}-\vec{y}| \to \infty$, the two-point function falls off like

$$\lim_{|\vec{x}-\vec{y}|\to\infty} \langle L(\vec{x})L^\dagger(\vec{y})\rangle_c \simeq \exp\left\{-\beta\,\sigma|\vec{x}-\vec{y}|\right\} . \tag{3.12}$$

Here, $\langle\cdots\rangle_c$ stands for the connected part of the related correlation function, i.e.

$$\langle L(\vec{x})L^\dagger(\vec{y})\rangle_c = \langle L(\vec{x})L^\dagger(\vec{y})\rangle - \langle L(\vec{x})\rangle\langle L(\vec{y})\rangle. \tag{3.13}$$

In turn, its Fourier transform shows the momentum dependence

$$\lim_{|p|\to 0} \langle L(0)L^\dagger(p)\rangle_c \simeq \lim_{|p|\to 0} \frac{1}{\pi^2}\frac{\beta\sigma}{((\beta\sigma)^2+p^2)^2} = \frac{1}{\pi^2}\frac{1}{(\beta\sigma)^3} . \tag{3.14}$$

From this we conclude that the Polyakov loop variable has a massive propagator. This directly relates to a massive propagator of A_0 in Polyakov gauge. Therefore, we can use a truncation with a simple momentum structure, similar to the local potential approximation frequently used when investigating scalar theories with the fRG. We compute the flow of the effective action $\Gamma[A_0, \vec{A}_\perp]$ in the following truncation

$$\begin{aligned}\Gamma_k[A_0,\vec{A}_\perp] &= \beta\int d^3x\left(-\frac{Z_0}{2}A_0\vec{\partial}^{\,2}A_0 + V_k[A_0]\right)\\ &\quad -\frac{1}{2}\int_T d^4x\, Z_i\vec{A}^a_\perp\left[(D_0^2)^{ab}+\vec{\partial}^{\,2}\delta^{ab}\right]\vec{A}^a_\perp ,\end{aligned} \tag{3.15}$$

with k-dependent wave function renormalisations Z_0, Z_i. The effective action eq. (3.15) relates to the order parameter $\langle L(\vec{x})\rangle$ as well as its two point correlation function $\langle L(\vec{x})L^\dagger(\vec{y})\rangle$ via the effective potential $V_{\text{eff}}[A_0] = V_k[A_0]$ as explained above. The expectation value $\langle L(\vec{x})\rangle$, or $L[\langle A_0\rangle]$, is used to determine the phase transition temperature T_c as well as critical exponents. The temperature-dependence of the Polyakov loop two-point function relates to the string tension. As explained at the beginning of this chapter, the Polyakov loop has a massive propagator in the confining phase.

In our study, we will set $Z_i = 1$ right from the start, as we assume the backreactions of the temporal on the spatial gluons to be a subleading effect for confinement. The backreaction modifies the potential generated by the spatial gluons. This modification changes the effective potential generated by the temporal gluons only through the denominator of the flow equation. Therefore, the effect on the confining properties of the theory is small. In an extended truncation, we would have to loosen this restriction.

Next we discuss the relation between Z_0 and the running gauge coupling. In order to do so, consider the four-gluon vertex, which is present in the original YM action. We have

$$\Gamma_k^{(2,2)} = \frac{\delta^4 \Gamma_k}{\delta A_0^2 \delta A_i^2} = (4\pi\alpha_s) Z_0 Z_i = g_k Z_0. \tag{3.16}$$

The strong coupling $4\pi\alpha_s$ has to be an RG invariant as the wave function renormalisations carry the RG running. Note that the strong coupling $(4\pi\alpha_s)$ is not a constant, it still has a momentum dependence. In our truncation we identify the momentum running of the strong coupling with its fRG running. We have

$$\alpha_s = \alpha_s(p^2 = k^2_{\text{phys}}). \tag{3.17}$$

Consequently we get the running coupling of YM theory from

$$g_k = \frac{g}{Z_0} = 4\pi\alpha_s(p^2 = k^2_{\text{phys}}) \tag{3.18}$$

This also entails that the anomalous dimension η_0 is linked to the running coupling by

$$\eta_0 = -\partial_t \log \alpha_s(k^2_{\text{phys}})\,. \tag{3.19}$$

In order to proceed and solve the flow equation, we need to specify a regulator function. As we treat temporal and spatial gluons separately, we also choose a regulator that treats the two components in a non-uniform way. The approximation scheme is fully set by specifying the regulators $R_{0,k}$ and $R_{\perp,k}$. Naively one would identify the cut-off parameter k in the regulators with the physical cut-off scale k_{phys}. For general regulators this is not possible and one deals with two distinct physical cut-off scales, $k_{0,\text{phys}}$ and $k_{\perp,\text{phys}}$ related to $R_{0,k}$ and $R_{\perp,k}$ respectively, for a detailed discussion see [41]. However, within the approximation eq. (3.15) it is crucial to have a unique effective cut-off scale $k_{\text{phys}} = k_{0,\text{phys}} = k_{\perp,\text{phys}}$, as different physical cut-off scales $k_{0,\text{phys}} \neq k_{\perp,\text{phys}}$ necessarily introduce a momentum transfer into the flow which carries part of the physics. This momentum transfer is only fully captured with a non-local approximation to the effective action. In turn, a local approximation such as eq. (3.15) requires $k_{0,\text{phys}} = k_{\perp,\text{phys}}$. In other words, a local approximation works best if the momentum transfer in the flow is minimised. This requires a matching of the cut-off scales. More details about such a scale matching and its connection to optimisation [59–61] can be found in [41]. Note in this context that in the present case we also have to deal with the subtlety that A_0 only depends on spatial coordinates whereas $\vec{A}_\perp$ is space-time dependent. However, the requirement of minimal momentum transfer in the flow is a simple criterion which is technically accessible. The regulator can be written as one single regulator $R_{A,\mu\nu}$

which is a block-diagonal matrix in field space. More specifically we restrict ourselves to regulators [62]

$$R_{A,00} = R_{0,k} = Z_0 R_{\mathrm{opt},k}(\vec{p}^2)\,, \quad R_{A,ij} = Z_i \Pi_{\perp,ij}(\vec{p}) R_{\mathrm{opt,k}_\perp}(\vec{p}^2)\,, \tag{3.20}$$

where we introduced the transversal projector defined by

$$\Pi_{\perp,ij} = \delta_{ij} - \frac{p_i p_j}{\vec{p}^2}. \tag{3.21}$$

we use the following regulator shape function, called the 3D optimised regulator [59–61]

$$R_{\mathrm{opt},k}(\vec{p}^2) = (k^2 - \vec{p}^2)\theta(k^2 - \vec{p}^2)\,. \tag{3.22}$$

It has advantageous properties, particularly when working at finite temperature. Some calculations simplify drastically compared with other calculations for a different choice of regulator.

The regulators are optimised in the sense, that the flow has the shortest trajectory towards the final result.

The detailed scale-matching argument is deferred to App. B.3 and results in a relation $k_\perp = k_\perp(k)$ depicted in Fig. 3.3. It is left to determine the effective cut-off scale k_{phys}. This cut-off scale can be determined from the numerical comparison of the flows of appropriate observables: one computes the flow with the three-dimensional regulator $R_{\mathrm{opt},k_\perp}(\vec{p}^2)$ in eq. (3.20), as well as with the four-dimensional regulator $R_{\mathrm{opt},k_{\mathrm{phys}}}(p^2)$. The respective physical scales are then identified, i.e. $k_{\perp,\mathrm{phys}}(k_\perp) = k_{\mathrm{phys}}$. The results for this matching procedure are depicted in Fig. 3.3 and the details of the calculation are found in Appendix B.3. Another estimate comes from the flow related to the three-dimensional A_0-fluctuations where we can directly identity $k_{\mathrm{phys}} = k$. We use the above choices as limiting cases for an estimate of the systematic error in our computation. Our explicit results are obtained for the best choice that works with all physical constraints.

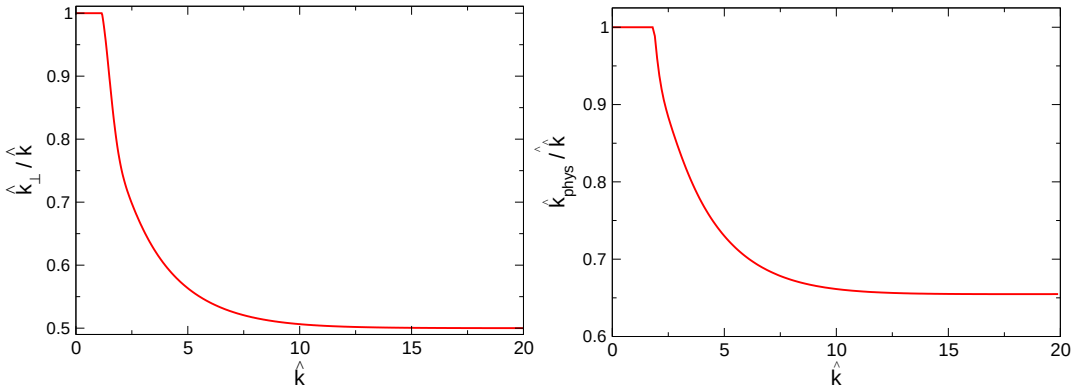

Figure 3.3: $\hat{k}_\perp/\hat{k}$ as function of $\hat{k}$ and $\hat{k}_{\mathrm{phys}}(\hat{k})$ from the comparison of flows with three-dimensional regulators and four-dimensional regulators.

3.1.2 RG Flow Equation

The flow of the cut-off dependent effective action Γ_k is governed by Wetterich's flow equation [44, 63–68] for Yang-Mills theory [41, 69, 70] in Polyakov gauge,

$$\begin{aligned}\partial_t \Gamma_k &= \frac{\beta}{2}\int \frac{d^3p}{(2\pi)^3}\left(\frac{1}{\Gamma_k^{(2)}+R_A}\right)_{00}\partial_t R_{0,k} \\ &\quad +\frac{T}{2}\sum_{n\in\mathbb{Z}}\int \frac{d^3p}{(2\pi)^3}\left(\frac{1}{\Gamma_k^{(2)}+R_A}\right)_{ii}\partial_t R_{opt,k_\perp}\,,\end{aligned} \tag{3.23}$$

where t is the RG time $t=\ln(k/\Lambda)$ and Λ is some reference scale.

Eq. (3.23) together with an initial effective action at some initial ultraviolet scale $k=\Lambda_{\rm UV}$ provides a definition of the full effective action at vanishing scale $k=0$ via the integrated flow. For the solution of eq. (3.23) we have to resort to approximations to the full effective action. In gauge theories such an approximation also requires the control of gauge invariance, see e.g. [41].

We are now in the position to integrate the flow equation eq. (3.23). To begin with, we can immediately integrate out the spatial gauge fields $\vec{A}_\perp$ for $Z_i=1$, that is the second line in eq. (3.23). This part of the flow only carries an explicit dependence on the cut-off k, details of the calculation can be found in App. B.2. It results in a non-trivial effective potential $V_{\perp,k}[A_0]$ that approaches the Weiss potential [52] in the limit $k/T\to 0$, and falls off like $\exp(-\beta k_\perp(k))\cos(g\beta A_0)$ in the UV limit $k/T\to\infty$, see Fig. 3.4. In terms of the effective action, after the integration over $\vec{A}_\perp$, we are led to an effective action of A_0,

$$\Gamma_k[A_0]=\beta\int d^3x\left(\frac{Z_0}{2}(\vec{\partial}A_0)^2+\Delta V_k[A_0]+V_{\perp,k}[A_0]\right). \tag{3.24}$$

Eq. (3.24) follows from eq. (3.15) with $\Gamma_k[A_0]=\Gamma_k[A_0,\vec{A}_\perp=0]$, and

$$V_k[A_0]=\Delta V_k[A_0]+V_{\perp,k}[A_0]\,. \tag{3.25}$$

The full effective potential is given by $V_{\rm eff}[A_0]=\Delta V_{k=0}[A_0]+V_{\perp,k=0}[A_0]$. We are left with the task to determine ΔV_k, which is the part of the effective potential induced by A_0-fluctuations. In Polyakov gauge, these fluctuations carry the confining properties of the Polyakov loop variable, whereas the spatial fluctuations generate a deconfining effective potential for A_0, see Appendix B.2. We emphasise that this structure is not present for spatial confinement which is necessarily also driven by the spatial fluctuations, and solely depends on these fluctuations in the high temperature limit. Work in this direction is in progress.

Here we proceed with the integration of the flow for the potential ΔV_k. To that end we reformulate eq. (3.23) as a flow for ΔV_k with the external input $V_{\perp,k}$, see eq. (B.18). The flow equation for ΔV_k reads

$$\beta\,\partial_t\Delta V_k=\frac{1}{2}\int\frac{d^3p}{(2\pi)^3}\frac{\partial_t R_{0,k}}{Z_0\vec{p}^{\,2}+\partial_{A_0}^2(\Delta V_k+V_{\perp,k})+R_{0,k}}\,. \tag{3.26}$$

With the specific regulator R_k in eq. (3.20) we can perform the momentum integration analytically. We also introduce the scalar field $\varphi = g\beta A_0$ and arrive at

$$\beta\partial_k \Delta V_k = \frac{2}{3(2\pi)^2} \frac{(1+\eta_0/5)k^2}{1+\frac{g_k^2\beta^2}{k^2}\partial_\varphi^2(V_{\perp,k}+\Delta V_k)}\,, \tag{3.27}$$

where the coupling g_k^2 has to run with the effective cut-off scale $k_{\rm phys}$ as explained above. Eq. (3.27) is an equation for the dimensionless effective potential $\hat{V} = \beta^4 V_k$ in terms of $\hat{V}_\perp = \beta^4 V_{\perp,k}$ and $\hat{\Delta}V = \beta^4 \Delta V_k$. The infrared RG-scale k naturally turns into the modified RG-scale $\hat{k} = k\beta$. Thus all scales are measured in temperature units. The flow equation is then of the form

$$\partial_{\hat{k}} \Delta\hat{V} = \frac{2}{3(2\pi)^2} \frac{(1+\eta_0/5)\hat{k}^2}{1+\frac{g_k^2}{\hat{k}^2}\partial_\varphi^2(\hat{V}_\perp+\Delta\hat{V})}\,. \tag{3.28}$$

The potential $\hat{V}$ and hence $\hat{\Delta}V$ has a field-independent contribution which is related to the pressure. For the present purpose it is irrelevant and we can conveniently normalise the flow eq. (3.28) such that it vanishes at fields where $\partial_\varphi^2(\hat{V}_\perp+\Delta\hat{V}) = 0$. This is achieved by subtracting $2(1+\eta_0/5)\,\hat{k}^2/(3(2\pi)^2)$ in eq. (3.28) and we are left with

$$\partial_{\hat{k}} \Delta\hat{V} = -\frac{1}{6\pi^2}\left(1+\frac{\eta_0}{5}\right) \frac{g_k^2\,\partial_\varphi^2\,(\hat{V}_\perp+\Delta\hat{V})}{1+\frac{g_k^2}{\hat{k}^2}\partial_\varphi^2\,(\hat{V}_\perp+\Delta\hat{V})}\,, \tag{3.29}$$

where we have kept the notation $\partial_{\hat{k}}\Delta\hat{V}$ for $\partial_{\hat{k}}\Delta\hat{V} - 2(1+\eta_0/5)\,\hat{k}^2/(3(2\pi)^2)$. In this form it is evident, that the flow vanishes for fields where $\partial_\varphi^2(\hat{V}_\perp+\Delta\hat{V}) = 0$, i.e. once a region of the potential becomes convex, this part is frozen, unless the external input $\hat{V}_\perp$ triggers the flow again.

We close this section with a discussion of the qualitative features of eq. (3.29). It resembles the flow equation of a real scalar field theory, and due to $V_\perp$, the flow is initialised in the broken phase. It relies on two external inputs, $V_\perp$ and α_s.

The first input, $\hat{V}_\perp$, is computed in a perturbative approximation to the spatial gluon sector, and its computation is deferred to App. B.2. It is shown in Fig. 3.4 for various values of the RG time $\hat{k}$, and approaches the perturbative Weiss potential [52] for vanishing cut-off $\hat{k} = 0$. We have argued that within Polyakov gauge this approximation should capture the qualitative feature of its contribution to the Polyakov loop potential. We emphasise again that this is not so for the question of spatial confinement, and the related potential of the spatial Wilson loops.

The second input is $\alpha_s = g_k^2/(4\pi)$, the running gauge coupling. It runs with the physical cut-off scale $k_{\rm phys}$ derived in Appendix B.3, $\alpha_s = \alpha_s(k_{\rm phys}^2)$. In the present work we model α_s with a temperature-dependent coupling that runs into a three-dimensional fixed point $\alpha_{*,3d} k_{\rm phys}/T$ for low cut-off scales $k_{\rm phys}/T \ll 1$. This choice carries some uncertainty as the running coupling in Yang-Mills theory is not universal beyond two loop order. Here we have chosen the Landau gauge couplings $\alpha_{{\rm Landau},4d}(k_{\rm phys}^2)$ at cut-off scales $k_{\rm phys}/T \gg 1$,

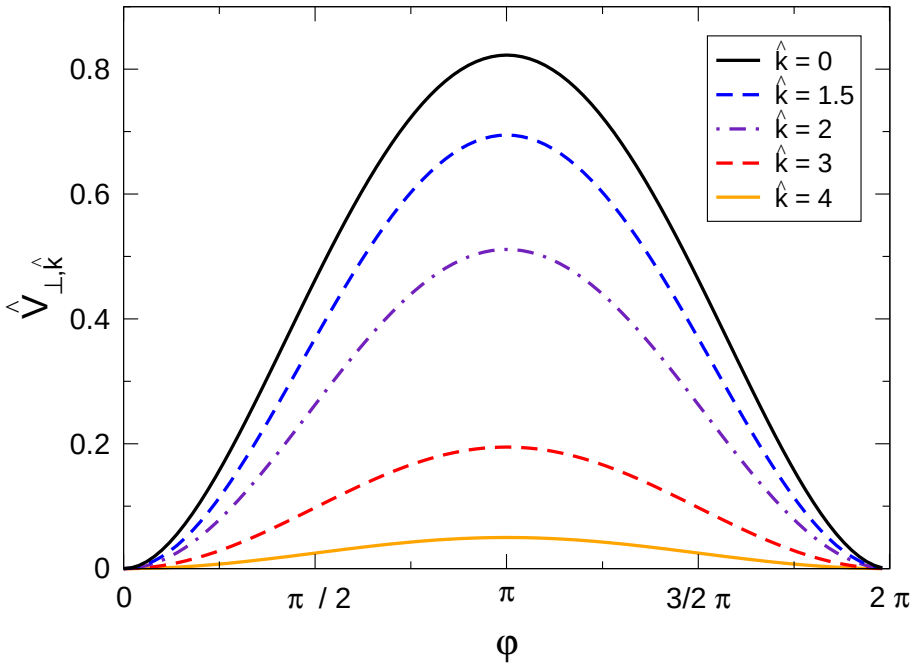

Figure 3.4: $\hat{V}_\perp$ for different values of $\hat{k}$

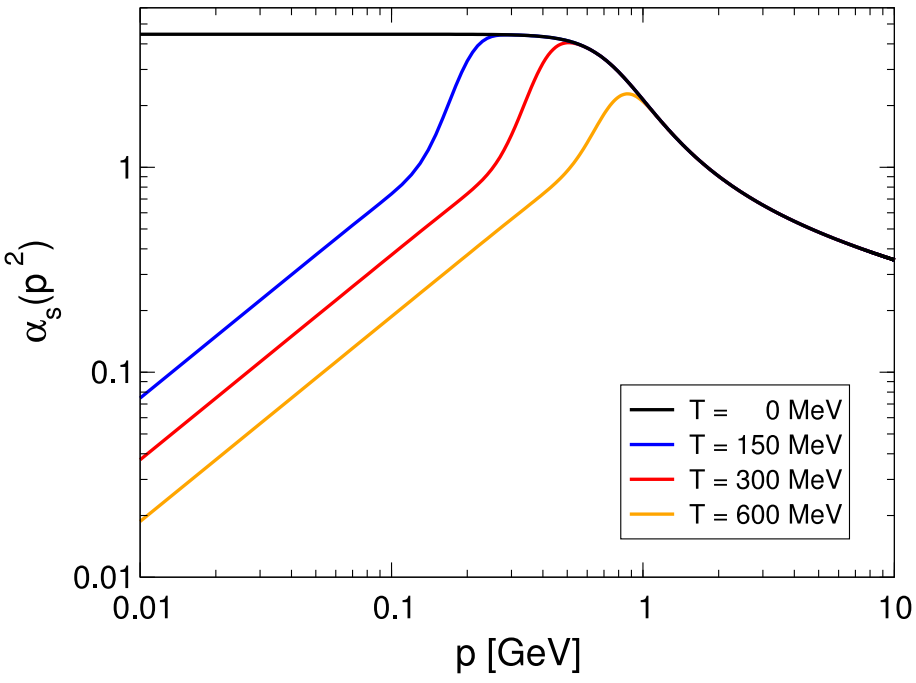

Figure 3.5: α_s for temperatures $T = 0, 150, 300, 600$ MeV

see [42, 71–75]. The corresponding three-dimensional fixed point $\alpha_{*,3d} = 1.12$ is obtained from [74, 75]. A specific choice for such a running coupling is displayed in Fig. 3.5.

The normalisation of the momentum scale has been done by the comparison of continuum Landau gauge propagators to their lattice analogues. Fixing the lattice string tension to $\sqrt{\sigma} = 440$ MeV, we are led to the above momentum scales. For a comparison with Landau gauge results obtained in [56] we have also computed the temperature-dependence of the Polyakov loop by using $\alpha_{\text{Landau},4d}$ for all cut-off scales. Indeed, this over-estimates the strength of α_s, as can be seen from Fig. 3.5, However, qualitatively this does not make a difference: for scales far below the temperature scale, $\hat{k} \to 0$, the flow switches off for fields φ with $\partial_\varphi^2(\hat{V}_\perp + \Delta\hat{V}) \geq 0$, i.e. for the convex part of the potential. This happens both for $g_k^2 \to \text{const}$, and for $g_k^2(\hat{k}^2 \to 0) \sim \hat{k}$. In other words, the minimum of the potential freezes out in this regime. For the non-convex part of the potential, $\partial_\varphi^2(\hat{V}_\perp + \Delta\hat{V}) < 0$, the flow does not tend to zero but simply flattens the potential, thus arranging for convexity of the effective potential $V_{\text{eff}} = V_{k=0}$. The uncertainty in g_k^2 is taken into account by evaluating the limiting cases. Together with the error estimate on the physical cut-off scale k_{phys} in App. B.3 this leads to an estimate for the systematic error of the results presented below. This error includes the error related to our specific choice of the running coupling. For example, a viable alternative choice to Fig. 3.5 is provided by the background field coupling derived in [76] which is covered by the above error estimate.

Integration

The numerical solution of eq. (3.29) is done on a suitably chosen grid or parameterisation of $\Delta\hat{V}$ and its derivatives. As $\hat{V}$, $\hat{V}_\perp$ and $\Delta\hat{V}$ are periodic, one is tempted to solve eq. (3.29) in a Fourier decomposition, see e.g. [55]. However, as can be seen already at the example of the perturbative Weiss potential $V_W = V_{\perp,0}$, eq. (3.9), this periodicity is deceiving. The Weiss potential is a polynomial of order four in $\tilde{\varphi} = \varphi \mod 2\pi$, its periodicity comes from the periodic $\tilde{\varphi}(\varphi)$ [52]. Consequently the third derivative $\partial_\varphi^3 V_W$ has a discontinuity at $\varphi = 2\pi n$ with $n \in \mathbb{Z}$.

Moreover, $\partial_\varphi^3 V_W[\varphi \to 0_+] = -\partial_\varphi^3 V_W[\varphi \to 0_-] \neq 0$. A periodic expansion of V_W, e.g. in trigonometric functions cannot capture this property at finite order. This does not only destabilise the parameterisation, but also fails to capture important physics: the flow of the position of the minima is proportional to $\partial_\varphi^3\hat{V}$. This follows from $\partial_t\hat{V}[\varphi_{\min,k}] = 0$. Expanding this identity leads to

$$\partial_t\varphi_{\min,k} = -\left.\frac{\partial_t\hat{V}'[\varphi]}{\hat{V}''[\varphi]}\right|_{\varphi=\varphi_{\min,k}}, \tag{3.30}$$

where $\hat{V}' = \partial_\varphi\hat{V}$ and $\hat{V}'' = \partial_\varphi^2\hat{V}$. The flow $\partial_t\hat{V}'[\varphi]$ is proportional to $\partial_\varphi^3\hat{V}$, which e.g. can be seen by taking the φ-derivative of eq. (3.23). Since a Fourier-decomposition enforces $\partial_\varphi^3\hat{V} = 0$ at any finite order, the minimum does not flow in such an approximation, and the theory always remains in the deconfined phase. Note also that the resulting effective

potential at $\hat{k} = 0$ for smooth periodic potentials and flows vanishes identically as it has to be convex. In the present case this is not so, as the potential is rather polynomial (in $\tilde{\varphi}$) and convexity does not enforce a vanishing effective potential.

In turn, a standard polynomial expansion about the minimum $\rho_{\min,k}$ already captures the flow towards the confining phase. Here, however, we use a grid evaluation of the flow of $\Delta\hat{V}$ with $\varphi \in [0\,,\,2\pi]$, taking special care of the boundary conditions at $\varphi = 0, 2\pi$: we have extrapolated the second derivative to $\varphi = 0$ and $\varphi = 2\pi$. It suffices to use a first order extrapolation, and we have explicitly checked that the resulting flow is insensitive to the precision of the extrapolation.

An alternative procedure is an expansion in terms of Chebyshev polynomials which also works quite well and provides a very fast and efficient way of integrating the flow. A comparison between the results obtained on a grid and with Chebyshev polynomials shows that both parameterisations agree nicely and the corresponding flows deviate from each other only for small values of k. This is due to an expected failure of the standard Chebyshev-expansion for those small $\hat{k}$ where the position of the minimum is almost settled and the potential flattens out in the regions that are not convex. This behaviour is better resolved with a grid than with polynomials because polynomials have difficulties resolving the transition from a flat to a non-flat region. On a grid implementation we see the potential becoming convex as $\hat{k} \to 0$.

3.1.3 Results

In Fig. 3.6 we show the full effective potential for temperatures ranging from $T = 500$ MeV in the deconfined phase to $T = 250$ MeV in the confined phase. The expectation value $\langle\varphi\rangle$ in the center-broken deconfined phase is given by the transition point between the decreasing part of the potential for small φ and the flat region in the middle of the φ-interval. It can also be explicitly computed from eq. (3.30). In the center-symmetric confined phase it is simply given by the minimum at $\varphi = \pi$.

The temperature-dependence of the order parameter $L[\langle A_0\rangle] = \cos(\langle\varphi/2\rangle)$ is shown in Fig. 3.7, and we observe a second order phase transition from the confined to the deconfined phase at a critical temperature

$$T_c = 305^{+40}_{-55}\,\text{MeV}, \qquad T_c/\sqrt{\sigma} = 0.69^{+.04}_{-.12}\,, \tag{3.31}$$

with the string tension $\sqrt{\sigma} = 440$ MeV. The corresponding value on the lattice is $T_c/\sqrt{\sigma} = .709$, [77–80] and agrees within the errors with our result. The estimate of the systematic error in eq. (3.31) is dominated by the uncertainty of the determination in the identification of k_{phys}, see App. B.3.

We would also like to comment on the difference of the temperature-dependence of $L[\langle A_0\rangle]$ depicted in Fig. 3.7 and that of the Polyakov loop $\langle L[A_0]\rangle$. It has been shown in sec. 3.1.1 that both vanish in the confined phase and both are non-zero in the deconfined phase. However, the Jensen inequality eq. (3.3) entails that the present observable $L[\langle A_0\rangle]$ takes bigger values than the Polyakov loop $\langle L[A_0]\rangle$ which is in agreement with lattice results.

The critical physics should not depend on this issue. Here we compute the critical exponent ν, a quantity well-studied in the $O(1)$ model which is in the same universality class as $SU(2)$ Yang-Mills theory. Moreover, in Polyakov gauge the effective action $\Gamma[A_0]$ after integrating-out the spatial gauge field is close to that of an $O(1)$-model. Studies using the fRG in local potential approximation with an optimised cut-off for the $O(1)$ model yield $\nu = 0.65$, see [81]. The critical exponent in $SU(2)$ YM is related to the screening mass of temporal gauge field by

$$m^2(T) \propto |T - T_c|^{2\nu}, \tag{3.32}$$

where $m^2 = V''(\varphi_{min,0})/2$. We have computed the temperature-dependence of the screening mass in the confined phase near the phase transition, and extracted the critical exponent ν from a linear fit to the data. This is shown in Fig. 3.8. The fit yields the anticipated value of

$$\nu = 0.65^{+0.02}_{-0.01}\,, \tag{3.33}$$

for the critical exponent ν. The critical exponent β agrees within the errors with the Ising exponent $\beta = 0.33$.

Finally we would like to compare the results obtained here with the results of [56]. There, the effective potential $V_{\text{eff}}[A_0]$ was computed from the flow [71, 82] of Landau gauge propagators [72–75, 83–85] within a background field approach in Landau-DeWitt gauge. In this gauge the confining properties of the theory are encoded in the non-trivial momentum dependence of the gluon and ghost propagators. Indeed, in [56] the

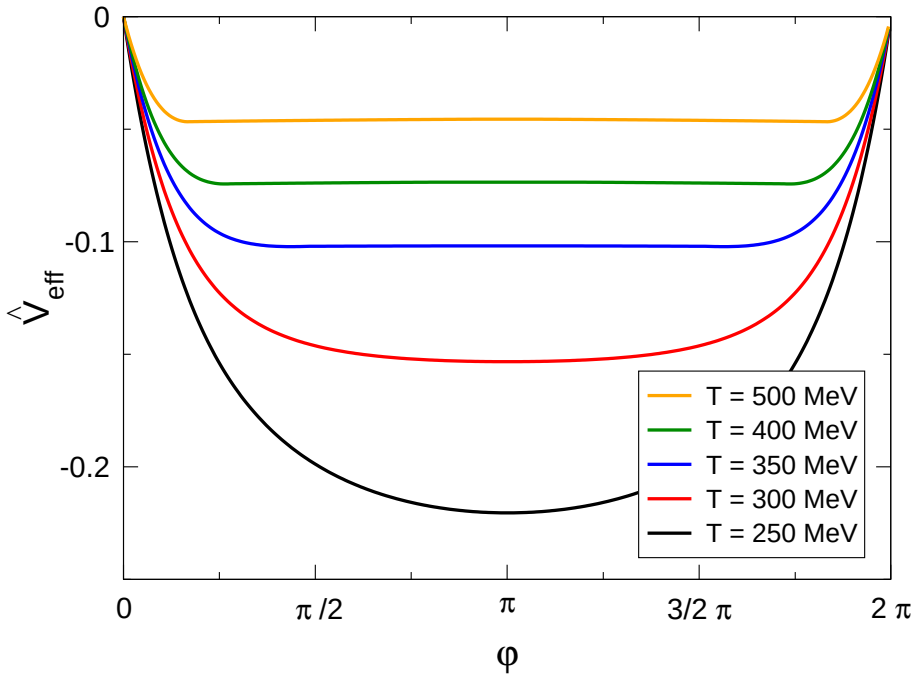

Figure 3.6: Full effective potential $\hat{V}_{\text{eff}}$, normalised to 0 at $\varphi = 0$

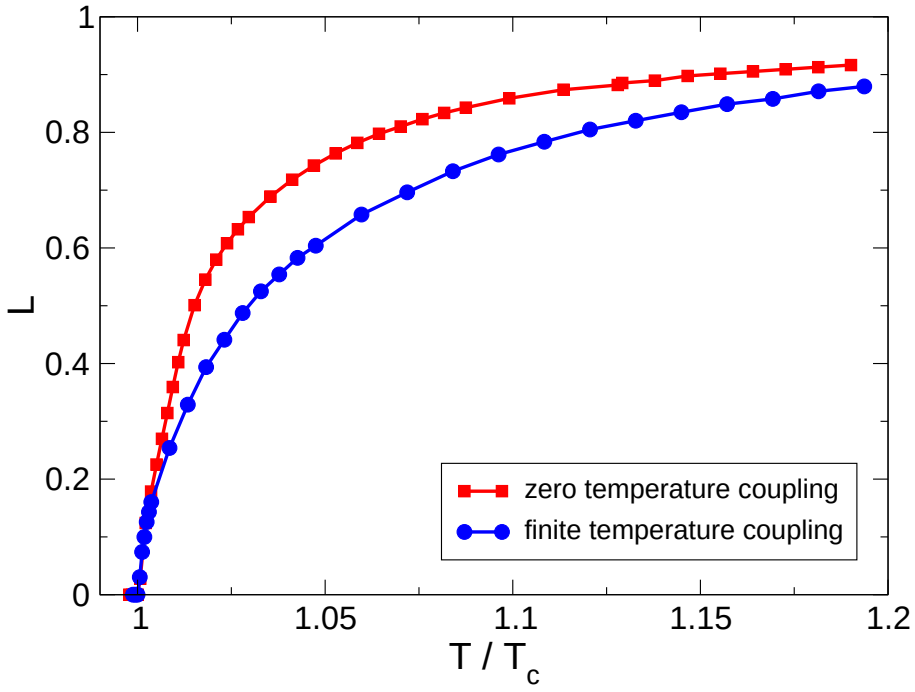

Figure 3.7: Temperature dependence of the Polyakov loop $L[\langle A_0 \rangle] = \cos(\langle \varphi \rangle / 2)$ in $SU(2)$

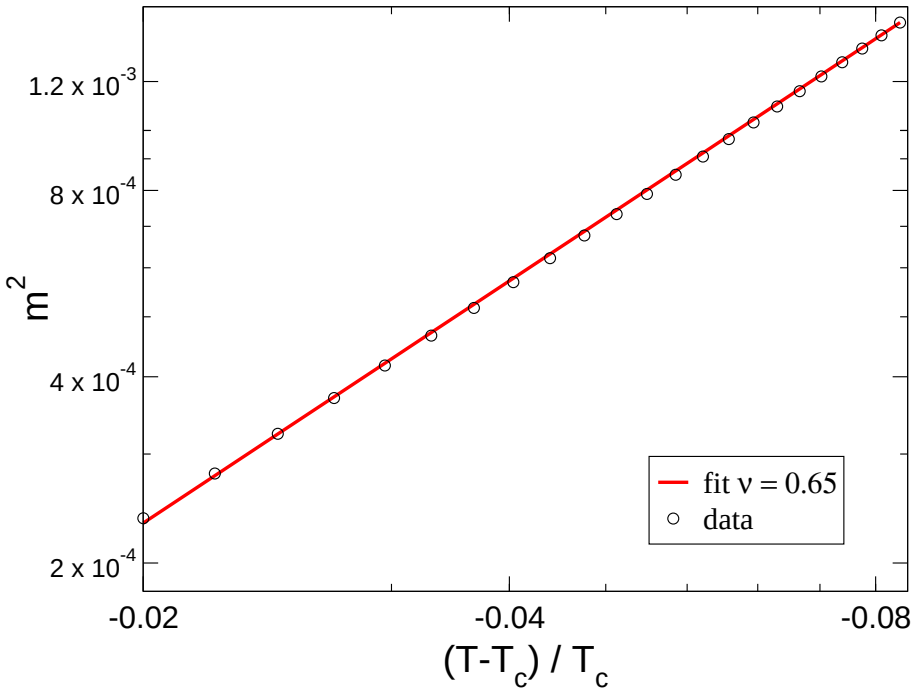

Figure 3.8: Critical exponent ν from $m^2 = V''(\varphi_{min,0})/2$

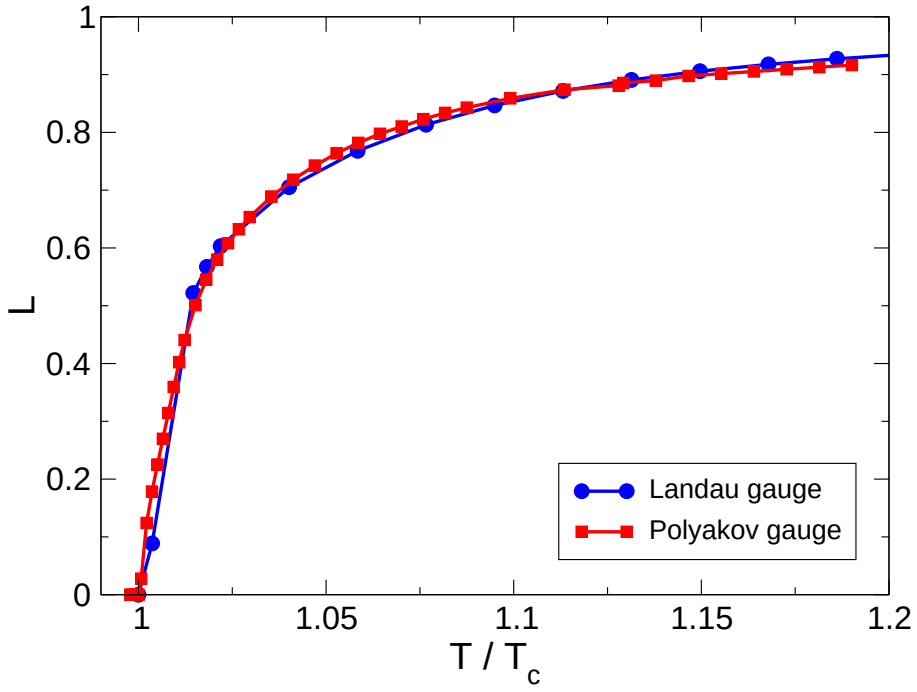

Figure 3.9: Comparison of $L[\langle A_0 \rangle]$ computed in Polyakov gauge and in Landau-DeWitt gauge from [56].

effective potential V_k was computed solely from this momentum dependence but its back-reaction in the form of its second derivative V'' has not been taken into account. In $SU(2)$ Landau gauge Yang-Mills this is expected to be a good approximation with the exception of temperatures close to the phase transition, see [56]. In the vicinity of the phase transition, the back-reaction of the effective potential is particularly important for the critical physics and the value of the critical temperature [86].

For the comparison we have computed the present flow with the zero-temperature running coupling in Fig. 3.5 for all temperatures. This mimics the approximation used in [56] which implicitly relies on the zero-temperature running coupling α_s. We also remark that the quantity $L[\langle A_0 \rangle]$ is gauge-dependent in general, and only the critical temperature derived from it is not. However, in Landau-DeWitt gauge with background fields A_0 in Polyakov gauge temporal fluctuations about this background resemble those in Polyakov gauge. For this reason we might expect a rather quantitative agreement for the quantity $L[\langle A_0 \rangle]$ in both approaches. The results for the temperature dependence of the Polyakov loop are depicted in Fig. 3.9. The coincidence between the two gauges is very remarkable, particularly since the mechanisms driving confinement are quite different in the different approaches, as are the approximations used in both cases. This provides further support for the results from these studies. It also sustains the argument concerning the lack of gauge dependence made above. The quantitative deviations in the vicinity of the phase transition are due to the truncation used in [56] that cannot encode the correct critical physics yet, as has been already discussed there.

3.2 Confinement Phase Transition Formulated in $L[\vec{x}]$

We mentioned before that there are physical situations where the appropriate degrees of freedom change with scale. In chapter 5 we will introduce an implementation of this in the fRG for a scalar $O(2)$ model. In our truncation, QCD can be treated like a scalar theory, it is therefore worthwhile to investigate how a change of degrees of freedom influences the deconfinement phase transition. In the previous section, we showed that we can use $\langle L[A_0(\vec{x})]\rangle$ as an order parameter instead of the original order parameter $\langle L(\vec{x})\rangle$. Doing so, we do not directly take the Polyakov loop fluctuations into account. The effect of taking these fluctuations into account is a phase transition that is less sharp. This can already be seen from the Jensen inequality, eq. (3.3) and has also been observed on the lattice. Finally there are also indications from the flow, as it is more deconfining above the critical temperature compared to the flow formulated in terms of the gauge field variable. A formulation of the theory in L also allows for a direct comparisson of the results with lattice data, because on the lattice one naturally computes $\langle L\rangle$.

Now we want to formulate the flow equation in terms of $L(\vec{x})$, thereby computing the order parameter $\langle L(\vec{x})\rangle$.

3.2.1 Flow Equation

The natural variable to formulate the flow in, is the Polyakov loop which is in $SU(2)$ related to the gauge field A_0 via

$$L(\vec{x}) = \cos\left(\frac{g\beta A_0^3(\vec{x})}{2}\right) = \cos\left(\frac{\varphi(\vec{x})}{2}\right) \tag{3.34}$$

The task at hand is to reformulate the theory in terms of the Polyakov loop variable $(\vec{x})$ and then write the flow in terms of this variable. Let us first rewrite the action, giving us guidance to the changes, that we will have to introduce in the flow equations.

The parametrisation of the action is now given by

$$\Gamma_{L,k}[A_0] = \frac{Z_L}{2}(\partial_\mu A_0^3(L))^2 + V_k[A_0(L)] = \frac{4Z_L}{2(1-L^2)}(\partial_\mu L)^2\frac{1}{g^2\beta^2} + V_k[\varphi(L)], \tag{3.35}$$

where we used $A_0^3[L(\vec{x})] = \frac{2}{g\beta}\arccos(L(\vec{x}))$ and $\partial_\mu\arccos(L(\vec{x})) = \frac{-2}{\sqrt{1-L^2}}\partial_\mu L(\vec{x})$. We renamed Z_0 into Z_L.

It is now obvious how to define the cut-off. The spatial gluons are not affected by the reformulation of the theory. We use the same cut-off shapes as in the previous section, only the pre factors are changed. Then the cut-off is given by

$$R_{A,LL} = R_{L,k} = Z_L\frac{2}{g^2\beta^2}R_{\mathrm{opt},k}(\vec{p}^2)\,, \quad R_{A,ij} = Z_i\Pi_{\perp,ij}(\vec{p})R_{\mathrm{opt,k}_\perp}(\vec{p}^2)\,, \tag{3.36}$$

where again [59–61]

$$R_{\mathrm{opt},k}(\vec{p}^2) = (k^2-\vec{p}^2)\theta(k^2-\vec{p}^2)\,. \tag{3.37}$$

The flow of the cut-off dependent effective action $\Gamma_{L,k}$ is governed by Wetterich's equation [44, 63–68]. For Yang-Mills theory [41, 69, 70] in Polyakov gauge, using the Polyakov loop variable L, it reads

$$\partial_t \Gamma_{L,k} = \int \frac{d^3p}{(2\pi)^3} \left(\frac{\beta}{2} \left(\frac{1}{\Gamma^{(2)}_{L,k} + R_A} \right)_{LL} \partial_t R_{L,k} + \frac{T}{2} \sum_{n\in\mathbb{Z}} \left(\frac{1}{\Gamma^{(2)}_{L,k} + R_A} \right)_{ii} \partial_t R_{opt,k} \right). \quad (3.38)$$

It is very similar to eq. (3.23), except for the fact, that we traded the zero component of the gauge field A_0 for the Polyakov loop variable L by means of the relation $L(\vec{x}) = \cos(g\beta A_0^3(\vec{x})/2)$. Effectively this will lead to modifications of the flow equation, which we discuss next.

As before we need to specify boundary conditions at some scale Λ_{UV} and solve the differential equation. At vanishing cut-off scale, $k = 0$, we recover the full effective action.

In the previous section definition of the boundary conditions was trivial, as we could start at some high scale, were QCD becomes perturbative and the effective action is nothing but the classical effective action. Here, we have to be more careful, because simple perturbative boundary conditions can lead to (unphysical) divergences in the flow. We will come back to this issue later.

What we can do similarly to our previous computation is integrating out the spatial gluons $\vec{A}_\perp$. The computation is exactly the same as in the previous section. Therefore, we do not show it here explicitly. Since we have integrated out the spatial gluons, the effective potential consists out of two contributions $V_{L,k}[L] = \Delta V_{L,k}[L] + V_{\perp,k}[A_0(L)]$. The latter contribution was introduced in the previous section and discussed there, a plot of it is in Fig. 3.4. It is the deconfining part of the effective potential, which triggers during the flow the confining part of the potential.

To compute the flow, we need the second derivative of the effective action. To compute it, note that we evaluate the flow equation at vanishing momenta, i.e. spatially homogeneus fields. Therefore, only the two field derivatives acting on the $(\partial L)^2$ terms contribute to the flow of the effective action, since other contributions to $\Gamma^{(2)}_k$ vanish $(\partial_\mu L|_{p\to 0} = 0)$. We therefore get:

$$\Gamma^{(2)}_{L,k} = Z_L \frac{4}{(1-L^2)g^2\beta^2} \vec{p}^2 + \partial_L^2 V_k[\varphi(L)], \quad (3.39)$$

We end up with the following flow equation, where we already integrated out the spatial gluons and absorbed their contribution into the effective potential as demonstrated in the last section. The resulting flow equation is given by (the step function of the regulator has already been used to specify the integration bounds)

$$\partial_t \Delta V = \frac{1}{2} \frac{4\pi}{(2\pi)^3} \int_0^k dp p^2 \frac{\frac{4}{g^2\beta^2} Z_L (2k^2 + \eta_L (k^2 - \vec{p}^2)}{Z_L \frac{4}{g^2\beta^2} \left(\frac{1}{1-L^2} - 1 \right) \vec{p}^2 + Z_L \frac{4}{g^2\beta^2} k^2 + \partial_L^2 V_k[\varphi(L)]}, \quad (3.40)$$

where $\eta_L = \dot{Z}_L / Z_L$. Again, we have the coupling g_k^2 running with the effective cut-off scale k_{phys}.

We perform the substitution $x = \vec{p}^2\beta^2$ and rescale the flow paramater $\hat{k} = \beta k$. Furthermore, we rescale the potential with temperature, $V = \beta^4 V_k$ The flow equations can then be expressed in terms of dimensionless quantities, details of the calculation can be found in App. B.4.

$$\hat{k}\,\partial_{\hat{k}} V = \frac{1}{(2\pi)^2}\int_0^{\hat{k}^2} dx \frac{\sqrt{x}(\hat{k}^2 + \eta_A(\hat{k}^2 - x))}{\frac{L^2}{1-L^2}x + \hat{k}^2 + \frac{g^2}{4}\partial_L^2 V[\varphi(L)]}. \tag{3.41}$$

We are left now with the computation of the second derivative of the potential $\partial_L^2 V[\varphi(L)]$. This is easily done, yielding

$$\partial_L^2 V[\varphi(L)] = -2\frac{\cos(\varphi/2)}{\sin^3(\varphi/2)}V' + \frac{4}{\sin^2(\varphi/2)}V'' = \frac{-2L}{(1-L^2)^{3/2}}V' + \frac{4}{1-L^2}V'', \tag{3.42}$$

where $V' = \partial V[\varphi]/\partial\varphi$. The momentum integration can be done analytically, however, there is a potential problem stemming from the points $L = \pm 1$, these are the points that relate to $\varphi \in \{0, 2\pi\}$. Thus, we have to be carefull about the boundaries of the potential again. Since the potential can be non-convex during the flow. It is easily seen from eq. (3.42), that near $L = \pm 1$ the flow at the boundaries of the potential may become very large. Especially at the begin of the flow, the potential is largely non-convex and therefore, these large contributions can lead to unphysical divergencies during the flow. Perturbatively we can see, that there are cancellations among the two contribution.

One way out, is to use the results for the potential obtained from the flow formulated in terms of the variable φ. At a specified point in the flow, we then switch to the formulation in L. The result of this procedure is unfortunately quite sensitive to the precise switching procedure, e.g. where the transition from one into the other formulation occurs.

3.2.2 Discussion

In summary, we see, that we devised a transformation of variables, that allows for a non-convex potential. This in turn invalidates the mean-field argument, that $L \propto \exp(i\beta A_0)$

We cannot simply substitute the variable A_0 in the previous calculation for the new variable L. This means, that $V_W[L] \neq V_{\text{eff}}[L]$, where $V_{\text{eff}}[L]$ is the effective potential, that we would have to use to get correct results.

To resolve this problem we need a transformation of variables, that takes this special feature into account. This could be of the form

$$L(A_0) \to \begin{cases} L \text{ for } g\beta\langle A_0\rangle \to \pi \\ A_0 \text{ for } g\beta\langle A_0\rangle \to 0 \end{cases} \tag{3.43}$$

3.3 Confinement Phase Transition for $SU(3)$

Having shown that we can describe the deconfinement phase transition within our truncation using the fRG. Next we want to tackle the real physical problem of $SU(3)$. $SU(3)$ is not too different from $SU(2)$, the mechanism driving confinement, i.e. the effective potential, is the same. $SU(2)$ YM in Polyakov gauge was particularly simple because the Cartan contained only one component. As we will see, in $SU(3)$, the Cartan now contains two components and therefore, the effective potential is 2-dimensional, which is technically more involved than the one-dimensional one for $SU(2)$. As we have seen in $SU(2)$ the boundaries of the region we compute the potential on are very important. In $SU(3)$ we have more boundaries and have to handle them carefully.

Gauge Fixing

For the case of $SU(3)$, Polyakov gauge is implemented by the gauge fixing conditions

$$\partial_0 \mathrm{Tr}\, \lambda_c A_0 = 0\,, \qquad \mathrm{Tr}\, \lambda_{a\neq c} A_0 = 0\,, \tag{3.44}$$

where the λ_c are the Gell-Mann matrices that lie in the Cartan subalgebra, i.e. $c \in \{3, 8\}$. $\lambda_{a\neq c}$ denotes the remaining Gell-Mann matrices. However, the gauge fixing eq. (3.44) is not complete. It is unchanged under time-independent gauge transformations in the Cartan sub-group. This residual gauge freedom is fixed by integral conditions, which for brevity we will not display here.

3.3.1 Flow Equation

Our truncation for $SU(3)$ Yang-Mills theory in Polyakov gauge is very similar to the truncation for $SU(2)$, except that the gauge field A_0 now has a more complex structure. It is given by $A_0 = A_0^3 T^3 + A_0^8 T^8$. The steps that led us in $SU(2)$ from eq. (3.23) to the flow equation for the effective potential eq. (3.29) are virtually unchanged apart from the fact that we have a more complex tensor structure. We would like to sketch the most important changes. Due to the higher dimensionality of the Cartan in $SU(3)$ the second derivative of the effective action will have an additional tensor structure in the Cartan components. This can already be seen by looking at the effective action that we want to use (compare with eq. (3.24))

$$\begin{aligned}\Gamma_k[A_0] &= \beta \int d^3x \left(Z_0 \mathrm{Tr}(\vec{\partial} A_0)^2 + \Delta V_k[A_0] + V_{\perp,k}[A_0] \right) \\ &= \beta \int d^3x \left(\frac{Z_0}{2} ((\vec{\partial} A_0^3)^2 + (\vec{\partial} A_0^8)^2) + \Delta V_k[A_0^3, A_0^8] + V_{\perp,k}[A_0^3, A_0^8] \right). \end{aligned} \tag{3.45}$$

The full effective potential is given by $V_{\mathrm{eff}}[A_0^3, A_0^8] = \Delta V_{k=0}[A_0^3, A_0^8] + V_{\perp,k=0}[A_0^3, A_0^8]$. We are left with the task to determine ΔV_k, which is the part of the effective potential induced by A_0-fluctuations. In Polyakov gauge these fluctuations carry the confining properties

of the Polyakov loop variable, whereas the spatial fluctuations generate a deconfining effective potential for A_0, see App. B.2.

The regulator for $SU(3)$ is unchanged in comparison with $SU(2)$, except for zero component of the gauge field,

$$R_{A,00} = \delta_{ab} R_{0,k} = Z_0 \delta_{ab} R_{\mathrm{opt},k}(\vec{p}^2)\,, \quad R_{A,ij} = Z_i \Pi_{\perp,ij}(\vec{p}) R_{\mathrm{opt},\mathrm{k}_\perp}(\vec{p}^2)\,, \tag{3.46}$$

where a, b run only in the Cartan, i.e. $a, b \in \{3, 8\}$ and $R_{\mathrm{opt},k}$ is the optimised regulator, already used in eq. (3.22).

The flow equation is the same as before except for an additional tensor structure , indicated by the superscript:

$$\partial_t \Gamma_k = \int \frac{d^3p}{(2\pi)^3} \left(\frac{\beta}{2} \left(\frac{1}{\Gamma_k^{(2)} + R_A} \right)^{aa}_{00} \partial_t R_{0,k} + \frac{T}{2} \sum_{n\in\mathbb{Z}} \left(\frac{1}{\Gamma_k^{(2)} + R_A} \right)_{ii} \partial_t R_{opt,k_\perp} \right). \tag{3.47}$$

The temporal component of the propagator, $(\Gamma^{(2)} + R)^{-1}_{00}$, is now matrix-valued in Cartan space. The inversion of the propagator is not difficult, though. The flow of the spatial gluons generates the Weiss potential for $SU(3)$.

At the example of the second derivative of the effective action, we exemplify the new structure appearing in the propagator. The second derivative of the effective action, $\Gamma^{(2)}$, is now matrix valued. Explicitly the second derivative reads, note that we omitted any field dependence other than the dependence on A_0,

$$\Gamma_k^{(2)}[A_0] = \begin{pmatrix} \frac{\delta^2}{\delta A_3^2} & \frac{\delta^2}{\delta A_3 \delta A_8} \\ \frac{\delta^2}{\delta A_3 \delta A_8} & \frac{\delta^2}{\delta A_8^2} \end{pmatrix} \Gamma[A_0] \tag{3.48}$$

Analogous expressions appear for the other components. With the specified regulator R_k in eq. (3.46) we can perform the momentum integration analytically. Introducing the scalar field $\varphi_{3/8} = g\beta A_0^{3/8}$, we find (details are deferred to App. B.5)

$$\begin{aligned} \beta \partial_k \Delta V_k \;=\; & \frac{2\beta^2 k^4}{3(2\pi)^2} \left(1 + \frac{\eta_0}{5}\right) \\ & \frac{2k^2 + g_k^2 \beta^2 \left((\partial_{\varphi_3}^2 + \partial_{\varphi_8}^2) V_k \right)}{(k^2 + g_k^2 \beta^2 \partial_{\varphi_3}^2 V_k)(k^2 + g_k^2 \beta^2 \partial_{\varphi_8}^2 V_k) - (g_k^2 \beta^2 \partial_{\varphi_3} \partial_{\varphi_8} V_k)^2}, \end{aligned} \tag{3.49}$$

where the coupling g_k^2 has to run with the effective cut-off scale k_{phys}, and is estimated by an appropriate choice of the running coupling α_s as before. Of course the running of the gauge coupling in $SU(3)$ is different from the running in $SU(2)$.

3.3.2 Integration of the Flow

Having derived the flow equation, we have to devise a method for solving them numerically. This is more involved than before. For $SU(2)$, the potential depends only on one variable, for the case of $SU(3)$ however, it depends on two variables. This increases the

numerical effort to solve the equations drastically but there are also conceptual complications stemming from the boundaries. As we detailed for the case of $SU(2)$ the boundaries are crucial for confinement. A potential depending on two variables has of course not only two boundary points, but instead boundary lines. Before discussing this more detail, let us discuss a trick which renders the equations more manageable.

Using the Weiss potential $V_{\perp,k}$ as an input into the flow equation is a disadvantageous choice. It is a non-convex potential that leads to a flow which always has to balance this non-convexity. Therefore, it is advantageous to use a more convex potential, i.e. a potential with second derivatives that are positive. From the solutions of the $SU(2)$ calculation, we have such a potential at hand and will use it as input. This is easily done by adding a "0", $0 = \partial_t(\Delta V_{SU(2),k} - \Delta V_{SU(2),k})$ to the flow equation, where $\Delta V_{SU(2),k}$ is the potential generated by the flow in $SU(2)$. After splitting the potential to be computed into two terms $\Delta V_k = \Delta V_{SU(2),k} + \Delta V_{SU(3),k}$, where $\Delta V_{SU(3),k}$ is the potential we want to compute, the flow is schematically given by

$$\begin{aligned} \partial_t \Delta V_k &= \mathrm{fRG}[\Delta V_k + V_{\perp,k}], \\ \Rightarrow \partial_t \Delta V_k &= -\partial_t \Delta V_{SU(2),k} + \mathrm{fRG}[\Delta V_k + \Delta V_{SU(2),k} + V_{\perp,k}], \end{aligned} \tag{3.50}$$

where we set $\Delta V_k = \Delta V_{SU(3),k}$ after having split the potential. The full effective potential is then $\Delta V_k + \Delta V_{SU(2),k} + V_{\perp,k}$

At its root eq. (3.50) is an equation for the dimensionless effective potential $\hat{V} = \beta^4 V_k$ in terms of $\hat{V}_\perp = \beta^4(V_{\perp,k} + \Delta V_{SU(2),k})$ and $\Delta\hat{V} = \beta^4 \Delta V_k$. The infrared RG-scale k naturally turns into the modified RG-scale $\hat{k} = k\beta$, that is all scales are measured in units of temperature. The flow equation then takes the following form

$$\begin{aligned} \partial_{\hat{k}} \Delta\hat{V}_{\hat{k}} &= -\partial_{\hat{k}} \Delta\hat{V}_{SU(2),k} + \frac{2\hat{k}^4}{3(2\pi)^2}\left(1 + \frac{\eta_0}{5}\right) \\ &\quad \frac{2\hat{k}^2 + g_k^2\left((\partial_{\varphi_3}^2 + \partial_{\varphi_8}^2)V_k\right)}{(\hat{k}^2 + g_k^2\partial_{\varphi_3}^2 V_k)(\hat{k}^2 + g_k^2\partial_{\varphi_8}^2 V_k) - (g_k^2 \partial_{\varphi_3}\partial_{\varphi_8} V_k)^2}. \end{aligned} \tag{3.51}$$

This equation governs the flow of the effective potential. It resembles the flow equation of a scalar $O(2)$-theory. In our case it is additionally driven by two external inputs, $V_\perp$ and α_s.

The first input, $\hat{V}_\perp$, is computed in a perturbative approximation to the spatial gluon sector. The potential $\hat{V}_\perp[\varphi_3, \varphi_8]$ is within our truncation a sum of contributions from a well known potential depending solely on one variable, $\hat{V}_{\perp,SU(2)}[\varphi]$. The corresponding expression is

$$\hat{V}_\perp[\varphi_3, \varphi_8] = \hat{V}_{\perp,SU(2)}[\varphi_3] + \hat{V}_{\perp,SU(2)}\left[\frac{\varphi_3 + \sqrt{3}\varphi_8}{2}\right] + \hat{V}_{\perp,SU(2)}\left[\frac{\varphi_3 - \sqrt{3}\varphi_8}{2}\right]. \tag{3.52}$$

$\hat{V}_{\perp,SU(2)}[\varphi]$ is shown in Fig. 3.4 for various values of the RG time $\hat{k}$. It approaches the perturbative $SU(2)$ Weiss potential [52] for vanishing cut-off $\hat{k} = 0$. Consequently $\hat{V}_\perp[\varphi_3, \varphi_8]$ yields the perturbative $SU(3)$ Weiss potential for $k \to 0$

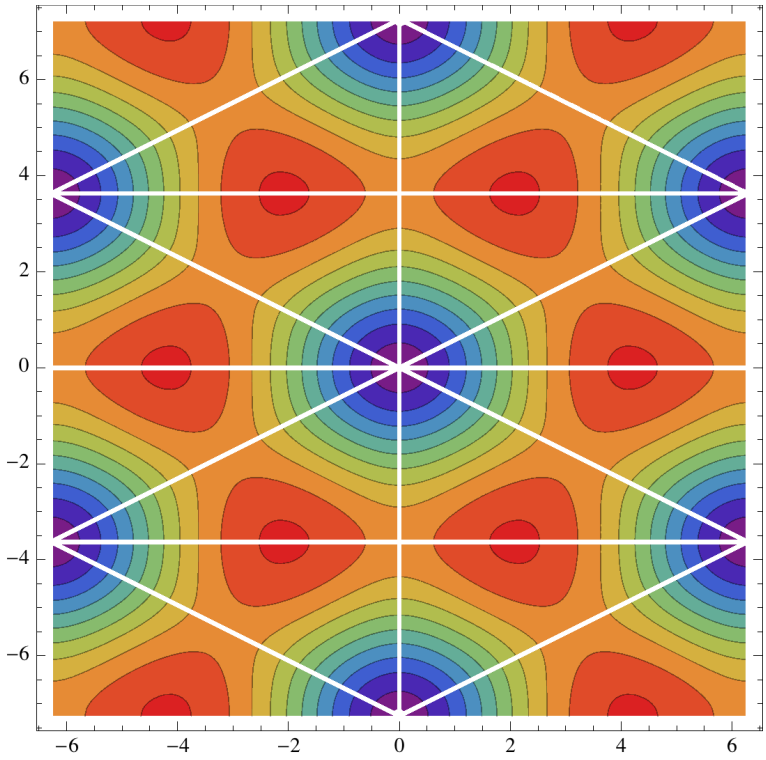

Figure 3.10: Contour Plot of the Weiss potential, in this projection, the symmetries of the potential indicated by the white lines.

When inspecting the landscape of the $SU(3)$ Weiss potential, we can immediately identify symmetries. In order to extract information about confinement, we therefore, do not need the potential over a full period, but can restrict our computations to the so called Weyl chambers. These are the triangular areas indicated by the white lines in Fig. 3.10. These triangular region originate from each other upon mirror symmetry. Along the lines parallel to the φ^3 or φ^8 axis, the symmetry is a simple reflection. Along the diagonal lines, we have to apply an inversion at the center of the diagonal.

It is tempting to use the symmetries of the Weyl chambers to define the second derivatives on the boundaries, that are not easily accessible otherwise. However, we cannot use these symmetries, as they result in a phase transition and a potential, that depends on the input $\Delta V_{SU(2),k}$ into the flow equation. This input should not alter the results, as we simply added a "0", c.f. eq. (3.50).

Still we can already in this setting observe confinement in $SU(3)$. As the potential depends on the input, also the phase transition temperature is dependent on that input. One might have hoped that there is a class of deformations, where a deformation of the potential does not drastically effect the phase transition temperature. Attempts, to find these deformations have failed so far and it seems that the solution to this problem has to be developed along other lines of reasoning.

Note that the coupling we employ is almost the same as the one depicted in Fig. 3.5, except that now the fixed points are different from the fixed points there. For the fixed points, we get $\alpha_{*,3D,SU(2)} = \frac{3}{2}\alpha_{*,3D,SU(3)}$

3.3.3 Results

Although the results obtained by using the trick eq. (3.50), do not give unique results, but rather depend on the precise shape of $\Delta V_{SU(2),k}$, we want to pursue this approach. This is a good exercise, since the flow using the symmetries of the potential, gives a good picture of the mechanisms driving the confinement phase transition. Therefore, let us use these results to describe the general features of the confinement mechanism in an fRG setting.

The Polyakov loop can vanish at various points in the $\varphi_3 - \varphi_8$-plane. It is given by

$$L = \frac{1}{3}\left(\exp(-\frac{i}{2\sqrt{3}}\varphi^8)\left[\exp(\frac{i}{2}\varphi^3) + \exp(-\frac{i}{2}\varphi^3)\right] + \exp(\frac{i}{\sqrt{3}}\varphi^8)\right). \tag{3.53}$$

Let us restrict ourselves to $\varphi^8 = 0$. In this case it is easy to see, that for $\cos\varphi^3/2 \stackrel{!}{=} -1/2$ the Polyakov loop vanishes. This is achieved for $\varphi^3 = \frac{4\pi}{3}$. Therefore, we require the potential to have an absolute minimum at this combination of field values, or any center transformed combination of them.

We restrict the domain of the gauge fields to one Weyl chamber[2]. In Fig. 3.11 we show the potential for different values of the scale $\hat{k}$ for a temperature well below the phase transition temperature. We can track the minimum of the potential which starts to move away from the edges the Weyl chamber. It is precisely at these edges, where $L = 1$. The observation that there are two minima coming from the edge of the Weyl chamber is owed to the fact that this domain of the variables still carries information redundantly. The minima are physically equivalent and eventually merge into one single minimum. It is located right at $\varphi^8 = 0$ and $\varphi^3 = \frac{4\pi}{3}$, i.e. confining.

For temperatures above the phase transition temperature, the minima do not evolve to the confining minimum. As we can restrict our observations to the $\varphi^8 = 0$ axis - all other minima can be obtained by center symmetry - a plot of the potential on this slice is sufficient to determine the phase we are in.

The flow of the potential on the $\varphi^8 = 0$ slice is depicted in Fig. 3.12 for a temperature well below the physical phase transition temperature. We clearly observe the development of a second minimum, which evolves towards a $\varphi^3 = \frac{4\pi}{3}$, where at the end of the flow, it remains the absolute minimum. For temperatures above the critical temperature, the second minimum that develops around $\varphi^3 = \frac{4\pi}{3}$ remains only a local minimum. Therefore, the ground state is deconfining.

[2]The domain we work on can be divided into even smaller regions that carry the physical information. However, the numerical implementation becomes more complicated.

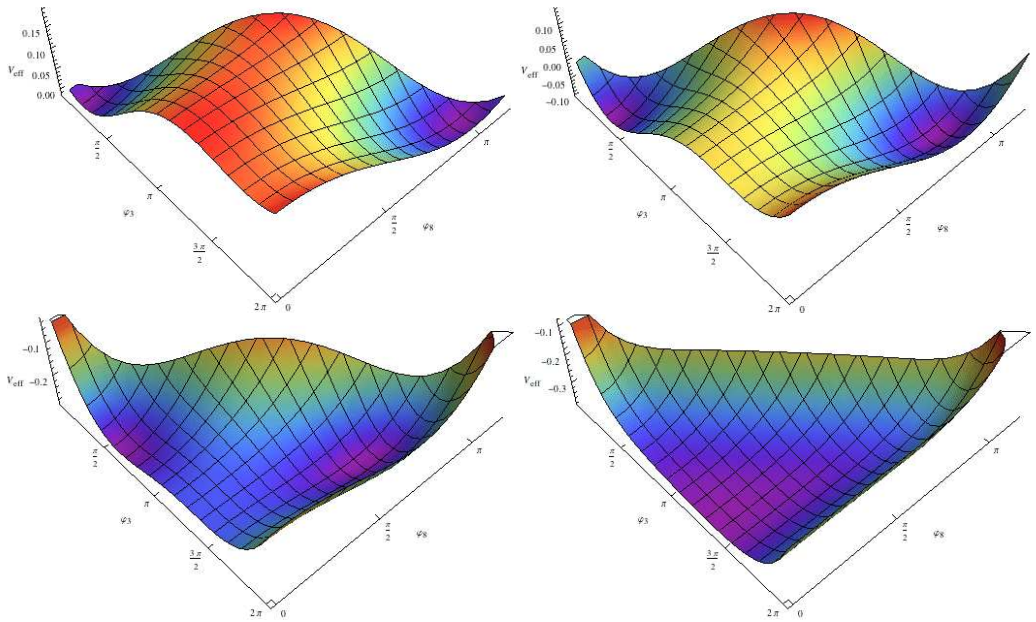

Figure 3.11: The effective potential plotted in one Weyl chamber for various values of the scale. From top left, to bottom right $\hat{k} = 18, 7, 5, 0$.

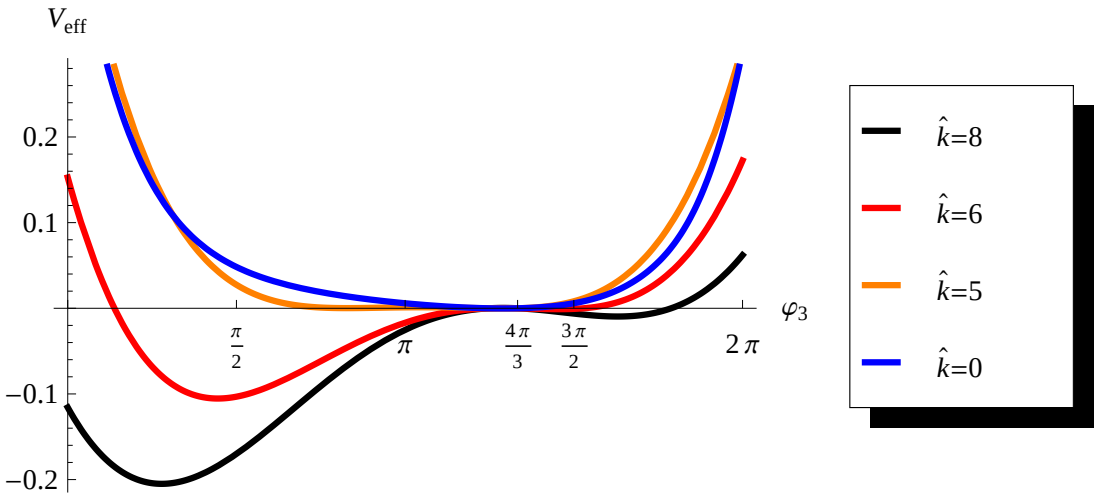

Figure 3.12: The effective potential on the slice $\varphi_8 = 0$ at $T = 200$ MeV.

4 QCD phase diagram

"Damit is der Käs gegessen"
Sprichwort

The QCD phase diagram has been an active area of research in the past two decades and it still is. Shortly after establishing QCD as the theory of strong interactions, it has already been argued, that hadrons, which consist of quarks and gluons, should dissociate at high temperatures or densities [3, 4]. This can be viewed as a prelude to the ideas of the quark-gluon plasma. From that time on a rich spectrum of other phase of strongly interacting matter has been conjectured and theoretically investigated.

Introduction

We want to investigate the properties of the deconfinement phase transition in the presence of a finite chemical potential and its relation to chiral symmetry breaking. This has been done in many phenomenological models, but still awaits a first principle calculation. Attempts to solve QCD at finite chemical potential on the lattice suffer from the notorious sign problem and are thus restricted to small chemical potential. Information about the phase diagram can be inferred using expansion techniques. Lattice QCD also faces problems in the investigation of the chiral phase transition, as on the lattice it is very difficult to impose chiral symmetry.

As a first approach towards the full QCD phase diagram, we investigate the confinement and the chiral phase transition in the presence of dynamical quarks without quark chemical potential. Once this is established, we can move to the next step and incorporate a finite chemical potential, which allows for a grip on the full phase diagram.

Of interest is also the relation between the chiral and the deconfinement phase transition, which has so far not been established. Most results on the lattice point towards a coincidence of the chiral and the deconfinement phase transition temperature, see e.g. Fig. 4. While lattice calculations are very precise, they do only provide limited insight into the physical mechanism at work. Therefore, the numerical coincidence of the phase transitions calls for further explanation.

Recently there has been a debate wheter the two transitions coincide or if the critical temperatures do not coincide in lattice simulations. While the Bielefeld group observes matching transition temperatures [88], the Wuppertal group on the other hand measures different transition temperatures [89].

So far, attempts to find an exact relation between the chiral and the deconfinement phase transition have sparked fruitful research, which lead to fruitful results. However, it

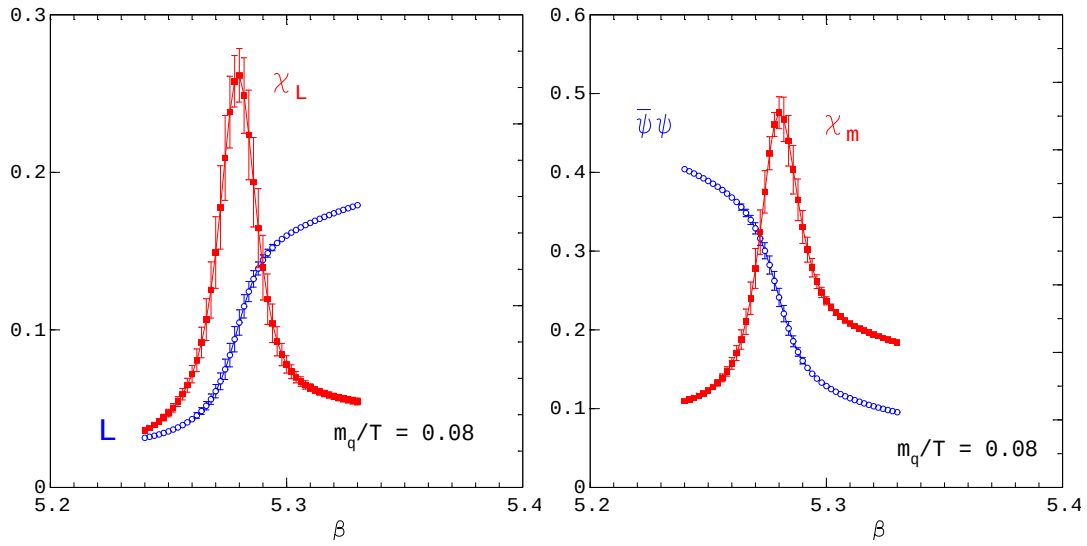

Figure 4.1: Polyakov loop (left) and chiral condensate (right), with their respective susceptibilities. Lattice data taken from [87]

was not possible to show a precise relation between the two phase transition temperatures. With our functional RG approach, we want to contribute to this ongoing debate.

We start with an investigation of the chiral transition, continuing with the deconfinement phase transition before investigating their interrelation.

4.1 Chiral Phase Transition

Our understanding of the nature of strong interactions in terms of QCD is that all hadrons are composite objects. These are build up from quarks and gluons, with masses dominantly generated by quark-gluon-dynamics. In simple models, chiral symmetry breaking can explain the emergence of the macroscopic hadron masses. The dynamically generated mass, the so-called constituent quark mass, of e.g. up-quarks in a non-perturbative treatment of QCD is about 1/3 of the proton mass. Thereby giving a glimpse at the mechanisms underlying the formations of hadrons. For the physics at hand, it is important to consider the transition from microscopic to macroscopic states [41, 49, 51, 90–93].

Current Status

The chiral phase transition in QCD has been investigated in various approaches. Predominantly in models like the well known (P)NJL model [94, 95]. and (P)QM models, but also employing the MIT bag model. We will introduce the NJL and the QM model shortly. The PQM and PNJL model are QM and NJL models supplemented with a potential for the Polyakov loop. The Polyakov loop is then coupled to the quarks by means of the covariant derivative leading to interesting results, for details see e.g. [96–106] The Polyakov

loop potential is usually taken from lattice calculations, ensuring the correct confinement phase transition temperature. Thereby the hard problem of describing confinement is taken out of the analysis and given to the lattice community.

A first calculation of the chiral phase boundary using functional renormalisation group techniques in one-flavour QCD has been performed in [18].We aim to improve this calculation for the zero temperature, finite density case, where quark fluctuations become important.

4.1.1 Dynamical Hadronisation

In a full treatment of QCD in a non-perturbative setting, the quark sector and the gauge sector feed back into each other non-linearly: the gluons generating quark self-interactions that can become the relevant interaction in the IR, where the theory is strongly coupled. Our analysis will make excessive use of this interaction, neglecting the complicated momentum structure, which could be generated by the gluons.

Eventually, we want to work with a quark-meson model, which has its roots in the Nambu-Jona-Lasinio (NJL) model. While not giving an exhaustive derivation of the quark-meson model from the NJL model, we want to outline the steps leading from one to the other. Particularly, we want to highlight, why it is useful for studying chiral symmetry breaking and its relation to confinement, as well as exploring the QCD phase diagram.

The NJL model is an extremely useful model for studying chiral symmetry breaking or other phenomena like colour superconductivity, whereas it lacks confinement. As it was originally conceived to model nuclear interactions of protons and neutrons this is not surprising as confinement was not an issue. The NJL model is in some sense complementary to the MIT bag model [107–109] which phenomenologically covers confinement, but violates chiral symmetry.

The pioneering idea of Nambu and Jona-Lasinio was to generate a mass gap in the Dirac spectrum analogously to the energy gap of a superconductor in BCS theory [25]. It was thereby possible to generate large masses, while keeping the Lagrangian free of a fermion mass and thus keeping it chirally symmetric.

Of course, the NJL model lacks confinement, which is a consequence of the neglect of gauge degrees of freedom. It has still been used to analyse many aspects of the QCD phase diagram. To include gauge dynamics, the NJL model can be extended with a confining potential for the Polyakov loop which couples to the quark fields. These so-called Polyakov NJL (PNJL) models have recently been applied successfully, see e.g. [104].

The action of the NJL model in the 2-flavour case is

$$S_{\mathrm{NJL}} = \int d^4x \left\{ \bar{\psi} \left(\mathrm{i}\partial\!\!\!/ + \mathrm{i}\gamma_0\mu \right) \psi + \frac{\bar{\lambda}_\psi}{2} [(\bar{\psi}\psi)^2 - (\bar{\psi}\gamma_5 \vec{\tau}\psi)^2] \right\} \tag{4.1}$$

with $\psi^T = (\psi_1, \psi_2)$ consisting of two fermion species and $\vec{\tau}^T = (\sigma_1, \sigma_2, \sigma_3)$, with σ_i being the Pauli matrices. The four-Fermi coupling $\bar{\lambda}_\sigma$ can be thought of as a remnant of gluonic interaction.

The generating functional for disconnected Green's function then reads

$$Z[\eta,\bar{\eta},J_0,\vec{J}]=\int\mathcal{D}\psi\mathcal{D}\bar{\psi}\exp\left(-S_{\mathrm{NJL}}+\bar{\eta}\psi+\bar{\psi}\eta+J_0(\bar{\psi}\psi)+\vec{J}\cdot(\bar{\psi}i\gamma_5\vec{\tau}\psi)\right) \tag{4.2}$$

The NJL model possesses particularly interesting symmetries for the investigation of the QCD phase diagram. The Lagrangian is invariant under vector (V) and axial-vector (A) rotations, the generators of which are defined by

$$U_V=\exp\left(i\vec{\tau}\vec{\Theta}\right)\quad\text{and}\quad U_A=\exp\left(i\gamma\vec{\tau}\vec{\Theta}\right), \tag{4.3}$$

where $\vec{\Theta}$ is a constant vector. The axial-vector transformations are the *chiral* transformations that we will put special emphasis on, an explicit mass term would destroy this symmetry. It can, however, still be broken dynamically by a vacuum expectation value of the chiral condensate $\langle 0|\bar{\psi}\psi|0\rangle$. This vacuum expectation value can be generated by vacuum fluctuations. According to Goldstone's theorem, there exist three massless pseudo-scalar excitations, that are not present in the NJL model action. Therefore, these must be excitations of the ground state. We have to find a method to incorporate these bound states into the theory.

Particularly when working with the fRG, the method of choice is (re-)bosonisation, in this context also know as dynamical hadronisation, which is precisely what we are aiming at. The procedure behind, the Hubbard-Stratonovich transformation [110, 111], introduces new scalar fields into the theory and trades quartic fermion interactions for mass terms of the scalars. Albeit this is at first a mathematical identity, the scalars acquire a physical meaning, i.e. in QCD they can be identified with (pseudo-) scalar mesons, the pions and the sigma meson. The pions can then be identified with the Nambu-Goldstone bosons related to chiral symmetry breaking. With this procedure, we naturally also generate a Yukawa interaction between fermions and bosons, which in turn regenerates the four-fermion interactions in the RG flow.

Formally the Hubbard-Stratonovic transformation can be implemented by multiplying the generating functional with a constant:

$$\exp\left(\int d^4x\frac{m^2}{h^2}(J_0^2+\vec{J}^2)\right)=\mathcal{N}\int\mathcal{D}\sigma\mathcal{D}\vec{\pi}\exp\left(-\int d^4x\frac{m^2}{2}(\sigma^2+\vec{\pi}^2)-\frac{m^2}{h^2}(J_0^2+\vec{J}^2)\right), \tag{4.4}$$

$\mathcal{N}$ is a normalisation constant, m and h are at this stage arbitrary constants. σ and $\vec{\pi}$ are auxiliary fields, to which we will give meaning later. Upon shiftig the variables of integration

$$\sigma\to\sigma-\frac{1}{h}J_0+\frac{h}{m^2}\bar{\psi}\psi\quad\text{and}\quad\vec{\pi}\to\vec{\pi}+\frac{1}{h}\vec{J}+\frac{h}{m^2}\bar{\psi}i\vec{\tau}\gamma_5\psi \tag{4.5}$$

the so-called bosonised action reads

$$S_{\mathrm{QM}}=\int d^4x\left\{\bar{\psi}\left(\mathrm{i}\partial\!\!\!/+\mathrm{i}\gamma_0\mu\right)\psi+\frac{m^2}{2}(\sigma^2+\vec{\pi}^2)+h\bar{\psi}(\sigma+i\gamma_5\vec{\tau}\vec{\pi})\psi\right\}. \tag{4.6}$$

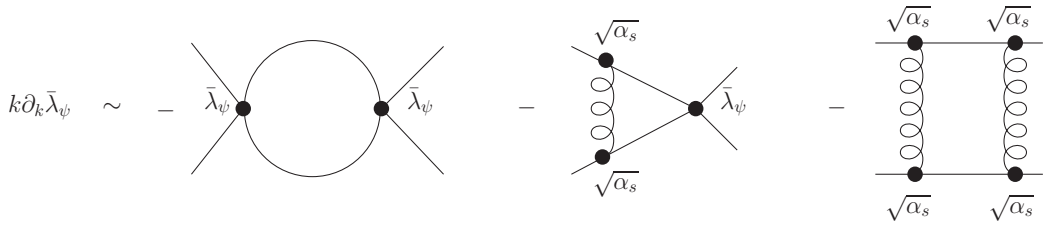

Figure 4.2: The flow equation of the four fermion coupling. Straight lines correspond to quark propagators, curly lines are gluons.

At this point, the auxiliary fields can be reinterpreted. In the action, we set $\bar{\lambda}_\psi = -h^2/m^2$. In the generating functional, we then have to rescale the source terms, which we do not explicitly display at this point. As advertised above, we now have the Yukawa interaction of strength h and a mass term with mass m for the scalar fields, which can be identified with the scalar meson and the Goldstone bosons - the pions - in low energy QCD.

To obtain a model of quarks and mesons, we only have to add a kinetic term for the meson fields that were previously auxiliary fields and a self interaction for the bosons. This can be conveniently parametrised by a potential U.

In the context of the fRG the Hubbard-Stratonovich transformation has to be upgraded with a procedure that keeps track of the four-fermion interactions, that are re-generated during the flow. The diagrams leading to this re-generation are shown in Fig. 4.2. They can be deduced from the model we introduce in the next section, see also [112]. There we already took into account, that we want to include gluons - at least partly - into our equations. Without gluons and starting from a bosonised theory, there would of course be no re-generation of the four-fermi coupling.

Within the our model, we aim at a vanishing four-fermi coupling and therefore have to bosonise this interaction. In first approximation these contributions can be neglected since they are small due to the large mass gap at small momentum scales. However, these contributions are essential for bridging the gap between the perturbative QCD sector and the low-energy limit of QCD.

If we think of the flow as being a series of discrete steps, it is obvious, that we have to bosonise at each step [49], such that the re-generated four-fermion interactions are always redirected into the boson sector. Starting from a completely bosonised action, the rebosonisation procedure ensures a vanishing four-fermi coupling throughout the flow. We have visualised this in Fig. 4.3. We conclude that the information from the four-fermion interaction can be conveniently stored in the bosonic sector.

In a flow equation approach, we can allow for four-fermi coupling along with a bosonised interaction. Applying the bosonisation technique we can allow for a coexistence of the sectors and a description in the appropriate degrees of freedom. As we will see below.

How does chiral symmetry breaking manifest itself in the quark-meson model? A quark mass term in S_{QM} arises, if σ acquires a vacuum expectation value, similar to the Higgs mechanism. Therefore, the boson potential must develop a non-trivial minimum,

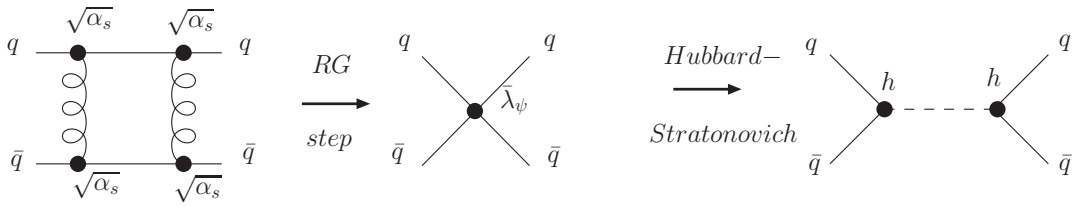

Figure 4.3: Dynamical hadronisation within the flow equation approach. Even for $\bar{\lambda}_\psi$ a four-fermi coupling is generated

i.e. the boson mass has to become negative. This, in turn, is equivalent to a diverging four-fermion coupling

$$\lambda_\psi = -\frac{h^2}{m^2} \to \infty. \tag{4.7}$$

In the bosonised theory, this corresponds to a vanishing boson mass, i.e. $m \to 0$. In the flow equation setting, this is a consequence of the running of the couplings with the scale. The scale at which the four-fermi coupling diverges, or in the rebosonised language, where the boson mass vanishes, is called chiral symmetry breaking scale k_{cr}. An example of the flow of the mass parameters is shown in Fig. 4.4 Fermions have the tendency to generate disorder due to the negative sign in the flow equation, i.e. they generate a non-trivial minimum in the boson potential. At large scales, we start with an unbosonized theory and the flow generates the boson fermion mass and thereby we eventually get chiral symmetry breaking.

4.1.2 The Model

Our analysis is based on the full QCD flow, including fermionic self-interactions that are generated by gluons. We also take bosonic terms into account representing mesons in the

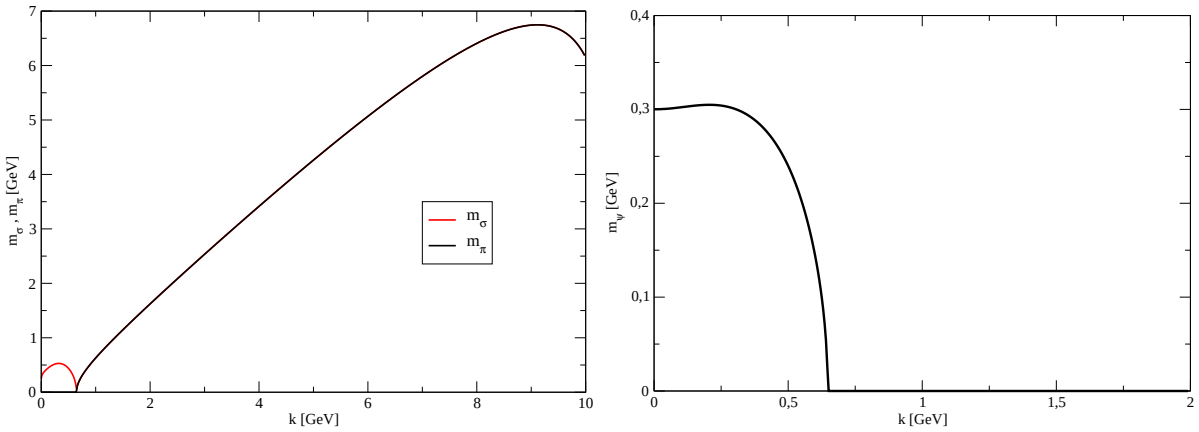

Figure 4.4: Flow of the masses, we clearly see the onset of chiral symmetry breaking

theory, as explained above. Note that we work only with one flavour, $N_f = 1$.

The truncation we use is similar to the one in [18], note that we do not work in Polyakov gauge as before, but in Landau gauge. Since we want to study the influence of the chemical potential and neglect the temperature for the moment, the integration is over all space-time, action consist of two contributions, the matter Γ_m and the gauge sector Γ_{YM}:

$$\begin{aligned}\Gamma_{\mathrm{m}} &= \int d^4x \left\{ \bar{\psi}\left(\mathrm{i}\not{D}[A] + \mathrm{i}\gamma_0\mu\right)\psi + \frac{\bar{\lambda}_\psi}{2}[(\bar{\psi}\psi)^2 - (\bar{\psi}\gamma_5\psi)^2] + \right. \\ &\qquad \left. \frac{1}{2}Z_\phi\left(\partial_\mu\Phi\right)^2 + U(\Phi^2) + \frac{\bar{h}}{\sqrt{2}}(\bar{\psi}(\vec{\tau}\cdot\Phi)\psi) \right\} \qquad (4.8) \\ \Gamma_{\mathrm{YM}} &= \int d^4x \, \frac{Z_{A_{QCD}}}{4} F^a_{\mu\nu}F^a_{\mu\nu} + \Gamma_{\mathrm{gauge}} \qquad (4.9)\end{aligned}$$

The term Γ_{gauge} contains contributions to the action which are not contained in the standard Yang-Mills term, such as ghosts or higher order terms in the gauge fields, that can be generated during the flow.

Since we work in 1-flavour QCD, there will be only one Nambu-Goldstone boson from chiral symmetry breaking, together with the scalar meson, we combine the two into the O(2) vector $\Phi^T = (\Phi_1, \Phi_2)$. Then we can write the Yukawa coupling term in a a compact form by means of $\vec{\tau} = (\gamma_5, \mathrm{i}\cdot\mathbf{1}_d)$. $U(\Phi)$ is the scalar potential, defined in [18] and Z_ϕ is the scalar wave function renormalisation. The first two terms describe quark dynamics and interactions, as know from the NJL model.

Note that there is a redundancy in this action, as the four-fermi coupling is related to the boson potential and the Yukawa coupling by a Hubbard-Stratonovich transformation. With the aforementioned re-bosonisation techniques which we apply in the following [41, 49, 50], we can use this to our advantage. We can initiate the flow at high scale with the appropriate high energy degrees of freedom, quarks and gluons. During the flow the mesonic degrees of freedom take over as we lower the scale. With this procedure we manage to describe strong interactions always in the degrees of freedom that give a good description of the physics at hand.

This model has successfully been applied in an investigation on the chiral phase boundary in 1-flavour QCD [18]. The curvature t_2 of the chiral phase boundary defined by

$$\frac{T_c(\mu)}{T_c(\mu)} = 1 - t_2\left(\frac{\mu}{\pi T_c(0)}\right)^2 + \cdots, \qquad (4.10)$$

was computed to a value of 0.97 when including global $U_A(1)$ symmetry and 0.4 with anomalously broken $U_A(1)$ symmetry.

Running coupling modifications

Before we solve the flow for these quantities, we discuss another very important quantity, particularly because it plays a crucial role in the investigation of the deconfinement phase transition: The running gauge coupling.

The running gauge coupling of QCD has been subject of many studies, particularly on the lattice and using functional methods like the fRG or DSEs. The behaviour of the running coupling in Landau gauge Yang-Mills theory is well established and has already been used in the previous chapter as an input into our calculation. There exists a vast literature on Landau gauge QCD, see e.g. [45, 46, 71, 72, 74–76, 83–85, 113–127].

Here we want to study its behaviour in the presence of a finite chemical potential. Obviously, a study of the full system of quarks and gluons is daring and not the scope of our work. Instead, we add the effect of the vacuum polarisation to the flow of the gluon wave-function renormalisation $Z_{A_{QCD}}$. The vacuum polarisation diagram is shown in Fig. 4.5.

Non-perturbative definitions of the strong coupling α_s hinge on the vertices. In most of the investigation the ghost-gluon vertex were used to the define the strong coupling, then it is given by a product of the wave function renormalisation of the ghosts and gluons. Due to the non-renormalisation theorem of the ghost-gluon vertex [72, 113, 128] in Landau gauge, the strong coupling can be defined in terms of the ghost and gluon propagator:

$$\alpha_s(p^2) = \frac{g^2}{4\pi} \frac{1}{Z_{A_{QCD}}(p^2) Z_C^2(p^2)}. \tag{4.11}$$

Other definitions of the running coupling are of course also possible and have been tested, four example the coupling defined by virtue of the four-gluon vertex [117]. They showed differences only in the low momentum regime, where the coupling does not influence hadron physics.

The propagators in Landau gauge YM have a very simple representation in terms of projectors and dressing functions. For the fRG setting, a detailed derivation can be found in [129], we state the result for the gluon propagator using a 4D optimised cut-off,

$$\begin{aligned} G_{AA}(p,k) &:= \left(\frac{\delta^2 \Gamma_k}{\delta A_\mu^a \delta A_\nu^b}(p) + R_{AA}(p,k) \right)^{-1} \\ &= \frac{1}{Z_A(p,k)} \Pi^t_{\mu\nu} \delta_{ab} \left(\theta(k^2 - p^2) \frac{1}{k^2} + \theta(p^2 - k^2) \frac{1}{p^2} \right), \end{aligned} \tag{4.12}$$

where $\Pi^t_{\mu\nu} = \delta_{\mu\nu} - \frac{p_\mu p_\nu}{p^2}$ is the transversal projector. At finite temperature, Lorentz symmetry is broken and it is advantageous to work with a 3D cut-off. The dressing

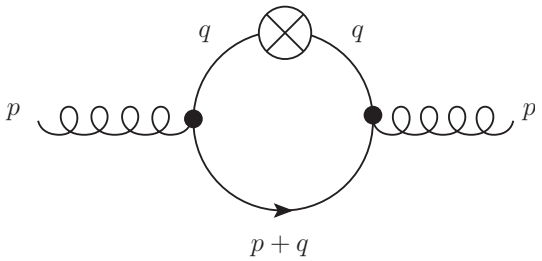

Figure 4.5: The vacuum polarisation diagram with regulator insertion

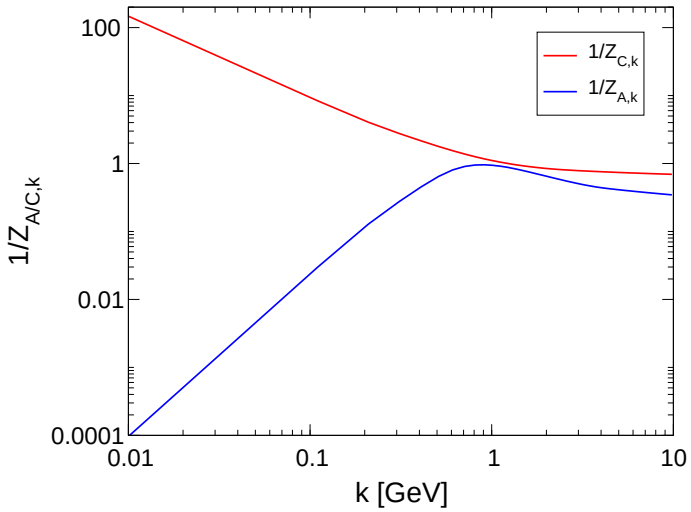

Figure 4.6: The gluon and ghost wave-function renormalisation functions Z_A and Z_C.

function for pure Yang-Mills theory for vanishing temperature and density, as computed e.g. in [71] are shown in Fig. 4.6

The flow of the wave function renormalisation $\Delta\dot{Z}_{A_{QCD}}$ of the gluons consists of a contribution from the ghost-gluon sector $\Delta\dot{Z}_{A_{YM}}$ and from the matter sector $\dot{Z}_{A_Q}$.

$$\partial_t Z_{A_{QCD}} = \partial_t Z_{A_{YM}}(p^2) + \dot{Z}_{A_Q}(m, \mu, k) \tag{4.13}$$

$\Delta\dot{Z}_{A_Q}$ is given by the quark loop displayed in Fig. 4.5, details of the calculation are found in App. C.1.

The logarithmic scale derivative of the gauge field wave function renormalisation, i.e. the anomalous dimension of the gauge field with contributions from quarks η_{A_Q} is given by:

$$\eta_{A_Q} = \partial_t \ln Z_{A_Q} = -\frac{g_k^2}{(4\pi)^2} 4 \cdot 16 \frac{k^3}{(k^2+m^2)^{\frac{3}{2}}} (1 - \theta(\mu - \sqrt{k^2+m^2})). \tag{4.14}$$

Here, we will use the approximation that $\dot{Z}_{A_Q}(p^2) = \dot{Z}_{A_{YM}}|_{p^2=k^2}$. This is a valid approximation as the scale derivative of the regulator ensures that the momentum integral receives only contributions around k^2,c.f. figure 2.2.

Let us discuss some properties of the anomalous dimension, as it will play an important role in the discussion of the results. It is proportional to the gauge coupling α_s, we will set $g_k^2/4\pi = \alpha_{s,k=0}(p^2 = k^2)$. As α_s is small in the UV and grows large in the IR, the largest contributions will come from the mid-momentum regime to the IR part of the flow.

For large fermion masses, the flow in the IR will be suppressed like $(k/m)^3$. As the fermion mass is generated in the IR part of the flow, we see already at this point, that there is a balance between the enhancement due to the coupling and a suppression due to the fermion masses.

Finally, the chemical potential μ comes into play via the step-function. For the step-function to be non-vanishing, the chemical potential has to be larger than the combination of the cutt-off scale and the fermion mass. Roughly speaking, this can only have an effect on the flow, when the chemical potential is of the order of the fermion mass. The quarks decouple then from the flow very early.

4.1.3 Results

Recent flow equation approaches towards chiral symmetry breaking in QCD were predominantly carried out in background field gauge [18, 76, 112]. We incorporated the scaling of the anomalous dimension into the flow equations for the scalar fields, the Yukawa coupling h, which occurs after bosonisation of a four-fermion vertex, and the four-fermion coupling λ_ϕ. The truncation yielded a space-like wave-function renormalisation η_ϕ and can be seen in [18].

This model is now extended through the replacement of the scale derivative of the field strength renormalisation in background formalism with $\Delta\dot{Z}_{A_Q}(m, \mu, k)$ derived above. The ghost and gluon propagators are obtained by using suitable fits from full Yang-Mills theory and lattice QCD [130]. The aim of our analysis is to find a relation between the chemical potential and the critical scale, which then yields a relation between the chemical potential and the chiral phase transition temperature.

The calculations are performed for a constant fermion mass, including a finite chemical potential. The initial conditions are fixed at the Z-boson mass scale of 90 GeV, as this corresponds to the perturbative regime and therefore the field strength renormalisations do not contribute. In this regime α_s is given by $\alpha_s(m_Z) \approx 0.118$ [131], the Yukawa coupling h by $h(m_Z) = 0.01$, and the four-boson coupling λ_ϕ by $\lambda_\phi = 0$. Note that the starting value of the Yukawa coupling is a free parameter and the results are independent of it [50].

For simplicity, the flow of the fermionic wave function renormalisation η_ψ, given by the self-energy diagrams of the fermion is neglected, i.e. we set $Z_\psi = 1$. It has been shown in other calculations, that this is a reasonable approximation, as the flow of Z_ψ is not very pronounced.

With the critical scale at vanishing chemical potential, we can set a relation between the temperature and the critical scale. Let us therefore first study, what happens at $\mu = 0$.

As explained above, we start at some high UV scale, where the theory can be treated perturbatively and we are in the chirally symmetric phase. Upon lowering the scale, the coupling strength α_s increases due to the gluonic self-interaction. When the coupling has grown large enough [1] , for the quarks to form bound states, they condense into these and chiral symmetry is spontaneously broken. This is reflected in the development of a non-trivial minimum in the bosonic potential U, as described above. The behaviour of the four-fermi coupling can nicely be visualised for different values of the coupling, see Fig. 4.7. For simplicity a constant coupling is assumed. The flow is based on the flow

[1] In the NJL model reflected by a diverging four-fermi coupling

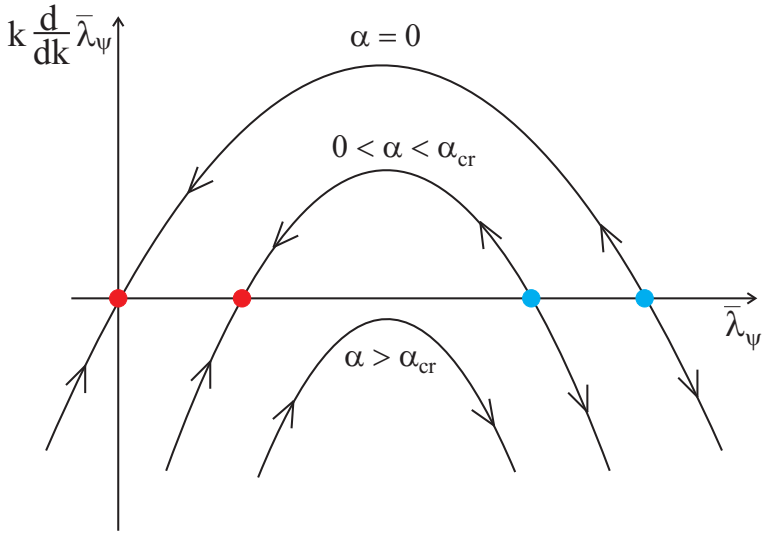

Figure 4.7: Fixed-point behaviour of the four-fermi coupling from Fig. 4.2, see also [76], for different values of the strong coupling. Arrows indicate the direction of the flow, i.e. decreasing the scale. Consequently red dots are IR fixed points, whereas blue dots are UV fixed points.

equation represented by Fig. 4.2.

When the strong coupling is zero, the flow always ends up at vanishing four-fermi coupling, as it should be, because the four-fermi coupling in the NJL model is generated by gluons. If their coupling vanishes, there should be no quark self-interaction. In the NJL model one can still observe chiral symmetry breaking by choosing a starting value of the four-fermi coupling larger than the UV fixed point. The effect of the gluonic interaction is to shift the flow trajectory downwards, allowing for a finite four-fermi coupling in the IR, until a critical coupling α_{cr} is reached. When increasing the strong coupling even further, there is no finite fixed point left and the flow always generates a diverging four-fermi coupling, signalling chiral symmetry breaking.

The fermionic flow increases the vacuum expectation value (VEV) of the bosonic potential, thereby increasing the dynamically generated fermion mass, which is proportional to $\langle\bar{\psi}\psi\rangle$. With increasing mass, the fermion propagator is more strongly suppressed.A large scales, k dominates the propagator. The further we lower the cut-off scale, the more the fermion mass has influence on the flow. At some scale, the strong dynamical chiral symmetry breaking generates a mass, that is large enough to decouple the quarks from the flow. The scale at which this happens is called freeze-out scale.

Below the freeze-out scale massless pion fluctuations drive the potential back towards the symmetric phase. It is the freeze-out scale, that determines, whether the theory turns back into the symmetric phase, or remains in the broken phase until the end of the flow. As we will see, the chemical potential has the largest impact on that.

Upon increasing the chemical potential μ, there is at first no significant change of the critical scale k_{cr}. This does not come unexpectedly. The chemical potential enters the

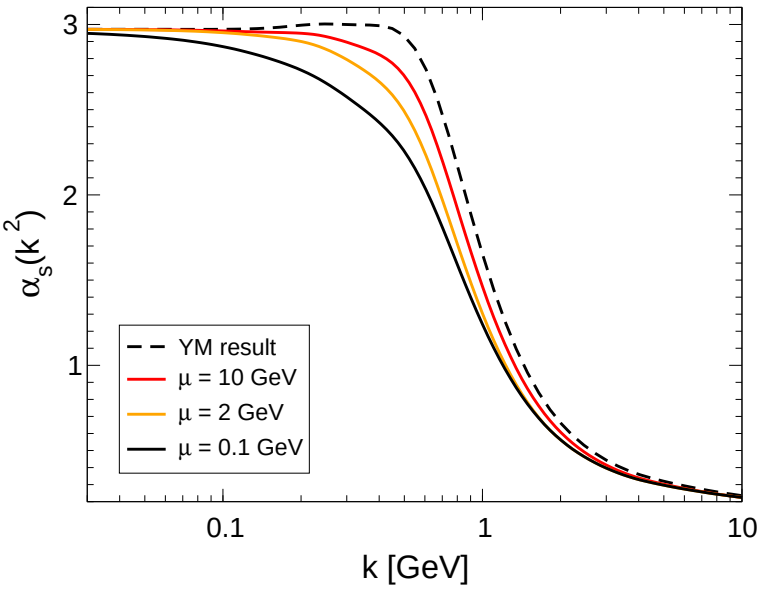

Figure 4.8: The dependence of the chemical potential on the running of the strong coupling α_s. With increasing μ the graph approaches the Yang-Mills result. However its dependence on μ is small. For $\mu > \mu_{cr}$ the fermions do not contribute to the flow.

flow only through the vacuum polarisation of the gluon, c.f. eq. (4.13) and eq. (4.14). As long as the chemical potential remains small compared to the fermion mass, or the cut-off scale, the modifications of the vacuum polarisation due to the chemical potential are small, the contribution comes only at the very end of the flow. Keep in mind, that the chemical potential does not have a direct influence on the chiral condensate, but only through the gluons.

By increasing the chemical potential further the vacuum polarisation is modified for longer RG-times during the flow. Thus the decoupling of the quarks occurs at larger scales in the flow. Eventually, we reach a chemical potential $\mu_{\rm cr}$, above which the bosons drive the theory back into the symmetric phase and chiral symmetry is restored again.

Let us now study these qualitative results in a little more detail and add some numerical results to it. We start with the running of the coupling α_s, defined from the ghost-gluon vertex, with the scale k, shown in Fig. 4.8. As mentioned, the initial conditions are fixed at the Z-boson mass scale m_Z. The dashed curve shows the behaviour of pure YM in Landau gauge [84, 122, 123]. We then see that the quark contributions to the anomalous dimension lower the value of the coupling. This is also observed perturbatively. We also observe that the modification in the mid-momentum regime become weaker with increasing chemical potential. This is not surprising, as the quarks decouple earlier, as explained above. In the IR α_s approaches the IR fix point behaviour of Landau gauge independent of μ. This is easily understood, as the vacuum polarisation switches off, once the cut-off scale falls below the chemical potential and we are left with the pure YM

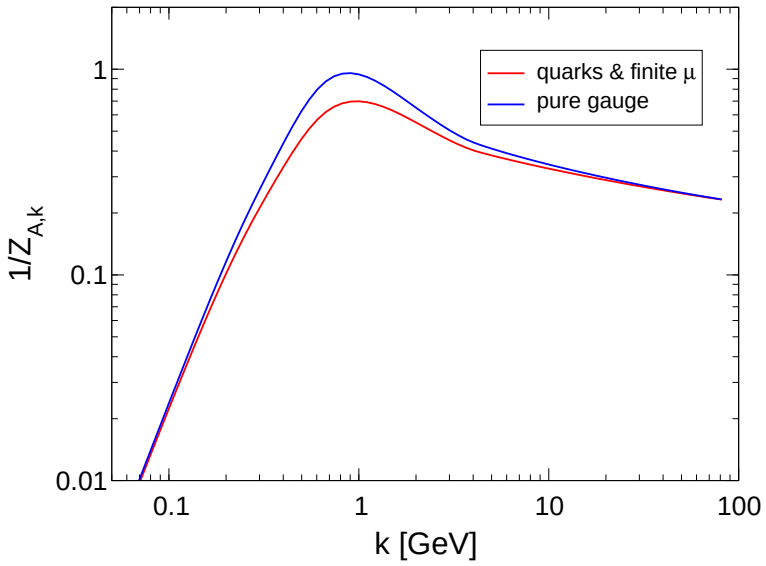

Figure 4.9: Plot of the dressing function of the gauge field versus k. The upper graph corresponds to the pure Yang-Mills solution, the lower includes quark contributions.

flow.

The behaviour of the strong coupling is reflected in the behaviour of the dressing function $1/Z_A$, see Fig. 4.9. In the perturbative regime the contributions of the polarisation vanishes with the coupling and approaches the pure gauge result. In the infrared, the fixed point behaviour dominates the flow and the changes induced by the vacuum polarisation become negligible.

In Fig. 4.10 we quantitatively see the feature of dynamical chiral symmetry breaking that we described above qualitatively: The quark mass increases rapidly below the chiral symmetry breaking scale and reaches a maximum. Then the evolution of the mass stops as the quarks decouple from the flow for scales smaller than the freeze-out scale.

Equally well, we can see the symmetry breaking scale in the plot of the boson masses in Fig. 4.11. With decreasing scale, we observe that also the boson mass decreases, at the chiral symmetry breaking scale k_{cr} it vanishes. Below the chiral symmetry breaking scale the massive excitation, the σ-meson becomes massive again.

Fig. 4.12 depicts the differences of the strong running coupling α_s with varying quark mass m_ψ at vanishing chemical potential.

The critical values we obtained for the chemical potential and the critical scale are $k_{cr} \approx 440$ MeV at $\mu = 0$ and μ_{cr} in between 350-400 MeV. This agrees with the values found in Dyson-Schwinger equations and other RG calculations [18].

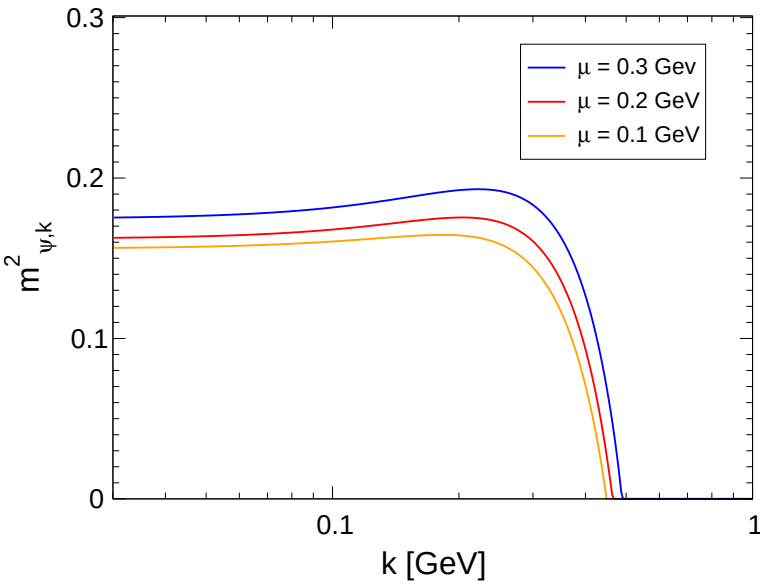

Figure 4.10: $m_\psi^2 = \bar{h}\langle\sigma\rangle$ as function of k for various μ. Up to a critical scale, no fermion mass is generated dynamically. This critical scale depends on the value of μ. k_{cr} is shifted to higher values for larger μ. At the maximum, the fermions decouple and hence the mass approaches to a constant.

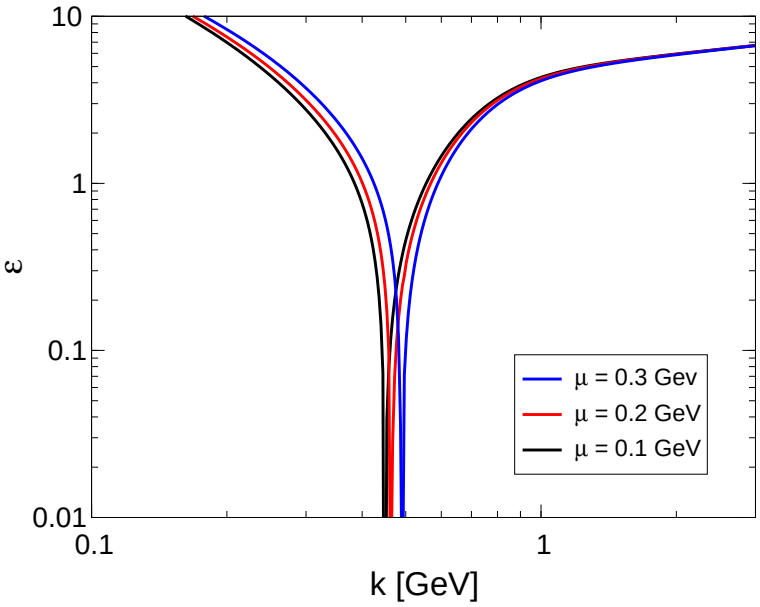

Figure 4.11: $\varepsilon = \frac{m_\phi^2}{Z_\phi k^2}$ as a function scale k where $m_\phi^2 = \frac{\partial^2 U}{\partial \Phi^2}\Big|_{\Phi_{min}}$. For increasing chemical potential the phase transition occurs at a higher critical scale.

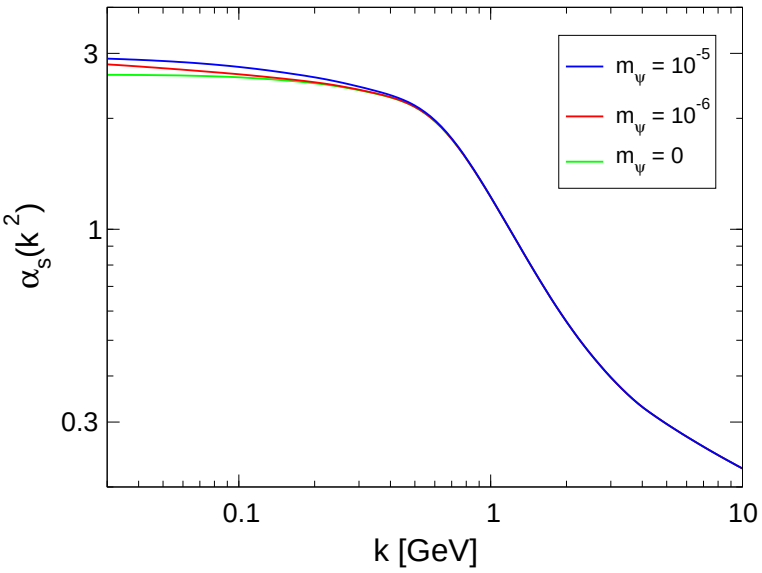

Figure 4.12: Plot of α_s versus k for massless quarks at $\mu = 0$. Different values of the dynamically generated fermion mass approach lower values of the IR fixed-points than the full Yang-Mills theory (compare values of fixed-points with plot 4.8). The fixed-points shown here correspond to the full QCD fixed-points.

4.2 Deconfinement Phase Transition

In earlier parts of this work we showed that within a simple truncation we can describe the deconfinement phase transition of Polyakov gauge Yang-Mills theory. Since gluons do not explicitly couple to the chemical potential, we have to extend our truncation and include dynamical quarks. This is interesting in its own right, as we can get a handle on the deconfinement phase transition in the entire QCD phase diagram. Moreover, the ideas developed in this section will play a role in the discussion of the relation between confinement and chiral symmetry breaking. There, we want to study the effects of quarks on the Polyakov loop potential, which is an important input into the calculation.

We can also study the phase transition behaviour of QCD for arbitrary quark masses and chemical potential. This can be used to map out the phase diagram in the quark mass directions. Related to these investigations is the search for the critical endpoint in QCD. The existence of a QCD critical point is still an active area of research and has not been settled. From the experimental side there is very little know about the critical endpoint, it is thus the hope to compute the location of the critical endpoint or the critical region theoretically, see e.g. [132], such that the experimental searches can be focused on a promising region. The standard view on this is, that there is a critical point as shown in Fig. 4.13. Albeit, recently it has been conjectured, that it might also be that the surface indicated there has another curvature and therefore there is no critical point. This matter is far from being settled, as from the theoretical side there are many uncertainties. Note that most of the investigations mentioned here focus on the chiral phase transition. We will give a discussion of the quark mass dependence of the deconfinement phase transition in our approximation. It is expected that the chiral and the deconfinement phase transition are closely related and the situation in both cases is similar.

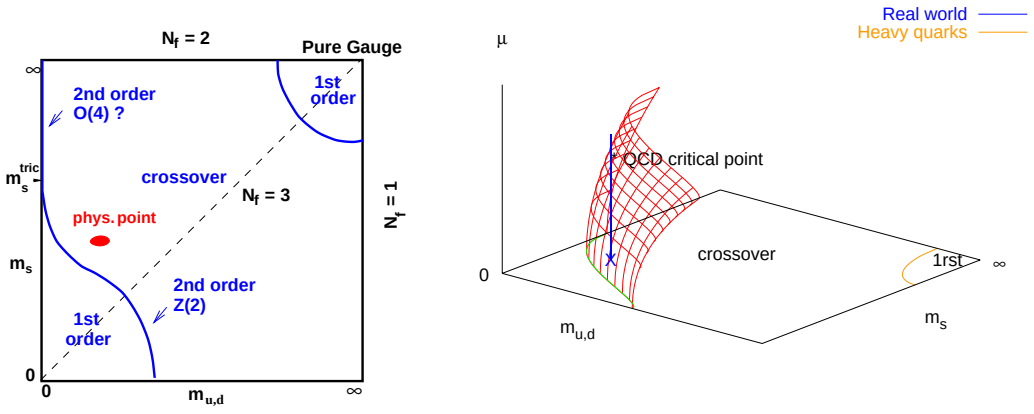

Figure 4.13: Schematic (chiral) phase transition behaviour in $SU(3)$ QCD for vanishing chemical potential with varying quark masses (left)[133]. Including chemical potential (right)[15].

We focus on the effect the quarks have on the gluons and neglect the backreaction of the gluons on the quarks. The backreaction is not a dominant effect for confinement, since confinement is generated in the gauge sector. The effect of the incorporation of quarks manifests itself in two instances. Remember that we had two crucial objects in the calculation of the full effective potential for Yang-Mills theory: the Weiss potential and the running gauge coupling. The Weiss potential is generated by the spatial gluons and is treated as an input. We include dynamical quarks in a similar fashion, by adding a quark determinant to the action. This will result in an additional contribution to the potential, which will obviously result in a modification of the phase transition temperature. Of course, at zero chemical potential with dynamical quarks, we expect a crossover rather than a phase transition and we will also observe this in our calculation. The second difference is that the gauge coupling will be modified in the presence of quarks. This can already be seen at the QCD β-function for the gauge coupling computed in perturbation theory

$$\beta_g = -\left(\frac{11N_c}{3} - \frac{2N_f}{3}\right)\frac{g^3}{16\pi^2}. \tag{4.15}$$

The N_f dependence comes with a different sign than the N_c dependence, i.e. the coupling is weakend by quark dynamics. In a non-perturbative treatment of QCD, e.g. using DSEs, fRGs or on the lattice, the amplitude of the gluon propagator is reduced particularly in the mid-momentum regime. As detailed before, a non-perturbative definition of the running coupling can be obtained from the gluon propagator. And we showed the influence of the quarks on the gauge coupling.

Neglecting backreactions of the gluons on the fermions implies, that we will be able to perform some calculations analytically.

4.2.1 Truncation

To include the quarks we add terms including fermionic operators to the effective action. For a full study of QCD with dynamical fermions this action includes a kinetic term with scale and momentum-dependent wave function renormalisation, scale dependent mass and vertex correction, as well as possible higher order corrections.

Here we resort to a simpler truncation, starting point is the action

$$\Gamma_\psi = \bar{\psi}(Z_\psi(D^2)i\not{D} + Z_m(D^2)m)\psi + O((\bar{\psi}\psi)^2) \quad \Rightarrow \quad \Gamma_\psi^{(2)} = Z_\psi(D^2)i\not{D} + Z_m(D^2)m. \tag{4.16}$$

In the presence of chiral symmetry breaking, we always have to compare momentum scales to the mass scale m_χ set by chiral symmetry breaking. We consider only momentum scales much smaller than m_χ, i.e. $(p/m_\chi)^2 \ll 1$. Therefore, we can assume momentum-independent wave function renormalisations, $Z_\psi(D^2) = Z_\psi(0) = Z_\psi$ and $Z_m(D^2) = Z_m(0) = Z_m$. We take the wave-function renormalisations to be field-independent. In the flow equation they can then be absorbed into the definition of a renormalised mass, such that we have $\Gamma_\psi^{(2)} = \not{D} + Z_m/Z_\psi m$. Furthermore, we have

$$\mu\frac{d}{d\mu}\left[\frac{Z_m}{Z_\psi}m\right] = 0. \tag{4.17}$$

This means, that this is a physical quantity and we can identify it with the physical mass.

It is now simple to write down the effective action. We work in $SU(2)$, which is a good model system to set up our method. In Polyakov gauge, i.e. setting any component of the gauge field except A_0^3 to zero, the action in momentum space reads

$$\Gamma_\psi^{(2)} = -(\not{\vec{p}} + \gamma_4(\omega_n + gA_0^3\sigma^3)) + m\,, \tag{4.18}$$

with fermionic Matsubara frequencies $\omega_n = \pi T(2n+1)$ and we introduced the notation $\not{\hat{p}} := \not{\vec{p}}/|\vec{p}|$. For the cut-off we impose the requirement that it has chiral properties, since we do not want to introduce any artificial chiral symmetry breaking, except due to the current quark mass. To be consistent with our preceding calculation, we choose a regulator function which is of the form as the one used for the spatial gluons. Therefore, the regulator is

$$R_\psi = -(k\not{\hat{p}} - \not{\vec{p}})\theta(k^2 - \vec{p}^2). \tag{4.19}$$

Now the inversion of the propagator is straightforward. The fermionic contribution to the flow equation reads

$$\mathrm{Tr}[(\Gamma_\psi^{(2)} + R_\psi)^{-1}\partial_t R_\psi] = \mathrm{Tr}\left[(-(k\not{\hat{p}} + \gamma_4(\omega_n + gA_0^3\frac{\sigma^3}{2})) + m)^{-1}(-k)\not{\hat{p}}\theta(k^2 - \vec{p}^2).\right] \tag{4.20}$$

Upon taking the trace only the term proportional to $\not{\hat{p}}^2$ survives. The color eigenvalues of σ^3 are $\{-1, 1\}$. The result of the trace in Dirac space is 4. The momentum integral is done analytically, resulting in a factor $k^3/(6\pi^2)$, and we are left with the following result for the trace

$$\begin{aligned}\mathrm{Tr}[(\Gamma_\psi^{(2)} + R_\psi)^{-1}\dot{R}_\psi] &= 4\cdot 2\frac{4\pi}{(2\pi)^3}\frac{k^3}{3}k^2\sum_{n=-\infty}^{\infty}\frac{1}{k^2 + ((2n+1)\pi T + gA_0^3/2)^2 + m^2} \\ &= \frac{2k^5}{3\pi^2}\frac{\beta}{\sqrt{k^2+m^2}}\frac{\sinh(\beta\sqrt{k^2+m^2})}{\cos(\varphi/2) + \cosh(\beta\sqrt{k^2+m^2})},\end{aligned} \tag{4.21}$$

which we can easily incorporate into our flow equation for the effective potential of A_0. It leads to a modification of the critical temperature depending on the current quark mass.

This result is very similar to the one obtained for the Weiss potential. When neglecting the fermion mass, the only difference is, that the period of the potential is changed. The Weiss potential has a period of 2π, whereas the potential generated by the fermions has period of 4π. This is a consequence of the different representation of the gauge group $SU(2)$, that quarks and gluons live in. Note that fermions in the adjoint representation would generate a potential having the same periodicity as the gluonic potential.

We rush to add that the incorporation of a chemical potential is not difficult. In the action, the term stemming from the chemical potential can be absorbed into the zero component of the Dirac operator. Therefore, we only have to perform the correct substitution for the Matsubara frequencies. The inclusion of the chemical potential can schematically be done in the following way:

$$\bar{\psi}(-i\not{D})\psi \to \bar{\psi}(i\not{D} + i\mu\gamma_4)\psi \quad \Rightarrow \quad \omega_n \to \omega_n + i\mu, \tag{4.22}$$

where ω_n are fermionic Matsubara frequencies.

Including the fermionic flow into the flow of the Polyakov loop potential is not difficult, we merely have to add the fermionic contributions. In our truncation we choose the quarks not to be coupled to the gluon sector, but to only include the effect the quarks have on the gauge sector. Therefore, the flow equation schematically reads:

$$\partial_t V = \mathrm{Tr}[(\Gamma_A^{(2)} + R_A)^{-1}\dot{R}_A] + \mathrm{Tr}[(\Gamma_\psi^{(2)} + R_\psi)^{-1}\dot{R}_\psi] \tag{4.23}$$

The first part of the flow equation can now be written as in Sec. 3.1, such that the flow is precisely the one given in eq. (3.29), plus the contribution stemming from the fermionic term. This contribution, we call it $\dot{V}_\psi$, to the flow can be computed analytically and we can absorb it into the flow of the Weiss potential $V_\perp$. Therefore, we simply shift $\Delta\tilde{V} = \Delta V + V_\psi$ and redefine $\tilde{V}_\perp = V_\psi + V_\perp$. Upon renaming the potentials, we are left with the flow equation for the effective potential

$$\partial_{\hat{k}}\Delta\hat{V} = -\frac{1}{6\pi^2}\left(1 + \frac{\eta_0}{5}\right)\frac{g_k^2\,\partial_\varphi^2\,(\hat{V}_\perp + \Delta\hat{V})}{1 + \frac{g_k^2}{\hat{k}^2}\partial_\varphi^2\,(\hat{V}_\perp + \Delta\hat{V})}\,. \tag{4.24}$$

As in the calculation of the Polyakov loop in pure gauge theory, we need to specify the running gauge coupling as input. It is here, where the modifications of the YM coupling, discussed in the previous section come into play. Of course, we have to make sure that there is no double counting of contributions, as the fermions already have an effect on the effective potential via the fermion determinant introduced in the flow. But the contribution of the quarks to the running coupling are an effect, that is certainly not included by including the determinant, this can be seen upon considering the diagrams contributing to the flow of the gauge coupling. The coupling we employ is almost the same as the coupling depicted in Fig. 3.5, except for the mid-momentum regime, where the influence of the quarks reduces the coupling strength, as found in the previous section.

4.2.2 Results

The calculation of the flow of the effective potential $\hat{V}_{eff}$ in the presence of dynamical quarks is very similar to the computation in Chap. 3. Therefore, we discuss only the changes induced by the quarks.

First of all the quarks generate an additional potential $\hat{V}_{\psi,\hat{k}}$. Fig. 4.14 shows the result for various values of the cut-off scale on the left panel. On the right panel we show the difference induced by the quark mass. We observe, that the potential $\hat{V}_{\psi,\hat{k}}$ gradually builds up during the flow and that it is stronger, i.e. more deconfining, for smaller quark masses.

The phase transition is shown in Fig. 4.15 for various fermion masses on the left panel. We nicely see, that now instead of a phase transition, we get a crossover, as it is expected. In a theory with dynamical fermions, the Polyakov loop is strictly speaking not an order parameter, but we can still use it to define a transition temperature by the maximum of the susceptibility of the Polyakov loop. We observe, that for larger quark masses, the

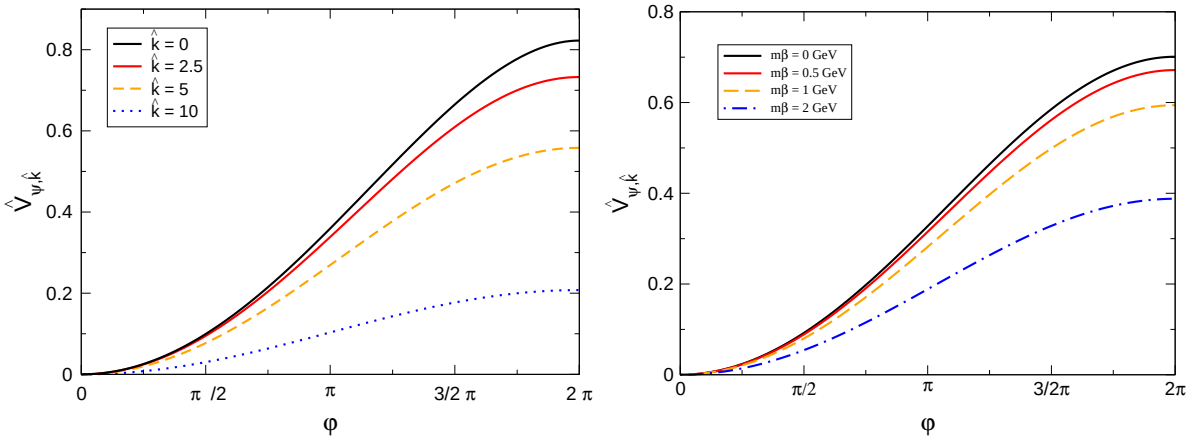

Figure 4.14: The potential generated by the fermions for different values of the cut-off scale (left). For fixed cut-off scale and varying quark mass (right).

transition becomes steeper. We conclude that for $m_\psi \to \infty$ we recover the second order phase transition that we got in pure gauge theory.

The resulting crossover temperature as a function the fermion mass is displayed in Fig. 4.15 on the right panel. We nicely see, that for $m_\psi \to \infty$ we recover the transition temperature, that we found in the previous chapter.

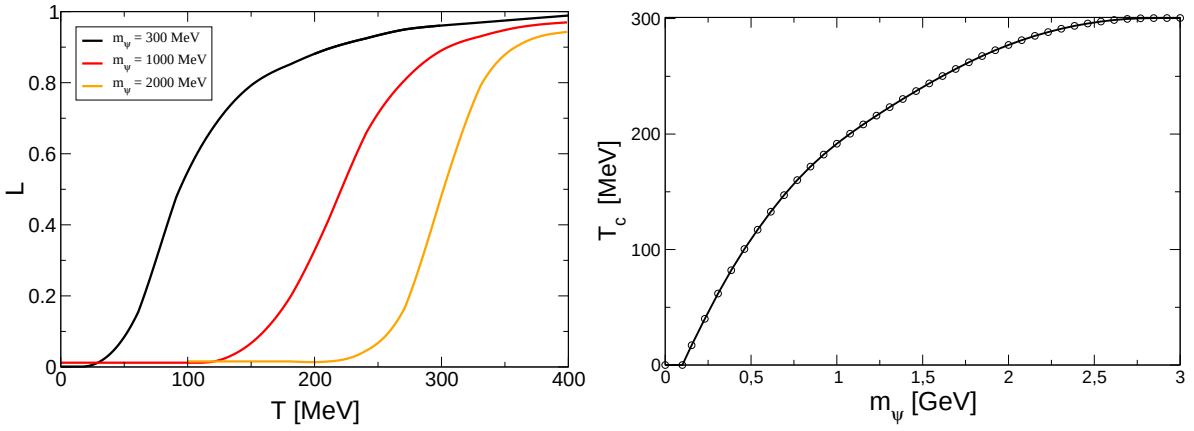

Figure 4.15: The crossover for various quark masses (left). The crossover temperature as a function of quark mass(right).

4.3 Relation Between Confinement and Chiral Symmetry Breaking

In the previous sections we focused on computing the order parameters for confinment and chiral symmtry breaking directly. Now we want to establish a relation between the two. As both phenomena are generated in different sectors of QCD, this is of course not a simple task and no analytical proof linking the two corresponding transition temperatures has been found.

Recently a relation between the two has been proposed by Gattringer [134] in a groundbreaking article, finding a connection between the dressed Polyakov loop and the dual chiral condensate on the lattice. While this is no direct relation between the two physical phenomena, it is worth exploring this relation.

In Chap. 3 we showed that not only the expectation value of the Polyakov loop is an order parameter for confinement, but also the Polyakov loop evaluated with the expectation value of the gauge field. With the same arguemen, it follows immediately that *any* observable which transforms non-trivially under center transformations, serves as an order parameter of confinement. This has been exploited in [134], and to full extend in [135, 136] for devising other order parameters for confinement. It has been shown in [134] how to relate the spectral properties of the Dirac operator to the expectation value of the Polyakov loop. In [137] the dual chiral condensate has been defined, and it has been shown that it also relates to the expectation value of the Polykov loop. A further generalisation has been put forward in [135, 136]. There it has been proven that *any* function $f(\lambda)$ of the spectral values of the Dirac operator serve as order parameter of confinement, if integrated over all possible fermionic boundary conditions and spectral values. Here we provide a shortened version of the arguments.

Within an fRG approach using a model of QCD similar to the model used in Chap. 4.2 we compute observables for confinement and chiral symmetry breaking. We can and have extended the model in various directions, including the effects of the quark dynamics on the gluons, which give additional contributions to the dual density. We were also able to relate the dual density to the Polyakov loop, which is also nicely reflected by the numerical results, giving a numerical check of the analytic findings.

Phase transformed fermions

Let us first give an introduction into the formalism of phase transformed fermions. The key to our results are the different transformation properties of fermion fields and gauge fields under center transformations. While a center transformation is a symmetry transformation of the gauge sector, the periodicity properties of the fermionic field changes upon applying the gauge transformation eq. (2.33). We deduce for the gauge transformed fermion field $\psi^U = U\psi$,

$$\psi^U(t+\beta,\vec{x}) = -z\psi^U(t,\vec{x})\,, \quad \text{with} \quad \beta = \frac{1}{T}\,, \tag{4.25}$$

for fermions with anti-periodic boundary conditions $\psi(t+\beta,\vec{x}) = -\psi(t,\vec{x})$. U_z are center transformations.

The question arises how we can use eq. (4.25) for a construction of observables that are sensitive to center transformations. This is easily done by considering more general boundary conditions for the fermion fields. It leads to the definition of phase transformed fermion fields. The defining property is given by the generalised boundary condition

$$\psi_\theta(t+\beta,\vec{x}) = -e^{2\pi i\theta}\psi_\theta(t,\vec{x}) \tag{4.26}$$

with $\theta = 0$ reproducing the standard antiperiodic boundary conditions of fermions in thermal field theory. It includes eq. (4.25) with the center phases $z = \mathbb{1}e^{2\pi i\theta_z}$. In $SU(2)$ the center elements are $\mathbb{1}_2$, $-\mathbb{1}_2$ and hence $\theta_z = 0, 1/2$, in $SU(3)$ the center elements are $\mathbb{1}_3$, $e^{2\pi i/3}\mathbb{1}_3$, $e^{4\pi i/3}\mathbb{1}_3$, and hence $\theta_z = 0, 1/3, 2/3$ for $\theta \in [0, 1)$.

The boundary condition (4.26) is easily implemented by

$$\psi_\theta(t,\vec{x}) = e^{i2\pi\theta t/\beta}\psi_{\theta=0}(t,\vec{x}) \quad \text{with} \quad \psi_{\theta=0} = \psi, \tag{4.27}$$

where ψ obeys the standard antiperiodic boundary conditions for fermions, with $\psi(t+\beta,\vec{x}) = \psi(t,\vec{x})$. Using this property, (4.26) is obviously fulfilled.

We can express an arbitrary function f of the Dirac operator $i\not{D}$ standing between phase transformed fermion fields in terms of antiperiodic fermion fields by means of the identity

$$\bar{\psi}_\theta f(i\not{D})\psi_\theta = \bar{\psi} f(i\not{D} - 2\pi\frac{\theta}{\beta}\gamma_0)\psi \tag{4.28}$$

With the use of this identity, we can write down an action for the phase transformed fermions. We choose a standard kinetic term for fermions. The action is then given by

$$S_D[\psi_\theta,\bar{\psi}_\theta,A] = \int d^4x\bar{\psi}_\theta(i\not{D}+m)\psi_\theta = \int d^4x\bar{\psi}(i\not{D} - 2\pi\frac{\theta}{\beta}\gamma_0 + m)\psi \tag{4.29}$$

Next we define the generating functional of phase transformed fermions. For brevity, we will use the collective variable $\Phi_\theta = (A, c, \bar{c}, \psi_\theta, \bar{\psi}_\theta)$ with the appropriate source J in our definition:

$$Z_\theta[J] = \int D\Phi \exp(-S_D[\Phi] + \int d^4x J\cdot\Phi). \tag{4.30}$$

The action in eq. (4.29) is the Dirac action with an imaginary chemical potential $\mu = 2\pi i\,\theta/\beta$. Imaginary chemical potential is of interest for lattice simulations, as the fermion determinant becomes real and importance sampling is still viable. With lattice simulations at imaginary chemical potential and an analytic continuation of the results towards real chemical potential, one aspires to gain access to the QCD phase diagram. The situation is depicted in Fig. 4.16, where also the Roberge-Weiss (RW) discontinuity [138], ending in an endpoint is depicted. It is still unclear if and how the Roberge-Weiss discontinuity merges with the chiral phase transition. The Roberge-Weiss discontinuity only arises in the deconfined phase, where center symmetry is broken. For a discussion of this point see Ref. [139]. Let us analyse how this discontinuity arises in our theory of phase

transformed fermions. If θ takes one of the center values θ_z, we can define $\psi^{U_z} = \psi_{\theta_z}$ with U_z as defined in eq. (4.25). We conclude with

$$\int \bar{\psi}_{\theta_z} \left(i\not{D}(A) + m \right) \psi_{\theta_z} = \int \bar{\psi} \left(i\not{D}(A^{U_z^\dagger}) + m \right) \psi \,, \tag{4.31}$$

that center phases θ_z can be absorbed in center transformations of the gauge field. As we know from the investigation of the gauge sector of QCD center symmetry is a symmetry of the gauge sector. Therefore, the action has the Roberge-Weiss periodicity [138], see also [139],[140], this is also a manifest symmetry of the generating funtional at vanishing source:

$$Z_\theta[0] = Z_{\theta+1/N_c}[0] \,. \tag{4.32}$$

This symmetry can be broken only in a non-center symmetric (deconfining) ground state, leading to the Roberge-Weiss discontinuity. We will come back to this point later, as a symmetry of the generating functional is also a symmetry of the effective action, we have to make sure that this symmetry is implemented in the flow equation. We will make sure that our flow, which we will use to compute the dual observables, respects the Roberge-Weiss periodicity.

Now we are in a position to define the flow of the phase transformed fermions. Moreover, this enables us to define order parameters for the confinement phase transition, such as the dual density, that we define in the next subsection. These quantities will allow us to analyse the relation between the chiral and the deconfinement phase transition.

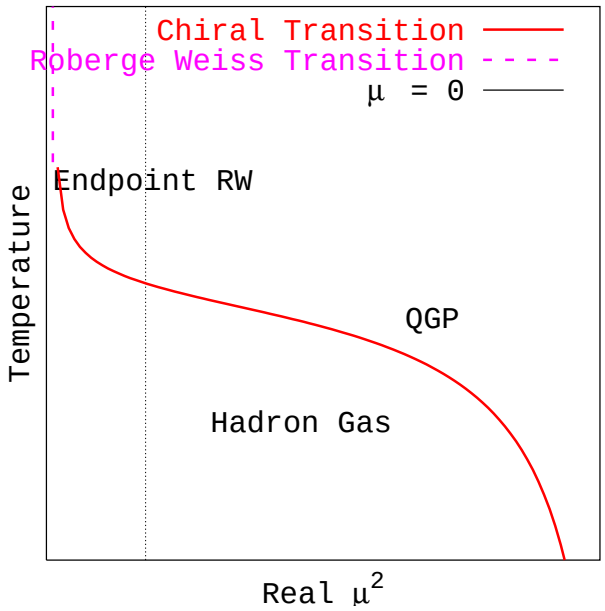

Figure 4.16: The phase diagram in the T, μ^2 plane taken from [139]. Lattice simulations are possible in the $\mu^2 \leq 0$ halfplane, physical results in the region of $\mu^2 \geq 0$ have to be inferred by an analytic continuation.

4.3.1 Dual Observables

Before studying the flow of the dual density and other dual observables, let us analyse some of the general properties of these.

From eq. (4.26) it is obvious, that the theory is periodic in θ, therefore, general observables $\mathcal{O}_\theta = \langle \mathcal{O}[\psi_\theta] \rangle$ can be represented in a Fourier decomposition,

$$\mathcal{O}_\theta = \sum_{l \in \mathbb{Z}} e^{2\pi i l \theta} O_l \,. \tag{4.33}$$

This implies that the dual observables O_l transforms under a gauge transformation in the center U_z into $z^l O_l$. Hence, in the center symmetric phase every moment O_l with $l \in \mathbb{Z}$ and $l \bmod N_c \neq 0$ has to vanish, as it is proportional to a sum over center elements z,

$$\sum_{z \in \mathcal{Z}} z^l = N_c \, \delta_{l \bmod N_c, 0} \,. \tag{4.34}$$

The above observables $\mathcal{O}_\theta$ can be either evaluated in QCD with anti-periodic fermions ψ, or in QCD$_\theta$ with fermions ψ_θ having θ-dependent boundary conditions. The first case was considered in previous work [134–137, 141], in which case the $\mathcal{O}_\theta$ constitute observables in the physical theory as do the dual observables O_l. Note that the definition $\mathcal{L}_\theta = e^{2\pi i \theta} \langle L \rangle$ reflects the boundary condition eq. (4.26). It fits into the definition of dual observables and it is a natural extension of the Polyakov loop defined before.

In this work we mainly concentrate on the case of QCD$_\theta$. Where we can interpret the phase as an imaginary chemical potential, $\mu = 2\pi i \, \theta / \beta$ as explained above. Then, the observables $\mathcal{O}_\theta$ constitute observables in *different* theories differentiated by the boundary conditions or imaginary chemical potential.

We conclude that the dual observables O_l with $l \mod N_c \neq 0$ only vanish if QCD$_\theta$ is in the center symmetric phase for all boundary conditions. Within the quenched approximation this reduces to the first case, as there are no dynamical quarks, therefore there is no imaginary chemical potential discriminating the theories.

We shall also show that the *physical* transition temperature $T_c(\theta = 0)$ is a lower bound for $T_c(\theta)$. Thus the dual phase transition temperature $\tilde{T}_c$, derived from an observable O_l, is expected to be identical with the physical one. In summary, the moments O_l with $l \mod N_c \neq 0$ are order parameters for the confinement phase transition in the physical theory in both approaches. In particular the first moment is an order parameter for all N_c,

$$\tilde{\mathcal{O}} = \int_0^1 d\theta \, e^{-2\pi i \theta} \mathcal{O}_\theta \,. \tag{4.35}$$

At imaginary chemical potential $\mathcal{O}_\theta$ obeys the RW-symmetry if the source term of the generating functional vanishes. Then it is easy to see that the dual observable vanishes:

$$\int_0^1 d\theta \, e^{-2\pi i \theta} \mathcal{O}_\theta = \int_0^{1/N_c} d\theta \, e^{-2\pi i \theta} \mathcal{O}_\theta \sum_{k=0}^{N_c - 1} z^k = 0, \tag{4.36}$$

where we used $\mathcal{O}_{\theta+\theta_z} = \mathcal{O}_\theta$ and the fact that the sum over all center elements z vanishes. Therefore, the dual observables at vanishing source vanish identically. In turn, a non-vanishing current J_A for the gauge field breaks the RW-symmetry, and leads to $O_l \neq 0$ for $l \mod N_c \neq 0$. This leads us to a simple and easily accessible confinement order parameter in QCD_θ, the dual density:

$$\tilde{n}[\phi_J] := \int_0^1 d\theta\, e^{-2\pi i\theta} n_\theta[\phi_J] \tag{4.37}$$

with $\phi_J = \langle\phi\rangle_J$, i.e. the field expectation values are evaluated at a non-vanishing source $J_A \neq 0$. The density n_θ is the derivative of the partition function w.r.t. the chemical potential $2\pi\,\theta/\beta$,

$$n_\theta[\phi_J] = \int d^4x\, \langle\bar{\psi}\gamma_0\psi\rangle_\theta = \frac{\beta}{2\pi}\partial_\theta \ln Z_\theta[J]\,. \tag{4.38}$$

The integration over space-time is equivalent to evaluating the generating functional in momentum space at $p = 0$.

Flow of the dual observables

Let us turn to computing the dual observables using functional methods. In [141] it has been shown how to compute the dual chiral condensate from functional methods, i.e. from Dyson-Schwinger equations (DSE). We want to use another approach, the fRG. Its advantage is that it provides expressions for the *renormalised* effective action. Consequently renormalisation problems as present within the lattice computations as well as the DSE computation, are absent here. The central quantity of the fRG is the effective action, consequently, we want to relate the dual observables to the effective action. Then the above expectation values are taken at fixed $\phi_J = \langle\phi\rangle_J$. At the example of the dual density, we illustrate the procedure. We observe, that n_θ is trivially related to the effective action $\Gamma_\theta[\phi_J] = J\cdot\phi_J - \ln Z[J]$:

$$n_\theta[\phi_J] = \frac{\beta}{2\pi}\frac{\partial}{\partial\theta}\ln Z_\theta[J] = \frac{\beta}{2\pi}\frac{\partial}{\partial\theta}(\ln Z_\theta[J] - J\cdot\phi_J) = -\frac{\beta}{2\pi}\frac{\partial}{\partial\theta}\Gamma_\theta[\phi_J]. \tag{4.39}$$

For the dual density we can perform an integration by parts, simplifying the equation significantly:

$$\tilde{n}[\phi_J] = -\frac{\beta}{2\pi}\int_0^1 d\theta e^{-2\pi i\theta}\frac{\partial\Gamma_\theta[\phi_j]}{\partial\theta} = -i\beta\int_0^1 d\theta e^{-2\pi i\theta}\Gamma_\theta[\phi_J]. \tag{4.40}$$

We used the fact that the effective action is periodic in θ: $\Gamma_1[\phi_J] = \Gamma_0[\phi_J]$. In other words, the dual density is proportional to the first moment of the grand canonical potential at imaginary chemical potential.

Similarly, we find for the dual chiral condensate an expression in terms of the effective action:

$$\tilde{\sigma}[\phi_J] = -\int_0^1 d\theta\, e^{-2\pi i\theta}\partial_m\Gamma_\theta[\phi_J]\,. \tag{4.41}$$

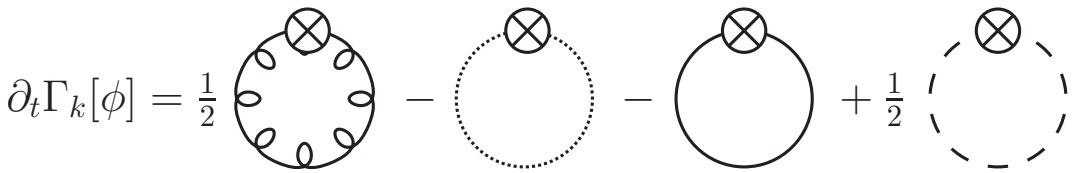

Figure 4.17: Functional flow for the effective action. Filled circles denote fully dressed field dependent propagators. Crosses denote the regulator insertion $\partial_t R$. This flow includes also the contributions of the mesons, indicated by the dashed lines.

Eq. (4.40) links the dual density $\tilde{n}$ to the grand canonical potential, therefore, we can easily read off its growth at high temperatures. The integrated θ-dependence is expected to be leading order in T. The grand canonical potential rises with T^4, and hence the dual density $\tilde{n}$ rises with T^3.

Having all dual observables expressed in terms of the effective action, it is simple to compute the dual observables by means of the flow equation. We get a flow of the dual observables by applying a scale derivative on the dual observables. The boundary condition of the flow is simply that the dual observable vanishes. Diagrammatically the flow of the effective action is shown in Fig. 4.17

Remember that the effective action retains all the symmetries of the generating functional. The source term is related to the effective action by $J = \delta\Gamma\theta[\phi]/\delta\phi|_{\phi=\phi_J}$ and $\bar{\phi}_\theta = \phi_{J=0}$. Therefore, the dual density evaluated at the expectation value of the fields vanishes $\tilde{n}[\bar{\phi}_\theta] = 0$, as explained above.

The flow of the dual density is given by

$$\partial_t \tilde{n}[\phi_J] = -i\beta \int_0^1 d\theta e^{-2\pi i\theta}\, \dot{\Gamma}_\theta[\phi_J]. \tag{4.42}$$

Note that $\partial_t \tilde{n}[\phi_J]$ is directly proportional to the flow depicted in Fig. 4.17.

We emphasise that this is an important property as the direct use of the flow for the effective action is least sensitive to the approximations involved. Moreover, the dual density guarantees the maximal disentanglement of the different field sectors as is obvious from the diagrammatic representation Fig. 4.17: the explicit change of introducing θ will only affect the fermionic loop, as the Matsubara freuqencies are shifted by $\mu = 2\pi\beta\theta$. As we shall see, this can be seen as a minor correction to the $\theta = 0$ behaviour. Then, the back-coupling to the gauge field loop will be sub-leading. The correction from the ghost loop is even more suppressed, as there is no direct (classical) coupling between quark and ghost. We conclude that in a first, but already good, approximation, the dual density is dominated by the quark loop. This has far-reaching consequences. The quark propagator has only a mild momentum dependence, and is in leading order is only sensitive to the chiral properties of the theory. In other words, if the dual condensate shows a cross-over or a phase transition, it can only be induce by the chiral cross-over or phase transition. Therefore we can already deduce that, at vanishing real chemical

potential, the confinement-deconfinement phase transition can only manifest itself in the dual density at the chiral critical temperature or below. Our explicit computation will show that this is indeed the case. We rush to add that in the case of a cross-over this strictly speaking only implies, that *one* of the possible definitions of the confinement-deconfinement temperature has this property.

We provide a further heuristic argument why at vanishing chemical potential this tightly relates the chiral and the confinement-deconfinement transition $T_{c,\chi}$ and $T_{c,\mathrm{conf}}$ respectively. To that end we concentrate on the Polyakov loop. In pure Yang-Mills with $N_c = 2, 3$ the transition temperature $T_{c,\mathrm{conf}}$ is roughly $3/2$ of $T_{c,\mathrm{conf}}$ in QCD with dynamical quarks. However, the chiral transition suppresses the quark loops and reduces the dynamics to that of pure Yang-Mills. Consequently the confinement-deconfinement transition has to follow at least closely to the chiral transition.

The flow representation allows to deduce some interesting properties of the dual density. First we show that our approach is manifestly invariant under the Roberge-Weiss transformation. Furthermore, we show that the dual observables can be related to the Polyakov loop, showing a close relation of these to confinement.

For the analytical arguments it is sufficient to use constant mean gauge field configurations A_0 in the Cartan subalgebra. For example, for $N_c = 3$ we have Cartan fields $\varphi_3 = \beta g A_0^3$ and $\varphi_8 = \beta g A_0^8$, that we encountered already in the computations of the deconfinement phase transition in $SU(3)$. The θ-dependence of the effective action $\Gamma[\phi]$ has its roots in the summation over fermionic Matsubara frequencies that we encounter in the zero component of the Dirac operator and the imaginary chemical potential $iD_0 - 2\pi T\theta$:

$$iD_0 - 2\pi T\theta = \omega_n + gA_0^a T^a - 2\pi T\theta \mathbb{1}_{N_c}. \tag{4.43}$$

Most of the θ-dependence can be reabsorbed in a θ-dependent gauge field $A_0(\theta)$. Details of the calculation can be found in App. C.2. After some algebra we are led to

$$(iD_0 - 2\pi T\theta)_{aa} = 2\pi T\left(n + \frac{1}{2} + \frac{1}{4\pi}\Phi_a - N_c\delta_{a1}\theta\right), \quad a = 1, ..., N_c\,. \tag{4.44}$$

were Φ_a are the eigenvalues of the matrix $2\beta g A_0(\theta)$ and the summation convention is *not* applied. In the Cartan there are no color matrices with non-vanishing off-diagonal components, thus there are also no off-diagonal components of the Dirac operator zero component in color space. For $N_c = 3$ we have $\Phi[\hat{\varphi}]$ having diagonal components

$$\Phi_1 = \frac{\hat{\varphi}_8}{\sqrt{3}} + \hat{\varphi}_3\,, \quad \Phi_2 = \frac{\hat{\varphi}_8}{\sqrt{3}} - \hat{\varphi}_3\,, \quad \Phi_3 = -2\frac{\hat{\varphi}_8}{\sqrt{3}}\,, \tag{4.45}$$

where $\beta g A_0(\theta) = \hat{\varphi}_3\tau^3 + \hat{\varphi}_8\tau^8$ with Gell-Mann matrices τ_3, τ_8. The $\hat{\varphi}$ are defined to be invariant under Roberge-Weiss transformatinons, they are given by

$$\hat{\varphi}_3 = \varphi_3 - 3(2\pi\beta)\theta \quad \text{and} \quad \hat{\varphi}_8 = \varphi_8 - \sqrt{3}(2\pi\beta)\theta. \tag{4.46}$$

Inserting the $\hat{\varphi}$ in eq. (4.44) we get back the original parameterisation of the fermionic Matsubara frequencies. The $\hat{\varphi}$, and hence the Φ_a, are invariant a Roberge-Weiss transformation, i.e. under shifts of the phase by a center phase and accompanied by shifts of

the gauge fields:

$$\theta \to \theta + \theta_z \quad , \quad \varphi_3 \to \varphi_3 + 3(2\pi\beta)\theta_z \quad , \quad \varphi_8 \to \varphi_8 + \sqrt{3}(2\pi\beta)\theta_z. \tag{4.47}$$

The latter is a center transformation $U_z^\dagger$ on the gauge field, see eq. (4.31) and leaves the action invariant. The shift of the full Matsubara frequencies eq. (4.44) under the above transformation can be undone with an appropriate shift of n. We conclude that any expansion scheme based on the field variables $\hat{\varphi}$ is form-invariant under $\theta \to \theta + \theta_z$. The same holds true for the observables $\mathcal{O}_\theta[\bar{\phi}_\theta]$ that are also invariant under this transformation. Consequently, the dual observable vanishes $\tilde{\mathcal{O}}[\bar{\phi}_\theta] = 0$. In turn, observables $\tilde{\mathcal{O}}[\phi]$ with θ-independent gauge field background φ are order parameters for confinement as such a background explicitly breaks the RW-symmetry. In particular this includes $\tilde{\mathcal{O}}[\phi]$ with $\varphi = \bar{\varphi} = \bar{\varphi}_{\theta=0}$ and $\varphi = 0$.

Simple observables $\tilde{\mathcal{O}}[\phi]$ follow directly from the vertices $\Gamma^{(n)}[\phi]$ in QCD$_\theta$. This includes the dual density eq. (4.40) as well as the dual chiral condensate with $\mathcal{O}_\theta[\phi_J] = \int d^4x \, \langle \bar{\psi}_\theta \psi_\theta \rangle_J$ for either $\varphi_J = \bar{\varphi}_{\theta=0}$ and $\varphi_J = 0$. The first case with $\bar{\varphi}$ relates to the lattice computations in QCD of dual order parameters [134, 135, 137]. The latter choice has been used implicitly in [141, 142]. An even simpler observable is the dual quark mass parameter $\tilde{\mathcal{M}}$ with $\mathcal{M}_\theta[\phi] \sim \mathrm{Tr}\, \Gamma^{(2)}_{\bar{\psi}\psi}[\phi](p=0)$. The specific choice $\mathcal{M}_\theta[\bar{\phi}_\theta]$ is directly related to the pion decay constant f_π in QCD$_\theta$. A further prominent example is the modified Polyakov loop variable $L_\theta = e^{2\pi i\,\theta} L$,

$$L_{-\theta}[\varphi] = \frac{1}{N_c} \sum_{i=1}^{N_c} e^{2\pi i \left(\frac{1}{4\pi} \Phi_i[\hat{\varphi}] + N_c \delta_{i1} \theta \right)} . \tag{4.48}$$

with $\mathcal{L}_\theta = \langle L_\theta \rangle$. $L_{-\theta}$ is invariant under $\theta \to \theta + \theta_z$ at fixed $\hat{\varphi}$, and hence $\tilde{\mathcal{L}}[\bar{\phi}_\theta] = 0$. However, $\tilde{L}[\bar{\varphi}] = L[\bar{\varphi}]$ simply is the Polyakov loop variable introduced in [23, 56] as an order parameter for confinement.

The representation of the Polyakov loop in eq. (4.48) leads to an interesting observation: in phase-quenched QCD$_\theta$ we are left with the explicit θ-dependence in the Matsubara frequencies eq. (4.44). Thus, any observable $\tilde{\mathcal{O}}$ in eq. (4.35) obeys

$$\tilde{\mathcal{O}}[\phi] = \int_0^1 d\theta \, e^{-2\pi i \theta} \mathcal{O}_\theta[0] L[\varphi] = \tilde{\mathcal{O}}[0] \, L[\varphi] \, , \tag{4.49}$$

for θ-independent gauge field background φ and vanishing quark and mesonic backgrounds. In fully dynamical QCD$_\theta$ the factorisation eq. (4.49) only holds approximately. For general φ_θ such as $\bar{\varphi}$ in QCD$_\theta$ this factorisation does not happen. However, in unquenched QCD we can use eq. (4.49) to measure the importance of the respective quantum fluctuations with

$$\Delta_{\mathcal{O}} = \frac{\tilde{\mathcal{O}}}{\tilde{\mathcal{O}}[0]} - L[\bar{\varphi}] \, , \qquad \Delta_{\mathcal{O}}[\varphi] = \frac{\tilde{\mathcal{O}}[\phi]}{\tilde{\mathcal{O}}[0]} - L[\varphi] \, , \tag{4.50}$$

for $\mathcal{O} = n$ or $\mathcal{O} = L$. For the latter case we have $\Delta_{\tilde{L}} = \tilde{L} - L[\bar{\varphi}]$ and $\Delta_{\tilde{L}}[\bar{\varphi}] = \tilde{L}[\bar{\varphi}] - L[\bar{\varphi}]$. We emphasise that the relations eq. (4.49) and eq. (4.50) are valid in both approaches

with and without imaginary chemical potential. Without chemical potential we have $\Delta_n = \Delta_n[\bar{\varphi}]$.

4.3.2 Approximation

We solve the flow equation for the effective action Γ within an approximation that is very similar to the one used in Chap. 4.1. For our study of two flavour QCD in the chiral limit, we solve the flow equation for the effective action Γ by combining results for the Yang-Mills part of QCD [56, 71], as well as the matter part [18, 50, 63]. The two sectors are coupled by the dynamical quark-gluon interaction. This setting incorporates the confining properties of QCD [56] via the full momentum dependence of gluon and ghost propagators [71]. The results for pure Yang-Mills agree quantitatively with the corresponding lattice results. In the matter sector mesonic degrees of freedom are dynamically included [18, 50, 63]. Such a treatment of the matter sector already provides quantitatively reliable results for the meson spectrum, see e.g. [63]. It has been also successfully implemented for the phase diagram of one flavour QCD at finite chemical potential [18].

In this approximation the flow of the density is governed by the equation

$$\begin{aligned}\frac{\dot{n}_\theta[\phi_J]}{T^3} &= \frac{8v_3}{3}\left(\frac{k}{T}\right)^4\left(\frac{1}{\sqrt{k^2+m_\sigma^2}}\left(\frac{1}{2}+n_B^{(\theta)}(m_\sigma)\right)+\frac{(N_f^2-1)}{\sqrt{1+m_\pi^2}}\right.\\ &\left.\left(\frac{1}{2}+n_B^{(\theta)}(m_\pi)\right)-\frac{2N_cN_f}{\sqrt{1+m_q^2(\theta)}}\left(\frac{1}{2}-n_F^{(\theta)}(m_\pi)\right)\right)+\frac{\dot{n}_{\theta,YM}[\phi_J]}{T^3},\end{aligned} \tag{4.51}$$

where n_B and n_F denote the standard bosonic and fermionic distribution functions, respectively. Note that m_π and m_σ are θ-dependent. While the fermion loop depends explicitly and implicitly on θ, the meson and gluon loop depend only implicitly on θ through fermionic contributions to their propagators. We have indicated the contribution from the gauge sector by the last term.

In order to compute the dual density, we expand the chiral order-parameter potential $U(\Phi^2)$ in a power series of Φ^2 up to order Φ^4 and drop all higher terms, i. e. $U(\Phi^2) = U_0 + (1/2)m^2\Phi^2 + (\lambda/4)\Phi^4$. Consequently, the expansion coefficients of the (chiral) order-parameter potential depend on θ as well. The RG flow equations for these couplings are straightforward generalizations from the RG equations in the case $\theta = 0$ which can be found elsewhere, see e. g. Ref. [18].

The gluonic contributions to the flow of the dual density is given by the the first two terms in Fig. 4.17. When neglecting backreactions of the quarks on the gluons, the integrated flow of these terms leads along the lines of [56] to the effective potential of the Polyakov loop. Since we evaluate our equations at the expectation values of the Polyakov loop, it will yield the value of the potential at the expectation value of the Polyakov loop. As we know, the potential obeys Roberge-Weiss symmetry manifestly. Therefore, upon integrating over the phase θ, this contribution to the dual density vanishes.

Including the vacuum polarisation gluons, we get a non-vanishing contribution, if we evaluate the vacuum polarisation for θ-independent ϕ. The inclusion of the vacuum po-

larisation modifies the gluon propagator, we split the propagator into the YM propagator in Landau gauge and an additional term. Thereby putting us into a position to split the gluonic contribution in the well-know vanishing part explained above and a non-vanishing part. The splitting of the propagator is similar to Chap. 4.2, c.f. eq. (4.12) and (4.13). The difference in this section is that the chemical potential is now imaginary and we work at finite temperature. Using the 3D optimised regulator , we obtain for the quark loop contribution [18]

$$\eta_{\mathrm{q}}(m_\psi,\tilde{t},\tilde{\mu}) = \frac{N_f}{\sqrt{1+m_\psi^2}}\left(1-\frac{1}{1+\mathrm{e}^{\frac{\sqrt{1+m_\psi^2}-\tilde{\mu}}{\tilde{t}}}}-\frac{1}{1+\mathrm{e}^{\frac{\sqrt{1+m_\psi^2}+\tilde{\mu}}{\tilde{t}}}}\right)\frac{4}{3}\frac{g^2}{(4\pi)^2}\,, \tag{4.52}$$

eq. (4.14) is the limiting case of this equation vanishing for vanishing temperature. $m_\psi = h\kappa$ denotes the dimensionless quark mass, which is a parameter that varies during the flow. We observed before, that we can identify the chemical potential here with the phase θ via the relation $\mu = i2\pi\beta\theta$.

Now we want to introduce our truncation of gluonic part of the flow equation that allows for a splitting of the contributions. Therefore we start with the 4D optimised regulator for Landau gauge YM, given by

$$R_{\mathrm{YM},k} = \left(\Gamma^{(2)}_{\mathrm{YM},k}(k^2) - \Gamma^{(2)}_{\mathrm{YM},k}(p^2)\right)\theta(k^2-p^2), \tag{4.53}$$

this cut-off entails also a cutting of the Matsubara frequencies. Then the inverse propagator is, c.f. also eq. (4.12) for the full expression of the propagator,

$$\Gamma^{(2)}_{\mathrm{YM},k}(p^2) + R_{\mathrm{YM},k} \;=\; \left[\Gamma^{(2)}_{\mathrm{YM},k}(k^2)\right]\theta(k^2-p^2) + \Gamma^{(2)}_{\mathrm{YM},k}(p^2)\theta(p^2-k^2). \tag{4.54}$$

The scale derivative of the cut-off would now be consist of various contributions. We want to resort to a simpler approximation that has proven to give good result. The truncation being that we identify the scale dependence with the momentum dependence $\partial_t\Gamma_k(p) \simeq \partial_t\Gamma_0(k)$ such that the scale-derivative of the propagator is simply given by

$$\partial_t R_{\mathrm{YM},k} = \partial_t\left(\Gamma^{(2)}_{\mathrm{YM},0}(k^2)\right)\theta(k^2-p^2). \tag{4.55}$$

Therefore, we have eliminated the momentum dependence of the propagator in the flow, $\partial_t\left[\Gamma^{(2)}_{\mathrm{YM},0}(k^2)\right]$ is related to the quark loop contribution after projecting onto the dressing function is given by

$$\frac{\partial_t\Gamma^{(2)}_{\mathrm{YM},0}(k^2)}{Z_A} \sim \frac{\dot{Z}_A}{Z_A} = \eta_A = \eta_{\mathrm{YM}} + \eta_{A,q}, \tag{4.56}$$

where Z_A is the dressing function appearing in $\Gamma^{(2)}_{YM,0}$. Then the first contribution together with the ghost term results in the Polyakov loop potential, as explained above and gives no contribution to the dual density. In contrast, the second term gives a non-vanishing contribution to the dual density. However, we found that the dual density is not very sensitive to this modification, the deviations are at the percent level.

4.3.3 Results

In Fig. 4.19 the temperature dependence of two order parameters for confinement are shown, namely the Polyakov loop variable $L[\bar{\varphi}]$ and the dual density $\tilde{n}[\bar{\phi}]$. The crossover temperature $T_{\rm conf}$ is determined by the peaks in the respective T-derivatives χ_L and $\chi_{\rm dual}$. Interestingly the factorisation eq. (4.49) works quantitatively for the dual density in the full theory: $\tilde{n}[\bar{\phi}]/\tilde{n}[0]$ and $L[\bar{\varphi}]$ agree on the percent level. This is shown in Fig. 4.18. We have checked further order parameters such as the dual pion decay constant. We find that the crossover temperatures extracted from the dual density, the dual pion decay constant and the Polyakov loop agree within a few MeV: $T_{\rm dual} \approx T_{\rm conf} \approx 178\,{\rm MeV}$. This provides further support for the quantitative reliability of the present approximation.

In Fig. 4.19 we also show the pion decay constant f_π. It is proportional to the quark mass parameter $\mathcal{M}_\theta$ evaluated at $\bar{\phi}_\theta$, and is an order parameter for the chiral phase transition. For $T \to 0$, f_π approaches 90 MeV. For $T > T_\chi \approx 181\,{\rm MeV}$ the pion decay constant tends to zero and chiral symmetry is restored. We observe a second order phase transition, and the critical exponents such as ν signal the $O(4)$-universality class. Most importantly, the chiral phase transition and the confinement crossover temperature agree at vanishing chemical potential. We have also shown the behaviour with phase and temperature of the pion decay constant and the density in Fig. 4.22.

An evaluation of the dual chiral condensate and the dual quark mass parameter in QCD$_\theta$ for vanishing gauge field background $\varphi = 0$ has been implicitly performed in [141] and [142] respectively. Evaluated at both, 0 and $\bar{\varphi}$, we find the expected periodicity of $\tilde{M}$ in $\theta \to \theta{+}1$, and no RW-symmetry. For $\theta = 1/2$ it can be shown analytically that it grows with $T^{1/2}$ for large T. In turn, for $\theta = 0$ and $\varphi = \bar{\varphi}_{\theta=0}$ it agrees with f_π and vanishes for large T, see Fig. 4.19. Below the chiral phase transition temperature T_χ the mass

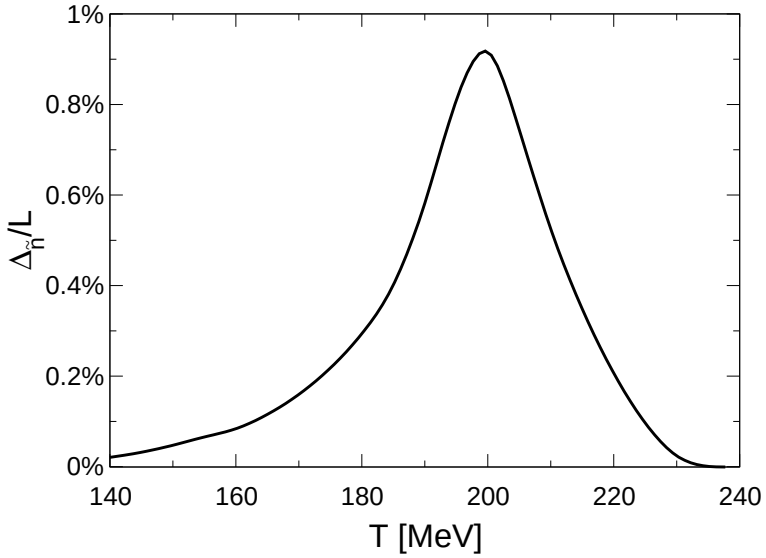

Figure 4.18: Deviation from the factorisation.

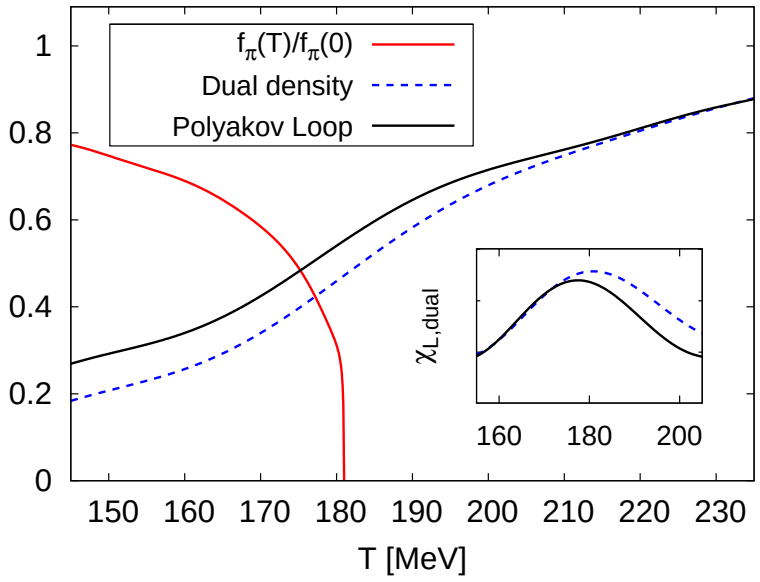

Figure 4.19: The pion decay constant $f_\pi(T)/f_\pi(0)$, the dual density $\tilde{n}(T)/\tilde{n}(\infty)$, and the Polyakov loop $L[\bar{\varphi}](T)$ as functions of temperature, $\chi_L = \partial_T L$, $\chi_{\text{dual}} = \partial_T \tilde{n}$.

parameter $\tilde{\mathcal{M}}$ is a smooth function of θ. However, a box-like behavior emerges above T_χ, see also [142]. For our calculation, this is shown in Fig. 4.20. We note, that $\mathcal{M}_\theta[\phi]$ is an expansion parameter of the effective action which only signals chiral symmetry breaking for $\phi = \bar{\phi}_\theta$.

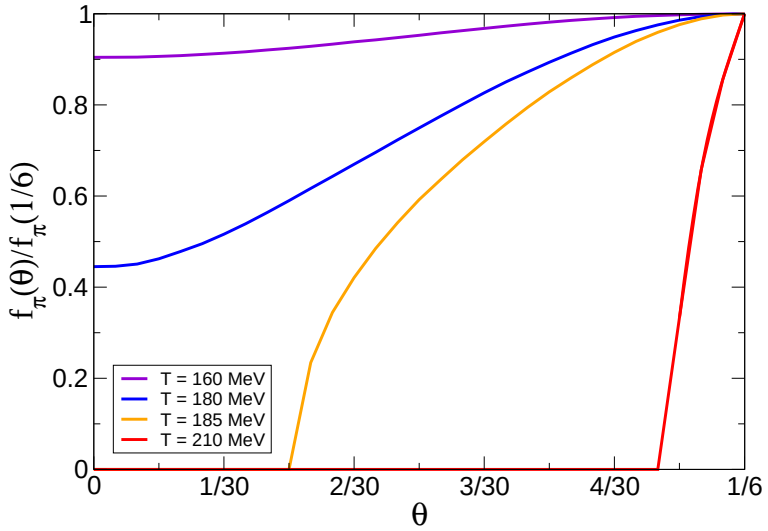

Figure 4.20: Pion decay constant f_π for various temperatures

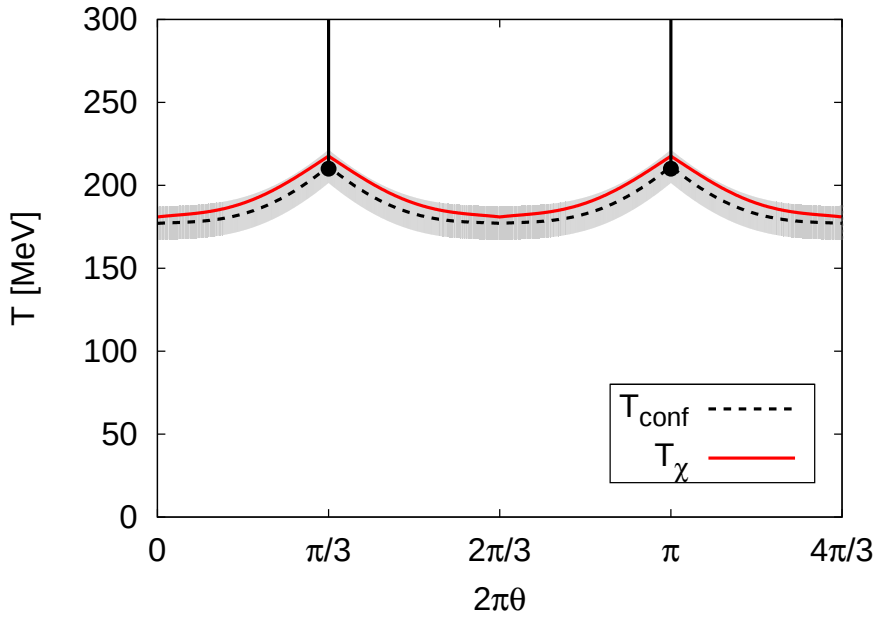

Figure 4.21: Chiral (T_χ) and confinement temperature ($T_{\rm conf}$) as functions of temperature and boundary angle θ. The width of $\chi_L = \partial_T L$ is displayed as a shaded area. The dots indicate the endpoints of the confinement RW-phase transitions.

In Fig. 4.21 we show the phase diagram of QCD$_\theta$. The confinement and the chiral temperatures lie close to each other for all imaginary chemical potentials. Their value at $\theta = 1/6$ is the endpoint $(T_{\rm RW}, \theta_{\rm RW}) \approx (210\text{MeV}, 1/6)$ of the corresponding RW phase transitions shown as a vertical line at $\theta = 1/6$ in Fig. 4.21. Our results compare well to the lattice results [143, 144]. In the PNJL-model [96, 104] the lattice results have been reproduced by adjusting model parameters connected to an eight quark interaction [105]. In our approach to full QCD$_\theta$ coinciding temperatures result from the interplay of quantum fluctuations and are not adjusted by hand. An estimate of the corresponding quantum fluctuation within a Polyakov–quark-meson model also leads to coinciding critical temperatures at real chemical potential [106]. These results suggest that the differences between $T_{\rm conf}$ and T_χ at both, real and imaginary chemical potential, are mainly due to mean field or large N_c approximations. The relevance of this observation for the quarkyonic phase proposed in [19] will be discussed elsewhere.

In summary our study suggests that the confinement and chiral critical temperatures $T_{\rm conf}$ and T_χ are dynamically related and agree within the error bars. At present, we extend our work to real chemical potential. This may help to shed some light on the current debate concerning lattice simulations at finite chemical potential.

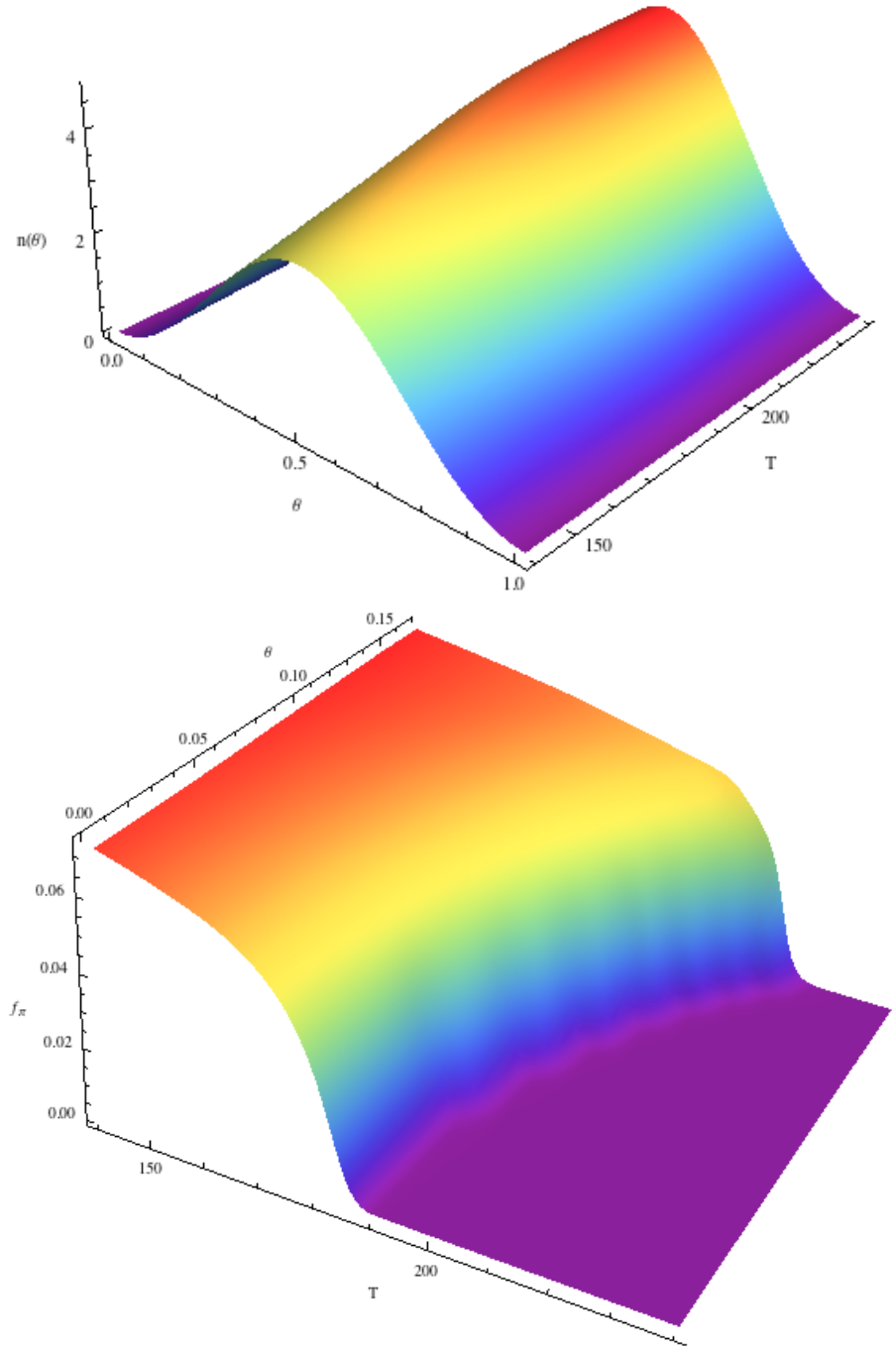

Figure 4.22: The density and the pion decay constant.

5 Dynamically Adjusted Degrees of Freedom

"All roads lead to Rome"

5.1 Motivation

The treatment of a physical problem is generally simplified if one chooses an appropriate language to describe the problem. If e.g. a charge distribution in electrodynamics is spherically symmetric, the computations are greatly simplified, upon using spherical coordinates.

At this point, we want to give a summary of the methods applied to choose the correct degrees of freedom and introduce a framework within which the appropriate degrees of freedom can be selected dynamically.

In the context of this work there are particularly two cases in which choosing the right degrees of freedom is essential for an adequate treatment of the theory. The first we encountered was the formulation of QCD in Polyakov gauge in terms of the Polyakov loop variable. The second was in the computation of the QM model, where we bosonised the fermions.

In the case of the Polyakov variable we saw, that it is important to change the mathematical description of our degrees of freedom in the right instance. Thereby we can cover the essential physics while avoiding unphysical singularities stemming from parametrisation artefacts. Recall that the Polyakov loop was defined by

$$\mathcal{P}(\vec{x}) = \mathcal{P} \exp\left(\mathrm{i}g \int_0^\beta dx_0\, A_0(x_0, \vec{x})\right) . \tag{5.1}$$

In the end we choose a parametrisation that could interpolate between a formulation in A_0 and $\mathcal{P}$. The close we got to the confining regime, the more we had to take fluctuations of $\mathcal{P}$ into account. At the beginning of the flow, where we started with a deconfining potential, we used a flow essentially of A_0.

On the contrary, for the QM model, we needed to modify our degrees of freedom because we dealt with a condensation phenomenon. There quarks formed bound states and we had to deal with a new physical situation, with new observables that we had to take into account, via the dynamical hadronization procedure. We added the bosonic field Φ to our theory and identified it with two quarks.

$$\Phi = \bar{\psi}\psi \tag{5.2}$$

A finite expectation value of Φ ammounted to a finite value of the chiral condensate, which is nothing but the condensation of quarks.

A model to demonstrate how the dynamical choice of degrees of freedom works, that makes it transparent is the $O(N)$ model. We choose this model because it is quite well understood and mathematically easier to handle than theories with gauge fields or fermions. Also, the basic notions can be visualised nicely.

5.2 $O(2)$ Model Intricacies

We specify to the $O(2)$ model because it is easier to write down everything explicitly and to visualise our results. The extension to an arbitrary number of fields is straightforward.

The classical action of the $O(2)$ model with two fields ϕ_1 and ϕ_2 is given by

$$S[\phi] = \int d^d x \frac{1}{2} \partial_\mu \phi^a \partial_\mu \phi^a + V[\phi^a \phi^a] \tag{5.3}$$

with an unspecified potential $V[\phi^a \phi^a]$. Obviously this action is symmetric under an orthogonal transformation $R \in O(2)$ of the two field components $S[\phi] = S[R\phi]$. Assuming a convex potential, we can expand the potential about the minimum and write the action as a sum of polynomials of the two individual fields, as all directions are equivalent. With this, we can e.g. do perturbation theory, or solve a flow equation. We do not expect anything special or problematic to happen.

However, if we assume a non-convex potential, for example $V(x) = (x - x_0)^2$, this are different. This potential is depicted in Fig 5.1. Now we have a continuum of minima

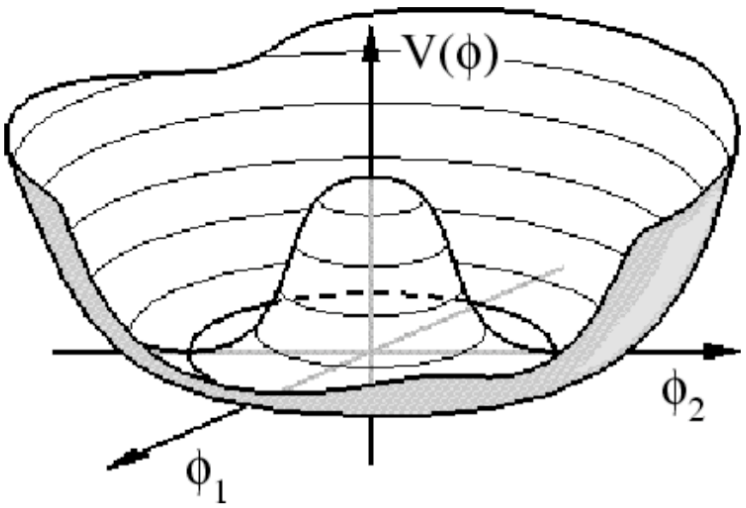

Figure 5.1: Typical shape of a mexican hat potential

that are physically equivalent. Picking one of those minima and expanding the potential about this minimum in terms of the two fields ϕ_1 and ϕ_2, we get an action with two different fields. In momentum space, it is given by

$$S = \int d^d x \frac{1}{2} \left(p^2 \phi_1^2 + m_1^2 \phi_1^2 \right) + \frac{1}{2} p^2 \phi_2^2 + \lambda (\phi_1^2 + \phi_2^2)^2 \Big) . \tag{5.4}$$

While this looks like a sensible action, there are some problems that are evident already in perturbation theory. To see this, let us consider the one-loop $2n$-point function with external legs of only the field ϕ_1 and internal propagators of the field ϕ_2. The propagator of ϕ_2 is simply $1/p^2$ and the vertex is momentum-independent. Now consider the limit where all external momenta vanish. There are n "2" propagators, they are the only structures carrying momentum, thus the momentum structure of this $2n$-point function is simply

$$\int d^d p \left(\frac{1}{p^2} \right)^n . \tag{5.5}$$

As long as $2n > d-1$, this $2n$-point function is divergent. This divergence is carried over into the flow equation. This problem can be circumvented by considering only the flow of correlation functions in which this divergence is cancelled out. It would however be nice, to have a formulation of the flow equation in terms operators that do not exhibit these divergences.

Let us first find out, what goes wrong when treating the theory the way we did and where the divergence arises. Obviously the divergence arises because the only momentum structure in the correlation function under consideration is the massless propagator of the field ϕ_2. Such a structure, however, is natural in a theory with spontaneously broken symmetry, the corresponding particles are the Goldstone bosons. An expansion around one of the minima of the mexican hat potential in terms of the fields ϕ_1 and ϕ_2 does not correctly capture the Goldstone physics, because as soon as the perturbations in ϕ_2 direction grow larger, we run up the potential hill again and this field should also acquire a mass. Therefore, we will introduce a field parameterisation, that is apt to deal with the Goldstone mode. This will also introduce a momentum dependent vertex, which will cure the IR divergence, we encountered in the more naive picture before.

A parameterisation of the field, that can correctly describe the Goldstone mode is written down right away:

$$\Phi = (\varphi + \rho_0^{1/2}) \exp(i\vartheta/\rho_0^{1/2}), \tag{5.6}$$

φ describes the radial mode, whereas ϑ describes the Goldstone mode. The action is

$$S = \int d^d p \frac{1}{2} \left(p^2 \varphi^2 + m^2 \varphi^2 \right) + \frac{(\varphi + \rho_0^{1/2})^2}{2\rho_0} p^2 \vartheta^2 + \lambda \varphi^4 + \frac{(\varphi + \rho_0^{1/2})}{\rho_0} (p_\mu \varphi)(p_\mu \vartheta). \tag{5.7}$$

It looks much similar to the previous action, but there is an important difference. There is three boson interaction, which is also momentum dependent. Let us now consider an $2n$-point function with external legs belonging to the radial field ϑ, which plays the role for ϕ_1 in the former parameterisation. In the loop there are Goldstone propagators,

which are of course massless, and radial mode propagators alternating after each vertex. Therefore, we get n massless propagators and $2n$ powers of the loop momentum p from the vertices, such that the momentum structure is

$$\int d^d p \left(\frac{1}{p^2}\right)^n (p)^{2n} = \int d^d p. \tag{5.8}$$

We have arrived at a correlation function, which is now not IR divergent and also captures Goldstone physics. There is, however, a drawback of the parameterisation. It cannot be used in the symmetric phase of the theory, as the Goldstone mode ϑ simply does not exist anymore. Here it is advantageous to resort to the Cartesion formulation.

On these results, we are going to show how to dynamically choose the appropriate degrees of freedom in an fRG setting.

5.3 Dynamical Parametrisation

The idea of the presented field parametrisation is to work in coordinates that are most appropriate for the physical situation. If we go back to the mexican hat potential for two field degrees of freedom, in an $O(2)$ symmetric scalar theory, it is immidiately clear that this would be best described in terms of a radial and an angular coordinate. Consequently, this parametrisation is good if we are in the regime of spontaniously broken symmetry. However, in the regime were the symmetry is restored, this is not a good parameterisation as explained above.

Therefore, we have to devise a parameterisation that allows us to dynamically choose the right degrees of freedom. We employ a nonlinear representation of the fields in terms of the collective variable

$$\Phi = (\varphi + b)e^{i\vartheta/b} + (\rho_0^{1/2} - b) \tag{5.9}$$

where $\rho_0 = \Phi^*\Phi$ and we introduced a parameter b that allows for an interpolation between the appropriate parametrisations in the symmetric and the broken phase. To see this we consider the limits $b \to \infty$ and $b \to \rho_0^{1/2}$:

$$b \to \infty \quad : \quad \Phi = (\varphi + b)(1 + i\frac{\vartheta}{b}) - b = \varphi + i\vartheta \tag{5.10}$$

$$b \to \rho_0^{1/2} \quad : \quad \Phi = (\varphi + \rho_0^{1/2})e^{i\vartheta/\rho_0^{1/2}} \tag{5.11}$$

We see that $b \to \infty$ corresponds to the appropriate field parametrisation in the symmetric phase and $b \to \rho_0^{1/2}$ is adequate in the case of spontaneously broken $O(2)$ symmetry.

Generically bosonic flows are symmetry breaking, therefore, if we start in the symmetric phase, we will have to adjust the parameter b during the flow. We will give a suitable prescription after we discuss the flow.

Since we now adjust the field in the course of the flow, there are modifications induced by the scale dependence of the fields. For a detailed discussion of these changes, see e.g.

[41, 49, 51, 145]. For the case of dynamical hadronisation, the scale dependence of the field is in a sense quadratic:

$$\hat{\Phi}_k = Z_k \bar{\psi}\psi, \tag{5.12}$$

where the only scale- (k-) dependence is in the factor Z_k. Therefore we get

$$\langle \partial_t \hat{\Phi}_k \rangle = \langle (\partial_t Z_k) \bar{\psi}\psi \rangle = (\partial_t Z_k) \langle \bar{\psi}\psi \rangle = \partial_t \langle \hat{\Phi}_k \rangle. \tag{5.13}$$

With this identity, the flow equation for scale dependent fields can be brought into a form close to the flow equation we know.

5.4 Flow of Scale Dependent Fields

We want to derive the flow equation for a scale dependent field Φ_k. The derivation is similar to the one for the well known flow equation (2.65). Here we only sketch the differences. Following the same steps that lead us to eq. (2.65), we arrive at

$$\Gamma_k[\Phi_k] = -W_k[J[\Phi_k]] + \int J\Phi_k - \Delta S_k[\Phi_k]. \tag{5.14}$$

Now we apply a total derivative w.r.t. $t = \ln(k/\Lambda)$ and write this total derivative by means of the chain rule as a partial derivative w.r.t. t, keeping the mean field $\Phi_k = \langle \hat{\Phi}_k \rangle$ fixed. The other term is a derivative w.r.t. the field Φ_k, times its scale derivative $\partial_t \Phi_k$. Analogously to eq. (2.55) we obtain for the scale derivative at fixed mean field

$$\partial_t|_{\Phi_k} W = -\frac{1}{2}\langle \hat{\Phi}_k \dot{R}_k \hat{\Phi}_k \rangle - \langle \dot{\hat{\Phi}}_k R_k \hat{\Phi}_k \rangle + \int J[\Phi_k] \langle \dot{\hat{\Phi}}_k \rangle. \tag{5.15}$$

From the first term, we can recover the flow equation as we did for a scale independent field. Assuming, that we can write $\langle \dot{\Phi} \rangle = \Phi$ as in eq. (5.13), the second term can be rearranged by means of functional derivatives w.r.t. J such that we end up with $\langle \dot{\hat{\Phi}}_k R_k \hat{\Phi}_k \rangle = G\delta(\dot{\Phi}_k)/\delta\Phi_k + \Phi_k R_k \dot{\Phi}_k$

The second term arising from applying a scale derivative on the RHS of eq. (5.14) is quickly computed. We arrive at

$$\dot{\Phi}_k \frac{\delta}{\delta \Phi_k} \left(-W_k + \int J\Phi_k - \Delta S_k \right) = -\dot{\Phi}_k \frac{\delta W}{\delta J} \frac{\delta J}{\delta \Phi} + \int \dot{\Phi}_k \left(J + \Phi_k \frac{\delta J}{\delta \Phi_k} \right) - \dot{\Phi}_k R_k \Phi. \tag{5.16}$$

Using $\delta W/\delta J = \Phi$, we observe, that only the terms $\int \dot{\Phi}_k J - \Phi_k R_k \dot{\Phi}_k$ survive.

Seeing that most of the terms cancel, we are left with the flow equation for the effective action of scale dependent fields

$$\dot{\Gamma}_k + \dot{\Phi}_{k,i} \frac{\delta \Gamma_k}{\delta \Phi_{k,i}} = \frac{1}{2} \mathrm{Tr} \frac{1}{\Gamma_k^{(2)} + R_k} \dot{R}_k + \mathrm{Tr} \frac{\delta \dot{\Phi}_{k,i}}{\delta \Phi_{k,j}} \left(\frac{1}{\Gamma_k^{(2)} + R_k} R_k \right)_{ij}, \tag{5.17}$$

where the trace runs over all internal indices and includes the momentum integration. We accounted for the possibility, that there is more than one scale dependent field by

including the indices Φ_i. For the $O(2)$ theory that we are going to discuss, the field has two components: $\Phi = (\varphi, \vartheta)$. We observe right away, that this flow equation comprises also the standard flow equation for constant fields, simply be noting that $\dot{\Phi}$ vanishes for constant fields.

To compute $\delta\dot{\Phi}/\delta\Phi$ we need explicit expression for the collective variable Φ_k in terms of the radial and angular component of the field. From eq. (5.9), it is not difficult to compute the expressions, details can be found in Appendix D.1:

$$\dot{\vartheta} = \frac{\dot{b}}{b}\vartheta + \frac{b(\dot{\sqrt{\rho_0}} - \dot{b})}{\varphi + b} \sin\left(\frac{\vartheta}{b}\right) \quad , \quad \dot{\varphi} = -\dot{b} - (\dot{\sqrt{\rho_0}} - \dot{b}) \cos\left(\frac{\vartheta}{b}\right). \tag{5.18}$$

Then it is straightforward to compute $\delta\dot{\Phi}/\delta\Phi$:

$$\frac{\delta\dot{\Phi}}{\delta\Phi} = \begin{pmatrix} \frac{\partial\dot{\varphi}}{\partial\varphi} & \frac{\partial\dot{\vartheta}}{\partial\varphi} \\ \frac{\partial\dot{\varphi}}{\partial\vartheta} & \frac{\partial\dot{\vartheta}}{\partial\vartheta} \end{pmatrix} = \begin{pmatrix} 0 & -b\frac{\dot{\sqrt{\rho_0}}-\dot{b}}{(\varphi+b)^2}\sin\left(\frac{\vartheta}{b}\right) \\ \frac{\dot{\sqrt{\rho_0}}-\dot{b}}{b}\sin\left(\frac{\vartheta}{b}\right) & \frac{\dot{b}}{b} + \frac{\dot{\sqrt{\rho_0}}-\dot{b}}{\varphi+b}\cos\left(\frac{\vartheta}{b}\right) \end{pmatrix}. \tag{5.19}$$

Guided by the classical action of the $O(2)$ theory in the phase of spontaneously broken symmetry, we write down the effective action for our theory. For reasons which will be apparent later, we extend the truncation to include more terms than the classical action. The effective action in an extended local potential approximation (LPA) reads

$$\Gamma_k = \int \frac{d^dx}{(2\pi)^d} \frac{1}{2} \left\{ Z_\varphi(\partial\varphi)^2 + (Z_\vartheta + U(\varphi))(\partial\vartheta)^2 + Z_4(\partial\vartheta)^4 \right\} + V[\rho], \tag{5.20}$$

where we introduced $\rho = \Phi^*\Phi$. It contains a standard kinetic term for the massive mode φ and an effective potential for the collective variable Φ, as well as a kinetic term for the Goldstone mode ϑ.

$U(\varphi)$ is a term in the effective action which is responsible for correct Goldstone physics. The necessity of this term is easily seen when inspecting $\partial\Phi^*\partial\Phi = (\partial\varphi)^2 + (\partial\vartheta)^2(1+\varphi/b)^2$. It is an extension of the interaction between Goldstone and radial mode that we have already in the classical action. If we did not allow for a general potential, the contribution of the Goldstone modes to the flow of the effective potential would vanish. In the large-N limit, this would certainly be wrong, as the flow of the radial mode is surpressed by $1/N$ compared to the flow of the Goldstone mode.

In the limit $b \to \rho_0$, U should be expanded in $(1 + \varphi/b)$, if b assumes a different value, a parametrisation in φ is appropriate. It is numerically advantageous to work exclusively with an expansion in φ and identifying the coefficients of this expansion with the coefficients of an expansion in $(1+\varphi/b)$. We will see that the variations of the results depending on the different parametrisations are minimal.

Flow of the Radial Mode Potential

The central quantity of the theory is the effective potential V, that provides information about the ground state of the system. The potential V is most conveniently parametrised by

$$V[\rho] = \frac{\lambda_k}{2}(\rho - \rho_{0,k})^2 + O(\rho^3). \tag{5.21}$$

We neglect higher terms in the expansion of the potential, as we are only interested in the behaviour of the vacuum expectation value. Higher terms are of importance in the calculation of critical exponents, see e.g. [63]. Note that we parametrised the effective potential in terms of the absolut value of the field, $\rho = \Phi^*\Phi$. The propagator in the flow equation, on the other hand, is obtained by taking derivates of the effective action Γ with respect to the field φ and ϑ. By means of the chain rule, we rewrite these derivates. To compute $\Gamma^{(2)}$, we can immediately set $\vartheta = 0$ from the start, since in the derivation of the flow of the coefficients of $V[\rho]$, no derivatives w.r.t. to ϑ appear.

The full flow equation (5.17) reduces to the flow equation for the effective potential:

$$\dot{V}_k + \dot{\Phi}_i \frac{\delta\Gamma}{\delta\Phi_i}\bigg|_{\vartheta=0=p} = \frac{1}{2}\int \frac{d^dp}{(2\pi)^d}\dot{R}_{ij}G_{ji}, \text{ where } \dot{R} = \begin{pmatrix} \dot{R}_{k,\varphi} & 0 \\ 0 & \dot{R}_{k,\vartheta} + 2\frac{\partial\dot{\vartheta}}{\partial\vartheta}R_{k,\vartheta} \end{pmatrix}. \quad (5.22)$$

Note that the second term in the $\vartheta\vartheta$-component of the regulator is a consequence of the second term on the RHS of eq. (5.17). In $\dot{R}_\varphi$ this term is zero, c.f. eq. (5.19).

The propagtor has only diagonal components, these are G_φ and G_ϑ. Explicitly they read

$$G_\varphi = \left(Z_\varphi p^2 + 2V' + 4\rho_0 V'' + R_{k,\varphi}\right)^{-1} \quad (5.23)$$

$$G_\vartheta = \left(p^2(Z_\vartheta + U(\varphi)) + \frac{\partial^2\rho}{\partial\vartheta^2}V' + R_{k,\vartheta}\right)^{-1}, \quad (5.24)$$

where we defined $V' = \partial V(\rho)/\partial\rho$ and used $\partial\rho/\partial\vartheta|_{\vartheta=0} = 0$. The optimised cut-off for the scalar fields is given by

$$R_{k,\varphi/\theta}(p^2) = Z_{\varphi/\theta}(k^2 - p^2)\ \theta(Z_{\varphi/\theta}(k^2 - p^2)) \quad (5.25)$$

In the flow equations for the effective potential V the second term is particularly simple, we defer the calculation to App. D.2. The flow equation for the effective potential V reads:

$$\dot{V} - \dot{\rho}_0\left(1 + \frac{\varphi}{\sqrt{\rho_0}}\right)V' = \frac{1}{2}\int\frac{d^dp}{(2\pi)^d}\left(\frac{\dot{R}_k(p^2)}{Z_\varphi k^2 + 2V' + 4\rho^2 V''} + \frac{\dot{R}_k(p^2) + 2\frac{\partial\dot{\vartheta}}{\partial\vartheta}R_k(p^2)}{Z_\vartheta k^2 + p^2 U(\varphi) + \frac{\partial^2\rho}{\partial\vartheta^2}V'}\right) \quad (5.26)$$

Getting the flow equations for λ and ρ_0 is straightforward, we project the flow equation onto the coefficients of the potential.

To compute the second term in the regulator eq. (D.3), we need to specify the behaviour of b during the flow. b determines wether our parametrisation is in the symmetric ($\Phi = \varphi + i\vartheta$)or in the spontaniously broken $\Phi = \varphi e^{i\vartheta}$ regime. We choose the following form of b:

$$b = \sqrt{\rho_0}\left(1 + \left(\frac{\alpha k^2}{\lambda\rho_0}\right)^\nu\right). \quad (5.27)$$

As mentioned above the function b interpolates between the different regimes of the theory. Via the parameters α and ν we can influence the location and strength/rapidity of the transion. The transition takes place around $\alpha k^2/\lambda\rho_0 = 1$. It is obvious, that smaller α corresponds to an earlier transiton into the Goldstone parameterisation $b = \rho_0$. ν determines the rapidity of the transition, larger ν induces a sharper transition. By varying the parameters α and ν we can get an intuition for the quality of the parametrisation. It would be desireable to have a parametrisation ot the theory that is as weakly dependend on the form of b as possible.

Flow of the Goldstone Potential

Getting the flow of U is more involved, since it comes with the term $\partial_m\vartheta$. Therefore, we have to take a second derivative w.r.t. to ϑ on Eq. (5.17) and a second derivative w.r.t. to momentum p, that we will set to zero at the end. Generically this will generate the loop and tadpole graphs, shown in Fig. 5.2, on which we will apply second derivatives w.r.t. external momentum. This complicates the evaluation of these graphs, as the momentum derivative could act on the propagators, yielding expressions that are difficult to handle. We will neglect these terms in our approximation, thus, we only consider terms that arise when a momentum derivative acts on the vertices, that have a trivial momentum dependence. The tadpole has a trivial dependence on external momenta.

This approximation is exact in the case of $\alpha = 0$, i.e. in the broken regime, since then all vertices with two Goldstone boson legs carry the momentum structure $p\dot{q}$, where p and q are the momenta of the Goldstone bosons. Therefore, if the momentum derivative does not act on the vertices, the whole graph vanishes upon setting $p = 0$.

The other limit $\alpha \to \infty$ is also not a problem since the contributions of the function U on the effective potential V are negligible and so are the contributions to U. Only in the range $\alpha \in (0.1...1000)$ the omitted terms induce small corrections.

We now give a derivation of the flow for the Goldstone potential. From the parameterisation eq. (5.20) and eq. (5.17), we can extract the flow of U by means of

$$\dot{Z}_\vartheta + \dot{U}\Big|_{\vartheta=0=p} = \frac{1}{2d}\left(\partial_p^2\frac{\delta^2}{\delta\vartheta^2}\dot{\Gamma} - \partial_p^2\frac{\delta^2}{\delta\vartheta^2}\dot{\Phi}_i\frac{\delta\Gamma}{\delta\Phi_i}\right)\Big|_{\vartheta=0=p}, \tag{5.28}$$

where we introduced the shorthand notation $\partial_p^2 = \partial_{p_\mu}\partial_{p_\mu}$. It is simple algebra to work out the second term on the RHS, we exhibit these calculations in App. D.3. We obtain for the second term

$$\partial_p^2\frac{\delta^2}{\delta\vartheta^2}\dot{\Phi}_i\frac{\delta\Gamma}{\delta\Phi_i} = 2d\left[(Z_\vartheta + U(\varphi))\left(\frac{\dot{b}}{b} + \frac{\dot{\sqrt{\rho_0}} - \dot{b}}{\varphi + b}\right) - \dot{\sqrt{\rho_0}}\,U'(\varphi) + Z_\varphi\,\varphi\,\frac{\dot{\sqrt{\rho_0}} - \dot{b}}{b^2}\right]. \tag{5.29}$$

There is a further approximation we make at this level. Namely, we neglect derivatives w.r.t. to ϑ acting on $\delta\dot{\Phi}/\delta\Phi$.

For the first term on the RHS, we have to take a second derivative of the effective

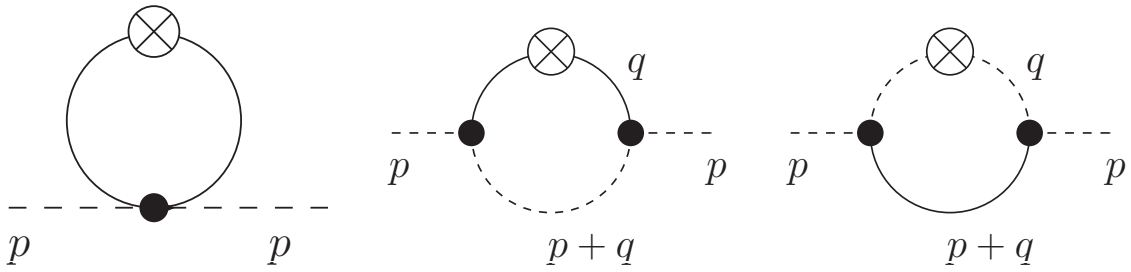

Figure 5.2: The graphs appearing in the computation of U, dashed lines represent Goldstone propagators G_ϑ, solid lines denote radial propagators G_φ. Full circles symbolise vertices, crossed circles signal regulator insertions.

action w.r.t. ϑ, schematically it reads

$$\frac{\delta^2}{\delta\vartheta^2}\dot{\Gamma} = -\frac{1}{2}\mathrm{Tr}\left[\dot{R}G\Gamma^{(4)}G - 2\dot{R}G\Gamma^{(3)}G\Gamma^{(3)}G\right]$$

where $\Gamma^{(4)}$ is the second derivative of $\Gamma^{(2)}$ with respect to ϑ. A detailed definition is in the appendix. From these terms, we get various loop graphs that contribute to the flow. These are shown in Fig. 5.2. Obviously the tadpole stems from the contribution with the four boson vertex $\Gamma^{(4)}$.

5.5 Results

As a first check of the parameterisation, we examine our choice of the control parameter b of the field parameterisation, which decides whether we are in the symmetric or the broken phase of the theory. b depends on two parameters α and ν, we will vary these independently. The results are shown in Fig. 5.3, showing the dependence of the field expectation value $\rho_{0,k\to 0}$ on the parameters α and ν. We see, that for a broad range of values of α the results of the flow is unaffected by a variation of α and ν, supporting the choice of b. Furthermore, we observe, that the region of small α entails to a higher value of ρ_0 than the one where α is large. Large α is corresponds to a flow in the linear basis, whereas small α implies a flow almost in the Goldstone basis.

This is reassuring in the sense that we are relatively independent of the shape of the function b, however, the dependence of the result on b is as expected.

It is interesting, to check, whether the terms in the flow equation that arise due to the scale dependence of the fields are significant. The results are shown in Fig. 5.4 for various combinations where we either took these terms into account or neglected them. The left plot displays the effects the term $\mathrm{Tr}\,\frac{\delta\dot{\Phi}_{k,i}}{\delta\Phi_{k,j}}\left(\frac{1}{\Gamma_k^{(2)}+R_k}R_k\right)_{ij}$, has on the flow. For $\alpha\to\infty$ the result is identical, this is as expected, as this corresponds to a flow in the Cartesian basis, the fields are not scale dependent. Since the term under discussion arises only for scale dependent fields, there should be no difference. In the Goldstone basis, where the

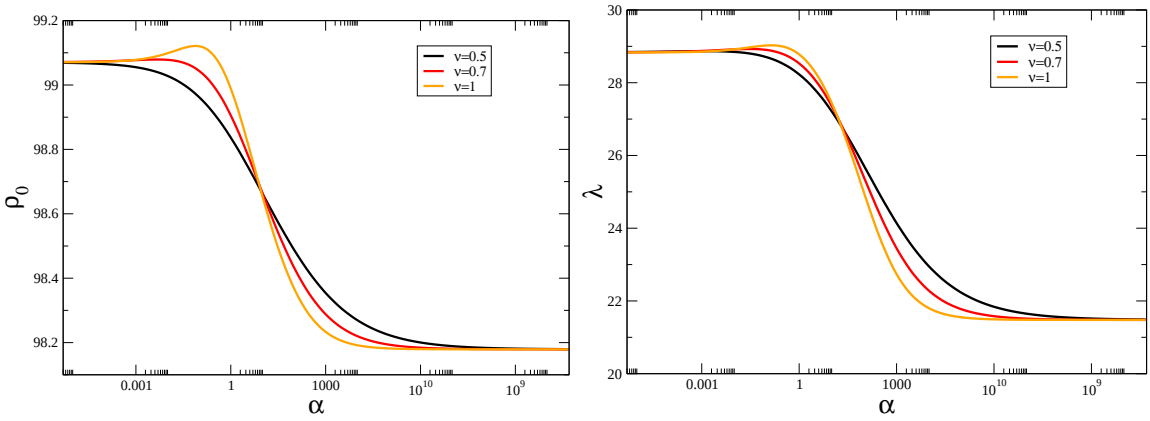

Figure 5.3: Dependence of ρ_0 and λ on the parameter α. The initialconditions for the fRG are $\Lambda = 100, rho_{0,\Lambda} = 60, \lambda_\Lambda = 40$. The red curve correspond to $\nu = 1$, black to $\nu = 0.7$ and orange to $\nu = 0.5$

fields are scale dependent, the difference of the flows is not very large, we conclude, that this term is not of great importance.

The term $\dot{\Phi}_{k,i}\frac{\delta\Gamma_k}{\delta\Phi_{k,i}}$ on the other hand appears to be significant, as it is responsible for the difference in the Goldstone regime that we observe in the graph on the right. Let us consider this in more detail. $\dot{\Phi}_{k,i}$ has two components $\dot{\phi}$ and $\dot{\vartheta}$. The blue and the black curve correspond to the equation with the $\dot{\phi}$-term, where for the blue curve we switched off the $\dot{\vartheta}$-term. Switching off the $\dot{\phi}$-term, we get the red and orange curves, where for the red curve, we also switched off the $\dot{\vartheta}$-term.

Note that we have normalised ρ_0 to agree in the Cartesian basis. If we do not normalise the curves, we observe that switching off the $\dot{\phi}$-term shifts the whole curve down. We mention, that the higher terms in the radial variable potential, are not sensitive on the terms in the flow equation that arises from the scale dependence.

We conclude that the term $\dot{\Phi}_{k,i}\frac{\delta\Gamma_k}{\delta\Phi_{k,i}}$ is important for a correct description of the physics.

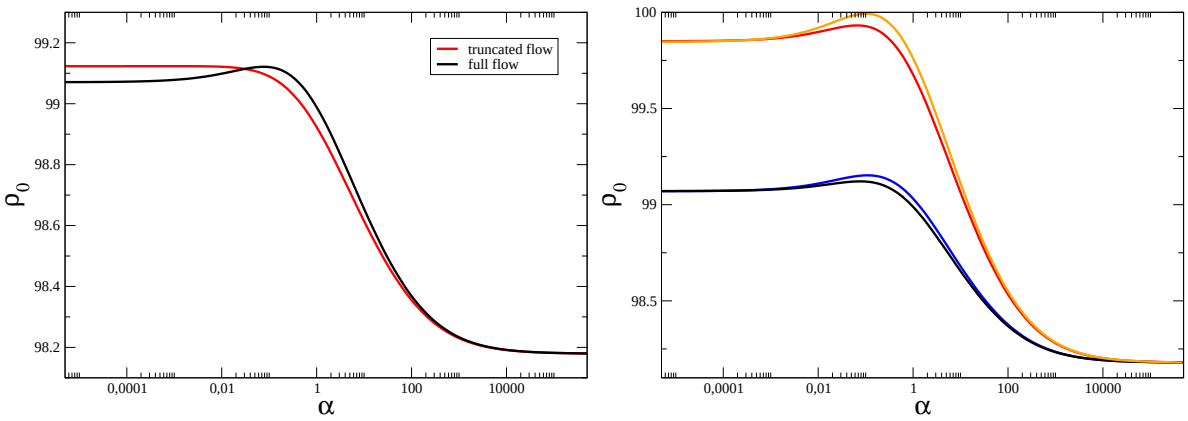

Figure 5.4: $\rho_{0,k\to 0}$ in various approximations to the full flow.

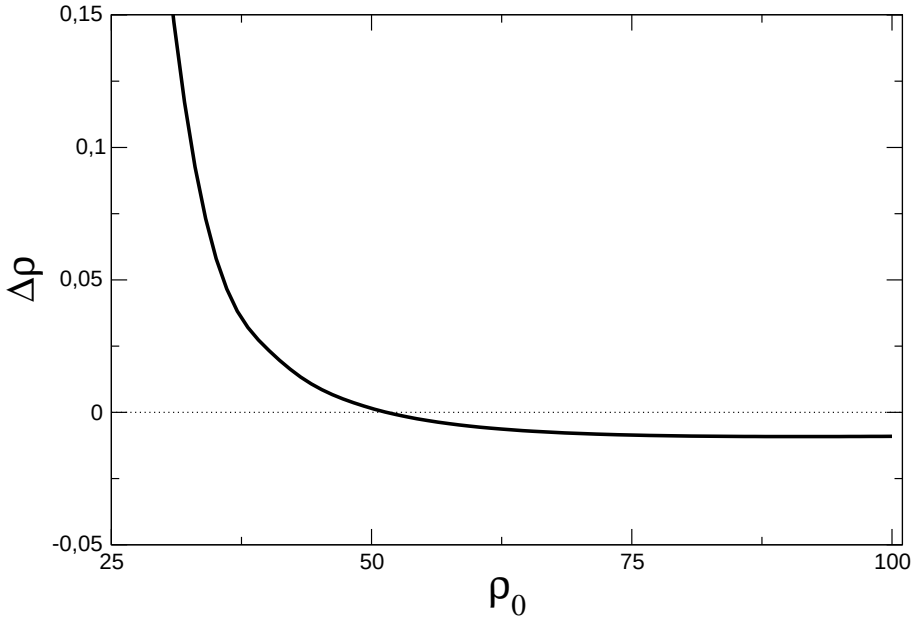

Figure 5.5: Dependence of $\Delta\rho_0$ on the initial condition $\rho_0(k \to \Lambda)$.

It is interesting to note, that the scale dependence of the radial field governs the dynamics of the theory more drastically than the scale dependence of the Goldstone field. For a $O(N)$ theory in the large-N limit, we expect the contrary, it will be interesting to investigate this.

We can also explore the difference in the results for different α in relation to the initial conditions. Therefore we consider

$$\Delta\rho_0 = \frac{\rho_0(k \to 0, \alpha \to 0) - \rho_0(k \to 0, \alpha \to \infty)}{\rho_0(k \to 0, \alpha \to 0)} \tag{5.30}$$

We observe that the closer we are to the symmetric regime, the larger the difference between the radial mode expectation value for the Goldstone and the linear basis. This is as expected, as we are closer to the parameterisation, in which the radial basis is appropriate. Comparing it to the Goldstone basis of course gives larger deviations, the more we are in the symmetric regime.

Finally, we want to check of the parametrisation of $U(\phi)$, in order to see how important the Goldstone mode potential is for the physics we investigate. We devised four different parametrisations of U. These are:

$$\text{(I)} \quad : \quad U(\varphi) = Z_\vartheta + d_1\varphi + d_2\varphi^2 + d_3\varphi^3 + d_4\varphi^4 \tag{5.31}$$

$$\text{(II)} \quad : \quad U(\varphi) = Z_\vartheta + d_1\varphi + d_2\varphi^2 \tag{5.32}$$

$$\text{(III)} \quad : \quad U(\varphi) = Z_\vartheta \left(1 + \frac{\varphi}{b}\right)^2 \tag{5.33}$$

$$\text{(IV)} \quad : \quad U(\varphi) = Z_\vartheta \left(1 + \frac{\varphi}{b}\right)^2 + a_1 \left(1 + \frac{\varphi}{b}\right)^3 + a_2 \left(1 + \frac{\varphi}{b}\right)^4. \tag{5.34}$$

Without showing numerical results, we state that particularly for small and moderate α the qualitity of the parametrisation of U plays a role. However, we also observe, that already parametrisation II gives almost identical results as parametrisation I. This is very fortunate since every additonal term in the parametrisation significantly amplifies the computational effort. There is however a little caveat, the results are computed neglecting the term $\delta\dot{\Psi}/\delta\Psi$, which gives only quantitative corrections. Hence we will mainly work with the numerically simpler parametrisation II. That the parametrisation is less important at small at large α is not unexpected since U plays a role in the Goldstone physics and this becomes important when we go away from the linear basis.

In summary we have shown that a dynamical reparameterisation of degrees of freedom within the fRG is feasible and exhibits non-trivial results. This is an important finding, because for a flow of the effective potential of the confinement order parameter formulated in the Polyakov loop variable we need such a reparameterisation.

6 Conclusion

"Veni, Vidi, Vici"
Gaius Iulius Caesar

6.1 Summary

We have studied the gluon and quark dynamics of QCD at finite temperature and chemical potential in a non-perturbative RG framework based on a simple flow equation for the effective action. It allows to relate full quantum effective action to the classical action of the theory at hand, giving us a powerful toolbox to study quantum field theories non-pertubatively. It is in a sense a complementary approach to lattice QCD, which allows to study QCD with high precision and virtually no approximations. Certain aspects of the theory, like chiral symmetry breaking or a finite chemical potential, are however hardly tractable in this approach. It is also difficult to see the physical mechanisms that are at work. Here the advantages of the fRG come into play and what seems to be a disadvantage, the necessity to truncate the system of flow equations, turns into an advantage: only within a finite system of equations, we can identify the relevant degrees of freedom. Extending the system, we can systematically check the validity of the assumptions made. Finally can we cross-check the results by comparing it with other non-perturbative methods, preferably in a regime where the two methods are assumed to be suitable.

In Chap. 3, we proposed a new formalism in which we can describe confinement in an elegant and simple way. In Polyakov gauge, which is a physical gauge, we were able to relate the confinement order parameter to the effective potential of the gluons. The gluonic theory effectively reduced to a scalar theory with a non-trivial effective potential that is imposed as an external input. The massive propagation of the Polyakov loop implied a simple truncation of the effective action, that led to a flow which we could solve numerically with a high accuracy. We showed that our results for the gauge group $SU(2)$ are compatible with lattice QCD data and also with result for the deconfinement phase transition obtained in another gauge, indicating gauge invariance of the results. The phase transition is of the correct order and exhibits the expected critical exponents. In the course of computing critical exponents, we showed that it is possible to compute critical exponents using Dyson-Schwinger equations, what has not been done so far, c.f. Appendix B.6.

A different formulation of the theory in terms of the natural variables, in which we compute the Polyakov loop in, was proposed. This formulation has to be parametrised correctly to obtain meaningful results. We have conjectured a parameterisation that

could do this.

Eventually, we extend the formalism to the physical gauge group $SU(3)$. It became apparent, that the results obtained up to this point are crucial, to find a phase transition. Numerically the situation is a lot more involved, but there are good indications, that a solution of the problem is within reach. Already within the results obtained so far, there is a clear indication, that the method works and that the phase transition is of correct order. The problems come with the boundary conditions of the potential, as we have to be carefull to define derivatives on them correctly. In $SU(2)$ we found a method to deal with this problem, so we expect it to be solvable for $SU(3)$ as well.

It is our hope that our research will spark further investigations on confinement in Polyakov gauge. We will discuss possible extensions in the outlook.

In Chap. 4 we discussed various approaches towards the QCD phase diagram. Starting from the NJL model, we explained the notion of dynamical hadronisation by means of the Hubbard-Stratonovich transformation and how it can be used to describe chiral symmetry breaking. In a model of QCD in Landau gauge, that incorporates much of the dynamics, we were able to solve flows of mesonic and quark degrees of freedom at finite chemical potential. It was possible to calculate the effects dynamical quarks have on the gauge coupling and the dependence of the chemical potential on these.

Regarding the deconfinement phase transition, we extend our analysis of Chap. 3 by including dynamical quarks into the flow. The phase transition becomes a cross-over and we could compute the quark-mass dependence of the cross-over temperature. The computation provides a basis for further investigations.

Concluding Chap. 4, we presented the first successful two-flavor continuum QCD computation at finite temperature in the chiral limit at imaginary chemical potential. We provided a framework to compute observables that allow to establish a relation between confinement and chiral symmetry breaking. The confinement-deconfinement and chiral phase transition temperatures $T_{c,\mathrm{conf}}$ and $T_{c,\chi}$ respectively agree within the error bars, as do $T_{c,\mathrm{conf}}$ and the critical temperature $\tilde{T}_{c,\mathrm{conf}}$ of the dual observable. The latter does not only provide a non-trivial reliability check of the approximations involved, but also gives an estimate on the potential broadness of the confinement-deconfinement temperature.

In Chap. 5 we discussed a formulation of the fRG with dynamically adjusted degrees of freedom, that we encountered in many instances throughout this work. In an $O(2)$ model, we investigated the importance of a correct parameterisation of the Goldstone physics and particularly the changes induced in the flow equation stemming from the scale dependence of the degrees of freedom. We found that the flow equation in a not too difficult truncation is already very stable under variation of the scale dependence. This give further support that the results obtained in Chap. 4 using dynamical hadronisation are reliable.

6.2 Outlook

There are various directions to extend the analysis of this work. Concluding this work, we want to present these directions.

The investigations of the deconfinement phase transition in Polyakov gauge are at present only in a exploratory state. First of all a full description of the deconfinement phase transition in terms of the effective potential computed on one Weyl chamber with appropriate boundary conditions should be the goal of further research. It is expected, that with an elaborate parameterisation of the potential, e.g. in terms of Chebyshev Polynomials or with a grid that implements the symmetry of the Weyl chamber appropriately, the phase transition can be observed.

The results obtained, apart from being interesting on their own, can serve as important inputs for other computations. PQM or PNJL models would benefit from these, as they allow for a cross-check with the current calculations in which the input is purely from the lattice. Within flow equation approaches towards these models, the scale dependence of the potential is of further interest. Such a calculation would already be very close to a full treatment of QCD in Polyakov gauge.

A comparison with results from other functional methods could shed further light on the gauge independence of the continuum approaches towards QCD.

Another interesting extension of the calculation is computing the running of the gauge coupling in Polyakov gauge. This eliminates the uncertainty in the results that comes from using an external input as coupling. This calculation is hampered by zero modes that still exist in the propagator of the spatial gauge fields.

An ambitious extension is to treat the full gluon system in the fRG. Therefore, we would have to set up flow equations for the coupled system of the spatial and temporal gauge fields. The effective potential would give a backreaction on the spatial gauge fields, thereby it would be impossible to integrate out the spatial gauge fields right from the start, as we did. We would also have to include the running of the three- and four- gluon vertex, which would again give us a handle on the running of the gauge coupling.

We already discussed how to include a chemical potential in Polyakov gauge in Sec. 4.3. As an approach towards the QCD phase diagram a tractable extension would be to compute the curvature of the deconfinement phase transition with increasing chemical potential. Thereby we could also comment on the whether there is a coincidence between the deconfinement and the chiral phase transition in the phase diagram.

At present we work on a refined analysis on the relation between confinement and chiral symmetry breaking. We work on employing a bettered approximation as well as on the extension of the present work to real chemical potential and 2+1 flavors. Apart from providing direct results on the physical phase diagram of QCD this should sheed some light in the current ongoing debate concerning lattice simulations at finite chemical potential.

The analysis of scale dependent fields should be extended towards general $O(N)$ theories, where we can establish the importance of Goldstone physics more evidently.

To wrap up, we have corroborated the capability of fRG methods to investigate Quantum Chromodynamics. With the determination of the deconfinement phase transition temperature compatible with lattice QCD and the gauge independence, we dare say to have made a worthy contribution to the knowledge about QCD. Still, as we saw, there remains much work to be done, part of it is already in progress.

A Appendix: Definitions

A.1 Conventions

We will use the following conventions throughout this work, following the conventions used in [42]

- The metric $g_{\mu\nu}$ that defines the inner product of two 4-vectors is Euclidian in all calculations:

$$g_{\mu\nu} = \delta_{\mu\nu}, \tag{A.1}$$

  where $\delta_{\mu\nu}$ is the Kronecker symbol. Consequently we do not need to distinguish between covariant and contravariant tensor structures.

- We work in natural units where

$$\hbar = c = 1.$$

- We use the Einstein sum convention.

- We use Euclidian gamma matrices. They are defined via the relation

$$\{\gamma_{mu}, \gamma_{nu}\} = -\delta_{\mu\nu} \tag{A.2}$$

- Greek indices run from 1 to 4.

A.2 Color Algebra

In this section, we show our conventions for the generators of the $SU(N_c)$ Lie-groups used throughout this work and discuss some of their properties particularly the ones important for evaluating the color traces appearing in this work.

The Color Group $SU(N_c)$

Though we use only $N_c \in 2, 3$ in this work, it is instructive and also not difficult to consider groups with an arbitrary N_c. $SU(N_c)$ is the group of unitary matrices U of rank N_c with unit determinant. It has $N_c^2 - 1$ generators T^a, obeying the commutation relation

$$[T^a, T^b] = i f^{abc} T^c, \tag{A.3}$$

where f^{abc} are the structure constants of the group. a, b, c take values in $1, \cdots, N_c^2 - 1$. The generators are normalised by the relation

$$\mathrm{Tr}[T^a T^b] = \frac{1}{2}\delta^{ab}\mathbb{1}_c. \tag{A.4}$$

Upon summation they fulfil the relation

$$\sum_a (T^a)_{\alpha\beta}(T^a)_{\gamma\delta} = \frac{1}{2}\delta_{\alpha\delta}\delta_{\beta\gamma} - \frac{1}{2N_c}\delta_{\alpha\beta}\delta_{\delta\gamma} \tag{A.5}$$

Specifying to $SU(2)$, the generators in the fundamental representation are proportional to the Pauli matrices τ^a by the relation $T^a = \frac{1}{2}\tau^a$, with eq. (A.3) it is a simple task to compute the structure constants. The structure constants are given by the totally antisymmetric tensor, $f^{abc} = \epsilon^{abc}$.

For $SU(3)$, the generators in the fundamental representation are given by the Gell-Mann matrices $T^a = \frac{1}{2}\lambda^a$

B Appendix: Polyakov gauge

B.1 Faddeev-Popov Determinant

When we introduced Polyakov gauge, we stated the result for the Faddeev-Popov determinant. Here, we want to give a detailed derivation of the result. For the gauge group $SU(2)$.

The general definition of the Faddeev-Popov determinant can be found e.g. in [146]. From the gauge fixing functionals eq. (2.36) and eq. (2.37) we can compute the Faddeev-Popov determinant given by

$$\Delta_{FP}[A] = \det\left[\frac{\delta F^a(A^\omega)}{\delta\omega^b}\right], \tag{B.1}$$

where A^ω is the gauge transformed gauge field A. a and b take values $+$, - and 3, analogously to the definition in the gauge fixing conditions. In order to compute the determinant we need to have an expression for A^ω. For infinitesimal gauge transformations it is given by

$$A^\omega_\mu = A_\mu - (\partial_\mu\sigma^a + igA^b_\mu[\sigma^a,\sigma^b])\omega^a\,. \tag{B.2}$$

In the following we use the representation $\omega^a\sigma^a = \omega^+\sigma^- + \omega^-\sigma^+ + \omega^3\sigma^3$, and the related derivatives w.r.t. $\omega^\pm, \omega^3$. We introduced $\sigma^\pm = \sigma^1 \pm i\sigma^2$, where the σ^i are the Pauli matrices. The matrix elements related to ω-derivatives of F^+ read

$$\begin{aligned}
\frac{\delta F^+(A^\omega)}{\delta\omega^+} &= -\mathrm{Tr}\,\sigma^+\left(\partial_0\sigma^- + iA^3_0[\sigma^-,\sigma^3]\right),\\
\frac{\delta F^+(A^\omega)}{\delta\omega^-} &= 0\,,\\
\frac{\delta F^+(A^\omega)}{\delta\omega^3} &= -\mathrm{Tr}\,\sigma^+\left(\partial_0\sigma^3 + iA^+_0[\sigma^3,\sigma^-]\right).
\end{aligned} \tag{B.3}$$

Analogously we get for the ω-derivatives of F^-

$$\begin{aligned}
\frac{\delta F^-(A^\omega)}{\delta\omega^+} &= 0\,,\\
\frac{\delta F^-(A^\omega)}{\delta\omega^-} &= -\mathrm{Tr}\,\sigma^-\left(\partial_0\sigma^+ + iA^3_0[\sigma^+,\sigma^3]\right),\\
\frac{\delta F^-(A^\omega)}{\delta\omega^3} &= -\mathrm{Tr}\,\sigma^-\left(\partial_0\sigma^3 + iA^-_0[\sigma^3,\sigma^+]\right).
\end{aligned} \tag{B.4}$$

The ω-derivatives of F^3 yield long expressions, and we only display the parts proportional to $\partial_0 \mathrm{Tr}\,\sigma^3 A_0$, where we have abbreviated additional terms proportional to the spatial gauge fields by dots,

$$\begin{aligned}
\frac{\delta F^3(A^\omega)}{\delta\omega^+} &= -i\partial_0 A_0^- \,\mathrm{Tr}\,\sigma^3[\sigma^-,\sigma^+] + \cdots\,, \\
\frac{\delta F^3(A^\omega)}{\delta\omega^-} &= -i\partial_0 A_0^+ \,\mathrm{Tr}\,\sigma^3[\sigma^+,\sigma^-] + \cdots\,, \\
\frac{\delta F^3(A^\omega)}{\delta\omega^3} &= -2\partial_0^2 + \cdots\,. \qquad \text{(B.5)}
\end{aligned}$$

The contributions that we left out only contribute a constant to the Faddeev-Popov determinant, which can be absorbed in the normalisation.

Evaluating the traces (B.3), (B.4), (B.5) we can compute the Faddeev-Popov determinant. Again we only concentrate on the terms dependent on A_0, and use the gauge fixing condition $A_0^+ = A_0^- = 0$ for eliminating some of the off-diagonal elements,

$$\begin{aligned}
\Delta_{FP}[A] &= -\mathrm{det}\left[\begin{pmatrix} \partial_0 + igA_0^3 & 0 & 0 \\ 0 & \partial_0 - igA_0^3 & 0 \\ -4ig\int dx_0 \partial_1 A_1^- & 4ig\int dx_0 \partial_1 A_1^+ & 1/2(\partial_0^2 + \int dx_0 \partial_1^2) \end{pmatrix}\right] \\
&= -\mathrm{det}\Bigg[(\partial_0 + igA_0^3)(\partial_0 - igA_0^3) \\
&\qquad \frac{1}{2}\left(\partial_0^2 + \int dx_0 \partial_1^2 + \int dx_0 dx_1 \partial_2^2 + \int dx_0 dx_1 dx_2 \partial_3^2\right)\Bigg]\,. \qquad \text{(B.6)}
\end{aligned}$$

We neglected terms that were previously abbreviated by dots. Using the third gauge fixing condition, $\partial_0 A_0^3 = 0$, we can simplify the first term, the second term in brackets is independent of A_0, therefore we will abbreviate it. We can write the Faddeev-Popov determinant as

$$\Delta_{FP}[A] = \frac{1}{2}\mathrm{det}\left[\left(\partial_0^2 + \left(gA_0^3\right)^2\right)\right]\mathrm{det}[\left(\partial_0^2 + \cdots\right)]\,.$$

We note again that the second determinant in eq. (B.7) is independent of the gauge fields and hence can be absorbed in the normalisation of the path integral. The first determinant is evaluated in frequency space, we get

$$\prod_{\vec{x}}\left((gA_0^3(\vec{x}))\prod_{n=1}^{n=\infty}\left((2\pi T n)^2 - (gA_0^3(\vec{x}))^2\right)\right)^2\,. \qquad \text{(B.7)}$$

Multiplying the determinant eq. (B.7) with a further constant normalisation

$$\mathcal{N} = \left(\prod_{n=1}^{n=\infty}(2\pi T n)^2\right)^{-2}\,, \qquad \text{(B.8)}$$

we arrive at

$$\mathcal{N}\det\left[G_{A_0}\right] = \prod_x (gA_0^3(x))^2 \prod_{n=1}^{n=\infty}\left(1-\left(\frac{gA_0^3(x)}{2\pi nT}\right)^2\right). \tag{B.9}$$

Eq. (B.9) is just a product representation of the sine-function, $\sin(x) = x\prod_{n=1}^{n=\infty}\left(1-\frac{x^2}{(\pi n)^2}\right)$, and the final result for the Faddeev-Popov determinant is

$$\Delta_{FP}[A] = \mathcal{N}'(2T)^2\left[\prod_x \sin^2\left(\frac{gA_0^3(x)}{2T}\right)\right], \tag{B.10}$$

where $\mathcal{N}'$ is a further normalisation constant.

B.2 Integrating Out Spatial Gluons

Weiss showed, that the Faddeeev-Popov determinant, that we computed in the previous section precisely cancels the contribution to the path-integral stemming from the longitudinal gluons, i.e. those gluon fields with $\vec{p}\vec{A}(p) \neq 0$. After integrating out the longitudinal gauge fields the Yang Mills action $S_{\text{eff}} = \frac{1}{4}\int_T d^4x F^a_{\perp,\mu\nu}F^a_{\perp,\mu\nu}$ explicitly reads:

$$\begin{aligned} S_{\text{eff}} &= -\frac{1}{2}\beta\int d^3x\, Z_0 A_0\vec{\partial}^2 A_0 - \frac{1}{2}\int_T d^4x\, A_i^a\left[(\partial_0^2+\vec{\partial}^2)\delta_{ij} - \partial_i\partial_j + \right. \\ &\qquad \left. 2gf^{a3b}(A_0\partial_0 + g^2A_0^2(\delta^{ab}-\delta^{a3}\delta^{b3})\delta_{ij}\right]A_j^b + O(A_i^3), \end{aligned} \tag{B.11}$$

where $\int_T$ indicates, that we are integrating over imaginary time only from 0 to β. Writing $A_0^3 = \varphi/(g\beta) + a_0$, where φ is a constant and a_0 the fluctuating field, this expression is given to second order in the fluctuating fields by

$$\begin{aligned} S_{YM} &\approx \frac{1}{2}\int d\tau d^3x\, \left\{Z_0(\vec{\partial}a_0)^2 - 2\varphi f^{a3c}(\partial_0 A_i^a)A_i^c + \right. \\ &\qquad \left. \varphi^2(\delta^{ab}-\delta^{a3}\delta^{b3})A_i^aA_i^b - A_i^a\left((\partial_0^2+\vec{\partial}^2)\delta_{ij}-\partial_i\partial_j\right)A_j^a\right\} \\ &= \frac{1}{2}\int d\tau d^3x\, \left\{(\vec{\partial}a_0)^2 - A_i^a(\vec{\partial}^2-\partial_i\partial_j)A_j^a - A_i^aD_0^{ac}D_0^{cb}A_i^b\right\}, \end{aligned} \tag{B.12}$$

where we have defined

$$D_0^{ab} = \partial_0\delta^{ab} + A_0^3 g f^{a3b}. \tag{B.13}$$

In the present work we neglect back-reactions of the A_0 potential on the transversal gauge fields. Assuming an expansion around $A_i^a = 0$, $\Gamma^{(2)}$ is block-diagonal, like the regulators, cf. eq. (3.20), and we can decompose the flow equation (2.65) into a sum of two contributions, schematically written as

$$\partial_t\Gamma_k = \frac{1}{2}\text{Tr}\left(\frac{1}{\Gamma_k^{(2)}+R_A}\right)_{00}\partial_t R_k + \text{Tr}\,\partial_t\left[\ln(S_{YM}^{(2)}+R_A)\right]_{ii}. \tag{B.14}$$

The first term on the RHS encodes the quantum fluctuations of A_0, the second line encodes those of the transversal spatial components of the gauge field. In the present truncation the second line is a total derivative w.r.t. t, and does not receive contributions from the first term. Therefore we can evaluate the flow of the second contribution, and use its output $V_{\perp,k}(A_0)$ as an input for the remaining flow.

The computation is done for the regulators eq. (3.20). As explained below eq. (3.14) in section 3.1.1, the cut-off parameters k, and $k_\perp$ in R_k for the fluctuations of A_0 and $R_{k,\perp}$ for the fluctuations of $\vec{A}_\perp$ respectively satisfy a non-trivial relation $k_\perp = k_\perp(k)$ for coinciding physical infrared cut-offs k_0 for A_0 and $k_\perp$ for $\vec{A}_\perp$. The computation is similar to those done in one loop perturbation theory in $SU(2)$ by Weiss [52], the only difference being the infrared cut-off. We infer from the second line in eq. (B.14) that

$$\begin{aligned} V_{\perp,k} &= V_{\perp,\Lambda_{\rm UV}} + \frac{1}{2}{\rm Tr}\,\Big[\ln(S^{(2)}_{YM}+R_A)\Big]_{ii}\Big|^{k}_{\Lambda_{\rm UV}} \\ &= V_W + T\sum_n \int \frac{d^3p}{(2\pi)^3}\theta(k_\perp^2-\vec{p}^2)\ln(k_\perp^2+D_0^2)\,. \end{aligned} \tag{B.15}$$

In eq. (B.15) we have used that $V_{\perp,\Lambda_{\rm UV}\to\infty}=0$ up to a constant term, and have added and subtracted the Weiss potential V_W [52],

$$V_W(\varphi) = -(\tilde\varphi-\pi)^2/(6\beta^4) + (\tilde\varphi-\pi)^4/(12\pi^2\beta^4)\,, \tag{B.16}$$

with the dimensionless $\varphi = g\beta A_0$, and $\tilde\varphi = \varphi \mod 2\pi$. Alternatively one can simple put $\Lambda_{\rm UV}=0$, even though this seems to be counter-intuitive. We also have used that with eq. (3.21) it follows ${\rm Tr}\,\Pi_\perp = 2$. Performing the Matsubara sum and neglecting terms independent of the temporal gauge fields, the resulting effective potential is given by

$$\begin{aligned} V_{\perp,k} &= \frac{4T}{(2\pi)^2}\int_0^{k_\perp} dp p^2 \Big\{\ln\Big(1-2\cos(\varphi)e^{-\beta k_\perp} \\ &\quad + e^{-2\beta k_\perp}\Big) - \ln(1-2\cos(\varphi)e^{-\beta p}+e^{-2\beta p})\Big\} + V_W\,. \end{aligned} \tag{B.17}$$

From eq. (B.17) we deduce that the potential $V_{k_\perp}$ approaches V_W in the limit $k\to 0$ and vanishes like $e^{-\beta k_\perp}\cos(\varphi)$ for $k\to\infty$. From eq. (B.14) we can now extract the flow of the effective potential, by setting $V_{{\rm eff},k} = \Delta V_k + V_{\perp,k}$. Then we get

$$\partial_t \Delta V_k = \frac{1}{2}\int \frac{d^3p}{(2\pi)^3}\frac{(\eta_0(k^2-\vec{p}^2)+2k^2)\theta(k^2-\vec{p}^2)}{k^2+g_k^2\beta^2(\Delta V_k'' + V_{\perp,k}'')}\,, \tag{B.18}$$

with the input $V_{\perp,k}$ given in eq. (B.17) and $\eta_0 = \partial_t \ln Z_0$. The factor $g^2\beta^2$ arises from the fact that we parametrise the potential in terms of φ rather than in A_0, and $g_k^2 = g^2/Z_0$ is nothing but the running coupling at momentum $\vec{p}^2 \sim k^2_{\rm phys}$. Thus we estimate $g_k^2 = 4\pi\alpha_s(\vec{p}^2 = k^2_{\rm phys})$. Note that g_k is an RG-invariant. The momentum integration can be performed analytically, and we are led to

$$\beta\partial_k\Delta V_k = \frac{2}{3(2\pi)^2}\frac{(1+\eta_0/5)k^2}{1+\frac{g_k^2\beta^2}{k^2}\partial_\varphi^2(V_{\perp,k}+\Delta V_k)}\,, \tag{B.19}$$

where η_0 is given by

$$\eta_0 = -\partial_t \log \alpha_s \,, \tag{B.20}$$

as the consistent choice in the given truncation.

B.3 Matching Scales

The flow of the temporal component of the gauge field, $A_0(\vec{x})$, is computed with a three-dimensional regulator, see eq. (3.20). In Polyakov gauge $A_0(\vec{x})$ only depends on the spatial coordinates, whereas the spatial components $A_\perp(x)$ are four-dimensional fields. For cut-off scales far lower than the temperature, $k/T \ll 1$, also the spatial gauge fields are effectively three-dimensional fields as only the Matsubara zero mode propagates. Hence in this regime we can identify $k = k_\perp$. For large cut-off scales, $k/T \gg 1$, the A_0-flow decouples from the theory. A comparison between the two flows can only be done after the summation of the spatial flow over the Matsubara frequencies. In the asymptotic regime $k/T \gg 1$ this leads to the relation

$$\frac{1}{k} \simeq \sum_{n=-\infty}^{\infty} \frac{1}{\omega_n^2 + k_\perp^2} \to \frac{1}{2k_\perp} \,, \tag{B.21}$$

The crossover between these asymptotic regimes happens at about $k/T = 1$. This crossover is implemented with the help of an appropriately chosen interpolating function f,

$$\frac{T}{k^2} f(k/T) \;=\; T \sum_{n=-\infty}^{\infty} \frac{1}{\omega_n^2 + k_\perp^2} \,, \tag{B.22}$$

A natural choice for $f(k/T)$ is depicted in Fig. B.1, and has been used in the computation. A more sophisticated adjustment of the relative scales can be performed within a comparison of the flow of momentum-dependent observables such as the wave function renormalisation Z_0. The peak of these flows in momentum space is directly related to the cut-off scale. Indeed, the function f carries the physical information of the peak of the flow at some momentum scale. Scanning the set of f gives some further access to the uncertainty in such a procedure. The effective cut-off scales $k_{\rm phys}(k_0)$ and $k_{\perp,{\rm phys}}(k_\perp)$ in the flows of the temporal gluons and of spatial gluons respectively do not match in general. If solving the flow within a local truncation as chosen in the present work we have to identify the two effective cut-off scales, $k_{\rm phys}(k_0) = k_{\perp,{\rm phys}}(k_\perp) = k_{\rm phys}$, leading to a non-trivial relation $k_0 = k_0(k_\perp)$. Moreover, the effective cut-off scale has to be used in the running coupling $\alpha_s = \alpha_s(\vec{p}^2 = k_{\rm phys}^2)$.

It is left to determine the physical cut-off scale $k_{\rm phys}$ from either the flow of the spatial gauge fields as $k_{\perp,{\rm phys}}(k_\perp)$ or from the temporal flow $k_{0,{\rm phys}}(k_0)$. We first discuss the spatial flow. For an optimised regulator depending on all momentum directions, p^2, we have the relation $k_{\rm phys} = k_\perp$. Hence the relation $k_{\perp,{\rm phys}}(k_\perp)$ can be computed if comparing the flows for a specific observable with three-dimensional regulator $R_{{\rm opt},k_\perp}(\vec{p}^2)$, eq. (3.22),

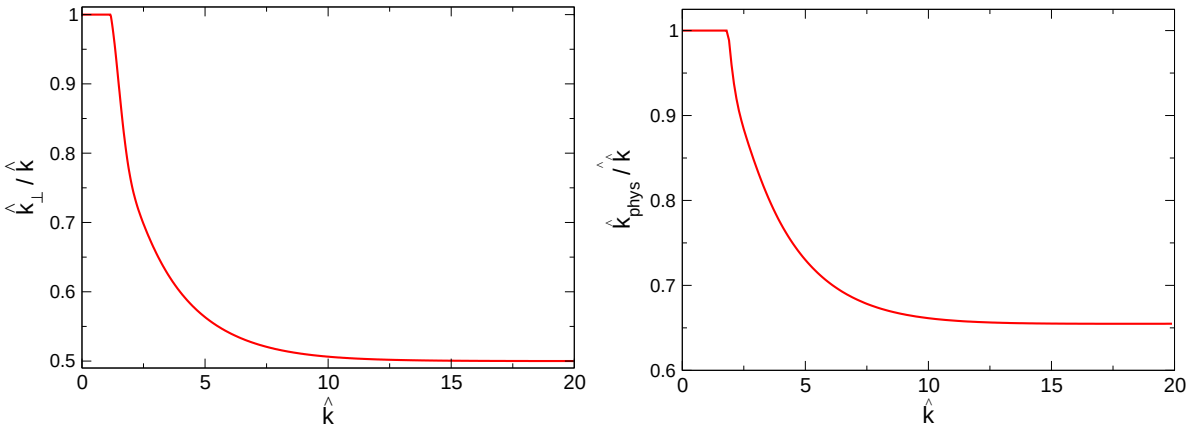

Figure B.1: $\hat{k}_\perp/\hat{k}$ as function of $\hat{k}$ (left panel).$\hat{k}_{\rm phys}(\hat{k})$ from the comparison of flows with three-dimensional regulators and four-dimensional regulators (right panel).

with flows with four-dimensional regulator $R_{{\rm opt},k_{\rm phys}}(p^2)$. Here, as a model example, we choose the effective potential of a ϕ^4-theory. This leads to the relation $k_{\rm phys}(k_\perp)$ displayed in Fig B.1. We remark that the relation in Fig. B.1 depends on the dimension d of the theory, and flatten to $k_{\rm phys}(k) = k$ for $d \to \infty$. In other words, $\lim_{k\to\infty} k_{\rm phys}(k)/k$ is proportional to $d/(d-1)$. Moreover, for momentum-dependent observables the crossover rather resembles the relation $k_\perp(k_0)$ as it is more sensitive to the propagator than to the momentum integral of the propagator. Indeed, for the three-dimensional field $A_0(\vec{x})$ the cut-off scale k_0 is another natural choice for the physical cut-off scale, $k_{0,{\rm phys}}(k_0) = k_0$, even though it underestimates the importance of the spatial flow for the correlations of the temporal gauge field. In summary, we take the above two extremal choices $k_{\rm phys} = k_{\perp,{\rm phys}}$ depicted in Fig. B.1 and $k_{\rm phys} = k_{0,{\rm phys}}(k_0) = k_0$ as a broad estimate of the systematic error in the present computation.

B.4 Flow Equation of the Polyakov Loop Variable L

The derivation of the flow equation formulated in terms of the Polyakov loop variable is very similar to the one for the effective potential of the gluons. The main difference being the kinetic term of the Polyakov loop variable. The propagator of the Polyakov loop variable $L(\vec{x})$ is now given by

$$\begin{aligned}(\Gamma^{(2)}_{L,k} + R_A)^{-1}_{LL} \;=\; & \left(Z_L \frac{4}{g^2\beta^2}\left(\frac{1}{1-L^2} - 1\right)\vec{p}^2 + Z_L \frac{4}{g^2\beta^2} k^2 + \partial_L^2 V_k[\varphi(L)] \right)^{-1} \theta(k^2 - \vec{p}^2) + \\ & \left(Z_L \frac{4}{g^2\beta^2}\left(\frac{1}{1-L^2}\right)\vec{p}^2 + \partial_L^2 V_k[\varphi(L)] \right)^{-1} \theta(\vec{p}^2 - k^2), \end{aligned} \tag{B.23}$$

Taking account of this modification, the equation for the potential is given by

$$\beta\Delta\dot{V}_{L,k} = \frac{1}{2}\frac{4\pi}{(2\pi)^3}\int_0^k dpp^2 \frac{\frac{4}{g^2\beta^2}Z_A(2k^2+\eta_A(k^2-\vec{p}^2)}{Z_A\frac{4}{g^2\beta^2}\left(\frac{1}{1-L^2}-1\right)\vec{p}^2 + Z_A\frac{4}{g^2\beta^2}k^2 + \partial_L^2 V_k[\varphi(L)]}. \quad \text{(B.24)}$$

We already absorbed the flow of the spatial gluons into the flow as we did in the other calculations. Then the full effective potential is $V_k = \Delta V_{L,k} + V_{\perp,k}$.

Performing a substitution $x = \vec{p}^2\beta^2 \Rightarrow dx = \beta^2 2pdp$ and $\hat{k} = k\beta$, we can write the flow in dimensionless variables,

$$\begin{aligned}
\beta\Delta\dot{V}_L &= \frac{1}{(2\pi)^2}\int_0^{\hat{k}^2}\frac{dx}{\beta^2}\frac{\sqrt{x}}{\beta}\frac{\hat{k}^2/\beta^2+\eta_a(\hat{k}^2/\beta^2-x/\beta^2)}{\frac{L^2}{1-L^2}x/\beta^2+\hat{k}^2/\beta^2+\frac{g^2\beta^2}{4Z_A}\partial_L^2 V_k[\varphi(L)]} && \text{(B.25)}\\
&= \frac{1}{\beta^3(2\pi)^2}\int_0^{\hat{k}^2} dx\sqrt{x}\frac{\hat{k}^2+\eta_a(x-\hat{k}^2)}{\frac{L^2}{1-L^2}x+\hat{k}^2+\frac{g^2\beta^4}{4Z_A}\partial_L^2 V_k[\varphi(L)]}. && \text{(B.26)}
\end{aligned}$$

The only thing left to do is rescale the potential $V \to \beta^4 V$ to end up with a flow defined in terms of dimensionless quantities:

$$\hat{k}\partial_{\hat{k}}\Delta V_L = \frac{1}{(2\pi)^2}\int_0^{\hat{k}^2} dx\frac{\sqrt{x}(\hat{k}^2+\eta_A(\hat{k}^2-x))}{\frac{L^2}{1-L^2}x+\hat{k}^2+\frac{g^2}{4}\partial_L^2 V_k[\varphi(L)]}. \quad \text{(B.27)}$$

As we want to write the flow in terms of the field φ, we compute $\partial_L^2 V[\varphi(L)]$ and express it in terms of φ. This is

$$\begin{aligned}
\partial_L^2 V[\varphi(L)] &= \partial_L^2 V[2\arccos(L)] = \partial_L\left(\frac{\partial 2\arccos(L)}{\partial L}\frac{\partial V}{\partial\varphi}\right) && \text{(B.28)}\\
&= \frac{\partial^2(2\arccos(L))}{\partial L^2}V' + \left(\frac{\partial 2\arccos(L)}{\partial L}\right)^2 V'' && \text{(B.29)}\\
&= -2\frac{\cos(\varphi/2)}{\sin^3(\varphi/2)}V' + 4\frac{1}{\sin^2(\varphi/2)}V'' && \text{(B.30)}
\end{aligned}$$

In the second line we introduced the abbreviation $\frac{\partial V}{\partial\varphi} = V'$

B.5 Derivation of the Flow for $SU(3)$

The flow equation for SU(3) YM theory in Polyakov gauge is much like the one for SU(2), the only difference being that the Cartan now has two field components. This introduces additional tensor structures into the objects we are dealing with. We will only discuss the changes to the flow equation in detail that change the flow of the zero-component of the gauge field. The spatial gluons generate the Weiss potential as in the case of $SU(2)$, only that it now is a potential of two fields. We need to get a representation of $\Gamma^{(2)}$,

therefore, we first need to specify the effective action Γ, we choose the parametrisation

$$\Gamma[A_0,\vec{A}_\perp] = -\frac{\beta}{2}\int d^3x\; Z_0\;(A_0^3\,\vec{\partial}^2\,A_0^3 + A_0^8\,\vec{\partial}^2\,A_0^8) + \tag{B.31}$$

$$\beta\int d^3x V_k[A_0] - \frac{1}{2}\int_T d^4x\; Z_i\vec{A}^a_\perp\left[(D_0^2)^{ab} + \vec{\partial}^2\delta^{ab}\right]\vec{A}^a_\perp\,. \tag{B.32}$$

We concentrate on the modifications in the flow equation, introduced by the additional Cartan components. These are the main modifications to the flow equation, the additional Cartan components lead to a modification of the Weiss potential in the sense, that it now depends on two variables. For the effective action we get for the second derivative w.r.t. the temporal gauge field A_0

$$\Gamma^{(2)}_{00}[A_0,\vec{A}_\perp]\Big|_{p=0} = \begin{pmatrix} \frac{\delta^2}{\delta(A^3)^2} & \frac{\delta^2}{\delta A^3\delta A^8} \\ \frac{\delta^2}{\delta A^3\delta A^8} & \frac{\delta^2}{\delta(A^8)^2}\end{pmatrix}\Gamma[A_0,\vec{A}_\perp]\Big|_{p=0}\,. \tag{B.33}$$

It is obvious how to compute the propagator, we choose as regulator the three-dimensional optimised cut-off $R_{A_0} = (k^2-\vec{p}^2)\mathbb{1}_{cartan}\theta(k^2-\vec{p}^2)$

$$\begin{aligned}
\left(\Gamma^{(2)}_{00} + \frac{\delta^2 V_k}{\delta A_0^2} + R_{00}\right)^{-1} &= \left(\Gamma^{(2)}_{A_0}[A_0,\vec{A}_\perp] + \frac{\delta^2}{\delta\varphi^2}V_k + R_{A_0}\right)^{-1} \\
&= \begin{pmatrix} k^2+\frac{g^2}{\beta^2}\frac{\delta^2 V}{\delta\varphi_3^2} & \frac{g^2}{\beta^2}\frac{\delta^2 V}{\delta\varphi_3\delta\varphi_8} \\ \frac{g^2}{\beta^2}\frac{\delta^2 V}{\delta\varphi_3\delta\varphi_8} & k^2+\frac{g^2}{\beta^2}\frac{\delta^2 V}{\delta\varphi_8^2}\end{pmatrix}^{-1}\theta(k^2-\vec{p}^2) + \\
&\quad \begin{pmatrix} \vec{p}^2+\frac{g^2}{\beta^2}\frac{\delta^2 V}{\delta\varphi_3^2} & \frac{g^2}{\beta^2}\frac{\delta^2 V}{\delta\varphi_3\delta\varphi_8} \\ \frac{g^2}{\beta^2}\frac{\delta^2 V}{\delta\varphi_3\delta\varphi_8} & \vec{p}^2+\frac{g^2}{\beta^2}\frac{\delta^2 V}{\delta\varphi_8^2}\end{pmatrix}^{-1}\theta(\vec{p}^2-k^2) \\
&= \frac{1}{(k^2+\frac{g^2}{\beta^2}\frac{\delta^2\hat{V}}{\delta\varphi_3^2})(k^2+\frac{g^2}{\beta^2}\frac{\delta^2\hat{V}}{\delta\varphi_3^2}) - (\frac{g^2}{\beta^2}\frac{\delta^2 V}{\delta\varphi_3\delta\varphi_8})^2} \\
&\quad \begin{pmatrix} k^2+\frac{g^2}{\beta^2}\frac{\delta^2 V}{\delta\varphi_8^2} & -\frac{g^2}{\beta^2}\frac{\delta^2 V}{\delta\varphi_3\delta\varphi_8} \\ -\frac{g^2}{\beta^2}\frac{\delta^2 V}{\delta\varphi_3\delta\varphi_8} & k^2+\frac{g^2}{\beta^2}\frac{\delta^2 V}{\delta\varphi_3^2}\end{pmatrix}\theta(k^2-\vec{p}^2) + G(\vec{p}^2)\,\theta(\vec{p}^2-k^2) \\
&= G(k^2)\,\theta(k^2-\vec{p}^2) + G(\vec{p}^2)\,\theta(\vec{p}^2-k^2),
\end{aligned}$$

where we implicitly introduced the propagator G. Taking the trace we get

$$\begin{aligned}
\mathrm{Tr}[(\Gamma^{(2)}_{00}+R_{00})^{-1}\dot{R}_{00}] &= \frac{2k^2+\frac{g^2}{\beta^2}\left(\frac{\delta^2\hat{V}}{\delta\varphi_3^2}+\frac{\delta^2\hat{V}}{\delta\varphi_8^2}\right)}{(k^2+\frac{g^2}{\beta^2}\frac{\delta^2\hat{V}}{\delta\varphi_3^2})(k^2+\frac{g^2}{\beta^2}\frac{\delta^2\hat{V}}{\delta\varphi_3^2}) - (\frac{g^2}{\beta^2}\frac{\delta^2\hat{V}}{\delta\varphi_3\delta\varphi_8})^2}\int d^3p\dot{R}_k(\vec{p}^2) \\
&= \frac{\beta^2 2\hat{k}^2+\beta^2 g^2\left(\frac{\delta^2\hat{V}}{\delta\varphi_3^2}+\frac{\delta^2\hat{V}}{\delta\varphi_8^2}\right)}{(\hat{k}^2+g^2\frac{\delta^2\hat{V}}{\delta\varphi_3^2})(\hat{k}^2+g^2\frac{\delta^2\hat{V}}{\delta\varphi_3^2}) - (g^2\frac{\delta^2\hat{V}}{\delta\varphi_3\delta\varphi_8})^2}\int d^3p\dot{R}_k,
\end{aligned} \tag{B.34}$$

in the last line, we introduced the dimensionless scale $\hat{k} = k\beta$. The integration in momentum space is not difficult. Combining this result with the flow of the spatial gluons,

we get the flow for the potential $\Delta V_{\hat{k}}$

$$\partial_{\hat{k}} \Delta \hat{V}_{\hat{k}} = \frac{2\hat{k}^4}{3(2\pi)^2} \left(1 + \frac{\eta_0}{5}\right) \frac{2\hat{k}^2 + g_k^2 \left((\partial_{\varphi_3}^2 + \partial_{\varphi_8}^2) V_k\right)}{(\hat{k}^2 + g_k^2 \partial_{\varphi_3}^2 V_k)(\hat{k}^2 + g_k^2 \partial_{\varphi_8}^2 V_k) - (g_k^2 \partial_{\varphi_3} \partial_{\varphi_8} V_k)^2} \tag{B.35}$$

Note that this flow equation contains the flow of $SU(2)$ as a limiting case, when restricting to a potential that is not dependent on the Cartan direction φ_8.

B.6 Critical Exponents

Critical exponents can be used to characterise a theory close to a second order phase transition. The interesting point to be taken is that critical exponents do *not* depend on the details of the interaction of a theory, but rather on the dimensionality and the internal symmetries, they are *universal*. Thus, critical exponents can be used to categorise theories into different universality classes. Also it is possible, to extract them experimentally and compare the theoretically computed critical exponents with the experimental ones for a system with the same universality class.

Critical exponents in the fRG

In $SU(2)$ we computed the critical exponent ν of the theory from the temperature dependence of the order parameter. While this is according to the definition of critical exponents, the (f)RG provides other means to extract critical exponents. One searches for a fixed point in the flow and extracts critical exponents from the stability matrix, first work on this with the RG has been done in e.g. [39, 147, 148]. The allows for controlled approximations, moreover, the results obtained allow for a simple unified picture of the critical exponents obtained. Within the fRG critical exponents have been computed a while later [149]. For reviews on this subject see e.g. [63, 81] and references therein.

Critical exponents from DSEs

Dyson Schwinger equations have been used to study various physical objects and theories. However, they have not been used to compute critical exponents. While at first this seems to be surprising, as DSEs have been established for quite a while, there is a reason, that this formalism has not been used to compute critical exponents.

The main obstacle for computing critical exponents from DSEs is that usually, renormalisation group invariance is broken in the DSE framework. For the purposes the DSEs are usually used for this is not an issue, however, it complicates things.

As DSEs are closely related to renormalisation group equations, i.e. DSEs are integrated RGs, it is to be expected, that we can extract critical exponents of a theory using DSEs. Therefore, let us try to calculate the effective potential of a scalar theory using

DSEs. Starting point is the functional form of the DSE

$$\begin{aligned}\frac{\delta\Gamma}{\delta\phi} &= \frac{\delta S}{\delta\phi} + \frac{\lambda}{2}\int\frac{d^3p}{(2\pi)^3}\frac{1}{p^2+V''}\phi - \\ &\quad \frac{\lambda}{3!}\int\frac{d^3p}{(2\pi)^3}\int\frac{d^3q}{(2\pi)^3}\frac{1}{p^2+V''}\frac{1}{q^2+V''}\frac{1}{(p+q)^2+V''}V^{(3)},\end{aligned} \tag{B.36}$$

where the classical action $S[\phi]$ in momentum space is given by

$$S[\phi] = \frac{1}{2}(p^2+m^2)\phi^2 + \frac{\lambda}{4!}\phi^4. \tag{B.37}$$

Note that the full equation is finite, however, there are divergences in the loop terms individually. These of course have to cancel, for calculational purposes, we will render each of these terms finite.

We start with the renormalisation of the tadpole term and write the mass of the scalar field as

$$m^2 = \bar{m}^2 + \Delta m^2 \qquad \text{where} \qquad \Delta m^2 = -\frac{\lambda}{2}\int\frac{d^3p}{(2\pi)^3}\frac{1}{p^2}. \tag{B.38}$$

$\bar{m}^2$ is the renormalised mass. With this renormalisation procedure, the first two terms on the RHS are now given by

$$\frac{\delta S}{\delta\phi} + \frac{\lambda}{2}\int\frac{d^3p}{(2\pi)^3}\frac{1}{p^2+V''}\phi = \frac{1}{2}(p^2+\bar{m}^2)\phi + \phi\frac{\lambda}{2}\int\frac{d^3p}{(2\pi)^3}\left(\frac{1}{p^2+V''}-\frac{1}{p^2}\right) \tag{B.39}$$

The integral in the tadpole term can be computed using the substitution $\tilde{p}^2 = p^2/V''$:

$$\begin{aligned}\int\frac{d^3p}{(2\pi)^3}\left(\frac{1}{p^2+V''}-\frac{1}{p^2}\right) &= -\int\frac{d^3p}{(2\pi)^3}\frac{V''}{(p^2+V'')p^2} = -\frac{1}{V''}\int\frac{d^3p}{(2\pi)^3}\frac{V''}{(1+\tilde{p}^2)\tilde{p}^2} \\ &= -\frac{(V'')^{3/2}}{V''}\frac{4\pi}{(2\pi)^3}\int_0^\infty d\tilde{p}\frac{\tilde{p}^2}{\tilde{p}^2(1+\tilde{p}^2)} \\ &= -\frac{(V'')^{3/2}}{V''}\frac{4\pi}{(2\pi)^3}\frac{\pi}{2} = -\frac{\sqrt{V''}}{4\pi}.\end{aligned} \tag{B.40}$$

While this calculation was straightforward, the last term in eq. (B.36) is logarithmically divergent and we cannot simply absorb this divergence by redefinition of a bare parameter. The problem of this divergence can be cured when taking a derivative w.r.t. the field ϕ. Before doing so, it is advantageous, to divide by $V^{(3)}$ first.

$$\begin{aligned}&\frac{\delta}{\delta\phi}\left(\int\frac{d^3p}{(2\pi)^3}\int\frac{d^3q}{(2\pi)^3}\frac{1}{p^2+V''}\frac{1}{q^2+V''}\frac{1}{(p+q)^2+V''}\right) = \\ &\quad -\int\frac{d^3p}{(2\pi)^3}\int\frac{d^3q}{(2\pi)^3}\left(\frac{1}{p^2+V''}\frac{1}{q^2+V''}\frac{1}{(p+q)^2+V''}\right) \\ &\qquad \left(\frac{V^{(3)}}{p^2+V''}+\frac{V^{(3)}}{q^2+V''}+\frac{V^{(3)}}{(p+q)^2+V''}\right) = \\ &\frac{-3V^{(3)}}{8\pi^4}\int_0^\infty dpp^2\int_0^\infty dqq^2\int_{-1}^1 dx\left(\frac{1}{p^2+V''}\frac{1}{q^2+V''}\left(\frac{1}{p^2+q^2+2pqx+V''}\right)^2\right)\end{aligned} \tag{B.41}$$

the integrals are easily solved using Mathematica. They evaluated to $\pi^2/(12V'')$, the full result for the equation is $V^{(3)}/(32\pi^2 V'')$.

Note that the renormalisation procedure for the two loop terms is different, as mentioned before.

The full functional DSE reads

$$\left(\frac{V'}{V^{(3)}}\right)' = \left(\frac{S'}{V^{(3)}}\right)' - \left(\phi\frac{\lambda}{8\pi}\frac{\sqrt{V''}}{V^{(3)}}\right)' + \lambda\frac{V^{(3)}}{192\pi^2 V''}. \tag{B.42}$$

This can now be used to compute the effective potential and from that we can compute the full scalar mass

$$m^2 = \frac{1}{2}\left.\frac{\partial^2 V}{\partial\phi^2}\right|_{\phi=\phi_{min}}, \tag{B.43}$$

which we need in order to compute the critical exponent ν. Therefore, we use the relation

$$m^2 \propto |\bar{m} - \bar{m}_{cr}|^{2\nu}, \tag{B.44}$$

to compute the critical exponent as a "function" of $\bar{m}/\bar{m}_{cr}$ and extrapolate it to $\bar{m}/\bar{m}_{cr} = 1$, c.f. Fig. B.2.

Before doing so, we write eq. (B.42) as a total derivative and perform the first integration of this differential equation analytically. Therefore, we observe, that $V^{(3)}/V'' = d\ln V''/d\phi$, we get:

$$0 = \frac{d}{d\phi}\left(-\frac{V'}{V^{(3)}} + \frac{S'}{V^{(3)}} - \phi\frac{\lambda}{8\pi}\frac{\sqrt{V''}}{V^{(3)}} + \lambda\frac{\ln(V'')}{192\pi^2}\right). \tag{B.45}$$

Upon integrating, we get a constant of integration, which we fix by the boundary condition $V(\phi_m) = S(\phi_m)|_{p=0}$, where we assume ϕ_m to be large. That is, at large values of the field, the full effective potential is given by the classical potential. We get the final form of the functional DSE:

$$-\frac{\sqrt{\bar{m} + \frac{\lambda}{2}\phi_m^2}}{8\pi} + \lambda\frac{\ln(\bar{m} + \frac{\lambda}{2}\phi_m^2)}{192\pi^2} = -\frac{V'}{V^{(3)}} + \frac{S'}{V^{(3)}} - \frac{\lambda\phi}{8\pi}\frac{\sqrt{V''}}{V^{(3)}} + \lambda\frac{\ln(V'')}{192\pi^2}. \tag{B.46}$$

While in principle this analytical computation could be left to a numerical solver that we use to get the results, practically we have to perform this step to get meaningful results. Note that all the analytical calculations are based on the neglect of the wave-function renormalisation of the scalar propagator. This will be the next extension of this model [150].

Now we compute the critical exponent ν. We get from Fig. B.2

$$2\nu = 0.995 \qquad \rightarrow \qquad \nu \simeq 0.5, \tag{B.47}$$

which is just the mean-field exponent.

This is not too surprising, as we did not take non-trivial momentum dependencies of the propagators into account. In an fRG approach, there are always at least some momentum dependencies taken into account, even in LPA, which is however done in a sense implicitly, as it comes from the inclusion of momentum modes shell by shell. Our findings support this claim that is often made when discussing the advantages of the fRG.

With the extension of this analysis to be done in Ref. [150], this should be overcome and we should get results closer to the physical value of the critical exponent ν.

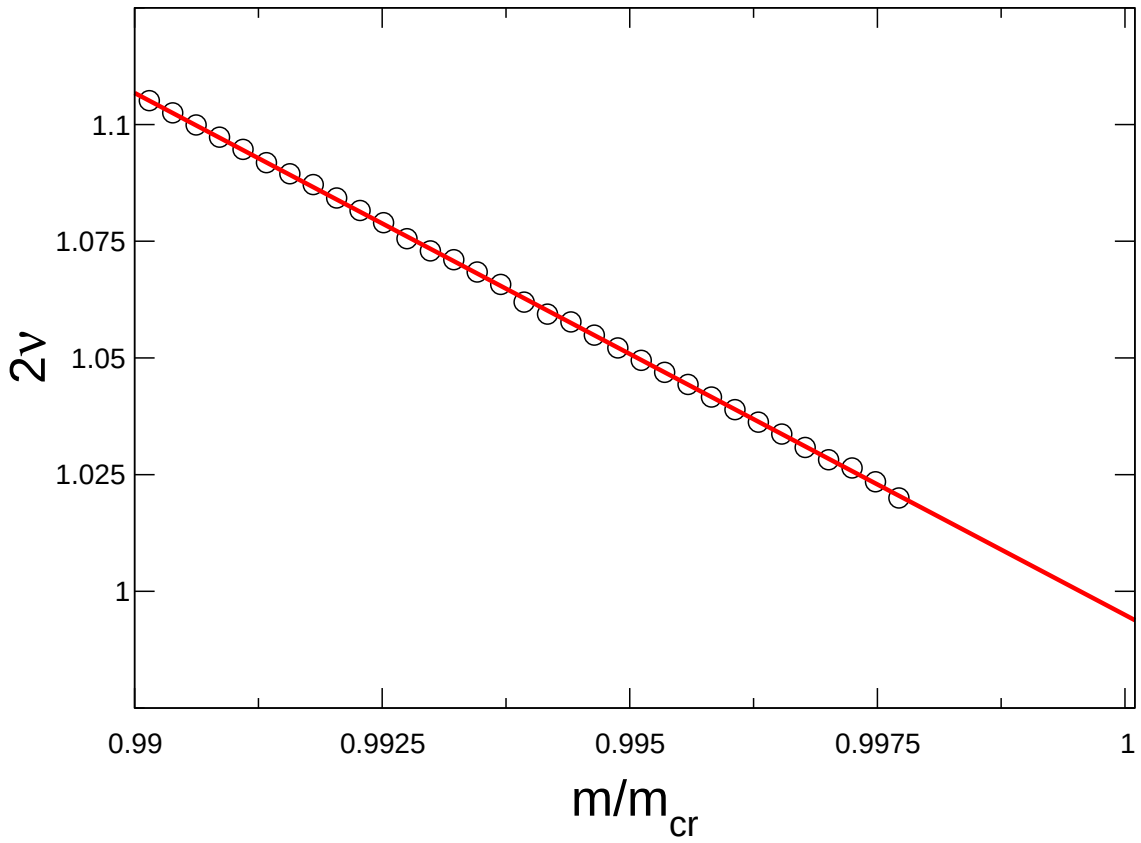

Figure B.2: The critical exponent ν, obtained from eq. (B.44)

C Appendix: Phase diagram

C.1 Deriving the Wave Function Renormalisation for the Gluons

For the derivation of the vacuum polarisation induced by the quarks, we need the quark propagator. As cut-off we will use the 3D optimised cut-off with chiral properties, as introduced in Chap. 4.3.

For the derivation of the flow equation of the gluon wave-function renormalisation, we neglect the tadpole diagram, and higher orders in Γ, as its contribution is proportional to g^4, and therefore does not belong to our truncation[1]. We can start to evaluate the diagram of figure 4.5

The RHS of the flow equation explicitly reads:

$$-\frac{1}{2}\left(G_{\psi_{k\sigma}\bar{\psi}_{r\alpha}}\dot{R}_{\psi_{k\sigma}\bar{\psi}_{t\beta}}G_{\psi_{m\lambda}\bar{\psi}_{t\beta}}\right)(q)\cdot\frac{\delta^3\Gamma_k}{\delta A_i^a(p)\delta\psi_{m\lambda}(q)\delta\bar{\psi}_{l\gamma}(q+p)}\cdot$$
$$\cdot G_{\psi_{n\rho}\bar{\psi}_{l\gamma}}(q+p)\cdot\frac{\delta^3\Gamma_k}{\delta A_j^b(p)\delta\psi_{n\rho}(q+p)\delta\bar{\psi}_{r\alpha}(q)}. \tag{C.1}$$

It is advantageous, to compute parts of the RHS separately and use properties of the cut-off and propagators, to simplify the intermediate results. All details of the calculation can be found in [129].

As an example we show the result for $(G\dot{R}G)_{\psi\bar{\psi}}$. We use the three dimensional optimised regulator with chiral properties.

Then the quark propagator is given by Then, using the above relations, the dressed propagator of the fermions in three dimensions reads

$$G_{\psi\bar{\psi}}=\frac{\delta_{ab}}{Z_\psi(\omega_n,\vec{p},k)}\left(\theta(k^2-\vec{p}^2)\frac{\left(\frac{\not{p}}{|\vec{p}|}\right)_{\alpha\beta}k-i(m_k)_{\alpha\beta}}{k^2+m_k^2}+\theta(\vec{p}^2-k^2)\frac{(\not{p})_{\alpha\beta}-i(m_k)_{\alpha\beta}}{p^2+m_k^2}\right) \tag{C.2}$$

[1] The tadpole diagram vanishes classically on one-loop order and hence the full diagram contains contributions of the order of box-diagrams and higher, which are at least proportional to g^4.

And finally we arrive at

$$
\begin{aligned}
&G_{\psi_{k\sigma}\bar{\psi}_{r\alpha}}\dot{R}_{\psi_{k\sigma}\bar{\psi}_{t\beta}}G_{\psi_{m\lambda}\bar{\psi}_{t\beta}} = \frac{1}{Z_\psi(\vec{p},\vec{k})}\theta(\vec{k}^2-\vec{p}^2)\cdot \\
&\Bigg\{\frac{(\eta_\psi+1)}{(k^2+\tilde{m}^2)^2}k\delta_{rm}\left[\left(\frac{\not{\vec{p}}}{|\vec{p}|}\right)_{\alpha\sigma}k+\check{m}_{\alpha\sigma}\right]\left(\frac{\not{\vec{p}}}{|\vec{p}|}\right)_{\sigma\beta}\left[\left(\frac{\not{\vec{p}}}{|\vec{p}|}\right)_{\beta\lambda}k+\check{m}_{\beta\lambda}\right] \\
&-\frac{(\eta_\psi+1)}{(k^2+\tilde{m}^2)^2}\delta_{rm}\left[\left(\frac{\not{\vec{p}}}{|\vec{p}|}\right)_{\alpha\sigma}k+\check{m}_{\alpha\sigma}\right](\not{\vec{p}})_{\sigma\beta}\left[\left(\frac{\not{\vec{p}}}{|\vec{p}|}\right)_{\beta\lambda}k+\check{m}_{\beta\lambda}\right] \\
&+\frac{\delta_{rm}}{(k^2+\tilde{m}^2)^2}\left[\left(\frac{\not{\vec{p}}}{|\vec{p}|}\right)_{\alpha\sigma}k+\check{m}_{\alpha\sigma}\right](\not{\vec{p}})_{\sigma\beta}\left[\left(\frac{\not{\vec{p}}}{|\vec{p}|}\right)_{\beta\lambda}k+\check{m}_{\beta\lambda}\right]\Bigg\}. \qquad \text{(C.3)}
\end{aligned}
$$

Deriving the anomalous dimension involves quite a bit of algebra and interchanging of derivatives and integrals. Neglecting the anomalous dimension of the fermion, we obtain:

$$
\partial_p^2\frac{\delta^2\dot{\Gamma}}{\delta A^2}\bigg|_{p=0} = -\frac{g^2}{(4\pi)^2}Z_{A_Q}\frac{k^3}{(k^2+m^2)^{\frac{3}{2}}}4\cdot 16\,\theta(\mu-\sqrt{k^2+m^2}). \qquad \text{(C.4)}
$$

Our result for the scaling of wave function renormalisation of the gauge field agrees with perturbation theory [146] in the limit $\mu \to 0$, $m \to 0$ and $\eta_\psi \to 0$.

C.2 Roberge-Weiss Invariance

We mentioned, that we can absorb the center shifts of the phase in the gauge fields. Here we give a detailed derivation of this statement. We start off by considering the Dirac operator and its eigenvalues. We only consider the case of $SU(3)$, which is also the gauge group we use in the calculations.

In the fundamental representation the generators in the 3- and 8- direction are given by:

$$
\tau_3 = \frac{1}{2}\begin{pmatrix}1&0&0\\0&-1&0\\0&0&0\end{pmatrix}, \qquad \tau_8 = \frac{1}{2\sqrt{3}}\begin{pmatrix}1&0&0\\0&1&0\\0&0&-2\end{pmatrix}. \qquad \text{(C.5)}
$$

The fermionic part of the effective action including the imaginary chemical potential like term is given by $\bar{\psi}\left(i\not{D}-2\pi T\theta\gamma_0\right)\psi$ and we can write the zero component of the Dirac operator in terms of the eigenvalues of the gauge fields in 3- and 8-direction $\varphi_3 = \beta g A_0^3$ and $\varphi_8 = \beta g A_0^8$:

$$
iD_0 - 2\pi T\theta = 2\pi T\left(\left(n+\frac{1}{2}-\theta\right)\mathbb{1}_3 + \frac{1}{4\pi}\begin{pmatrix}\varphi_3+\frac{\varphi_8}{\sqrt{3}}&0&0\\0&-\varphi_3+\frac{\varphi_8}{\sqrt{3}}&0\\0&0&-\frac{2\varphi_8}{\sqrt{3}}\end{pmatrix}\right) \qquad \text{(C.6)}
$$

Defining $\bar{\varphi}_3 \equiv \varphi_3 - 3(2\pi)\,\theta$ and $\bar{\varphi}_8 \equiv \varphi_8 - \sqrt{3}(2\pi)\,\theta$, we can rewrite D_0 in terms of $\bar{\varphi}_3$ and $\bar{\varphi}_8$:

$$iD_0 - 2\pi T\theta = 2\pi T \left(\left(n + \frac{1}{2} \right) \mathbb{1}_3 + \frac{1}{4\pi} \begin{pmatrix} \bar{\varphi}_3 + \frac{\bar{\varphi}_8}{\sqrt{3}} - 6\,\theta & 0 & 0 \\ 0 & -\bar{\varphi}_3 + \frac{\bar{\varphi}_8}{\sqrt{3}} & 0 \\ 0 & 0 & -\frac{2\bar{\varphi}_8}{\sqrt{3}} \end{pmatrix} \right). \quad \text{(C.7)}$$

Now only the first eigenvalue of the Dirac operator depends on θ.

Let us now consider the gluonic part of the theory, that we use to compute the Polyakov loop potential. In the adjoint representation D_0 is given by

$$D_0 = 2\pi T n\, \mathbb{1}_8 + T \begin{pmatrix} 0 & -\varphi_3 & 0 & 0 & 0 & 0 & 0 & 0 \\ \varphi_3 & 0 & 0 & 0 & 0 & 0 & 0 & 0 \\ 0 & 0 & 0 & 0 & 0 & 0 & 0 & 0 \\ 0 & 0 & 0 & 0 & -\frac{\varphi_3+\sqrt{3}\varphi_8}{2} & 0 & 0 & 0 \\ 0 & 0 & 0 & \frac{\varphi_3+\sqrt{3}\varphi_8}{2} & 0 & 0 & 0 & 0 \\ 0 & 0 & 0 & 0 & 0 & 0 & \frac{\varphi_3-\sqrt{3}\varphi_8}{2} & 0 \\ 0 & 0 & 0 & 0 & 0 & \frac{-\varphi_3+\sqrt{3}\varphi_8}{2} & 0 & 0 \\ 0 & 0 & 0 & 0 & 0 & 0 & 0 & 0 \end{pmatrix}. \quad \text{(C.8)}$$

The Polyakov loop potential is given as a sum of Yang-Mills and fermionic contribution depending on the Cartan gauge fields φ_3, φ_8 and on the phase θ. We write these functions in terms of their eigenvalues:

$$\begin{aligned} V_{Pol} &= V_{\mathrm{YM}} \left[\varphi_3, \frac{\varphi_3 + \sqrt{3}\,\varphi_8}{2}, \frac{\varphi_3 - \sqrt{3}\,\varphi_8}{2} \right] \\ &\quad + V_{\mathrm{ferm}} \left[\frac{\varphi_3 + \frac{\varphi_8}{\sqrt{3}}}{2} - 2\pi\,\theta, \frac{-\varphi_3 + \frac{\varphi_8}{\sqrt{3}}}{2} - 2\pi\,\theta, -\frac{\varphi_8}{\sqrt{3}} - 2\pi\,\theta \right] \end{aligned} \quad \text{(C.9)}$$

where the eigenvalues for V_{YM} are given by the generators in the adjoint representation and the eigenvalues for V_{ferm} are given by the generators in the fundamental representation. We can use the definitions of $\bar{\varphi}_3$ and $\bar{\varphi}_8$ to rewrite V_{Pol} in terms of the variables $\bar{\varphi}_3$ and $\bar{\varphi}_8$:

$$\begin{aligned} V_{Pol} &= V_{\mathrm{YM}} \left[\bar{\varphi}_3 + 3\,(2\pi)\,\theta, \frac{\bar{\varphi}_3 + \sqrt{3}\,\bar{\varphi}_8}{2} + 3\,(2\pi)\,\theta, \frac{\bar{\varphi}_3 - \sqrt{3}\,\bar{\varphi}_8}{2} \right] \\ &\quad + V_{ferm} \left[\frac{\bar{\varphi}_3 + \frac{\bar{\varphi}_8}{\sqrt{3}}}{2} - 3\,(2\pi)\,\theta, \frac{-\bar{\varphi}_3 + \frac{\bar{\varphi}_8}{\sqrt{3}}}{2}, -\frac{\bar{\varphi}_8}{\sqrt{3}} \right]. \end{aligned} \quad \text{(C.10)}$$

Performing a Roberge-Weiss transformation, we can check that the Polyakov loop potential is invariant under such a transformation:

$$\left.\begin{array}{rcl} \theta & \to & \theta + \theta_z \\ \varphi_3 & \to & \varphi_3 + 3\,(2\pi)\theta_z \\ \varphi_8 & \to & \varphi_8 + \sqrt{3}\,(2\pi)\theta_z \end{array}\right\} \quad \Rightarrow \quad \begin{array}{rcl} \bar{\varphi}_3 & \to & \bar{\varphi}_3 \\ \bar{\varphi}_8 & \to & \bar{\varphi}_8. \end{array}$$

As the center element θ_z has a $\frac{1}{3}$-symmetry, the fermionic potential shows this behaviour as well. The fermionic potential is symmetric under $\theta \to \theta + \theta_z$ where $\theta_z = 0, \frac{1}{3}, \frac{2}{3}, \ldots$. This invariance can be seen by performing the transformation $\theta \to \theta + \frac{1}{3}$ and absorbing the remaining "1" into the Matsubara sums. Therefore, the Matsubara sum is invariant under a Roberge-Weiss transformation. The YM potential is also invariant under such transformations as a shift of the gauge fields caused by a center element θ_z can be compensated by a gauge transformation, i.e. the gluonic action is invariant under center transformations.

C.3 Numerics of the QM Model for the Dual Density

We have used the quark-meson model in local potential approximation (LPA) for a first explicit computation of the dual density. The action of the quark-meson model reads:

$$\begin{aligned}\Gamma &= \int d^4x \left(\bar{\psi} \left(i\not{D} + \frac{2\pi\theta}{\beta}\gamma_0 \right) \psi + \frac{\bar{h}}{\sqrt{2}} \bar{\psi}(\vec{\tau}\cdot\Phi)\psi + \frac{1}{2}\left(\partial_\mu \Phi\right)^2 + U(\Phi^2) - c\sigma \right) \\ &\quad + \int d^4x \left(\frac{Z_{A_{QCD}}}{4} F^a_{\mu\nu} F^a_{\mu\nu} + \Gamma_{\text{gauge}} \right), \end{aligned} \tag{C.11}$$

where $\Phi^T = (\sigma, \vec{\pi})$. For two quark flavors, the Yukawa interaction is determined by $\vec{\tau} = (1, \mathrm{i}\vec{\sigma}\gamma_5)$ where $\vec{\sigma}$ denote the Pauli matrices [2]. In LPA we employ, the wave function renormalisations are trivial, $Z_\psi = Z_\phi = 1$ and the Yukawa coupling is taken to be constant. In order to compute the dual density, we expand the chiral order-parameter potential $U(\Phi^2)$ in a power series of Φ^2 up to order Φ^4 and drop all higher terms, i. e.

$$U(\Phi^T\Phi) = U_0 + \frac{\lambda}{4}\left(\Phi^T\Phi - \Phi_0^2\right)^2, \tag{C.12}$$

where we have introduced the expecation value Φ_0. Due to the fact that we have generalized the fermionic boundary conditions, the expansion coefficient of the potential depend on θ as well. Note that we have an explicit symmetry breaking term $-c\sigma$.

The gauge action will be used to compute the Polyakov loop potential V_{YM} that we already mentioned in the discussion of the Roberge-Weiss periodicity of our approach. It contains a standard Yang-Mills term and the term Γ_{gauge} entails gauge fixing terms and probable higher order terms in the gauge fields. The confining properties of the gluons are reflected in the Polyakov loop potential V_{YM} and will be computed in the spirit of [56]. Thereby we achieve a full decoupling of the quark, meson and gauge sector. Of course, via the dynamical hadronisation procedure, the gluons couple back to the quarks and mesons. This is described in detail in Ref. [18, 49]. At the present stage, we have neglected the contributions to the flow arising from this procedure, it will be an extension of the truncation that should be incorporated straightforwardly.

[2] The Pauli matrices should not be confused with the zeroth component of the vector Φ, namely the σ field.

In our fRG setting, we use dimensionless couplings, that are defined as:

$$\lambda_\phi = \frac{\bar{\lambda}_\phi}{Z_\phi^2}\,, \quad \kappa = \frac{1}{2}\frac{Z_\phi \Phi_0^2}{k^2}\,, \quad h^2 = \frac{\bar{h}^2}{Z_\phi}\,. \tag{C.13}$$

Where λ_ϕ is the scalar coupling, m the boson mass in the symmetric phase and Φ_0 the VEV of the scalar fields. λ_ϕ and Φ_0 are used to parametrise the effective potential in the chiral symmetric and broken phases. h is the dimensionless Yukawa coupling, ϵ stands for the dimensionless fermionic mass.

The QM model has been investigated in many works, using the fRG there has also been quite some effort to compute the phase structure of QCD using extended QM models [18, 93, 106, 151]. Thereby investigation the effects of the inclusion of the gauge sector or the phase diagram for three-flavour QCD.

A detailed discussion of the flow equations for the model 4.9 can be found in Ref. [18]. Here we want to give a glimpse at the changes of the two-flavour theory compared to the one-flavour case. Loosely speaking it can be said, that all terms that stem from the Goldstone bosons carry an N_f dependence. This can be seen easily, since chiral symmetry breaking has the symmetry breaking pattern

$$SU_{N_f} \otimes SU_{N_f} \to SU_{N_f}, \tag{C.14}$$

therefore, we get $N_f^2 - 1$ Goldstone bosons. The scaling of the fermionic contributions is trivially given by N_f, as in the chiral limit every quark flavour contributes equivalently.

At the example of the flow for the parameter κ, we demonstrate this. In Ref. [18] it was computed for the one-flavour case, where the threshold functions $l_1^{(B),(4)}$ used here, can be found, it reads:

$$\partial_t \kappa = -(\eta_\phi^\perp + 2)\kappa + 6v_3\, l_1^{(B),(4)}(\tilde{t}, m_\sigma) + 2v_3\, l_1^{(B),(4)}(\tilde{t}, m_\pi) + \partial_t \epsilon_{\text{ferm}}, \tag{C.15}$$

where $m_{psi} = 0$. Note that we absorbed the fermionic contributions in the last term $\partial_t \epsilon_{\text{ferm}}$. In the presence of the phase θ, this term receives modifications and we have to make sure, that we correctly incorporate the Roberge-Weiss symmetry, as described in the previous section.

In the two flavour case, the flow of κ reads

$$\partial_t \kappa = -(\eta_\phi^\perp + 2)\kappa + 6v_3\, l_1^{(B),(4)}(\tilde{t}, m_\sigma) + (N_f^2 - 1)2v_3\, l_1^{(B),(4)}(\tilde{t}, m_\pi) + N_f \partial_t \epsilon_{\text{ferm}}. \tag{C.16}$$

Note that in the presence of an explicit symmetry breaking term c this term receives an additional contribution, that we do not display. We see that the threshold function, that contain a Goldstone propagator, gets multiplied with a factor of $N_f^2 - 1$ as we hinted at before. The fermion contributions is trivially scaled by a factor N_f as explained above.

The flow of the four-boson coupling λ is modified equally.

On the contrary, the flow of the Yukawa coupling is not modified in the presence of additional flavours. This is a consequence of our truncation in which we do not allow for a flavour changing Yukawa interaction.

Parameter Fixing

We fix the parameters of the model at vanishing θ, which corresponds to standard fermions. For the numerical study, we have fixed the UV parameters of the model such that we find a quark mass $m_q = 0.3\,\mathrm{GeV}$ and $f_\pi = (1/2)\Phi_0^2 = (0.090\,\mathrm{GeV})^2$ in the IR. These two IR-parameters fix our choice for the Yukawa coupling: $\bar{h} = 10/3$. Note that $m_q^2 = h^2(\Phi_0^2/2)$. To be more specific, we use the following set of initial conditions for our studies of QCD in the chiral limit:

$$\begin{aligned} \Lambda_{\mathrm{UV}} &= 10\,\mathrm{GeV}\,, \\ \bar{c} = c_{\mathrm{UV}}\Lambda_{\mathrm{UV}}^3 &= -510^{-8}\,, \\ \epsilon_{\mathrm{UV}} = \frac{m^2}{k^2} &= 0.37803 \\ \lambda_{\mathrm{UV}} &= 300\,. \end{aligned}$$

We then find:

$$\begin{aligned} c(k\to 0) &= -10^{-8}\,, \\ \kappa_{\mathrm{UV}}(k\to 0) = \frac{1}{2}\frac{\Phi_0^2(k\to 0)}{k^2} &= 4082.01 \\ \lambda_{\mathrm{UV}}(k\to 0) &= 8.023\,, \end{aligned}$$

which translates into

$$\begin{aligned} m_q(k\to 0) &= 0.3\,\mathrm{GeV} \\ m_\sigma(k\to 0) &= 0.255\,\mathrm{GeV} \\ \frac{1}{2}\Phi_0^2(k\to 0) &= 0.090\,\mathrm{GeV}\,. \end{aligned} \tag{C.17}$$

D Appendix: Non-linear basis

D.1 Scale Dependence of the Fields

For the evaluation of these derivatives we need $\dot{\varphi}$ and $\dot{\vartheta}$ in terms of φ and ϑ. This is achieved by solving Eq. (5.9) for φ and ϑ, on which we can then take a derivative w.r.t. to t. ($t = ln(k/\Lambda)$). We make use of the fact the Φ is t-independent, $\dot{\Phi} = 0$, in particular we get

$$\begin{aligned} e^{2i\vartheta/b} &= \frac{\Phi - (\sqrt{\rho_0} - b)}{\Phi^* - (\sqrt{\rho_0} - b)} \quad \Rightarrow \quad \vartheta = \frac{b}{2i} ln \left(\frac{\Phi - (\sqrt{\rho_0} - b)}{\Phi^* - (\sqrt{\rho_0} - b)} \right) \\ \dot{\vartheta} &= \frac{\dot{b}}{b}\vartheta + \frac{b}{2i} \left\{ \frac{-\partial_t(\sqrt{\rho_0} - b)}{\Phi - (\sqrt{\rho_0} - b)} - \frac{-\partial_t(\sqrt{\rho_0} - b)}{\Phi^* - (\sqrt{\rho_0} - b)} \right\} \\ &= \frac{\dot{b}}{b}\vartheta + \frac{b(\dot{\sqrt{\rho_0}} - \dot{b})}{2i(\varphi + b)}(e^{i\vartheta/b} - e^{-i\vartheta/b}) \end{aligned}$$

and

$$\begin{aligned} (\varphi + b)^2 &= [\Phi - (\sqrt{\rho_0} - b)]\,[\Phi^* - (\sqrt{\rho_0} - b)] \\ \Rightarrow \quad \varphi &= \sqrt{[\Phi - (\sqrt{\rho_0} - b)]\,[\Phi^* - (\sqrt{\rho_0} - b)]} - b \\ \dot{\varphi} &= -\dot{b} - \frac{(\partial_t(\sqrt{\rho_0} - b))(\left[\Phi - (\sqrt{\rho_0} - b)\right] + \left[\Phi^* - (\sqrt{\rho_0} - b)\right])}{2\sqrt{\left[\Phi - (\sqrt{\rho_0} - b)\right]\left[\Phi^* - (\sqrt{\rho_0} - b)\right]}} \\ &= -\dot{b} - \frac{(\dot{\sqrt{\rho_0}} - \dot{b})(\varphi + b)}{2(\varphi + b)}(e^{i\vartheta/b} + e^{-i\vartheta/b}). \end{aligned}$$

D.2 Flow of the Radial Mode Potential

As introduced above, the potential V is most conveniently parametrised by

$$V[\rho] = \frac{\lambda_k}{2}(\rho - \rho_{0,k})^2. \tag{D.1}$$

The propagator in the flow equation, is obtained by taking derivates of the effective action Γ with respect to the field φ and ϑ. By means of the chain rule, we rewrite these derivates

$$\frac{\partial^2}{\partial\varphi^2} = \frac{\partial^2\rho}{\partial\varphi^2}\frac{\partial}{\partial\rho} + \left(\frac{\partial\rho}{\partial\varphi}\right)^2 \frac{\partial^2}{\partial\rho^2} \tag{D.2}$$

and similiar expressions for the other derivatives that appear in the computation of $\Gamma^{(2)}$.

We display explicit expressions for the propagators and regulators in field space here:

$$G|_{\vartheta=0} = \left((\Gamma^{(2)}+R)|_{\vartheta=0}\right)^{-1} = \begin{pmatrix} G_\varphi & 0 \\ 0 & G_\vartheta \end{pmatrix}, \tag{D.3}$$

$$\dot{R} = \begin{pmatrix} \dot{R}_\varphi & 0 \\ 0 & \dot{R}_\vartheta \end{pmatrix} = \begin{pmatrix} \dot{R}_{k,\varphi} & 0 \\ 0 & \dot{R}_{k,\vartheta} + 2\frac{\partial\dot{\vartheta}}{\partial\vartheta} R_{k,\vartheta} \end{pmatrix}. \tag{D.4}$$

Note that the second term in the regulator $\dot{R}_\vartheta$ is a consequence of the second term on the RHS of eq. (5.17). In $\dot{R}_\varphi$ this term is zero, c.f. eq. (5.19).

We introduced the components of the propagtor, G_φ and G_ϑ

$$G_\varphi = \left(Z_\varphi p^2 + 2V' + 4\rho_0 V'' + R_{k,\varphi}\right)^{-1} \tag{D.5}$$

$$G_\vartheta = \left(p^2(Z_\vartheta + U(\varphi)) + \frac{\partial^2\rho}{\partial\vartheta^2}V' + R_{k,\vartheta}\right)^{-1}. \tag{D.6}$$

We introduced the shorthand $V' = \partial V(\rho)/\partial\rho$ and used $\partial\rho/\partial\vartheta|_{\vartheta=0} = 0$. The optimised cut-off is given by

$$R_{k,\varphi/\theta}(p^2) = Z_{\varphi/\theta}(k^2 - p^2)\ \theta(Z_{\varphi/\theta}(k^2-p^2)) \tag{D.7}$$

In the flow equations for the effective potential V the term $\dot{\Psi}_i \frac{\delta\Gamma}{\delta\Psi_i}$ is particularly simple, since we can set $\vartheta = 0 = p$ from the beginning of the calculation. We get:

$$\dot{\vartheta}\Big|_{\vartheta=0} = 0 \quad , \quad \dot{\varphi}|_{\vartheta=0} = -\partial_t\sqrt{\rho_0} \quad , \quad \frac{\delta\Gamma}{\delta\varphi}\Big|_{\vartheta=0} = 2(\varphi+\sqrt{\rho_0})V' \tag{D.8}$$

The flow equation for the effective potential V reads:

$$\dot{V} - \dot{\rho}_0\left(1+\frac{\varphi}{\sqrt{\rho_0}}\right)V' = \frac{1}{2}\int\frac{d^dp}{(2\pi)^d}\left\{\frac{\dot{R}_k(p^2)}{Z_\varphi k^2 + 2V' + 4\rho^2V''} + \frac{\dot{R}_k(p^2) + 2\frac{\partial\dot{\vartheta}}{\partial\vartheta}R_k(p^2)}{Z_\vartheta k^2 + p^2U(\varphi) + \frac{\partial^2\rho}{\partial\vartheta^2}V'}\right\} \tag{D.9}$$

Getting the flow equations for λ and ρ_0 is straightforward.

D.3 Flow of the Goldstone Potential

Getting the flow for U is more involved, since we have to take a second derivative w.r.t. to φ on Eq. (5.17) and a second derivative w.r.t. momentum p which we will set to zero at the end of the computation. Generically this will generate loop and tadpole graphs, shown in Fig. 5.2 We will give a detailed derivation how this arise here.

From the parameterisation eq. (5.20) and the flow equation eq. (5.17), we get the flow of U by means of the formula

$$\dot{Z}_\vartheta + \dot{U}\Big|_{\vartheta=0=p} = \frac{1}{2d}\left(\partial_p^2\frac{\delta^2}{\delta\vartheta^2}\dot{\Gamma} - \partial_p^2\frac{\delta^2}{\delta\vartheta^2}\dot{\Phi}_i\frac{\delta\Gamma}{\delta\Phi_i}\right)\Big|_{\vartheta=0=p}. \tag{D.10}$$

Here we introduced the shorthand $\partial_p^2 = \partial_{p_\mu}\partial_{p_\mu}$.

It is simple algebra to work out the second term on the RHS:

$$\begin{array}{lll} \dot{\vartheta}\Big|_{\vartheta=0} = 0 & \frac{\partial\dot{\vartheta}}{\partial\vartheta}\Big|_{\vartheta=0} = \frac{\dot{b}}{b} + \frac{\sqrt{\dot{\rho_0}}-\dot{b}}{\varphi+b} & \frac{\partial^2\dot{\vartheta}}{\partial\vartheta^2}\Big|_{\vartheta=0} = 0 \\ \dot{\varphi}|_{\vartheta=0} = -\sqrt{\dot{\rho_0}} & \frac{\partial\dot{\varphi}}{\partial\vartheta}|_{\vartheta=0} = 0 & \frac{\partial^2\dot{\varphi}}{\partial\vartheta^2}\Big|_{\vartheta=0} = \frac{\sqrt{\dot{\rho_0}}-\dot{b}}{b^2} \end{array} \tag{D.11}$$

Thus we only need the compute the following three terms, evaluated at zero momentum p and $\vartheta = 0$,

$$\partial_p^2\frac{\delta^2\Gamma}{\delta\vartheta^2} = 2d(Z_\vartheta + U(\varphi)) \quad \partial_p^2\frac{\delta\Gamma}{\delta\varphi} = 2dZ_\varphi\varphi \quad \partial_p^2\frac{\delta^3\Gamma}{\delta\varphi\delta\vartheta^2} = 2dU'(\varphi) \tag{D.12}$$

and sum up all the contributions. We get eventually:

$$\partial_p^2\frac{\delta^2}{\delta\vartheta^2}\dot{\Psi}_i\frac{\delta\Gamma}{\delta\Psi_i} = 2d\left[(Z_\vartheta + U(\varphi))\left(\frac{\dot{b}}{b} + \frac{\sqrt{\dot{\rho_0}}-\dot{b}}{\varphi+b}\right) - \sqrt{\dot{\rho_0}}\;U'(\varphi) + Z_\varphi\;\varphi\;\frac{\sqrt{\dot{\rho_0}}-\dot{b}}{b^2}\right] \tag{D.13}$$

There is however a further approximation we make at this level. Namely, we neglect derivatives w.r.t. to ϑ acting on $\delta\dot{\Phi}/\delta\Phi$.

We now evaluate the second derivative of the flow of the effective action with respect to ϑ. We start by evaluating the first (functional) derivative

$$\frac{\delta}{\delta\vartheta}\dot{\Gamma} = -\frac{1}{2}\mathrm{Tr}\left[\frac{\dot{R}}{\Gamma_k^{(2)}+R}\Gamma^{(3)}\frac{1}{\Gamma_k^{(2)}+R}\right]$$

where $\Gamma^{(3)}$ is a derivative of $\Gamma^{(2)}$ with respect to ϑ. Then the second derivative reads:

$$\frac{\delta^2}{\delta\vartheta^2}\dot{\Gamma} = -\frac{1}{2}\mathrm{Tr}\left[\frac{\dot{R}}{\Gamma_k^{(2)}+R}\Gamma^{(4)}\frac{1}{\Gamma_k^{(2)}+R} - 2\frac{\dot{R}}{\Gamma_k^{(2)}+R}\Gamma^{(3)}\frac{1}{\Gamma_k^{(2)}+R}\Gamma^{(3)}\frac{1}{\Gamma_k^{(2)}+R}\right]$$

where $\Gamma^{(4)}$ is the second derivative of $\Gamma^{(2)}$ with respect to ϑ.

$\Gamma^{(4)}$ and $\Gamma^{(3)}$ are of course matrix-valued in field space and we should display explicit expressions for them at this place.

$$\begin{aligned} \Gamma^{(3)}|_{\vartheta=0} &= \begin{pmatrix} \Gamma_{(\varphi\varphi\vartheta)} & \Gamma_{(\varphi\vartheta\vartheta)} \\ \Gamma_{(\varphi\vartheta\vartheta)} & \Gamma_{(\vartheta\vartheta\vartheta)} \end{pmatrix} \\ &= \left[p_{\vartheta_1}p_{\vartheta_2}U'(\varphi) + \frac{\partial^3}{\partial\vartheta^2\partial\varphi}V(\rho(\varphi,\vartheta))\right]\begin{pmatrix} 0 & 1 \\ 1 & 0 \end{pmatrix} \qquad \text{(D.14)} \\ \Gamma^{(4)}|_{\vartheta=0} &= \begin{pmatrix} \Gamma_{(\varphi\varphi\vartheta\vartheta)} & \Gamma_{(\varphi\vartheta\vartheta\vartheta)} \\ \Gamma_{(\varphi\vartheta\vartheta\vartheta)} & \Gamma_{(\vartheta\vartheta\vartheta\vartheta)} \end{pmatrix} = \begin{pmatrix} \Gamma_{(\varphi\varphi\vartheta\vartheta)} & 0 \\ 0 & \Gamma_{(\vartheta\vartheta\vartheta\vartheta)} \end{pmatrix} \qquad \text{(D.15)} \end{aligned}$$

where we define

$$\begin{aligned} \Gamma_{(\varphi\varphi\vartheta\vartheta)} &= p_{\vartheta_1}p_{\vartheta_2}U''(\varphi) + \frac{\partial^4}{\partial\vartheta^2\partial\varphi^2}V(\rho(\varphi,\vartheta)), \qquad \text{(D.16)} \\ \Gamma_{(\vartheta\vartheta\vartheta\vartheta)} &= \frac{\partial^4}{\partial\vartheta^4}V(\rho(\varphi,\vartheta)). \qquad \text{(D.17)} \end{aligned}$$

In a shorthand notation, we can write using the propagators and regulators defined before

$$\frac{\delta^2}{\delta\vartheta^2}\dot{\Gamma} = -\frac{1}{2}\mathrm{Tr}\left[\dot{R}G\Gamma^{(4)}G - 2\dot{R}G\Gamma^{(3)}G\Gamma^{(3)}G\right] \tag{D.18}$$

The first term is the tadpole term and the last term is a loop graph.

Here we can nicely see how our approximation works. Consider the derivative terms of V in $\Gamma^{(4)}$ and $\Gamma^{(3)}$. We assume ρ and hence also $V(\rho)$ to be a function exclusively of φ. Therefore, all these derivates vanish, remember that there are derivatives w.r.t. ϑ, and we get vertices that are always proportianal to external momenta at least of order p^2. Then if the momentum derivative acts on anything other than the vertex, the contribution from this diagram vanishes. It is now simple algebra to evaluate the first term in eq. (D.18) at vanishings field ϑ:

$$\mathrm{Tr}\left[\frac{\dot{R}}{\Gamma_k^{(2)}+R}\Gamma^{(4)}\frac{1}{\Gamma_k^{(2)}+R}\right]\Big|_{\vartheta=0} = \mathrm{Tr}\left[\begin{array}{cc} \dot{R}_\varphi G_\varphi \Gamma_{(\varphi\varphi\vartheta\vartheta)} G_\varphi & 0 \\ 0 & \dot{R}_\vartheta G_\vartheta \Gamma_{(\vartheta\vartheta\vartheta\vartheta)} G_\vartheta \end{array}\right]\Big|_{\vartheta=0}$$

There are two tadpole graphs arising from this trace. However the tadpole with the Goldstone boson propagator in the loop vanishes. This can be seen easily: Upon taking a derivative with respect to momentum p the tadpole with the Goldstone boson in the loop vanishes, since the four-Goldstone vertex is momentum independent, c.f. eq. (D.16).

The remaining tadpole diagram is shown in Fig 5.2. Thus the tadpole contribution to the flow of the potential U is given by

$$\partial_p^2 \mathrm{Tr}\left[\left(\begin{array}{cc} \dot{R}_\varphi G_\varphi \Gamma_{(\varphi\varphi\vartheta\vartheta)} G_\varphi & 0 \\ 0 & \dot{R}_\vartheta G_\vartheta \Gamma_{(\vartheta\vartheta\vartheta\vartheta)} G_\vartheta \end{array}\right)\right] = -\frac{1}{2}\int_q G_\varphi^2(q)\dot{R}_\varphi(q) 2d U''(\varphi), \tag{D.19}$$

where the factor of $2d$ is a consequence of the derivative w.r.t. momentum p.

In our approximation, we have $Z_\varphi(t) = 1$. Plugging in the optimised regulator and specifying to three dimensions, we finally get for the tadpole contribution:

$$-\frac{1}{2}\,\partial_p^2 \mathrm{Tr}\left[\dot{R}G\Gamma^{(4)}G\right] = \frac{4}{(2\pi)^2}\frac{k^5 U''(\varphi)}{(k^2 + \frac{\partial^2}{\partial\varphi^2}V(\rho(\varphi,\vartheta))|_{\vartheta=0})^2}. \tag{D.20}$$

The second term in eq. (5.30) results in two one-loop graphs.

Looking at the structure we see that it will give more complicated one-loop structures. However the computation of the trace is readily done. The result, neglecting off-diagonal terms, that drop out of the trace, is:

$$\mathrm{Tr}\left[2\dot{R}G\Gamma^{(3)}G\Gamma^{(3)}G\right]\Big|_{\vartheta=0} = \mathrm{Tr}\left[\begin{array}{cc} \dot{R}_\varphi G_\varphi \Gamma_{(\varphi\vartheta\vartheta)} G_\vartheta \Gamma_{(\varphi\vartheta\vartheta)} G_\varphi & 0 \\ 0 & \dot{R}_\vartheta G_\vartheta \Gamma_{(\varphi\vartheta\vartheta)} G_\varphi \Gamma_{(\varphi\vartheta\vartheta)} G_\vartheta \end{array}\right]. \tag{D.21}$$

We do not explicitly give the algebraic derivation of the loop graphs. We call them L_1 and L_2. L_1 is the graph with the regulator insertion into the radial mode propagator, correspondingly, L_2 has a regulator insertion in the Goldstone propagator. The correspondig

diagrams are shown in Fig 5.2. They read explicitly

$$
\begin{aligned}
L_1 &= \int \frac{d^dq}{(2\pi)^d} \frac{(p\cdot(p+q)U' + V''')^2 \dot{R}_k(q^2)}{(Z_\varphi q^2 + 2V' + 4\rho_0 V'' + R_k(q^2))^2((p+q)^2(Z_\vartheta + U) + \frac{\partial^2\rho}{\partial\vartheta^2}V' + R_k((p+q)2))} \\
L_2 &= \int \frac{d^dq}{(2\pi)^d} \frac{(p\cdot(p+q)U' + V''')^2 (\dot{R}_k(q^2) + 2\frac{\partial\dot{\vartheta}}{\partial\vartheta}R_k(q^2))}{(Z_\varphi(p+q)^2 + 2V' + 4\rho_0 V'' + R_k((p+q)^2))(q^2(Z_\vartheta + U) + \frac{\partial^2\rho}{\partial\vartheta^2}V' + R_k(q^2))^2},
\end{aligned}
$$

where we introduced the shorthand $V''' = \frac{\partial^3}{\partial\vartheta^2\partial\varphi}V(\rho(\varphi,\vartheta))|_{\vartheta=0}$.

To get the flow of the Goldstone mode potential, we also have to apply momentum derivatives. As mentioned above, we only consider derivatives w.r.t. momentum p acting on the vertices. Therefore we need only evaluate the terms

$$
\begin{aligned}
\partial_p^2(p\cdot(p+q)U' + V''')^2 &= 2(\partial_p)_\mu((2p+q)_\mu p\cdot(p+q)U'^2 + (2p+q)_\mu U'V''') \\
&= 2((2p+q)^2U'^2 + 2dU'V''') \xrightarrow{p\to 0} 2(q^2U'^2 + 2dU'V''').
\end{aligned}
$$

Bibliography

[1] H. D. Politzer, "Reliable perturbative results for strong interactions?," *Phys. Rev. Lett.* **30** (1973) 1346–1349.

[2] D. J. Gross and F. Wilczek, "Ultravioler behavior of non-abelian gauge theories," *Phys. Rev. Lett.* **30** (1973) 1343–1346.

[3] J. C. Collins and M. J. Perry, "Superdense matter: Neutrons or asymptotically free quarks?," *Phys. Rev. Lett.* **34** (1975) 1353.

[4] N. Cabibbo and G. Parisi, "Exponential Hadronic Spectrum and Quark Liberation," *Phys. Lett.* **B59** (1975) 67–69.

[5] GSI Darmstadt, "The QCD phase diagram."

[6] M. Buballa, "NJL model analysis of dense quark matter," *Phys. Rept.* **407** (2005) 205–376, `hep-ph/0402234`.

[7] F. Karsch and E. Laermann, "Thermodynamics and in-medium hadron properties from lattice QCD," `hep-lat/0305025`.

[8] H. J. Rothe, "Lattice gauge theories: An Introduction," *World Sci. Lect. Notes Phys.* **74** (2005) 1–605.

[9] P. de Forcrand and O. Philipsen, "The QCD phase diagram for small densities from imaginary chemical potential," *Nucl. Phys.* **B642** (2002) 290–306, `hep-lat/0205016`.

[10] P. de Forcrand and O. Philipsen, "The QCD Phase Diagram for Three Degenerate Flavors and Small Baryon Density," *Nucl. Phys.* **B673** (2003) 170–186, `hep-lat/0307020`.

[11] G. Endrodi, Z. Fodor, S. D. Katz, and K. K. Szabo, "The curvature of the QCD phase transition line," *PoS* **LATTICE2008** (2008) 205, `0901.3018`.

[12] Z. Fodor and S. D. Katz, "A new method to study lattice QCD at finite temperature and chemical potential," *Phys. Lett.* **B534** (2002) 87–92, `hep-lat/0104001`.

[13] Z. Fodor and S. D. Katz, "Critical point of QCD at finite T and mu, lattice results for physical quark masses," *JHEP* **04** (2004) 050, `hep-lat/0402006`.

[14] Z. Fodor, C. Guse, S. D. Katz, and K. K. Szabo, "Curvature of the phase transition line in the mu-T plane," *PoS* **LAT2007** (2007) 189, 0712.2702.

[15] P. de Forcrand and O. Philipsen, "The chiral critical line of Nf=2+1 QCD at zero and non- zero baryon density," *JHEP* **01** (2007) 077, hep-lat/0607017.

[16] M. D'Elia and M.-P. Lombardo, "Finite density QCD via imaginary chemical potential," *Phys. Rev.* **D67** (2003) 014505.

[17] F. Karsch *et al.*, "Where is the chiral critical point in 3-flavor QCD?," *Nucl. Phys. Proc. Suppl.* **129** (2004) 614–616, hep-lat/0309116.

[18] J. Braun, "The QCD Phase Boundary from Quark-Gluon Dynamics," 0810.1727.

[19] L. McLerran and R. D. Pisarski, "Phases of Cold, Dense Quarks at Large N_c," *Nucl. Phys.* **A796** (2007) 83–100, 0706.2191.

[20] P. Braun-Munzinger, K. Redlich, and J. Stachel, "Particle production in heavy ion collisions," nucl-th/0304013.

[21] P. Braun-Munzinger, J. Stachel, and C. Wetterich, "Chemical freeze-out and the QCD phase transition temperature," *Phys. Lett.* **B596** (2004) 61–69, nucl-th/0311005.

[22] A. M. Polyakov, "Thermal Properties of Gauge Fields and Quark Liberation," *Phys. Lett.* **B72** (1978) 477–480.

[23] F. Marhauser and J. M. Pawlowski, "Confinement in Polyakov Gauge," 0812.1144.

[24] J. Braun, L. M. Haas, F. Marhauser, and J. M. Pawlowski, "On the relation of quark confinement and chiral symmetry breaking," 0908.0008.

[25] J. Bardeen, L. N. Cooper, and J. R. Schrieffer, "Theory of superconductivity," *Phys. Rev.* **108** (1957) 1175–1204.

[26] V. N. Gribov, "Quantization of non-Abelian gauge theories," *Nucl. Phys.* **B139** (1978) 1.

[27] J. I. Kapusta, "Finite temperature field theory,". Cambridge University Press, Cambridge, 1989.

[28] M. Le Bellac, "Thermal Field Theory,". Cambridge University Press, Cambridge, 1996.

[29] N. Seiberg and E. Witten, "Monopole Condensation, And Confinement In N=2 Supersymmetric Yang-Mills Theory," *Nucl. Phys.* **B426** (1994) 19–52, hep-th/9407087.

[30] W. Hollik, "The electroweak standard model,". Prepared for ICTP Summer School in Particle Physics, Trieste, Italy, 21 Jun - 9 Jul 1999.

[31] H. Leutwyler, "Principles of chiral perturbation theory," `hep-ph/9406283`.

[32] G. Ecker, "Chiral perturbation theory," *Prog. Part. Nucl. Phys.* **35** (1995) 1–80, `hep-ph/9501357`.

[33] A. V. Manohar, "Effective field theories," `hep-ph/9606222`.

[34] G. Ecker, "Chiral symmetry," `hep-ph/9805500`.

[35] B. Svetitsky, "Symmetry Aspects of Finite Temperature Confinement Transitions," *Phys. Rept.* **132** (1986) 1–53.

[36] C. Ford, U. G. Mitreuter, T. Tok, A. Wipf, and J. M. Pawlowski, "Monopoles, Polyakov loops, and gauge fixing on the torus," *Annals Phys.* **269** (1998) 26–50, `hep-th/9802191`.

[37] C. Ford, T. Tok, and A. Wipf, "SU(N)-gauge theories in Polyakov gauge on the torus," *Phys. Lett.* **B456** (1999) 155–161, `hep-th/9811248`.

[38] L. P. Kadanoff, "Scaling laws for Ising models near T(c)," *Physics* **2** (1966) 263–272.

[39] F. J. Wegner and A. Houghton, "Renormalization group equation for critical phenomena," *Phys. Rev.* **A8** (1973) 401–412.

[40] K. G. Wilson, "Renormalization group and critical phenomena. 1. Renormalization group and the Kadanoff scaling picture," *Phys. Rev.* **B4** (1971) 3174–3183.

[41] J. M. Pawlowski, "Aspects of the functional renormalisation group," *Annals Phys.* **322** (2007) 2831–2915, `hep-th/0512261`.

[42] R. Alkofer and L. von Smekal, "The infrared behavior of QCD Green's functions: Confinement, dynamical symmetry breaking, and hadrons as relativistic bound states," *Phys. Rept.* **353** (2001) 281, `hep-ph/0007355`.

[43] C. S. Fischer, "Infrared properties of QCD from Dyson-Schwinger equations," *J. Phys.* **G32** (2006) R253–R291, `hep-ph/0605173`.

[44] C. Wetterich, "Exact evolution equation for the effective potential," *Phys. Lett.* **B301** (1993) 90–94.

[45] U. Ellwanger, M. Hirsch, and A. Weber, "The heavy quark potential from Wilson's exact renormalization group," *Eur. Phys. J.* **C1** (1998) 563–578, `hep-ph/9606468`.

[46] U. Ellwanger, M. Hirsch, and A. Weber, "Flow equations for the relevant part of the pure Yang- Mills action," *Z. Phys.* **C69** (1996) 687–698, hep-th/9506019.

[47] M. Bonini, M. D'Attanasio, and G. Marchesini, "BRS symmetry from renormalization group flow," *Phys. Lett.* **B346** (1995) 87–93, hep-th/9412195.

[48] D. F. Litim and J. M. Pawlowski, "Completeness and consistency of renormalisation group flows," *Phys. Rev.* **D66** (2002) 025030, hep-th/0202188.

[49] H. Gies and C. Wetterich, "Renormalization flow of bound states," *Phys. Rev.* **D65** (2002) 065001, hep-th/0107221.

[50] H. Gies and C. Wetterich, "Universality of spontaneous chiral symmetry breaking in gauge theories," *Phys. Rev.* **D69** (2004) 025001, hep-th/0209183.

[51] H. Gies and C. Wetterich, "Renormalization flow from UV to IR degrees of freedom," *Acta Phys. Slov.* **52** (2002) 215–220, hep-ph/0205226.

[52] N. Weiss, "The Effective Potential for the Order Parameter of Gauge Theories at Finite Temperature," *Phys. Rev.* **D24** (1981) 475.

[53] M. Engelhardt and H. Reinhardt, "Effective potential for the order parameter of the SU(2) Yang-Mills deconfinement transition," *Phys. Lett.* **B430** (1998) 161–167, hep-th/9709115.

[54] H. Gies, "Effective action for the order parameter of the deconfinement transition of Yang-Mills theories," *Phys. Rev.* **D63** (2001) 025013, hep-th/0005252.

[55] J. Braun, H. Gies, and H. J. Pirner, "RG flow of the Polyakov-loop potential: First status report," *AIP Conf. Proc.* **775** (2005) 162–172, hep-ph/0610341.

[56] J. Braun, H. Gies, and J. M. Pawlowski, "Quark Confinement from Color Confinement," 0708.2413.

[57] H. Reinhardt, "Resolution of Gauss' law in Yang-Mills theory by Gauge Invariant Projection: Topology and Magnetic Monopoles," *Nucl. Phys.* **B503** (1997) 505–529, hep-th/9702049.

[58] O. Jahn and F. Lenz, "Structure and dynamics of monopoles in axial gauge QCD," *Phys. Rev.* **D58** (1998) 085006, hep-th/9803177.

[59] D. F. Litim, "Optimisation of the exact renormalisation group," *Phys. Lett.* **B486** (2000) 92–99, hep-th/0005245.

[60] D. F. Litim, "Optimised renormalisation group flows," *Phys. Rev.* **D64** (2001) 105007, hep-th/0103195.

[61] D. F. Litim, "Mind the gap," *Int. J. Mod. Phys.* **A16** (2001) 2081–2088, hep-th/0104221.

[62] D. F. Litim and J. M. Pawlowski, "Non-perturbative thermal flows and resummations," *JHEP* **11** (2006) 026, hep-th/0609122.

[63] J. Berges, N. Tetradis, and C. Wetterich, "Non-perturbative renormalization flow in quantum field theory and statistical physics," *Phys. Rept.* **363** (2002) 223–386, hep-ph/0005122.

[64] C. Bagnuls and C. Bervillier, "Exact renormalization group equations: An introductory review," *Phys. Rept.* **348** (2001) 91, hep-th/0002034.

[65] K. Aoki, "Introduction to the nonperturbative renormalization group and its recent applications," *Int. J. Mod. Phys.* **B14** (2000) 1249–1326.

[66] M. Salmhofer and C. Honerkamp, "Fermionic renormalization group flows: Technique and theory," *Prog. Theor. Phys.* **105** (2001) 1–35.

[67] J. Polonyi, "Lectures on the functional renormalization group method," *Central Eur. J. Phys.* **1** (2003) 1–71, hep-th/0110026.

[68] B. Delamotte, "An introduction to the nonperturbative renormalization group," cond-mat/0702365.

[69] D. F. Litim and J. M. Pawlowski, "On gauge invariant Wilsonian flows," hep-th/9901063.

[70] H. Gies, "Introduction to the functional RG and applications to gauge theories," hep-ph/0611146.

[71] C. S. Fischer, A. Maas, and J. M. Pawlowski, "On the infrared behavior of Landau gauge Yang-Mills theory," 0810.1987.

[72] L. von Smekal, R. Alkofer, and A. Hauck, "The infrared behavior of gluon and ghost propagators in Landau gauge QCD," *Phys. Rev. Lett.* **79** (1997) 3591–3594, hep-ph/9705242.

[73] F. D. R. Bonnet, P. O. Bowman, D. B. Leinweber, A. G. Williams, and J. M. Zanotti, "Infinite volume and continuum limits of the Landau-gauge gluon propagator," *Phys. Rev.* **D64** (2001) 034501, hep-lat/0101013.

[74] C. Lerche and L. von Smekal, "On the infrared exponent for gluon and ghost propagation in Landau gauge QCD," *Phys. Rev.* **D65** (2002) 125006, hep-ph/0202194.

[75] A. Maas, J. Wambach, B. Gruter, and R. Alkofer, "High-temperature limit of Landau-gauge Yang-Mills theory," *Eur. Phys. J.* **C37** (2004) 335–357, hep-ph/0408074.

[76] J. Braun and H. Gies, "Running coupling at finite temperature and chiral symmetry restoration in QCD," *Phys. Lett.* **B645** (2007) 53–58, hep-ph/0512085.

[77] J. Fingberg, U. M. Heller, and F. Karsch, "Scaling and asymptotic scaling in the SU(2) gauge theory," *Nucl. Phys.* **B392** (1993) 493–517, hep-lat/9208012.

[78] O. Kaczmarek, F. Karsch, P. Petreczky, and F. Zantow, "Heavy Quark Anti-Quark Free Energy and the Renormalized Polyakov Loop," *Phys. Lett.* **B543** (2002) 41–47, hep-lat/0207002.

[79] B. Lucini, M. Teper, and U. Wenger, "Properties of the deconfining phase transition in SU(N) gauge theories," *JHEP* **02** (2005) 033, hep-lat/0502003.

[80] C. Wozar, T. Kaestner, A. Wipf, and T. Heinzl, "Inverse Monte-Carlo determination of effective lattice models for SU(3) Yang-Mills theory at finite temperature," *Phys. Rev.* **D76** (2007) 085004, 0704.2570.

[81] D. F. Litim and J. M. Pawlowski, "Predictive power of renormalisation group flows: A comparison," *Phys. Lett.* **B516** (2001) 197–207, hep-th/0107020.

[82] J. M. Pawlowski in preparation.

[83] C. S. Fischer, R. Alkofer, and H. Reinhardt, "The elusiveness of infrared critical exponents in Landau gauge Yang-Mills theories," *Phys. Rev.* **D65** (2002) 094008, hep-ph/0202195.

[84] J. M. Pawlowski, D. F. Litim, S. Nedelko, and L. von Smekal, "Infrared behaviour and fixed points in Landau gauge QCD," *Phys. Rev. Lett.* **93** (2004) 152002, hep-th/0312324.

[85] C. S. Fischer and H. Gies, "Renormalization flow of Yang-Mills propagators," *JHEP* **10** (2004) 048, hep-ph/0408089.

[86] J. Braun, H. Gies, F. Marhauser, and J. M. Pawlowski in preparation.

[87] F. Karsch, "Lattice QCD at high temperature and density," *Lect. Notes Phys.* **583** (2002) 209–249, hep-lat/0106019.

[88] M. Cheng *et al.*, "The QCD Equation of State with almost Physical Quark Masses," *Phys. Rev.* **D77** (2008) 014511, 0710.0354.

[89] Z. Fodor, "QCD Thermodynamics," *PoS* **LAT2007** (2007) 011, 0711.0336.

[90] J. Polonyi and K. Sailer, "Renormalization of composite operators," *Phys. Rev.* **D63** (2001) 105006, hep-th/0011083.

[91] K. Harada, K. Inoue, and H. Kubo, "Wilsonian RG and Redundant Operators in Nonrelativistic Effective Field Theory," *Phys. Lett.* **B636** (2006) 305–309, nucl-th/0511020.

[92] J. Berges, D. U. Jungnickel, and C. Wetterich, "Two flavor chiral phase transition from nonperturbative flow equations," *Phys. Rev.* **D59** (1999) 034010, hep-ph/9705474.

[93] B.-J. Schaefer and J. Wambach, "Renormalization group approach towards the QCD phase diagram," *Phys. Part. Nucl.* **39** (2008) 1025–1032, hep-ph/0611191.

[94] Y. Nambu and G. Jona-Lasinio, "Dynamical model of elementary particles based on an analogy with superconductivity. II," *Phys. Rev.* **124** (1961) 246–254.

[95] Y. Nambu and G. Jona-Lasinio, "Dynamical model of elementary particles based on an analogy with superconductivity. I," *Phys. Rev.* **122** (1961) 345–358.

[96] K. Fukushima, "Chiral effective model with the Polyakov loop," *Phys. Lett.* **B591** (2004) 277–284, hep-ph/0310121.

[97] P. N. Meisinger and M. C. Ogilvie, "Chiral Symmetry Restoration and Z_N Symmetry," *Phys. Lett.* **B379** (1996) 163–168, hep-lat/9512011.

[98] E. Megias, E. Ruiz Arriola, and L. L. Salcedo, "Chiral Lagrangian at finite temperature from the Polyakov- Chiral Quark Model," *Phys. Rev.* **D74** (2006) 114014, hep-ph/0607338.

[99] K. Fukushima, "Thermodynamic limit of the canonical partition function with respect to the quark number in QCD," *Ann. Phys.* **304** (2003) 72–88, hep-ph/0204302.

[100] P. N. Meisinger, T. R. Miller, and M. C. Ogilvie, "A phenomenological treatment of chiral symmetry restoration and deconfinement," *Nucl. Phys. Proc. Suppl.* **119** (2003) 511–513, hep-lat/0208073.

[101] P. N. Meisinger, T. R. Miller, and M. C. Ogilvie, "Theory and phenomenology of the Polyakov loop in QCD thermodynamics," *Nucl. Phys. Proc. Suppl.* **129** (2004) 563–565, hep-lat/0309097.

[102] C. Ratti and W. Weise, "Thermodynamics of two-colour QCD and the Nambu Jona- Lasinio model," *Phys. Rev.* **D70** (2004) 054013, hep-ph/0406159.

[103] C. Ratti, M. A. Thaler, and W. Weise, "Phases of QCD: Lattice thermodynamics and a field theoretical model," *Phys. Rev.* **D73** (2006) 014019, hep-ph/0506234.

[104] S. Roessner, C. Ratti, and W. Weise, "Polyakov loop, diquarks and the two-flavour phase diagram," *Phys. Rev.* **D75** (2007) 034007, hep-ph/0609281.

[105] Y. Sakai, K. Kashiwa, H. Kouno, and M. Yahiro, "Polyakov loop extended NJL model with imaginary chemical potential," *Phys. Rev.* **D77** (2008) 051901, 0801.0034.

[106] B.-J. Schaefer, J. M. Pawlowski, and J. Wambach, "The Phase Structure of the Polyakov–Quark-Meson Model," *Phys. Rev.* **D76** (2007) 074023, 0704.3234.

[107] A. Chodos, R. L. Jaffe, K. Johnson, C. B. Thorn, and V. F. Weisskopf, "A New Extended Model of Hadrons," *Phys. Rev.* **D9** (1974) 3471–3495.

[108] A. Chodos, R. L. Jaffe, K. Johnson, and C. B. Thorn, "Baryon Structure in the Bag Theory," *Phys. Rev.* **D10** (1974) 2599.

[109] T. A. DeGrand, R. L. Jaffe, K. Johnson, and J. E. Kiskis, "Masses and Other Parameters of the Light Hadrons," *Phys. Rev.* **D12** (1975) 2060.

[110] J. Hubbard, "Calculation of partition functions," *Phys. Rev. Lett.* **3** (1959) 77–80.

[111] R. L. Stratonovich, "On a method fo calculating quantum distribution functions.," *Soviet. Phys. Doklady* (1958) 2:416.

[112] J. Braun and H. Gies, "Chiral phase boundary of QCD at finite temperature," *JHEP* **06** (2006) 024, hep-ph/0602226.

[113] L. von Smekal, A. Hauck, and R. Alkofer, "A solution to coupled Dyson-Schwinger equations for gluons and ghosts in Landau gauge," *Ann. Phys.* **267** (1998) 1, hep-ph/9707327.

[114] C. S. Fischer and R. Alkofer, "Infrared exponents and running coupling of SU(N) Yang- Mills theories," *Phys. Lett.* **B536** (2002) 177–184, hep-ph/0202202.

[115] C. S. Fischer and J. M. Pawlowski, "Uniqueness of infrared asymptotics in Landau gauge Yang- Mills theory," *Phys. Rev.* **D75** (2007) 025012, hep-th/0609009.

[116] C. S. Fischer, A. Maas, J. M. Pawlowski, and L. von Smekal, "Large volume behaviour of Yang-Mills propagators," *Annals Phys.* **322** (2007) 2916–2944, hep-ph/0701050.

[117] C. Kellermann and C. S. Fischer, "The running coupling from the four-gluon vertex in Landau gauge Yang-Mills theory," *Phys. Rev.* **D78** (2008) 025015, 0801.2697.

[118] F. D. R. Bonnet, P. O. Bowman, D. B. Leinweber, and A. G. Williams, "Infrared behavior of the gluon propagator on a large volume lattice," *Phys. Rev.* **D62** (2000) 051501, hep-lat/0002020.

[119] A. Cucchieri, A. Maas, and T. Mendes, "Infrared properties of propagators in Landau-gauge pure Yang-Mills theory at finite temperature," *Phys. Rev.* **D75** (2007) 076003, hep-lat/0702022.

[120] J. Gattnar, K. Langfeld, and H. Reinhardt, "Signals of confinement in Green functions of SU(2) Yang- Mills theory," *Phys. Rev. Lett.* **93** (2004) 061601, hep-lat/0403011.

[121] A. Sternbeck, E. M. Ilgenfritz, M. Muller-Preussker, A. Schiller, and I. L. Bogolubsky, "Lattice study of the infrared behavior of QCD Green's functions in Landau gauge," *PoS* **LAT2006** (2006) 076, `hep-lat/0610053`.

[122] H. Gies, "Running coupling in Yang-Mills theory: A flow equation study," *Phys. Rev.* **D66** (2002) 025006, `hep-th/0202207`.

[123] D. F. Litim, J. M. Pawlowski, S. Nedelko, and L. von Smekal, "Infrared QCD and the renormalisation group," `hep-th/0410241`.

[124] B. Bergerhoff and C. Wetterich, "Effective quark interactions and QCD propagators," *Phys. Rev.* **D57** (1998) 1591–1604, `hep-ph/9708425`.

[125] J. M. Pawlowski, D. F. Litim, S. Nedelko, and L. von Smekal, "Signatures of confinement in Landau gauge QCD," *AIP Conf. Proc.* **756** (2005) 278–280, `hep-th/0412326`.

[126] J. Kato, "Infrared non-perturbative propagators of gluon and ghost via exact renormalization group," `hep-th/0401068`.

[127] H. Gies, "Renormalizability of gauge theories in extra dimensions," *Phys. Rev.* **D68** (2003) 085015, `hep-th/0305208`.

[128] S. Mandelstam, "Approximation Scheme for QCD," *Phys. Rev.* **D20** (1979) 3223.

[129] L. M. Haas, "On the QCD Phase Diagram with the Renormalisation Group." Diplomarbeit, 2008.

[130] J. M. Pawlowski *in preparation*.

[131] S. Bethke, "α_s at Zinnowitz 2004," *Nucl. Phys. Proc. Suppl.* **135** (2004) 345–352, `hep-ex/0407021`.

[132] B.-J. Schaefer and J. Wambach, "Susceptibilities near the QCD (tri)critical point," *Phys. Rev.* **D75** (2007) 085015, `hep-ph/0603256`.

[133] F. R. Brown, N. H. Christ, Y. F. Deng, M. S. Gao, and T. J. Woch, "Nature of the Deconfining Phase Transition in SU(3) Lattice Gauge Theory," *Phys. Rev. Lett.* **61** (1988) 2058.

[134] C. Gattringer, "Linking confinement to spectral properties of the Dirac operator," *Phys. Rev. Lett.* **97** (2006) 032003, `hep-lat/0605018`.

[135] F. Synatschke, A. Wipf, and C. Wozar, "Spectral sums of the Dirac-Wilson operator and their relation to the Polyakov loop," *Phys. Rev.* **D75** (2007) 114003, `hep-lat/0703018`.

[136] F. Synatschke, A. Wipf, and K. Langfeld, "Relation between chiral symmetry breaking and confinement in YM-theories," *Phys. Rev.* **D77** (2008) 114018, 0803.0271.

[137] F. Bruckmann, C. Hagen, E. Bilgici, and C. Gattringer, "Dual condensate, dressed Polyakov loops and center symmetry from Dirac spectra," *PoS* **LATTICE2008** (2008) 262, 0810.0899.

[138] A. Roberge and N. Weiss, "Gauge theories with imaginary chemical potential and the phases of QCD," *Nucl. Phys.* **B275** (1986) 734.

[139] M. P. Lombardo, "Lattice QCD at finite density: Imaginary chemical potential," *PoS* **CPOD2006** (2006) 003, hep-lat/0612017.

[140] H. Kouno, Y. Sakai, K. Kashiwa, and M. Yahiro, "Roberge-Weiss phase transition and its endpoint," 0904.0925.

[141] C. S. Fischer, "Deconfinement phase transition and the quark condensate," 0904.2700.

[142] C. S. Fischer and J. A. Mueller, "Chiral and deconfinement transition from Dyson-Schwinger equations," 0908.0007.

[143] S. Kratochvila and P. de Forcrand, "QCD at zero baryon density and the Polyakov loop paradox," *Phys. Rev.* **D73** (2006) 114512, hep-lat/0602005.

[144] L.-K. Wu, X.-Q. Luo, and H.-S. Chen, "Phase structure of lattice QCD with two flavors of Wilson quarks at finite temperature and chemical potential," *Phys. Rev.* **D76** (2007) 034505, hep-lat/0611035.

[145] S. Floerchinger and C. Wetterich, "Exact flow equation for composite operators," 0905.0915.

[146] M. E. Peskin and D. V. Schroeder, "An Introduction to quantum field theory,". Reading, USA: Addison-Wesley (1995) 842 p.

[147] K. G. Wilson and M. E. Fisher, "Critical exponents in 3.99 dimensions," *Phys. Rev. Lett.* **28** (1972) 240–243.

[148] F. J. Wegner, "Critical Exponents in Isotropic Spin Systems," *Phys. Rev.* **B6** (1972) 1891–1893.

[149] N. Tetradis and C. Wetterich, "Critical exponents from effective average action," *Nucl. Phys.* **B422** (1994) 541–592, hep-ph/9308214.

[150] C. S. Fischer, L. Fister, F. Marhauser, and J. M. Pawlowski, "Critical exponents from Dyson-Schwinger equations." work in progress.

[151] B.-J. Schaefer and M. Wagner, "The three-flavor chiral phase structure in hot and dense QCD matter," *Phys. Rev.* **D79** (2009) 014018, 0808.1491.

Danksagungen

Ohne die Beiträge verschiedenster Menschen wäre diese Arbeit nicht gelungen und es ist mir eine Freude, mich bei ihnen zu bedanken!

Zuerst geht mein Dank natürlich an meinen Doktorvater Prof. Dr. Jan Martin Pawlowski, der mir die Möglichkeit gab in seiner Arbeitsgruppe zu promovieren. Ich bin ihm sehr dankbar für unzählige erhellende Diskussionen und seine manigfaltige Unterstützung während meiner Promotion. Seine Begeisterung für die Physik im Allgemeinen und seine Expertise auf dem Gebiet der Quantenchromodynamik waren entscheidend für meine Entwicklung im Laufe meiner Promotion. Ich bin ihm sehr dankbar, es mir ermöglicht zu haben an diversen Workshops und Konferenzen teilzunehmen, um dort meine Arbeit vorzustellen und zu diskutieren.

Herrn Prof. Dr. Jürgen Schaffner-Bielich danke ich für seine Bereitschaft, der Zweitkorrektor dieser Arbeit zu sein und für sein starkes Interesse an meiner Forschung.

Herrn Prof. Dr. Christof Wetterich and Frau Prof. Dr. Johanna Stachel bin ich dankbar für ihre Mitwirkung in meinem Promotionskomitee und ihr Interesse an meiner Arbeit.

Für die produktive und erfolgreiche Zusammenarbeit, sowie für viele interessante Diskussionen danke ich Dr. Jens Braun. Seine zahlreichen Anregungen zu dieser Arbeit haben entscheidend dazu beigetragen, sie zu verbessern.

Herrn Prof. Dr. Holger Gies danke ich für viele spannende und lehrreiche Diskussionen.

Für die Zusammenarbeit und die Diskussionen bin ich Herrn Prof. Christian S. Fischer sehr dankbar.

Frau Lisa Marie Haas danke ich sehr für die Zusammenarbeit und viele anregende Diskussionen. Ebenso danke ich den Teilnehmern des Kalten Quanten Kaffees und den Kollegen aus meinem Büro, für vielerlei anregende Diskussionen.

Ich bin der Heidelberg Graduate School of Fundamental Physics sehr dankbar für ihre Unterstützung meiner Arbeit.